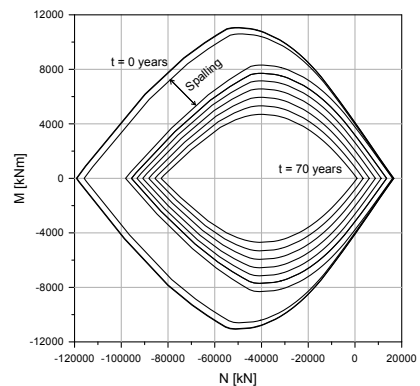
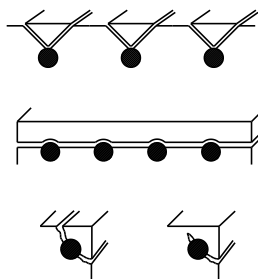
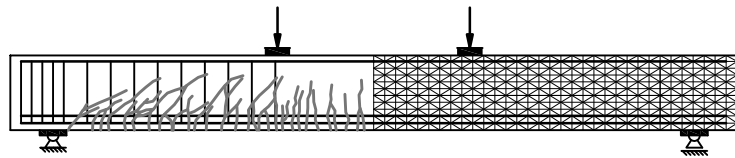


MANUEL QUAGLIAROLI

Doctoral Dissertation

From Bidimensional towards Monodimensional  
Modeling of Sound and Damaged  
Reinforced Concrete Structures



MARCH 2014



POLITECNICO DI MILANO

Department of Civil & Environmental Engineering

Doctoral School in Structural, Earthquake and Geotechnical Engineering

XXVI Cycle



# POLITECNICO DI MILANO

DEPARTMENT OF CIVIL & ENVIRONMENTAL ENGINEERING



DOCTORAL SCHOOL IN  
STRUCTURAL, EARTHQUAKE AND GEOTECHNICAL ENGINEERING  
XXVI Cycle

PHD THESIS

---

---

FROM BIDIMENSIONAL TOWARDS MONODIMENSIONAL  
MODELING OF SOUND AND DAMAGED  
REINFORCED CONCRETE STRUCTURES

---

Manuel QUAGLIAROLI

SUPERVISOR:

Prof. Pier Giorgio MALERBA

THE CHAIR OF THE DOCTORAL PROGRAM:

Prof. Roberto PAOLUCCI

---

MILAN - MARCH 2014

M. Quagliaroli  
*From Bidimensional towards Monodimensional  
Modeling of Sound and Damaged Reinforced Con-  
crete Structures*

© March 2014

[manuel.quagliaroli@polimi.it](mailto:manuel.quagliaroli@polimi.it)

---

*Department of Civil & Environmental Engineering*  
Politecnico di Milano

FROM BIDIMENSIONAL TOWARDS MONODIMENSIONAL MODELING  
OF SOUND AND DAMAGED REINFORCED CONCRETE STRUCTURES

A THESIS  
PRESENTED TO  
THE ACADEMIC FACULTY

by

**Manuel Quagliaroli**

IN PARTIAL FULLFILMENT  
OF THE REQUIREMENTS FOR THE DEGREE OF  
DOCTOR OF PHILOSOPHY

IN  
STRUCTURAL, SEISMIC AND GEOTECHNICAL ENGINEERING

MARCH 2014



FROM BIDIMENSIONAL TOWARDS MONODIMENSIONAL MODELING  
OF SOUND AND DAMAGED REINFORCED CONCRETE STRUCTURES

PhD thesis by Manuel Quagliaroli

Supervisor: Prof. Pier Giorgio Malerba

© March 2014

DOCTORAL SCHOOL IN STRUCTURAL, EARTHQUAKE AND GEOTECHNICAL  
ENGINEERING  
DEPARTMENT OF CIVIL & ENVIRONMENTAL ENGINEERING  
POLITECNICO DI MILANO

XXVI CYCLE - 2011-2014

BOARD COMMITTEE:

Prof. Raffele Ardito

Prof. Fabio Biondini

Prof. Gabriella Bolzon

Prof. Claudia Comi

Prof. Alberto Corigliano

Prof. Dario Coronelli

Prof. Marco Di Prisco

Prof. Claudio Di Prisco

Prof. Liberato Ferrara

Prof. Attilio Frangi

Prof. Elsa Garavaglia

Prof. Cristina Jommi

Prof. Pier Giorgio Malerba

Prof. Anna Pandolfi

Prof. Roberto Paolucci

Prof. Umberto Perego

Prof. Federico Perotti

Prof. Lorenza Petrini

Prof. Gianpaolo Rosati

Prof. Luigi Zanzi





Simplicity is the  
ultimate  
*Sophistication*

*To my Mother  
Caterina Boselli*

*To my Father  
Andrea Quagliaroli*



# Preface

This thesis was carried out at the Department of Civil and Environmental Engineering - Politecnico di Milano, between January 2011 and March 2014.

Firstly, I thank my supervisor Prof. Pier Giorgio Malerba. His vast knowledge of structures has been invaluable for the development of this research and his contributions to my education will be retained throughout my professional life.

A debt of gratitude is owed to Prof. Fabio Biondini, for the expert and precise advice he always provided during my studies.

Thanks to Prof. Franco Bontempi. His continuous encouragements and guidance have transformed this work in a motivated challenge.

This thesis benefited from the suggestions of several Professors of the Department. A special thank to: Prof. Luigi Cedolin, Prof. Giuseppe Cocchetti, Prof. Claudia Comi, Prof. Alberto Corigliano, Prof. Pietro Gambarova, Prof. Gabriella Mulas, Dr. Raffaele Ardito, Dr. Luca Martinelli and Dr. Luca Sgambi.

Thanks also to Prof. Evan Bentz and to Prof. Filip Filippou, for their advice from Toronto and Berkeley, and to Prof. Enrique Hernández and Prof. Luisa Gil-Martín, for their course on Reinforced Concrete taken during my PhD path.

A thank goes to colleagues and former colleagues: Dr. Elena Camnasio, because my study on RC structures starts with her; Dr. Francesco Foti, for teaching me object-oriented coding; Dr. Roberto Guidotti, for our great weekly football matches; Eng. Zdenek Matous, for explaining me that we don't need a computer at all; Dr. Ehssan Muhasami, for his help also from Iran; Eng. Visar Krelani, for all the time that we spent together; Eng. Juan Pazmino Flores, he knows the reasons; and Dr. Andrea Titi, for his suggestions on damage modeling.

My last special gratitude goes to Eng. Matteo Colussi, Eng. Elisa Conti and Eng. Diego Scaperrotta. At the beginning, they were my students, but then they became my "team work". I was honored to supervise their master thesis and I'm sure that this work would not have been the same without them: thank you all.

Finally, the financial assistance of the government of Italy is gratefully acknowledged.

*Milan, March 2014*  
*Manuel Quagliaroli*



# Abstract

Reinforced and Prestressed Concrete Structures exposed to aggressive environments, more or less severe, exhibit a progressive deterioration that reduce their bearing capacity over time, as well as their residual service life. Carbonation, spalling, cracking, corrosion due to chlorides and consequent reduction of bar and tendon areas are what we are used to see in surveying buildings and bridges forty/fifty years old.

The social and economic relevance of the safety of the structure and infrastructures gave rise to an intense research activity and was the motivation that led to undertake the present work.

After having deepened the main physical and mechanical aspects that rule the time variant capacity of a structure, the attention have been focused on the effects induced by the most frequent damaging causes on the behavioral and collapse mechanisms of RC elements. Such a problem involves (I) a representative modeling of the damage diffusion inside the volume of the RC element; (II) a reliable and robust modeling of RC cracked element working in membrane state and (III) a methodology of coupling the physical and the mechanical behaviors over time.

The mechanical aspects are prevailing. Therefore, the work starts by examining different approaches to the analysis of RC frame and membrane structures. These approaches have been introduced and developed through ad hoc computer codes, then tested and compared. In particular, two renowned RC smeared approaches for bidimensional FE analyses and hands-on verifications have been reviewed and a wide set of comparisons with experiments concerning shear critical panels and beams have been carried out. As known, a FE bidimensional analysis is quite heavy to do for practice. So, in order to search for a synthetic approach, a shear flexible beam column RC element has been proposed. With reference to the infinitesimal segment of beam, the evolution of the sectional kinematic from the Navier-Bernoulli, to Timoshenko and to the generalized beam theory is analyzed, showing how each new grade of refinement requires necessarily a more refined stress-strain relationship (linear or non-linear). Hence, by proposing two particular section state determinations, the structural analysis moved from bidimensional towards monodimensional one. The element formulation is accomplished with proposal that allows computing the stresses in the stirrups and representing, in a conventional way, the crack pattern in the web of the beam. Also such a model has been validated with reference to a set of experimental results.

After the analyses oriented to sound RC structures, the damage diffusion process and its modeling through the diffusivity equation is presented. The diffusion problem is solved through the Cellular Automata algorithm. Introductory examples show the effectiveness of such a numerical approach. The effects of the damage are then specialized to Reinforced Concrete Elements. New damage indexes, concerning both steel and concrete, are introduced and then tested for different reinforcement assemblies.

A wide set of applications confirm the soundness of both of theoretic proposals and of the algorithms used to reduce the problems to a numerical form. Moreover, significant comparisons have been made between the results given by non-linear analyses and those given by the limit analyses. Such comparisons led to introduce an efficiency factor that takes into account the different nature of these two approaches, as well as the different criteria to model the material properties with respect to the ultimate behavior. The types of applications stand out the effectiveness of all the proposed models in dealing with actual and complex structures, both in sound and damaged conditions, and show their usefulness among the methodologies for life-cycle appraisals.

**KEYWORDS:** Concrete structures; Shear modeling; Shear flexible beam column elements; Non linear analysis; Limit analysis; Corrosion; Environmental damage.

# Contents

<b>Preface</b>	<b>ix</b>
<b>Abstract</b>	<b>xi</b>
<b>List of Symbols</b>	<b>xix</b>
<b>List of Figures</b>	<b>xxvii</b>
<b>List of Tables</b>	<b>xxx</b>
<b>1 Introduction</b>	<b>3</b>
1.1 Motivation and Problem Statement . . . . .	3
1.1.1 Concerning the Structural Model . . . . .	4
1.1.2 Concerning the Damage Model . . . . .	5
1.2 Scope and objectives . . . . .	6
1.3 Research significance . . . . .	7
1.4 Contents of this document . . . . .	8
<b>I Sound RC Structures</b>	<b>11</b>
<b>2 A Review of the Non Linear Beam Problem</b>	<b>13</b>
2.1 Introduction . . . . .	13
2.2 The Virtual Work Principle . . . . .	14
2.3 Displacement Based Element (Stiffness Approach) . . . . .	16
2.3.1 Element state determination . . . . .	17
2.4 Force Based Element (Flexibility Approach) . . . . .	17
2.4.1 Reference systems: with and without rigid body modes . . . . .	17
2.4.1.1 Static field . . . . .	18
2.4.1.2 Kinematic field . . . . .	19
2.4.1.3 Additional considerations . . . . .	19
2.4.1.4 Summary of the Main Transformations . . . . .	21
2.4.2 Element State Determination . . . . .	21
2.4.3 Different types of state determination algorithms and additional comments . . . . .	23
2.5 Treatment of distributed loads . . . . .	26

2.5.1	Displacement-based element . . . . .	26
2.5.2	Force-based element . . . . .	27
2.6	Geometric non linearities . . . . .	28
2.7	Displacement-based vs force-based element: comparisons . . . . .	29
2.8	Shear Modeling . . . . .	32
2.8.1	Displacement-based Element . . . . .	32
2.8.1.1	Shear Locking Prevention . . . . .	33
2.8.2	Force-based Element . . . . .	34
2.9	Closing Remarks . . . . .	34
<b>3</b>	<b>RC Sectional Models: Problem Statement &amp; State of the Art</b>	<b>35</b>
3.1	Definition of the Problem . . . . .	35
3.1.1	Dealing with Normal Forces . . . . .	36
3.1.2	Dealing with Normal and Tangential Forces . . . . .	37
3.1.3	Shear in RC sections: the main difficulty . . . . .	40
3.2	Sectional kinematic approaches considering shear effects . . . . .	41
3.2.1	Strut & Tie based Models . . . . .	43
3.2.1.1	Martinelli’s Modeling Strategy . . . . .	43
3.2.2	Inter-Fibre Equilibrium Approaches . . . . .	44
3.2.2.1	The Dual Sectional Analysis . . . . .	44
3.2.2.2	The Longitudinal Stiffness Method . . . . .	45
3.2.2.3	The Theory of Bairán-Marí . . . . .	46
3.2.2.4	The Theory of Mohr-Bairán-Marí . . . . .	47
3.2.3	Fixed Pattern Approaches . . . . .	49
3.3	Closing Remarks . . . . .	50
<b>4</b>	<b>Bidimensional Modeling</b>	<b>53</b>
4.1	From trusses analogies to the smeared approaches . . . . .	53
4.2	Modified Compression Field Theory (MCFT) . . . . .	55
4.2.1	Hypothesis and sign conventions . . . . .	55
4.2.2	Compatibility Conditions . . . . .	57
4.2.3	Equilibrium Conditions . . . . .	57
4.2.4	Constitutive laws . . . . .	57
4.2.4.1	Concrete . . . . .	57
4.2.4.2	Steel . . . . .	59
4.2.5	Loading transmission across the cracks . . . . .	59
4.2.6	Additional conditions . . . . .	61
4.2.6.1	Crack width limit . . . . .	61
4.2.6.2	Residual Tension . . . . .	61
4.3	Disturbed Stress Field Model (DSFM) . . . . .	62
4.3.1	Hypothesis and sign conventions . . . . .	62
4.3.2	Compatibility Conditions . . . . .	62
4.3.3	Equilibrium Conditions . . . . .	64
4.3.4	Constitutive laws . . . . .	64
4.3.4.1	Concrete . . . . .	64
4.3.4.2	Steel . . . . .	65
4.3.5	Crack slip modeling . . . . .	66



4.4	Reduction of the Problem to Algebraic Form . . . . .	67
4.4.1	Displacement Field . . . . .	67
4.4.2	Reference Systems . . . . .	68
4.4.3	The RC Triangular Element . . . . .	68
4.4.3.1	Concrete . . . . .	69
4.4.3.2	Smearred Steel . . . . .	70
4.4.3.3	Reinforced Concrete: Concrete & Smearred Steel . . . . .	71
4.4.3.4	Resisting Forces and Element Stiffness . . . . .	71
4.4.4	Secant Solution and Convergence Criterion . . . . .	72
4.5	Validation and Comments . . . . .	74
4.5.1	PV20 Panel . . . . .	74
4.5.2	PV23 Panel . . . . .	75
4.5.3	PB20 Panel . . . . .	75
4.5.4	PW3-2 Cervenka Panel . . . . .	76
4.5.5	A1 Bresler & Scordelis Beam . . . . .	79
4.6	Closing Remarks . . . . .	80
<b>5</b>	<b>Monodimensional Modeling</b>	<b>81</b>
5.1	Global Framework . . . . .	81
5.1.1	Element: Resisting Forces and Stiffness Matrix . . . . .	82
5.1.2	Section: Resisting Forces and Stiffness Matrix . . . . .	83
5.2	Specialization to RC sections . . . . .	85
5.2.1	Concrete Fibers with Smearred Transversal Steel . . . . .	85
5.2.2	Longitudinal Steel . . . . .	86
5.3	Section State Determination . . . . .	87
5.3.1	Fixed Strain Approaches . . . . .	87
5.3.2	Fixed Stress Approaches . . . . .	88
5.3.3	Comparison and Flow Charts . . . . .	89
5.4	Validation: the “Stuttgart Shear Test” . . . . .	91
5.5	Concluding Remarks . . . . .	97
<b>II</b>	<b>Damaged RC Structures</b>	<b>99</b>
<b>6</b>	<b>Damage modeling in RC structures exposed to corrosion</b>	<b>101</b>
6.1	Introduction . . . . .	101
6.1.1	Initiation phase . . . . .	102
6.1.2	Propagation phase . . . . .	102
6.2	Diffusion Processes and Cellular Automata . . . . .	104
6.2.1	Modeling of Diffusion Processes . . . . .	104
6.2.2	An Introduction to Cellular Automata . . . . .	105
6.2.3	Cellular Automata Solution of Diffusion Equations . . . . .	106
6.3	From Diffusion Process to Damage Indexes . . . . .	107
6.3.1	Definition of the dimensionless damage index $\delta_s$ . . . . .	108
6.3.2	Reduction of the cross-section of reinforcing bars . . . . .	109
6.3.2.1	Uniform corrosion . . . . .	109
6.3.2.2	Localized corrosion . . . . .	110

6.3.3	Reduction of ductility of reinforcing steel . . . . .	110
6.3.4	Effects of corrosion on concrete . . . . .	110
6.4	Critical Comparison . . . . .	112
6.5	Closing Remarks . . . . .	114
<b>III</b>	<b>Applications</b>	<b>117</b>
<b>7</b>	<b>Damage Effects on Structural Performances of Bridges</b>	<b>119</b>
7.1	Introduction . . . . .	119
7.2	Sound Cable Stayed Bridge . . . . .	120
7.2.1	Cable Prestressing Forces Evaluation . . . . .	122
7.2.2	Non Linear Analysis . . . . .	123
7.2.3	Limit Analysis and Comparisons . . . . .	125
7.3	Sound Arch Bridge (Corace River, Calabria, Italy) . . . . .	126
7.3.1	Non Linear Analysis . . . . .	129
7.3.2	Limit Analysis and Comparisons . . . . .	130
7.4	Damaged Arch Bridge (Corace River, Calabria, Italy) . . . . .	131
7.4.1	Corrosion scenarios . . . . .	131
7.4.2	Solution of the diffusion process . . . . .	132
7.4.3	Mechanical damage induced by corrosion . . . . .	134
7.4.4	Effects on Service Performance . . . . .	137
7.4.5	Effects on Ultimate Performance . . . . .	138
7.5	Concluding Comments . . . . .	143
<b>8</b>	<b>Damage Effects on Shear Resisting Mechanisms</b>	<b>145</b>
8.1	Problem statement and diffusive process . . . . .	145
8.1.1	Corrosion Scenario . . . . .	146
8.1.2	Cellular Automata solution of the diffusion process . . . . .	147
8.2	Time variant structural analysis . . . . .	147
8.3	Closing Remarks . . . . .	150
<b>IV</b>	<b>Other Items suggested &amp; Further Improvements</b>	<b>151</b>
<b>A</b>	<b>A sectional parametric sub-domains discretization</b>	<b>153</b>
A.1	Introduction . . . . .	153
A.2	Numerical Integration by Parametric Transformations . . . . .	155
A.2.1	Quadrilateral sub-domain . . . . .	156
A.2.2	Circular sectorial sub-domain . . . . .	156
A.2.3	Integration Rules . . . . .	157
A.2.4	Sampling Points and Weights Factors . . . . .	158
A.3	RC Section based on Navier-Bernoulli kinematic . . . . .	162
A.3.1	Section Equilibrium . . . . .	163
A.3.2	The two types of Section Problems . . . . .	164
A.3.2.1	Type 1 Problem . . . . .	164
A.3.2.2	Type 2 Problem . . . . .	164

A.3.3	Remarks on the Section Stiffness Matrix . . . . .	166
A.3.4	Interaction Domains . . . . .	166
A.4	Validation and Applications . . . . .	167
A.4.1	Square section. Comparisons among different discretizations . . . . .	169
A.4.2	Multiaxial interaction domains . . . . .	173
A.4.2.1	A square R.C. section . . . . .	173
A.4.2.2	An L shaped R.C. section . . . . .	174
A.4.2.3	An hollow circular R.C. section . . . . .	175
<b>B</b>	<b>Limit analysis</b>	<b>177</b>
B.1	Introduction and Basic Hypothesis . . . . .	177
B.2	Global Equilibrium and Compatibility Equations . . . . .	179
B.2.1	Equilibrium Equations . . . . .	180
B.2.2	Compatibility Equations . . . . .	181
B.2.3	About Equilibrium and Compatibility matrices . . . . .	181
B.3	Material Constitutive Models . . . . .	182
B.3.1	Yield condition . . . . .	182
B.3.2	Flow rule . . . . .	183
B.4	Static and kinematic approach (duality) . . . . .	184
B.5	Benchmarks . . . . .	186
B.5.1	A portal frame . . . . .	186
B.5.2	A clamped RC arch . . . . .	187
B.5.3	A collaborating beam-arch system . . . . .	189
	<b>Conclusions</b>	<b>193</b>
	<b>References</b>	<b>199</b>
	<b>Index</b>	<b>211</b>



# List of Symbols

*The following is a list of the most important symbols and abbreviations that appear in the chapters of the thesis. Symbols not included in this list are defined when they first appear.*

## LATIN LETTERS

$a$	maximum aggregate size
$\mathcal{A}$	assembling process
$A_c$	area of concrete fiber
$A_s$	area of steel bar
$\mathbf{a}_s$	sectional interpolating matrix
$\mathbf{b}$	force's shape functions matrix
$\mathbf{B}$	displacement's shape functions matrix (derivatives)
$C$	concentration of the aggressive agent
$C_0$	initial concentration of the aggressive agent
$\mathbf{c}$	nodal coordinate vector
$D_e$	effective diffusion coefficient
$\mathbf{D}$	material's stiffness matrix $[3 \times 3]$
$\bar{\mathbf{D}}$	reduced material's stiffness matrix $[2 \times 2]$
$E_c$	concrete elastic modulus
$E_{c1}$	concrete modulus in direction 1
$E_{c2}$	concrete modulus in direction 2
$E_s$	steel elastic modulus
$\mathbf{e}_s$	generalized sectional strains vector
$f_{cr}$	tensile cracking stress
$f_y$	steel yielding stress
$F_{P0}$	prestressing force
$\mathbf{f}_{ne}$	equivalent nodal forces vector
$\mathbf{f}_p$	distributed loads vector
$\mathbf{f}_s$	generalized sectional stresses vector

$\mathbf{f}_{s,r}$	sectional resisting force (complete RC section)
$\mathbf{f}_{s,r}^C$	sectional resisting force (Concrete contribution)
$\mathbf{f}_{s,r}^S$	sectional resisting force (Steel contribution)
$\mathbf{F}_e$	structural external nodal forces vector
$\mathbf{F}_r$	structural restoring nodal forces vector
$\mathbf{F}_{r,e}$	triangular element's nodal forces
$G_c$	concrete tangential modulus
$\mathbf{g}$	residual vector (problem in homogeneous form)
$\mathbf{h}_l$	beam element's compatibility matrix
$\mathbf{h}_l^T$	beam element's equilibrium matrix
$\mathbf{H}$	structure's equilibrium matrix
$\mathbf{H}^T$	structure's compatibility matrix
$\mathbf{J}$	Jacobian matrix
$\mathbf{J}_p$	Jacobian matrix of the polar transformation
$\mathbf{J}_t$	Jacobian matrix of the quadrilateral transformation
$\mathbf{k}$	beam element's stiffness matrix
$\bar{\mathbf{k}}$	beam element's stiffness matrix (system without rigid body modes)
$\mathbf{k}_g$	geometric contribution to beam element's stiffness matrix
$\mathbf{k}_s$	section's stiffness matrix (complete RC section)
$\mathbf{k}_s^C$	section's stiffness matrix (Concrete contribution)
$\mathbf{k}_s^S$	section's stiffness matrix (Steel contribution)
$M$	bending moment
$M_p$	plastic moment
$\mathbf{M}$	stays prestressing forces matrix
$N$	axial force
$\mathbf{N}$	displacements shape functions matrix
$p$	corrosion penetration depth
$\mathbf{q}$	beam element's nodal displacements vector
$\bar{\mathbf{q}}$	beam element's basic displacements vector
$\mathbf{Q}$	beam element's nodal forces vector
$\bar{\mathbf{Q}}$	beam element's basic forces vector
$\mathbf{Q}_g$	geometric contribution to beam element's nodal forces
$\mathbf{Q}_t$	structural basic forces vector
$R$	pitting factor
$s_i$	state of the cellular automaton
$\mathbf{s}$	structural nodal displacements

$\mathbf{t}$	stays prestressing forces vector
$\mathbf{T}_\alpha$	beam element transformation matrix (local to global system)
$\mathbf{T}_\varepsilon$	transformation matrix of the strain tensor
$\mathbf{T}_\sigma$	transformation matrix of the stress tensor
$u$	local horizontal displacement of the generic point
$\mathbf{u}$	displacements vector in the generic point $[u \ v]^T$
$\mathbf{u}_s$	sectional generalized displacements vector $[u_0 \ v_0 \ \varphi]^T$
$\mathbf{U}$	triangular element's nodal displacements
$v$	local vertical displacement of the generic point
$V$	shear force
$w$	crack width opening
$W_e$	external work
$W_i$	internal work
$x$	x axis
$y$	y axis
$z$	z axis

## GREEK LETTERS

$\alpha$	reinforcing steel inclination
$\chi_0$	curvature
$\delta_s$	dimensionless damage index
$\Delta t$	automaton time step
$\Delta x$	automaton grid dimension
$\varepsilon_0$	axial strain
$\varepsilon_1$	greater principal strain
$\varepsilon_2$	lower principal strain
$\varepsilon_{cr}$	concrete cracking strain
$\varepsilon_\perp$	strain in the perpendicular direction
$\boldsymbol{\varepsilon}$	strain tensor $[\varepsilon_x \ \varepsilon_y \ \gamma_{xy}]^T$
$\bar{\boldsymbol{\varepsilon}}$	reduced strain tensor $[\varepsilon_x \ \gamma_{xy}]^T$
$\boldsymbol{\varepsilon}_c$	concrete strain tensor
$\boldsymbol{\varepsilon}^s$	strain tensor relative to average crack slip
$\phi$	evolutionary rule of the automaton
$\phi_s$	section flexibility matrix
$\bar{\boldsymbol{\Phi}}$	beam element's flexibility matrix (system without rigid body modes)

$\gamma_0$	mean shear strain
$\eta$	dimensionless axis in the parent domain
$\lambda_c$	collapse multiplier
$\mu$	flow parameters vector
$\nu_e$	effectiveness factor
$\vartheta$	angle between axis $y$ and axis 1
$\vartheta_\varepsilon$	principal strains direction angle
$\vartheta_\sigma$	principal stresses direction angle
$\Theta$	plastic potential vector
$\rho_{s,i}$	geometric percentage of the $i - th$ smeared reinforcement
$\sigma$	stress tensor $[\sigma_x \sigma_y \tau_{xy}]^T$
$\bar{\sigma}$	reduced stress tensor $[\sigma_x \tau_{xy}]^T$
$\zeta$	dimensionless axis in the parent domain

### ABBREVIATIONS

CFT	Compression Field Theory
DSFM	Disturbed Stress Field Model
FA-STM	Fixed-Angle Softened Truss Model
LA	Limit Analysis
MCFT	Modified Compression Field Theory
NLA	Non Linear Analysis
NLG	Non Linear Geometry
NLM	Non Linear Mechanic
NR	Newton-Raphson solution scheme
PS	Plane Section hypothesis
RA-STM	Rotating-Angle Softened Truss Model
RC	Reinforced Concrete



# List of Figures

1.1	Life steps of a bridge over the Po River, Italy. . . . .	3
1.2	Comparisons between Finite Element Models. . . . .	4
1.3	Scope of the thesis. The proposed procedure is the combination of two independent parts. . . . .	6
2.1	Shape functions for a conventional frame element. . . . .	16
2.2	Static field: element with and without rigid body modes. . . . .	18
2.3	Kinematic field: element with and without rigid body modes. . . . .	19
2.4	Logic comparison between displacement-based (only a global non linear system of eqs.) and force-based elements (additional nested non linear systems). . . . .	25
2.5	Distributed loads on the element. . . . .	26
2.6	Distributed loads and associated reaction forces. . . . .	27
2.7	Second order geometrical non-linearity. . . . .	28
2.8	Shape functions. . . . .	33
2.9	Bubble shape function. . . . .	33
2.10	Inclusion of shear in a force-based element. . . . .	34
3.1	Fibers Sectional Approach (normal stresses). . . . .	36
3.2	Membrane RC element, (Vecchio and Collins, 1986). . . . .	37
3.3	Enhancement of 1D solution, adapted from (Bairán, 2005). . . . .	38
3.4	In plane shear stresses in a beam deduced by Jourawski (1856). . . . .	40
3.5	Martinelli's Modeling Strategy (Martinelli, 2008). . . . .	43
3.6	The Dual Section Analysis, (Vecchio and Collins, 1988). . . . .	44
3.7	Longitudinal Stiffness Method, (Bentz, 2000). . . . .	45
3.8	TINSA Model, (Bairán, 2005). . . . .	46
3.9	The Theory of Mohr-Bairán-Marí, (Mohr <i>et al.</i> , 2010). . . . .	47
3.10	Comparisons between shear flow and strain (Vecchio and Collins, 1988). . . . .	49
4.1	Truss Analogies Model for concrete beams in shear, adapted from (Vecchio and Collins, 1988). . . . .	53
4.2	Metal beam with very thin webs studied by Wagner (1929). . . . .	54
4.3	Compression softening phenomena, (Robinson and Demorieux, 1968). . . . .	54
4.4	Membrane tester. . . . .	55

4.5	MCFT: Equilibrium and Compatibility Conditions. . . . .	56
4.6	Convention for average stresses and strains and equilibrium and compatibility conditions. . . . .	58
4.7	Compression softening effects in the constitutive laws. . . . .	58
4.8	Concrete constitutive law. . . . .	59
4.9	Stresses and strains for reinforcement in principal direction. . . . .	59
4.10	Steel constitutive law. . . . .	60
4.11	Comparisons of local stresses at a crack with calculated average stresses. . . . .	60
4.12	Comparisons between principal stresses and strains directions, (Vecchio and Collins, 1986). . . . .	63
4.13	DSFM: Equilibrium and Compatibility (only for concrete) Conditions. . . . .	64
4.14	DSFM: constitutive law for concrete in compression. . . . .	65
4.15	Discretization of the continuum domain with a triangular finite element. . . . .	67
4.16	Global ( $0 - xy$ ) and local ( $0 - 12$ ) reference systems. . . . .	68
4.17	Secant concrete modulus. . . . .	69
4.18	Secant steel modulus. . . . .	71
4.19	Secant solution scheme. . . . .	73
4.20	MCFT & DSFM: flow chart. . . . .	73
4.21	PV20 Panel: geometry and forces. . . . .	74
4.22	PV20 Panel: comparisons between MCFT and DSFM results. . . . .	75
4.23	PV23 Panel: geometry and forces. . . . .	76
4.25	PB20 Panel: geometry and forces. . . . .	76
4.24	PV23 Panel: shear stress versus shear strain. . . . .	77
4.26	PB20 Panel: shear stress versus shear strain. . . . .	77
4.27	PW3-2 Cervenka Panel: geometry and mesh. . . . .	78
4.28	PW3-2 Cervenka Panel: numerical crack patterns. . . . .	78
4.29	PW3-2 Cervenka Panel: force versus displacement. . . . .	78
4.30	A1 Bresler & Scordelis Beam: geometry, mesh and results. . . . .	79
4.31	A1 Bresler & Scordelis Beam: geometry of the section. . . . .	80
5.1	Global Analysis Framework. Real structure, structural mesh and element's nodal quantities. . . . .	81
5.2	The 2 Node shear-flexible beam-column element. . . . .	82
5.3	Timoshenko's kinematic. . . . .	83
5.4	RC section: fibers with smeared steel and longitudinal bars. . . . .	85
5.5	Fixed Strain Approaches: Input quantities. . . . .	87
5.6	Fixed Stress Approaches: Input quantities. . . . .	88
5.7	Flow chart of the two proposed Section State Determination. . . . .	90
5.8	Stuttgart Shear Test: meshes of the two numerical models used. . . . .	91
5.9	Stuttgart Shear Test: geometriy, sections and material's properties. . . . .	92
5.10	Stuttgart Shear Test: comparisons between principal tension strains. . . . .	93
5.11	Stuttgart Shear Test: comparisons of load-displacement curves and stresses in the stirrups. . . . .	95
5.12	Stuttgart Shear Test: comparisons between crack patterns. . . . .	96

6.1	Initiation and propagation periods for corrosion in RC structures. . .	102
6.2	Examples of consequences of corrosion of steel in concrete (Bertolini, 2006). . . . .	103
6.3	Typical neighborhoods for 1D and 2D cellular automata. . . . .	106
6.4	Modeling of mechanical damage: (a) time evolution of damage indices during diffusion process; (b) linear relationship between rate of damage and concentration of aggressive agent. . . . .	108
6.5	Modeling of cross section reduction of a steel bar, adapted from (Titi, 2012). . . . .	109
6.6	Corrosion effects on concrete cracking. . . . .	110
6.7	Model. . . . .	111
6.8	Schematic representation of corrosion rate of steel in different concretes and exposure conditions (Camnasio, 2013). . . . .	112
6.9	Cellular automata grid and steel bars sampling points position. . . .	112
6.10	Normalized concentration maps in time. . . . .	113
6.11	Comparisons between different formulations for the dimensionless damage index $\delta_s$ . . . . .	113
6.12	Flow chart of the proposed procedure. The structural models are nested in a loop that deals with damage in the time domain. . . . .	115
7.1	Cable Stayed Harp Bridge: geometry, sections and prestress levels. .	120
7.2	Cable Stayed Harp Bridge: geometry of the sections. . . . .	120
7.3	Cable Stayed Harp Bridge: Axial Force-Bending Moment Resistance Diagrams. . . . .	121
7.4	Histogram of the prestressing forces in the cables. . . . .	122
7.5	Cable Stayed Harp Bridge: deformed configurations until collapse. .	123
7.6	Cable Stayed Harp Bridge: displacements and bending moments in the deck and bending moments in the pylons. . . . .	124
7.7	Corace Bridge (Calabria, Italy), (Franciosi, 1959). . . . .	126
7.8	Geometry of the bridge. . . . .	127
7.9	Corace Bridge: geometry of the sections and reinforcement positions.	128
7.10	Non Linear Analysis: deformed configuration until collapse. . . . .	129
7.11	Corrosion scenarios: longitudinal distribution of the aggressive agent.	131
7.12	Corrosion scenarios: sectional distribution of the aggressive agent. .	132
7.13	Evolution in time of the normalized concentration maps for the arch.	132
7.14	Evolution in time of the normalized concentration maps for the beam.	133
7.15	Damage effects on the section of the beam. . . . .	135
7.16	Damage effects on the section of the arch. . . . .	136
7.17	Axial Force-Bending Moment Resistance Diagrams. . . . .	136
7.18	Corace Bridge: influence line of the vertical displacement in the mid-span of the beam due to a moving load with intensity equal to 30 tons. . . . .	137
7.19	Time evolution of the collapse multiplier. . . . .	138
8.1	Geometry of the beams [mm]. . . . .	145
8.2	Geometry of the sections ET1-ET2. . . . .	146
8.3	ET1-ET2 corrosion scenario: sectional position of the aggressive agent.	146

8.4 Time evolution of the normalized concentration maps for the cross-sections. . . . . 147

8.5 Evolution in time of the stresses for a constant total load equal to  $240 kN$ . . . . . 148

A.1 A generic RC section and his reference system. . . . . 153

A.2 Fibers Approach (Riemann Mid-Point Integration Rule). . . . . 154

A.3 Integration strategies. The section is divided into sub-domains and the integration works sampling in a parent domain by using parametric transformations. The so called fibers approach is a particular case of these integration procedures. . . . . 155

A.4 Transformation between real quadrilateral sub-domain and square parent domain. . . . . 156

A.5 From a quadratic shape to a circular sector: a double transformation. 157

A.6 Gauss-Legendre quadrature, (Abramowitz and Stegun, 1964). . . . . 158

A.7 Gauss-Lobatto quadrature, (Abramowitz and Stegun, 1964). . . . . 158

A.8 RC section and generalized normal stresses. . . . . 162

A.9 Generic 3D Interaction Domain. . . . . 167

A.10 R.C. sections considered for benchmarking. . . . . 168

A.11 Example of sub-domains discretization and sampling points position. 168

A.12 Moment-curvature diagrams for different axial forces. . . . . 169

A.13 Stresses in the concrete at different states ( $N = -240 kN$ ). . . . . 169

A.14 Moment-curvature diagrams for different sectional discretizations. . . 170

A.15 First discretization strategy. Real (black) and approximated (blue) distributions of stresses at the final state of moment-curvature curve. Comparison between the exact resultant of stresses (grey area) and approximate distribution (cyan area). . . . . 171

A.16 Second discretization strategy. Real (black) and approximated (blue) distributions of stresses at the final state of moment-curvature curve. Comparison between the exact resultant of stresses (grey area) and approximate distribution (cyan area). . . . . 172

A.17 Dense discretization. Real (black) and approximated (blue) distributions of stresses at the final state of moment-curvature curve. Comparison between the exact resultant of stresses (grey area) and approximate distribution (cyan area). . . . . 172

A.18 Interaction domain for the square section of Fig. A.10(a). . . . . 173

A.19 Interaction domain for the L shaped section of Fig. A.10(b). . . . . 174

A.20 Interaction domain for the circular hollow section of Fig. A.10(c). . . 175

B.1 Effectiveness factor. . . . . 178

B.2 Rigid perfectly-plastic behavior. . . . . 179

B.3 Limit Interaction Domains. . . . . 179

B.4 Limit analysis: structural geometry, structural mesh and reference system. . . . . 179

B.5 Static field: element with and without rigid body modes. . . . . 180

B.6 Kinematic field: element with and without rigid body modes. . . . . 181

B.7 Yielding criterion. . . . . 182

B.8 Portal frame with two variable concentrate loads. . . . . 186

B.9 Clamped RC arch. Geometry and discretization. . . . . 187

B.10 Clamped RC arch: limit analysis results. . . . . 187

B.11 Clamped RC arch: plastic hinges position in the interaction domains. 188

B.12 Clamped RC arch: comparisons with the solution obtained by (Cera-  
dini and Gavarini, 1965). . . . . 188

B.13 Geometry and loads of the beam-arch system. . . . . 189

B.14 Collaborating beam-arch system: plastic hinge positions. . . . . 189

B.15 Collaborating beam-arch system: limit analysis solution and com-  
parisons (Ronca and Cohn, 1979a).  $\lambda_c = 3.835$ . . . . . 190



# List of Tables

2.1	The two way of using the Virtual Work Principle. . . . .	14
2.2	Comparisons between displaced-based and force-based element state determination. . . . .	24
2.3	Some comparisons between displacement-based (dotted lines) and force-based approach (continuous line). . . . .	31
3.1	Navier-Bernoulli, Timoshenko and Generalized sectional kinematic. . . . .	39
4.1	PV20 Panel: materials characteristics. . . . .	74
4.2	PV23 Panel: materials characteristics. . . . .	76
4.3	PB20 Panel: materials characteristics. . . . .	77
4.4	PW3-2 Cervenka Panel: concrete characteristics. . . . .	77
4.5	PW3-2 Cervenka Panel: reinforcing steel characteristics. . . . .	77
4.6	A1 Bresler & Scordelis Beam: materials characteristics. . . . .	80
7.1	Cable Stayed Harp Bridge: geometrical/mechanical characteristics and prestressing levels. . . . .	121
7.2	Different analysis for the Cable Stayed Bridge. N.L.G. = Non Linear Geometry, N.L.M. = Non Linear Mechanics. . . . .	123
7.3	Cable Stayed Harp Bridge: Non Linear Versus Limit Analysis. . . . .	125
7.4	Corace Bridge: reinforcing steel and material's characteristics. . . . .	127
7.5	Different analysis for the Corace Bridge. N.L.G. = Non Linear Geometry, N.L.M. = Non Linear Mechanics. . . . .	129
7.6	Arch Bridge: Non Linear Versus Limit Analysis. . . . .	130
7.7	Arch corrosion scenario: axial forces, bending moments and collapse mechanisms in time. . . . .	140
7.8	Beam corrosion scenario: axial forces, bending moments and collapse mechanisms in time. . . . .	141
7.9	Arch and Beam corrosion scenario: axial forces, bending moments and collapse mechanisms in time. . . . .	142
8.1	Time evolution of the principal tension strain for ET1 and ET2 beams. . . . .	149
8.2	Time evolution of the maximum stresses in longitudinal bars and stirrups. . . . .	149
A.1	Navier-Bernoulli and Timoshenko sectional kinematics. . . . .	154

A.2 Newton-Cotes Quadrature Rule: sampling points and weight factors. 159  
A.3 Gauss-Legendre Quadrature Rule: sampling points and weight factors.160  
A.4 Gauss-Lobatto Quadrature Rule: sampling points and weight factors.161  
A.5 Material characteristics. . . . . 168  
  
B.1 Limit Analysis Theorem: Input & Output variables. . . . . 185



---

# INTRODUCTION



# 1 | Introduction

*The objectives of the thesis are presented and outlined with the aim of proposing a robust methodology handling the assessment of concrete structures based on time-variant capacity that account for environmental hazards. Focus is given to the main reasons for which a study on sound and damaged reinforced concrete has been carried out.*

## 1.1 MOTIVATION AND PROBLEM STATEMENT

---

The majority of buildings and infrastructures, like bridges, has today reached more than an half of a century of age. In a research carried out for the Lombardia Region (Italy), in which the Author collaborate, the bridges that across the Po River have been inspected. The main result of such a research is that today, a lot of Reinforced Concrete (RC) structures are reaching their ultimate lifetime. Damage scenarios, like corrosion due to chlorides, spalling of the concrete cover, reduction of area of reinforcing, are clearly evident. In some case, a repair intervention is already present, Fig. 1.1.

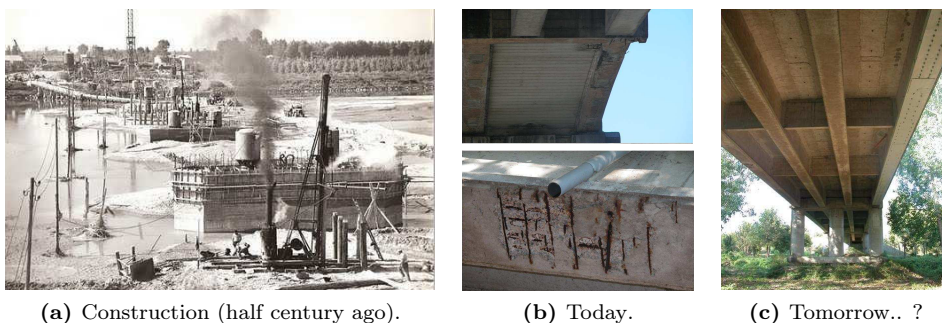


**Figure 1.1:** Life steps of a bridge over the Po River, Italy.

Region ask questions such as: what about the future of these bridges? Are they safe? How much are they safe? And if they are not, what we can do? The answers to these questions are not so simple as the questions are.

The phenomena involved in damage processes are not so clear and, in addition, not so certain due to dependability on aleatory quantities such as the humidity of the air, the chlorides content and so on. Hence, a robust assessment of concrete structures based on time-variant capacity that account for environmental hazards is needed.

The object of the thesis is to propose a methodology that can be applied in engineering practice in order to couple the structural analysis with the damage processes, and able to adequately evaluate the time-evolution of the structural performances.

### 1.1.1 CONCERNING THE STRUCTURAL MODEL

In recent years, structural modeling and nonlinear analysis are very common and the Finite Element Method (FEM) is the mainly used computational tool. Several models dealing with RC structures (Fig. 1.2) can be proposed but, in design or assessment of real frame structures, the use of complex 2D or 3D FE programs can turn to be impracticable, not only for the high computational cost (that in future will certainly decrease), but for the huge amount of generated data from which a difficult results interpretation process descends.

For these reasons, it's clear that between the main characteristics of a model there are not only accuracy, precision and robustness, but also clarity and simplicity.

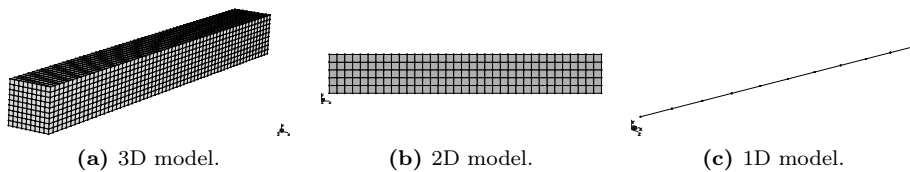


**Figure 1.2:** Comparisons between Finite Element Models.

In this framework, 1D modeling with distributed nonlinearity seems a good compromise. In this models, the generic section of the element is studied by using the so called “fiber approach”, in which the section is subdivide in sub-domains, called fibers. When fiber discretization is combined with a force-based element, the highest degree of accuracy and stability is obtained in a frame structural model at the current state of knowledge.

Usually, this models are based on the Navier-Bernoulli (plane section) kinematic, through which only longitudinal strain is described. As a consequence, only the problem of normal stresses is addressed.

In dealing with RC structures, such a descending restriction is generally considered valid, since the interaction with shear stresses is not so common. In fact, concrete structures design is currently based on the so-called “capacity design”, through which the shear failures must be avoided a priori. This statement can be reasonable acceptable regarding new and *sound* structures, but with respect existing or *damaged* ones it cannot be considered no longer valid.

Three are the main reasons:

1. it's not so certain that an existing structure has been design considering the current shear provisions;
2. also admitting that a proper capacity design has been performed, if the structures is interested by environmental hazards, its structural performances can varying in time and a change of the failure mode, not considered in the initial design process, can occur;
3. concerning repair interventions, if a strengthened in bending is performed, bending load capacity increase. This can produce, once again, a switch between the failure mechanisms and the structure can became critical with respect to shear.

Hence, classical beam column elements based on Navier-Bernoulli sectional kinematic are not enough, but specific improvements of the beam structural theory must be considered. This leads to formulate new 1D models with distributed non-linearity that can adequately address not only the problem of normal forces, but also the one of shear force. This is not an easy task and, despite severals Authors have already deal with such a problem, the research is actually open.

### 1.1.2 CONCERNING THE DAMAGE MODEL

Corrosion is a complex phenomenon, involving different mechanisms and depending on many parameters. In literature different studies can be found, in order to understand the fundamental factors. Both experimental tests and numerical simulations has been carried out, with the purpose to investigate the effects on a local and a global level, and also to develop analytical models. Among different aggressive agents, the presence of chlorides plays a fundamental role in damage processes of RC structures. For this reason, in this thesis, despite the proposed approach is general and effectively applicable to other phenomena, the attention is concentrated on *chlorides induced corrosion*.

Since corrosion depends on many parameters, such as the relative humidity, the temperature and the internal stress field, a damage model should considering both the thermal effects and the material constitutive laws in a full coupled physical-mechanical process. However, the so-obtained models are at first too complex, but secondly they need a wide calibration process that seems too far from the nature of the problem that, in addition, is not so certain.

For these reasons, in lifetime structural assessment, it seems more convenient the adoption of a *macroscopic* approach that neglect all the above mentioned interaction process but that, for his simplicity, can be easily extended in the non deterministic field.

In this work, it is hence assumed that Fick's law holds and, in order to consider different geometric domains or different positions of steel bars or different attack scenarios, a special evolutionary computation technique is used in order to solve the diffusion process: the *cellular automata*.

## 1.2 SCOPE AND OBJECTIVES

The thesis is focused on plane RC structures. The general objective is to *couple* the structural behavior with the damage process in order to obtain a framework that permits to perform lifetime predictions. All the phenomena that characterize the mechanical behavior are dealt with. The thesis is identified by two big parts:

- (1) focused on the study of sound RC structures. From bidimensional modeling, the objective is to move towards monodimensional modeling by including shear's effects;
- (2) focused on the study of the damage processes interesting RC structures exposed to environmental hazard.

### PART 1 & PART 2 = LIFETIME PREDICTIONS OF RC STRUCTURES

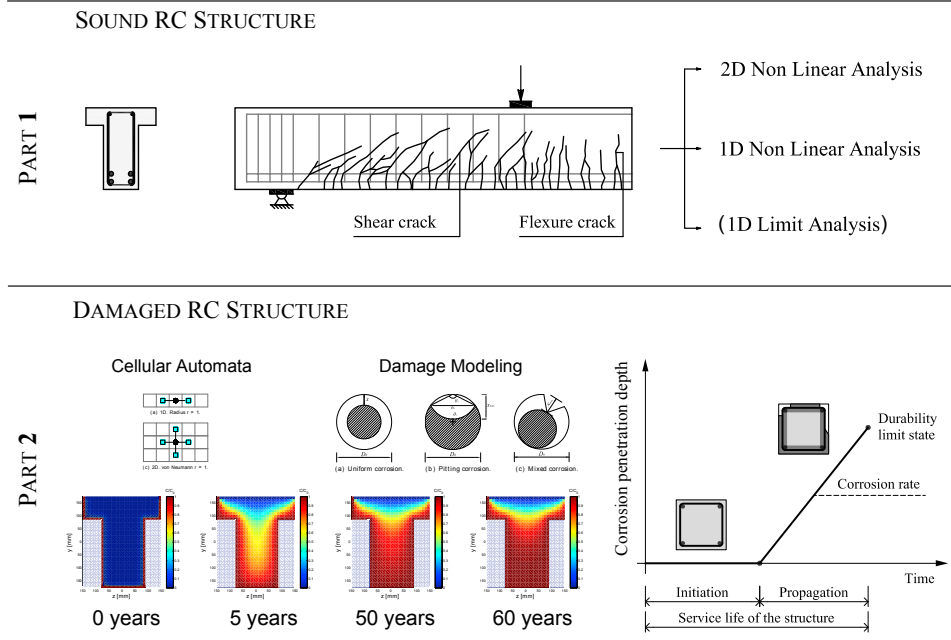


**Figure 1.3:** Scope of the thesis. The proposed procedure is the combination of two independent parts.

This two parts are initially completely independent. In particular, the first addresses the structural modeling, the second the damage modeling. However, if Part 1 is used as sub-module of Part 2, structural behavior results coupled with damage process and lifetime prediction can be performed.

In detailing, with the aim of proposing an efficient computational tools, the attention is focused on monodimensional modeling. Concerning the constitutive relationship adopted for reinforced concrete, two different smeared type models have been considered and compared.

It is well known that a structural theory, with respect to the full 2D problem, contains some intrinsic approximations. For this reason and also aiming to better understand the complex shear interaction mechanism, at first, a 2D FE modeling is considered. Such a computational technique deals with the definition of a triangular RC finite element. It has been proved that a bidimensional modeling of RC structures with smeared approaches can be considered effectively a robust technique that gives very accurate results.

Then, the computational tool is moved *towards monodimensional modeling*. In particular, a beam element with two types of sectional strategies is proposed, implemented and validated not only with respect to literature results, but also with the previous 2D numerical technique.

Finally, a general and versatile method handling the damage process and their effects on RC structural performance is proposed. The approach deals with chloride attacks and handles the problem regarding sections with arbitrary shape, with arbitrary position of reinforcements and with arbitrary corrosion scenarios. All the principal effects of chlorides-induced corrosion are considered:

1. reduction of the cross-section of reinforcing bars;
2. reduction of ductility of reinforcing steel;
3. reduction of concrete strength;
4. spalling of the concrete cover.

In developing applications concerning damage effects on structural performance, some interesting concepts that must be clearly taken into account in the design of refurbishment interventions have been obtained. Such applications are dealt with non linear analysis but these concepts have been better outlined by using another procedure considered in this thesis: the Limit Analysis. In this case, only axial force and bending moment interaction is taken into account and linear programming methods are used. Such a computational technique, despite its limitation in dealing with RC problems, is the most synthetic between all the others considered. It would be hence very useful to try to extend Limit Analysis with shear-bending-axial forces interaction.

### 1.3 RESEARCH SIGNIFICANCE

---

This thesis proposes a methodology dealing with the lifetime assessment of RC structures exposed to environmental hazard.

A very general computational technique concerning damage modeling is presented. Such an approach is based on the Cellular Automata algorithm and treats RC arbitrary shaped sections, with arbitrary reinforcements layouts. New damage indexes, that account for the phenomena previously exposed, are proposed and compared. The so-obtained model, consisting in a loop over the time domain, is able to predict the mechanical degradation of a generic RC domain.

Due to his generality, several structural models can be nested in it in order to perform lifetime predictions. The main aim of this work is to consider the possibilities of shear-flexible beam column elements in the study of RC framed structures. In order to reach such a result, two renown RC membrane theories are at first reviewed, developed and coded in a bidimensional finite element based program. Wide comparisons with reference to shear critical panels and beams are carried out. Then, by proposing two particular section state determinations, the structural analysis is moved from bidimensional towards monodimensional modeling and the formulation of the finite beam element with distributed nonlinearity is exposed. An additional structural analysis technique, based on limit analysis, is considered in order to outline specific comments related on the so-called effectiveness factor.

The proposed structural models are nested as sub-modules in the damage model and several case studied permits to point out as the proposed methodology is able not only to evaluate the structural behavior when the structure is sound, but also in time, when the structures progressively became damaged.

All the numerical procedures proposed in this thesis have been coded in specific computer programs written in MatLab<sup>(1)</sup>, by using some basic techniques from object oriented programming philosophy. The so-obtained codes interacts with other structural objects and future improvements are easily permitted. The architecture of the complete program strictly corresponds to the union of the two parts in which this thesis is subdivide. In particular, there is a global procedure that handle the damage processes and the time evolution of the structural performances and, nested in it, there are the structural models, based on: (a) 2D non linear analysis, (b) 1D non linear analysis without considering shear's effects, (c) 1D non linear analysis with the shear-flexible beam column element and (d) limit analysis for axial force - bending moment interaction.

Between the several future developments of the work, due to the object oriented programming philosophy adopted, a stand-alone application can be compiled or easily translated to a more efficient language.

## 1.4 CONTENTS OF THIS DOCUMENT

---

The thesis is composed in these sections:

1. Part I - Sound RC Structures - concerns the methods of structural analysis suitable to deal with non-linear behavior of RC structures. The main aim of this part is to propose a shear sensitive beam element. In particular:
  - Chapter 2 reviews the basic characteristics of non-linear beam elements formulation. By applying the Principle of Virtual Work, the longitudinal formulation of the problem is dealt both with a displacement based element and with a force based element (dual approach). The formulation is general applicable, with no matter about the non linear material that compose the element;

---

<sup>(1)</sup>Matlab is a registered trademark of The MathWorks Inc., 24 Prime Park Way, Natick, MA 01760-1500, U.S.A. Web: <http://www.mathworks.com>.



- Chapter 3 outlines the problem with respect RC structures. It shows that the normal forces problem can be successfully solved with classical beam-column elements, by adopting Navier-Bernoulli sectional kinematic, but the problem of shear stresses is more complex and not straightforward. With this aim, the State of the Art of RC sectional models is recalled and the principal models are exposed and compared;
  - due to the necessity of a bi-dimensional stress-strain relationships, in Chapter 4 two known and widely used Theories are examined: the Modified Compression Field Theory (MCFT) and the Disturbed Stress Field Theory (DSFT). Both Theories are discussed and tested with an original code and with reference to panels and beams having shear critical behaviors. Results and methods are compared and widely discussed in order to choose the most effective for the formulation of a shear sensitive beam element;
  - in Chapter 5, the finite element beam suitable to deal with the shear effects is then proposed and developed both with a fixed strain approach and a fixed stress approach. The difference between these two approaches depends on the type of the additional condition to be imposed in order to make the problem determinate. The element formulation is accomplished with proposal that allows to compute the stresses in the stirrups and of a proposal of conventional representation of the crack pattern in the web of the beam;
2. Part II - Damaged RC Structures - presents the damage process and its modeling through a diffusivity equation. The problem is solved through the Cellular Automata algorithm. Introductory examples show the effectiveness of such a numerical approach. The effects of the damage are then specialized to RC elements. New damage indexes, concerning both steel and concrete, are introduced and then tested for different reinforcement layouts. For its generality, the so-obtained damage models can be jointed with each structural analysis procedure. The final flow chart of the methodology proposed in the thesis is hence a loop in the time domain that deals with damage process and the structural models proposed in Part I are nested in it;
3. Part III - Applications - composed of two Chapters:
- Chapter 7 studies cable stayed and arch bridges and presents a coherent set of applications involving one or more of the aforementioned problems. In particular, significant comparisons are made between non-linear analyses and limit analyses results, that led to introduce an efficiency factor that takes into account the different nature of these two approaches, as well as the different criteria to model the material properties with respect to the ultimate behavior;
  - Chapter 8 deals with the effects of damage on shear resisting mechanisms. Once again, the FE models exposed in part I have been coupled with the damage models detailed in part II, and lifetime predictions have

been performed. The main conclusion of these investigations is that the effects of damage can produce a variation in the failure modes;

4. Part [IV](#) - Other Items suggested & Further Improvements - contains two appendices, collecting notes, comments and deepening emerged in developing the theoretical formulations and in setting up the numerical algorithms. In particular:
  - [Appendix A](#) contains a set of notes on the so-called fiber method and outlines some hidden aspects associated to the numerical integration of section properties;
  - [Appendix B](#) recalls the limit analysis theory. A set of basic as well as actual applications put in evidence the powerful and also the care to be adopted in using this type of analysis.

Finally, the main conclusions and the future developments are given.

# I

---

## SOUND RC STRUCTURES



# 2

## A Review of the Non Linear Beam Problem

*This chapter presents the nonlinear beam problem. Since the sectional state is a sub-module of the beam formulation, only the longitudinal problem is presented by considering two dual approaches: a displacement-based and a force-based (or mixed) one. By using standard finite element techniques, the two approaches are discussed and compared.*

### 2.1 INTRODUCTION

---

Beam-column finite elements are commonly derived with the displacement method of analysis, but recent studies have highlighted the benefits of frame models that are based on force interpolation functions. These benefits derive from the fact that models with force interpolation functions, that reproduce the variation of internal element forces in a strict sense, yield the exact solution of the governing equations in the absence of geometric nonlinearity (Neuenhofer and Filippou, 1997).

The structural theory of the beam requires, at first, the definition of sectional kinematics. Here there are many proposals, for instance the Navier-Bernoulli's theory, the Timoshenko's theory, the Reddy's third order theory, in which the complexity of the sectional kinematics progressively grows. Today many research proposals, focused on the aim of enhance the beam theory are available. Between them, the most elegant approach is the so-called *Generalized Beam Theory*, in which the sectional kinematic presents a very high level of generality.

Once a proper choice of the sectional kinematic is done, the beam formulation can be based on the application of the Virtual Work Principle or on the Hu-Washizu Variational Theorem (Taylor *et al.*, 2003).

For these reasons, and also for the sake of clarity, the attention is given to the dual formulations used in the developing of finite beam element models and the section will be presented in the next chapter. Here, it must be viewed as a module able to solve two types of problems:

- Type 1 Problem (direct):  
given a strain state (the sectional strains)  $\mathbf{e}_s$ , determine the stress state (the

Static Field (1): $\sigma, \mathbf{f}_s, \mathbf{Q}$	Kinematic Field (2): $\varepsilon, \mathbf{e}_s, \mathbf{q}$
<b>VIRTUAL DISPLACEMENT PRINCIPLE</b> (1) Real Static Field (2) Real Kinematic Field Variation $\Rightarrow$ EQUILIBRIUM	<b>VIRTUAL FORCE PRINCIPLE</b> (1) Real Static Field Variation (2) Real Kinematic Field $\Rightarrow$ COMPATIBILITY

**Table 2.1:** The two way of using the Virtual Work Principle.

resultant, or restoring, or resisting section forces)  $\mathbf{f}_{s,r}$ :

$$\mathbf{e}_s \rightarrow \mathbf{f}_{s,r} \quad (2.1)$$

- Type 2 Problem (indirect):

given a stress state  $\mathbf{f}_{s,e}$ , determine the sectional strain state  $\mathbf{e}_s$ :

$$\mathbf{f}_s \rightarrow \mathbf{e}_s \quad (2.2)$$

As it will be shown in the next, in a displacement-based approach the section is used in a direct way (type 1 problem); in a force-based approach, instead, the section is used in an indirect way (type 2 problem), but some simplifications has been proposed in order to avoid that.

## 2.2 THE VIRTUAL WORK PRINCIPLE

The Virtual Work Principle sets the equilibrium conditions of a deformable solid. It states that:

$$W_e = W_i \quad (2.3)$$

where  $W_e$  is the external work and  $W_i$  is the internal work. The work is done by the static quantities of an equilibrated field (1) and the kinematics quantities of a compatible field (2). Any choice about fields (1) and (2) can be done. If we chose as static field the real one and as kinematic field a virtual variation of the real field, the Virtual Displacement Principle is obtained; if we chose as static field a virtual variation of the real one and as kinematic field the real field, we find the Virtual Force Principle. The first imposes equilibrium, the second compatibility, as reported in the Tab. 2.1.

In formulating beam finite elements, both the approaches can be used. If we apply the Principle of Virtual Displacements (PVD) we have to compute the internal

work produced by a variation of the real kinematic field with the real static field, by assigning the nodal displacements  $\mathbf{q}$ . In general, we don't know the kinematic quantities in a generic section of the element as a function of  $\mathbf{q}$ . However, we can interpolate them by using specific shape functions that can be ordered in a matrix called  $\mathbf{B}(x)$ . The element formulated in this way is a *displacement-based element* and it will be discussed in par. 2.3.

If we apply the Principle of Virtual Forces (PVF), we have to compute the internal work produced by a variation of the real static field with the real kinematic field, by assigning the nodal forces  $\mathbf{Q}$ . Similar to before, in order to compute the internal work we have to know the static quantities in a generic section of the element as a function of  $\mathbf{Q}$ . Now, however, this can be done in very simple way: by using equilibrium statements. The result is that we can find exact shape functions  $\mathbf{b}(x)$  and the consequence is that, now, intrinsic approximations are not present. The element formulated in this way is a *force-based element* and it will be discussed in par. 2.4.

It is important to observe that by working with the PVF two major obstacles arise. First, global equilibrium equations through a structural flexibility matrix cannot be easily automated. In addition, only if we deal with a structural theory is straightforward to find directly matrix  $\mathbf{b}$ , but in general it is easier to postulate the kinematic field than the static one (let's think to a brick element with non linear behavior for instance). For these reasons, the global equilibrium equations are derived with the direct stiffness method, which allows the direct superposition of individual element contributions to yield the structure stiffness and resisting forces.

Second, the section constitutive relation is commonly given in the form  $\sigma = \sigma(\varepsilon)$ , but is seldom available in the inverse form  $\varepsilon = \varepsilon(\sigma)$ , which is necessary for a pure flexibility-based approach (Neuenhofer and Filippou, 1997).

In concluding, a flexibility based element presents several advantages with respect a displacement based element, but the major obstacle of the flexibility formulation is its numerical implementation in a standard finite element analysis program that imposes kinematic, rather than static, boundary conditions at the element ends (Spacone *et al.*, 1995). These aspects produce an *Element State Determination* process that is more complex with respect displacement based elements. The input are nodal displacements, and the output are nodal forces and element stiffness matrix. However, a flexibility based element does not interpolate the nodal displacements (known terms), but the nodal forces (unknown terms). There is the so-called *lack-of-fit* and additional calculations are needed.

In order to define the State of the Element for a standard finite element analysis program, that imposes kinematic boundary conditions at the element ends, we have to find the nodal forces  $\mathbf{Q}$  associated to the nodal displacements  $\mathbf{q}$ . These quantities, for a plane element, are (see Tab. 2.1):

$$\mathbf{q} = [q_1 \quad q_2 \quad q_3 \quad q_4 \quad q_5 \quad q_6]^T \quad (2.4)$$

$$\mathbf{Q} = [Q_1 \quad Q_2 \quad Q_3 \quad Q_4 \quad Q_5 \quad Q_6]^T \quad (2.5)$$

### 2.3 DISPLACEMENT BASED ELEMENT (STIFFNESS APPROACH)

In the stiffness method the displacement field of the element is discretized and interpolated in terms of generalized displacement degrees of freedom  $\mathbf{q}$  such that:

$$\mathbf{u}(x) = \begin{bmatrix} u_0(x) \\ v_0(x) \end{bmatrix} = \mathbf{N}(x)\mathbf{q} \quad (2.6)$$

Conventional frame elements are based on cubic Hermitian polynomials for the transverse displacement fields and linear Lagrangian shape functions for the axial displacement, as reported in Fig. 2.1.

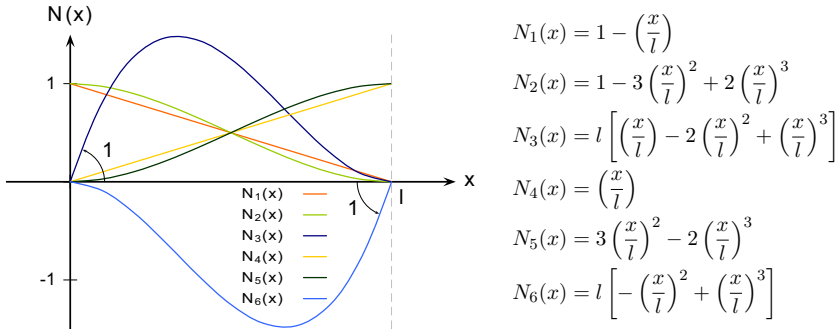


**Figure 2.1:** Shape functions for a conventional frame element.

The expression for the deformation fields is then:

$$\mathbf{e}_s(x) = \begin{bmatrix} \varepsilon_0 \\ \chi \end{bmatrix} = \begin{bmatrix} N_{1,x} & 0 & 0 & N_{4,x} & 0 & 0 \\ 0 & N_{2,xx} & N_{3,xx} & 0 & N_{5,xx} & N_{6,xx} \end{bmatrix} \mathbf{q} = \mathbf{B}(x)\mathbf{q} \quad (2.7)$$

According to the Principle of Virtual Displacements, the internal work is:

$$\begin{aligned} \delta W_i &= \int_0^l \delta \mathbf{e}_s^T(x) \cdot \mathbf{f}_s(x) dx = \\ &= \int_0^l \delta \mathbf{q}^T \mathbf{B}^T(x) \cdot \mathbf{f}_s(x) dx \\ &= \delta \mathbf{q}^T \int_0^l \mathbf{B}^T(x) \cdot \mathbf{f}_s(x) dx \\ &= \delta \mathbf{q}^T \mathbf{Q} \end{aligned} \quad (2.8)$$

in which we can recognize the element resisting forces  $\mathbf{Q}$ :

$$\mathbf{Q} = \int_0^l \mathbf{B}^T(x) \mathbf{f}_s(x) dx \quad (2.9)$$

In order to solve the non linear problem, a tangent approach is used. The Jacobian matrix involved in the iterations is equal to the tangent stiffness matrix



$\mathbf{k}$  of the element and it is defined by:

$$\mathbf{k} = \int_0^l \mathbf{B}^T(x) \mathbf{k}_s(x) \mathbf{B}(x) dx \quad (2.10)$$

in which  $\mathbf{k}_s(x)$  is the tangent stiffness matrix of the section at the abscissa  $x$  of the element.

### 2.3.1 ELEMENT STATE DETERMINATION

Given the nodal displacements  $\mathbf{q}$ , the element state determination process (finding nodal forces and stiffness matrix) for a displacement based element can be done through the following steps:

1. for each section, in direct form (type 1 sectional problem):
  - calculate the section deformations  $\mathbf{e}_s$  by using eq. (2.7);
  - calculate the section forces  $\mathbf{f}_s$  as the integral over the section domain of the stresses produced by  $\mathbf{e}_s$ ;
  - calculate the section stiffness matrix  $\mathbf{k}_s$ ;
2. weighting the section states to obtain the state of the element:
  - resisting forces  $\mathbf{Q}$  by using eq. (2.9);
  - element stiffness matrix  $\mathbf{k}$  by using eq. (2.10).

As shown, the Element State Determination process is direct and straightforward.

---

## 2.4 FORCE BASED ELEMENT (FLEXIBILITY APPROACH)

In a force-based element the static field is defined by using equilibrium. Then, the application of the Virtual Force Principle gives compatibility equations. For the previous exposed reasons, global equilibrium equations are, once again, derived with the direct stiffness method. However, a force-based element do not interpolate the nodal displacements (known terms), but the nodal forces (unknown terms). There is the so-called *lack-of-fit* that produces an element state determination more complex with respect the displacement-based element. The scope of that procedure is to determine, by using a flexibility approach, the nodal forces and the element stiffness matrix in order to write global equilibrium equations. It is not a pure flexibility approach, but a *mixed approach* as reported in (Taylor *et al.*, 2003). In order to do that, the definition of two reference systems is required.

### 2.4.1 REFERENCE SYSTEMS: WITH AND WITHOUT RIGID BODY MODES

In the following, the quantities referred to the system without rigid body modes are conventionally over-lined.

## 2.4.1.1 STATIC FIELD

Let's considered the element reported in Fig. 2.2. Since the element is free in the space, this system is indicated as element "with rigid body modes". The nodal forces  $\mathbf{Q}$  act in nodes  $n_1$  and  $n_2$ .

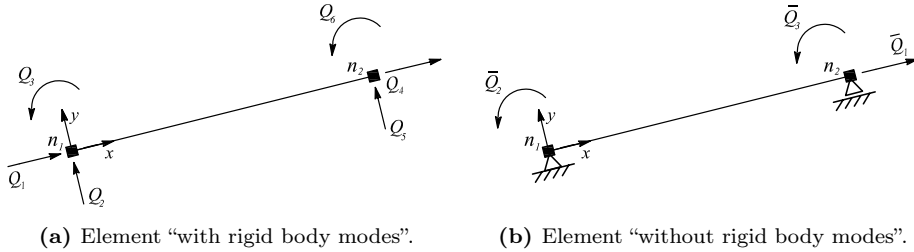


**Figure 2.2:** Static field: element with and without rigid body modes.

By writing equilibrium, a system of three equations in six unknowns can be obtained:

$$\begin{aligned} Q_1 + Q_4 &= 0 \\ Q_2 + Q_5 &= 0 \\ Q_3 + Q_6 + Q_5 \cdot l &= 0 \end{aligned} \quad (2.11)$$

In other words, between six nodal forces only three of them are independent: we call it *basic forces*  $\bar{\mathbf{Q}}$ . They act on a system that can be viewed as the element "without rigid body modes", Fig. 2.2b. By choosing as basic forces the force in the second node  $Q_4$  and the two nodal moments  $Q_3$  and  $Q_6$ , we define:

$$\bar{Q}_1 = Q_4 \quad \bar{Q}_2 = Q_3 \quad \bar{Q}_3 = Q_6 \quad (2.12)$$

and

$$\bar{\mathbf{Q}} = [\bar{Q}_1 \quad \bar{Q}_2 \quad \bar{Q}_3] \quad (2.13)$$

The relation between the nodal forces  $\mathbf{Q}$  and the basic forces  $\bar{\mathbf{Q}}$  can be obtained by using equilibrium. In matrix form we have:

$$\begin{aligned} \begin{bmatrix} Q_1 \\ Q_2 \\ Q_3 \\ Q_4 \\ Q_5 \\ Q_6 \end{bmatrix} &= \begin{bmatrix} -1 & 0 & 0 \\ 0 & 1/l & 1/l \\ 0 & 1 & 0 \\ 1 & 0 & 0 \\ 0 & -1/l & -1/l \\ 0 & 0 & 1 \end{bmatrix} \begin{bmatrix} \bar{Q}_1 \\ \bar{Q}_2 \\ \bar{Q}_3 \end{bmatrix} \\ \mathbf{Q} &= \mathbf{h}_l^T \bar{\mathbf{Q}} \end{aligned} \quad (2.14)$$

where  $l$  is the length of the element.

2.4.1.2 KINEMATIC FIELD

Similar to the static field, we can define two types of nodal displacements (Fig. 2.3): the ones that act on the element “with rigid body modes”, marked with  $\mathbf{q}$ , and the ones that act on the element “without rigid body modes”, marked with  $\bar{\mathbf{q}}$ .

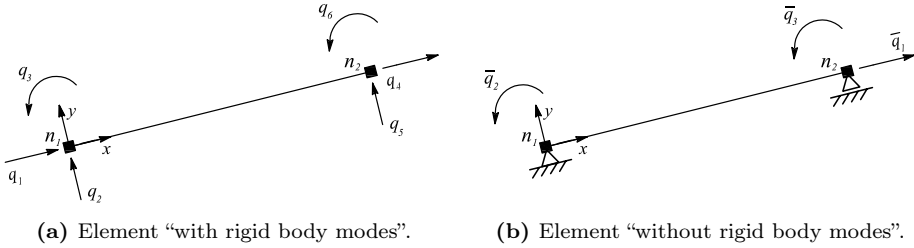


Figure 2.3: Kinematic field: element with and without rigid body modes.

The relation between the two can be obtained by using the Virtual Work Principle. The following condition holds:

$$\begin{bmatrix} \bar{q}_1 \\ \bar{q}_2 \\ \bar{q}_3 \end{bmatrix} = \begin{bmatrix} -1 & 0 & 0 & 1 & 0 & 0 \\ 0 & 1/l & 1 & 0 & -1/l & 0 \\ 0 & 1/l & 0 & 0 & -1/l & 1 \end{bmatrix} \begin{bmatrix} q_1 \\ q_2 \\ q_3 \\ q_4 \\ q_5 \\ q_6 \end{bmatrix} \quad (2.15)$$

$$\bar{\mathbf{q}} = \mathbf{h}_l \mathbf{q}$$

in which we can observe that the transformation matrix is the transpose of the one relative to the static field (see eq. (2.14)).

2.4.1.3 ADDITIONAL CONSIDERATIONS

Let’s suppose that we know the nodal forces  $\mathbf{Q}$  and we want to find, by using a flexibility approach, the element stiffness matrix  $\mathbf{k}$ . We can do that by inverting the element flexibility matrix. It’s clear that the flexibility matrix in the system with rigid body modes is rank deficient (3 times in plane) and so that development can not be performed. However, we can at first work in the reference system without rigid body modes (in which matrices have full rank), and then we can move the information in the reference system with rigid body modes. The following passages are required:

1. by working in the element without rigid body modes, we can find the static quantities  $\mathbf{f}_s(x)$  in a generic section by using the static shape functions matrix

$\mathbf{b}(x)$ :

$$\begin{bmatrix} N \\ M \end{bmatrix} = \begin{bmatrix} 1 & 0 & 0 \\ 0 & (x/l - 1) & x/l \end{bmatrix} \begin{bmatrix} \bar{Q}_1 \\ \bar{Q}_2 \\ \bar{Q}_3 \end{bmatrix} \quad (2.16)$$

$$\mathbf{f}_s(x) = \mathbf{b}(x) \bar{\mathbf{Q}}$$

2. eq. (2.16) gives the section forces. By using the section in *indirect way* (type 2 problem), we can find the sectional deformations  $\mathbf{e}_s(x)$ :

$$\mathbf{e}_s(x) = (\mathbf{k}_s)^{-1} \mathbf{f}_s(x) = \phi_s \mathbf{f}_s(x) \quad (2.17)$$

where  $\mathbf{k}_s$  is the section stiffness matrix and  $\phi_s$  is the section flexibility matrix;

3. according to the Principle of Virtual Forces the internal work is:

$$\begin{aligned} \delta W_i &= \int_0^l \delta \mathbf{f}_s^T(x) \cdot \mathbf{e}_s(x) dx = \\ &= \int_0^l \delta \mathbf{Q}^T \mathbf{b}^T(x) \cdot \mathbf{e}_s(x) dx \\ &= \delta \mathbf{Q}^T \int_0^l \mathbf{b}^T(x) \cdot \mathbf{e}_s(x) dx \\ &= \delta \mathbf{Q}^T \bar{\mathbf{q}} \end{aligned} \quad (2.18)$$

in which we can recognize the element nodal displacements  $\bar{\mathbf{q}}$ , associate to the nodal forces  $\bar{\mathbf{Q}}$ , as the integral of section deformations  $\mathbf{e}_s(x)$  (produced by section forces  $\mathbf{f}_s(x)$ , interpolated from  $\mathbf{Q}$  in an exact way):

$$\bar{\mathbf{q}} = \int_0^l \mathbf{b}(x)^T \mathbf{e}_s(x) dx \quad (2.19)$$

whose derivatives gives the flexibility matrix  $\bar{\Phi}$ :

$$\bar{\Phi} = \int_0^l \mathbf{b}(x)^T \phi_s \mathbf{b}(x) dx \quad (2.20)$$

4. flexibility matrix defined in eq. (2.20) is referred to the system without rigid body modes. For that reason, matrix  $\bar{\Phi}$  has full rank and it can be inverted in order to obtain the stiffness matrix  $\bar{\mathbf{k}}$ :

$$\bar{\mathbf{k}} = (\bar{\Phi})^{-1} \quad (2.21)$$

5. matrix  $\bar{\mathbf{k}}$  is the operator that gives:

$$\bar{\mathbf{k}} \bar{\mathbf{q}} = \bar{\mathbf{Q}} \quad (2.22)$$

What we need, however, is the stiffness matrix referred to the system with rigid body modes  $\mathbf{k}$ , so that:

$$\mathbf{k} \mathbf{q} = \mathbf{Q} \quad (2.23)$$

We can define that matrix through the following developments:

(a) we introduce in (2.22) the expression given by eq. (2.15):

$$\bar{\mathbf{k}} \mathbf{h}_l \mathbf{q} = \bar{\mathbf{Q}} \quad (2.24)$$

(b) we pre-multiply by  $\mathbf{h}_l^T$ :

$$\mathbf{h}_l^T \bar{\mathbf{k}} \mathbf{h}_l \mathbf{q} = \mathbf{h}_l^T \bar{\mathbf{Q}} \quad (2.25)$$

(c) for the right term, by remembering eq. (2.14), we can write:

$$(\mathbf{h}_l^T \bar{\mathbf{k}} \mathbf{h}_l) \mathbf{q} = \mathbf{Q} \quad (2.26)$$

(d) and we have find the definition of matrix  $\mathbf{k}$ :

$$\mathbf{k} = \mathbf{h}_l^T \bar{\mathbf{k}} \mathbf{h}_l \quad (2.27)$$

#### 2.4.1.4 SUMMARY OF THE MAIN TRANSFORMATIONS

$$\begin{aligned} \mathbf{Q} &= \mathbf{h}_l^T \bar{\mathbf{Q}} \\ \bar{\mathbf{q}} &= \mathbf{h}_l \mathbf{q} \\ \mathbf{k} &= \mathbf{h}_l^T \bar{\mathbf{k}} \mathbf{h}_l \end{aligned}$$

Once the transformations between the two reference systems are defined, the element state determination algorithm can be explained.

#### 2.4.2 ELEMENT STATE DETERMINATION

Since we use a mixed method, the input and output quantities of the element state determination are the same exposed in par. 2.3.1. In input we have nodal displacements  $\mathbf{q}$ , in output we have element resisting forces  $\mathbf{Q}$  and element stiffness matrix  $\mathbf{k}$ .

It's clear that we can't directly use the procedure exposed in par. 2.4.1.3 since we don't know  $\mathbf{Q}$ . This fact is know as *lack-of-fit* and it produces a non linear system of equations at the element level. The problem can be solved through the following steps:

1. given the nodal displacement in the element with rigid body modes  $\mathbf{q}$ , calculate the displacements in the system without rigid body modes:

$$\bar{\mathbf{q}} = \mathbf{h}_l \mathbf{q} \quad (2.28)$$

2. determine  $\bar{\mathbf{Q}}$  so that:  $\bar{\mathbf{q}}_r = \bar{\mathbf{q}}$  with:

$$\bar{\mathbf{q}}_r = \int_0^l \mathbf{b}(x)^T \mathbf{e}_s(x) dx \quad (2.29)$$

Such a condition is written in homogeneous form as follows:

$$\mathbf{g}(\bar{\mathbf{Q}}) = \bar{\mathbf{q}} - \bar{\mathbf{q}}_r = \mathbf{0} \quad (2.30)$$

and solved by Newton-Raphson (NR) method. The main steps of the NR solution are:

- (a) choice of an initial solution  $\bar{\mathbf{Q}}_0$ ;  
 (b) linearization of the problem as follows:

$$\mathbf{g}(\bar{\mathbf{Q}}) \cong \mathbf{g}(\bar{\mathbf{Q}}_0) + \mathbf{J}(\bar{\mathbf{Q}}_0) \cdot (\bar{\mathbf{Q}} - \bar{\mathbf{Q}}_0) = \mathbf{0} \quad (2.31)$$

where  $\mathbf{J}(\bar{\mathbf{Q}}_0)$  is the Jacobian matrix evaluated in  $\bar{\mathbf{Q}}_0$ ;

- (c) search for a new solution, by solving Eq. (2.31):

$$\bar{\mathbf{Q}}_1 = \bar{\mathbf{Q}}_0 - [\mathbf{J}(\bar{\mathbf{Q}}_0)]^{-1} \cdot \mathbf{g}(\bar{\mathbf{Q}}_0) \quad (2.32)$$

- (d) iteration until convergence.

In a more explicit form, the Jacobian matrix is:

$$\begin{aligned} \mathbf{J}(\bar{\mathbf{Q}}) &= \frac{\partial \mathbf{g}(\bar{\mathbf{Q}})}{\partial \bar{\mathbf{Q}}} = \frac{\partial}{\partial \bar{\mathbf{Q}}} (\bar{\mathbf{q}} - \bar{\mathbf{q}}_r(\bar{\mathbf{Q}})) = -\frac{\partial}{\partial \bar{\mathbf{Q}}} (\bar{\mathbf{q}}_r(\bar{\mathbf{Q}})) \\ &= -\frac{\partial}{\partial \bar{\mathbf{Q}}} \left( \int_0^l \mathbf{b}(x)^T \mathbf{e}_s(x) dx \right) = -\int_0^l \mathbf{b}(x)^T \frac{\partial}{\partial \bar{\mathbf{Q}}} (\mathbf{e}_s(x)) dx \\ &= -\int_0^l \mathbf{b}(x)^T \frac{\partial}{\partial \bar{\mathbf{Q}}} (\phi_s(x) \mathbf{f}_s(x, \bar{\mathbf{Q}})) dx = \\ &= -\int_0^l \mathbf{b}(x)^T \phi_s(x) \frac{\partial}{\partial \bar{\mathbf{Q}}} (\mathbf{b}(x) \bar{\mathbf{Q}}) dx = \\ &= -\int_0^l \mathbf{b}(x)^T \phi_s(x) \mathbf{b}(x) dx = \\ &= -\bar{\Phi} \end{aligned} \quad (2.33)$$

which shows how  $\mathbf{J}(\bar{\mathbf{Q}})$  equals the element flexibility matrix  $\bar{\Phi}$  (in the system without rigid body modes).

The recursive equation of the NR solution results:

$$\begin{aligned} \bar{\mathbf{Q}}_{i+1} &= \bar{\mathbf{Q}}_i + [\bar{\Phi}_i]^{-1} \cdot \mathbf{g}(\bar{\mathbf{Q}}_i) = \\ &= \bar{\mathbf{Q}}_i + \Delta \bar{\mathbf{Q}}_i \end{aligned} \quad (2.34)$$

and will be iterated until convergence.

At each element iteration, we have to compute the residual deformations:

$$\mathbf{g}(\bar{\mathbf{Q}}_i) = \bar{\mathbf{q}} - \bar{\mathbf{q}}_{r,i} \quad (2.35)$$

The restoring displacements are computed by using eq. (2.29) as integral of section deformations. In order to do that, the generic section of the element is used in an indirect way as highlighted by eq. (2.2): for each section, hence, a non linear system of equations must be solved.

- once convergence is achieved, we move to the system with rigid body modes in order to calculate:

- the element resisting forces:

$$\mathbf{Q} = \mathbf{h}_l^T \bar{\mathbf{Q}} \quad (2.36)$$

- the element stiffness matrix:

$$\mathbf{k} = \mathbf{h}_l^T [\bar{\Phi}_i]^{-1} \mathbf{h}_l = \mathbf{h}_l^T \bar{\mathbf{k}} \mathbf{h}_l \quad (2.37)$$

and the Element State Determination process is completed.

In conclusion, the Element State Determination is a non linear system of equations at the element level, due to a lack-of-fit between the force based element and the global displacement based approach. The non linear solution strategy here exposed is the classical Newton-Raphson approach (NR). Then, at the sectional level, since we have to compute deformations from interpolated forces, another system of non linear equations (NR) is present. This holds for each sectional iteration (*loop k*), for each element iteration (*loop j*), for each structural iteration (*loop i*) (see Fig. 2.4).

The procedure here exposed is not the unique way to handle the lack-of-fit problem, in fact there are several procedures that can be used as exposed in the next.

### 2.4.3 DIFFERENT TYPES OF STATE DETERMINATION ALGORITHMS AND ADDITIONAL COMMENTS

In (Nukala and White, 2004) four state determination algorithms, referred to as the L-L, L-N, N-L and N-N procedures, are discussed and compared. The first symbol indicates the element level, the second one indicates the section level. Furthermore, the symbol N indicates that local nonlinear iteration is performed prior to returning to the higher level, whereas the symbol L indicates that only the linearized equations are satisfied at the corresponding local level.

1. *N-N algorithm*: iterative element, iterative section.  
Conventional Newton iterations on both the element and section level (procedure previously exposed).
2. *N-L algorithm*: iterative element, non-iterative section.  
At the section level only the linearized equations are satisfied, at the element level the complete nonlinear iteration is performed. This procedure has been proposed in (Taucer *et al.*, 1991) and it has been largely used ((Petrangeli and Ciampi, 1997), (Spacone *et al.*, 1996), (Monti and Spacone, 2000)).
3. *L-N algorithm*: non-iterative element, iterative section.  
Complete iteration at the section level, linearized approach at the element level.
4. *L-L algorithm*: non-iterative element, non-iterative section.  
It entails the iterative satisfaction of the nonlinear element compatibility and section constitutive equations for each global iteration. This approach has been proposed in (Neuenhofer and Filippou, 1997).

By comparing these procedures, it is clear that the L-L state determination algorithm resembles more closely the computational steps in a stiffness-based element state determination, because only the global Newton type iteration is present. However, it needs more element storage requirements and it is not particularly advantageous for cases in which a large number of elements remain elastic and inelasticity is concentrated in a few elements. In general, as indicated in (Nukala and White, 2004), the N-N algorithm seems the most efficient of the four algorithms.

Actually, the most complete and update formulation can be found in (Lee and Filippou, 2009), that in addition addresses the issue of a singular section stiffness (the plastic hinge case). In particular, by using the singular value decomposition method, it is mathematically proved that a singular section stiffness is not a problem since one inverts it to get the section flexibility but then inverts it again after weighting to get the element stiffness, as reported in eq. (2.37).

In Tab. 2.2 a brief summary for displaced-based and force-based element state determination is reported. Fig. 2.4 shows the logical differences between the two approaches; in particular, it remarks the attention on the lack-of-fit problem that produce an element state determination more computational involved in the case of force-based elements.

	Displacement-based	Force-based
Section deformations	$\mathbf{e}_s(x) = \mathbf{B}(x)\mathbf{q}$	
Section forces		$\mathbf{f}_s(x) = \mathbf{b}(x) \bar{\mathbf{Q}}$
Section state determination	$\mathbf{f}_s(x), \mathbf{k}_s(x)$	$\mathbf{e}_s(x), \phi_s = (\mathbf{k}_s)^{-1}$
Restoring displacements <sup>(*)</sup>		$\bar{\mathbf{q}} = \int_0^l \mathbf{b}(x)^T \mathbf{e}_s(x) dx$
Flexibility matrix <sup>(*)</sup>		$\bar{\Phi} = \int_0^l \mathbf{b}(x)^T \phi_s \mathbf{b}(x) dx$
Stiffness matrix <sup>(*)</sup>		$\bar{\mathbf{k}} = (\bar{\Phi})^{-1}$
Element restoring forces	$\mathbf{Q} = \int_0^l \mathbf{B}^T(x) \mathbf{f}_s(x) dx$	
Element stiffness matrix	$\mathbf{k}$	$\mathbf{k} = \mathbf{h}_l^T \bar{\mathbf{k}} \mathbf{h}_l$

<sup>(\*)</sup> = quantities in the reference system without rigid body modes

**Table 2.2:** Comparisons between displaced-based and force-based element state determination.



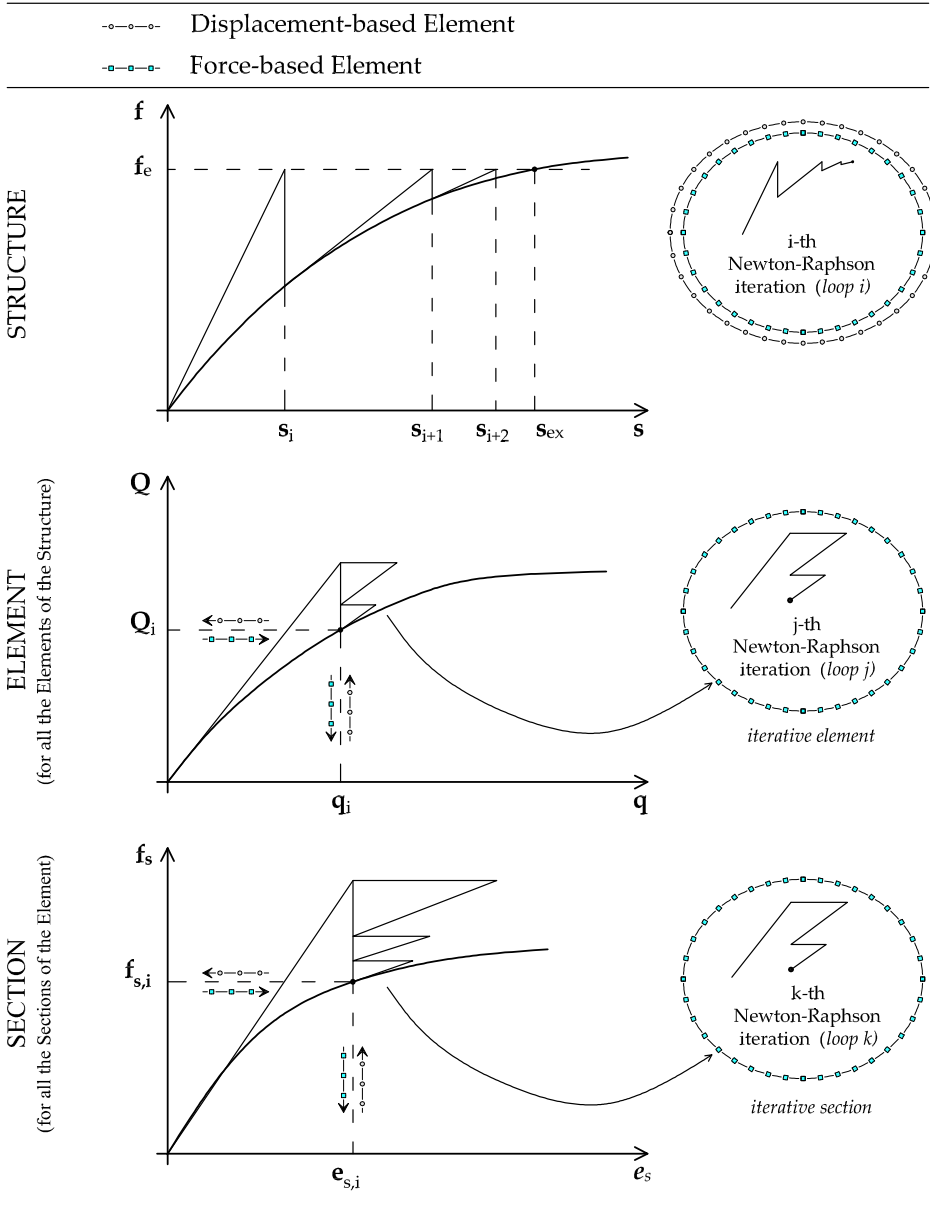


**Figure 2.4:** Logic comparison between displacement-based (only a global non linear system of eqs.) and force-based elements (additional nested non linear systems).

## 2.5 TREATMENT OF DISTRIBUTED LOADS

Let's considered the element in Fig. 2.5 on which the distributed loads  $f_x$  and  $f_y$  act. The loads define a vector  $\mathbf{f}_p$  so that:

$$\mathbf{f}_p = [f_x \quad f_y]^T \quad (2.38)$$

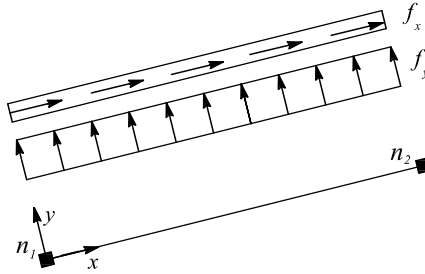


Figure 2.5: Distributed loads on the element.

### 2.5.1 DISPLACEMENT-BASED ELEMENT

In a displacement-based element, distributed loads can be included by means of equivalent nodal forces, whose definition is given by the virtual external work  $\delta W_e$ , produced by the displacements  $\mathbf{u}$  and the distributed forces  $\mathbf{f}_p$ , and computed in all the sections of the element:

$$\delta W_e = \int_0^l \delta \mathbf{u}^T(x) \cdot \mathbf{f}_p(x) dx \quad (2.39)$$

By introducing eq. (2.6) in eq. (2.39) we obtain:

$$\begin{aligned} \delta W_e &= \int_0^l \delta \mathbf{u}^T(x) \cdot \mathbf{f}_p(x) dx = \int_0^l \delta(\mathbf{N}(x)\mathbf{q})^T \cdot \mathbf{f}_p dx = \\ &= \int_0^l \delta \mathbf{q}^T \mathbf{N}(x)^T \mathbf{f}_p dx = \\ &= \delta \mathbf{q}^T \int_0^l \mathbf{N}(x)^T \cdot \mathbf{f}_p dx \\ &= \delta \mathbf{q}^T \mathbf{f}_{ne} \end{aligned} \quad (2.40)$$

from which we can define the equivalent nodal forces  $\mathbf{f}_{ne}$ :

$$\mathbf{f}_{ne} = \int_0^l \mathbf{N}(x)^T \cdot \mathbf{f}_p dx \quad (2.41)$$

These nodal forces depends on the shape functions  $\mathbf{N}(x)$  used to discretize and interpolate the displacement field in terms of generalized displacement degrees of

freedom  $\mathbf{q}$ . If cubic Hermitian polynomials for the transverse displacement fields and linear Lagrangian shape functions for the axial displacement are chosen (see Fig. 2.1), the following equivalent nodal forces result:

$$\mathbf{f}_{ne} = \begin{bmatrix} \frac{f_x l}{2} & \frac{f_y l}{2} & \frac{f_y l^2}{12} & \frac{f_x l}{2} & \frac{f_y l}{2} & -\frac{f_y l^2}{12} \end{bmatrix}^T \quad (2.42)$$

### 2.5.2 FORCE-BASED ELEMENT

In a force-based element, the inclusion of distributed forces is straightforward. Here in fact, we don't interpolate the displacement field, but the static field, and we do that in an exact way by using equilibrium statements. With respect the formulation presented in par. 2.4.1.3 on page 19, we just have to add the contribution, in terms of equilibrium, of the distributed loads represented in Fig. 2.6.

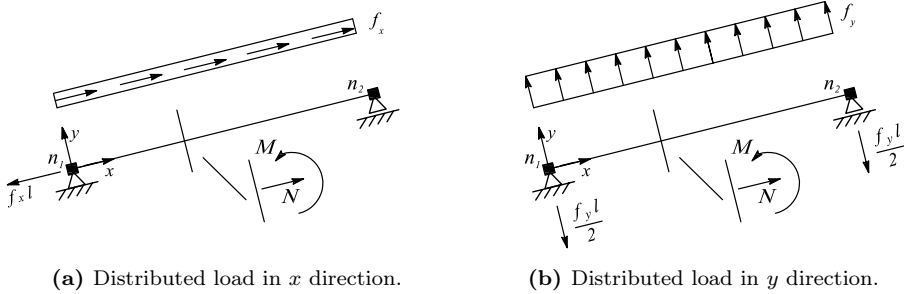


Figure 2.6: Distributed loads and associated reaction forces.

In particular, eq. (2.14) became:

$$\begin{bmatrix} Q_1 \\ Q_2 \\ Q_3 \\ Q_4 \\ Q_5 \\ Q_6 \end{bmatrix} = \begin{bmatrix} -1 & 0 & 0 \\ 0 & 1/l & 1/l \\ 0 & 1 & 0 \\ 1 & 0 & 0 \\ 0 & -1/l & -1/l \\ 0 & 0 & 1 \end{bmatrix} \begin{bmatrix} \bar{Q}_1 \\ \bar{Q}_2 \\ \bar{Q}_3 \end{bmatrix} + \begin{bmatrix} -l & 0 \\ 0 & -l/2 \\ 0 & 0 \\ 0 & 0 \\ 0 & -l/2 \\ 0 & 0 \end{bmatrix} \begin{bmatrix} f_x \\ f_y \end{bmatrix} \quad (2.43)$$

$$\mathbf{Q} = \mathbf{h}_l^T \bar{\mathbf{Q}} + \mathbf{h}_f \mathbf{f}_p$$

and for eq. (2.16) the following relation holds:

$$\begin{bmatrix} N \\ M \end{bmatrix} = \begin{bmatrix} 1 & 0 & 0 \\ 0 & (x/l - 1) & x/l \end{bmatrix} \begin{bmatrix} \bar{Q}_1 \\ \bar{Q}_2 \\ \bar{Q}_3 \end{bmatrix} + \begin{bmatrix} (l-x) & 0 \\ 0 & (x^2/2 - xl/2) \end{bmatrix} \begin{bmatrix} f_x \\ f_y \end{bmatrix} \quad (2.44)$$

$$\mathbf{f}_s(x) = \mathbf{b}(x) \bar{\mathbf{Q}} + \mathbf{b}_f(x) \mathbf{f}_p$$

These additional terms enter in the element state determination algorithm and the

restoring displacements (eq. (2.29)) became:

$$\begin{aligned}
 \bar{\mathbf{q}}_r &= \int_0^l \mathbf{b}(x)^T \mathbf{e}_s(x) dx \\
 &= \int_0^l \mathbf{b}(x)^T \phi_s(x) \mathbf{f}_s(x) dx \\
 &= \int_0^l \mathbf{b}(x)^T \phi_s(x) (\mathbf{b}(x) \bar{\mathbf{Q}} + \mathbf{b}_f(x) \mathbf{f}_p(x)) dx \\
 &= \left( \int_0^l \mathbf{b}(x)^T \phi_s(x) \mathbf{b}(x) dx \right) \bar{\mathbf{Q}} + \int_0^l \mathbf{b}(x)^T \phi_s(x) \mathbf{b}_f(x) \mathbf{f}_p(x) dx \\
 &= \bar{\Phi} \bar{\mathbf{Q}} + \bar{\mathbf{q}}_{r,f}
 \end{aligned} \tag{2.45}$$

## 2.6 GEOMETRIC NON LINEARITIES

Let  $P$  be an axial force applied to the ends of the beam element, and let  $\Delta$  be the corresponding displacement (Fig. 2.7), (Malerba and Bontempi, 1989), (Biondini *et al.*, 2004a). This displacement is congruent with the deformed shape and equals the difference between the length of the bent beam, assumed as axially rigid, and the length of the cord of its deformed axis:

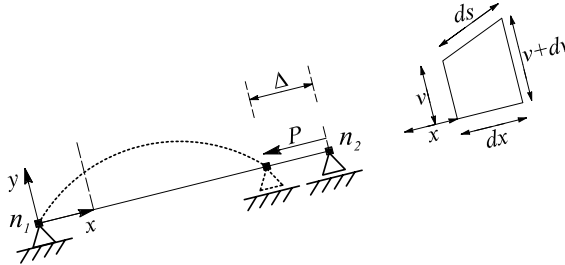


**Figure 2.7:** Second order geometrical non-linearity.

$$\begin{aligned}
 ds - dx &= \sqrt{(dx^2 + dy^2)} - dx = \\
 &= dx \left[ 1 + \frac{1}{2} \left( \frac{dv}{dx} \right)^2 - \frac{1}{4} \left( \frac{dv}{dx} \right)^4 + \dots \right] = \frac{1}{2} \left( \frac{dv}{dx} \right)^2 dx + \dots
 \end{aligned} \tag{2.46}$$

By neglecting the higher order terms,  $\Delta$  became:

$$\Delta = \int_0^l (ds - dx) dx = \frac{1}{2} \int_0^l \left( \frac{dv}{dx} \right)^2 dx \tag{2.47}$$

and adopting the beam's displacement functions in the following form:

$$\frac{dv}{dx} = [0 \quad N_{2,x} \quad N_{3,x} \quad 0 \quad N_{5,x} \quad N_{6,x}] \mathbf{q} = \mathbf{G} \cdot \mathbf{q} \tag{2.48}$$

the displacement and his virtual variation can be written as:

$$\begin{aligned} \Delta &= \frac{1}{2} \mathbf{q}^T \int_0^l \mathbf{G}^T(x) \cdot \mathbf{G}(x) dx \cdot \mathbf{q} \\ \delta\Delta &= \delta\mathbf{q}^T \int_0^l \mathbf{G}^T(x) \cdot \mathbf{G}(x) dx \cdot \mathbf{q} \end{aligned} \tag{2.49}$$

The external virtual work can be hence written as:

$$\delta W_G = P \cdot \delta\Delta = \delta\mathbf{q}^T \int_0^l P \mathbf{G}^T(x) \cdot \mathbf{G}(x) dx \cdot \mathbf{q} \tag{2.50}$$

By using the same notation introduce before, we can find a geometric contribution to the element resisting forces  $\mathbf{Q}$ :

$$\begin{aligned} \mathbf{Q}_g &= \delta\mathbf{q}^T \left( \int_0^l P \mathbf{G}^T(x) \cdot \mathbf{G}(x) dx \right) \mathbf{q} = \\ &= \delta\mathbf{q}^T \quad \mathbf{k}_g \quad \mathbf{q} \end{aligned} \tag{2.51}$$

in which  $\mathbf{k}_g$  is the geometric stiffness matrix of the element.

In the special case of constant axial force, the geometric stiffness matrix can be evaluated in close form:

$$\mathbf{k}_g = P \int_0^l \mathbf{G}^T(x) \mathbf{G}(x) dx = \frac{P}{10l} \begin{bmatrix} 0 & 0 & 0 & 0 & 0 & 0 \\ 0 & 12 & l & 0 & -12 & l \\ 0 & l & \frac{4}{3}l^2 & 0 & -l & -\frac{l^2}{3} \\ 0 & 0 & 0 & 0 & 0 & 0 \\ 0 & -12 & -l & 0 & 12 & -l \\ 0 & l & -\frac{l^2}{3} & 0 & -l & -\frac{4}{3}l^2 \end{bmatrix} \tag{2.52}$$

In general, however, also the effects due to geometric non linearities must be evaluated by numerical integration since axial forces derive from variable sectional states.

**2.7 DISPLACEMENT-BASED VS FORCE-BASED ELEMENT: COMPARISONS**

In a *displacement-based* element, the formulation is based on interpolation functions for the transverse and axial displacements of the member; the functions here used are cubic Hermitian polynomials for the transverse displacement fields and linear Lagrangian shape functions for the axial displacement, so that linear curvature and constant axial strain along the element result. Such a choice represents the exact solution only for a linear elastic, prismatic beam, without distributed loads. This is an approximation that, in nonlinear analysis, has well-known shortcomings. These limitations can be overcome with two types of approaches:

- by using higher-order displacement interpolation functions in connection with internal element nodes;

- by increase the discretization used, for example each structural element is divided in more finite beam elements.

The formulation of *flexibility-based* elements, on the other hand, is based on interpolation functions for the internal forces. For geometrically linear structures it is straightforward to select polynomials that satisfy the element equilibrium in a strict sense, such as constant axial force and linearly varying bending moments in absence of element loads. These interpolation functions represent the exact solution to the governing equations, irrespective of the geometry and constitutive law of the beam element. A discretization error, as generally encountered in stiffness-based formulations, does not occur (Neuenhofer and Filippou, 1997).

Many comparisons between displacement-based and force-based elements has been done in recent years, by showing the superior behavior of the second approach. Usually the comparisons are done in the non linear field, because this is the research goal. However, it is more useful to present comparisons in the elastic field, so that we can compare the two approaches in a very simple way.

Let's considering the simple beam shows in Tab.2.3. The beam is prismatic and linear elastic. Four examples are considered:

1. *Case 1:*

the first node is clamped and the second is free; a concentrated force  $F$  acts in the second node.

In this case, the deformed configuration is a 3<sup>th</sup> order curve and the bending moment distribution is linear. Hence, both displacement-based and force-based elements give the exact solution.

2. *Case 2:*

the first node is clamped and the second is free; a distributed loads  $p$  acts on the beam.

In this case, the deformed configuration is a 4<sup>th</sup> order curve and the bending moment distribution is parabolic. Both displacement-based and force-based elements give the exact nodal displacement solution, but only the force-based formulation is able to catch the complete deformed shape. In fact, with a displacement-based approach we describe at least a 3<sup>th</sup> order curve and linear curvature.

It follows that the deformed configuration is approximate, and the bending moment distribution is not correct.

3. *Case 3:*

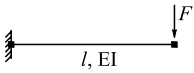
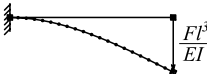
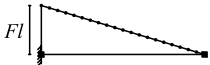
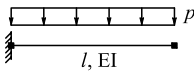
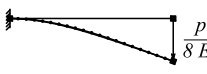
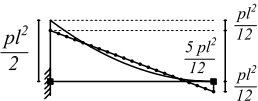
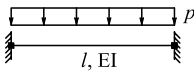
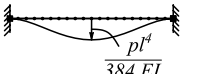
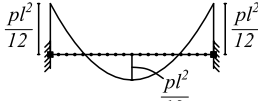
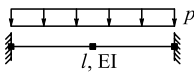
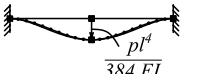
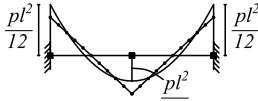
with respect *Case 2*, also the second node is clamped.

In this case, all nodal displacements are equal to zero. Since a displacement-based element interpolates that displacements, the complete deformed configuration is equal to zero; hence, zero curvatures and zero bending moments in all the sections descend. In contrast, a force-based approach is able, once again, to find the exact solution.

4. *Case 4:*

it is equal to *Case 3*, but the beam is studied by using two finite elements. We

can observe that now also the displacement-based element gives a deformed configuration with exact nodal displacements but, as happen in *Case 2*, the shape is approximated and the the bending moments are not correct.

CASE	Deformed configurations	Bending moments
Dotted lines = displacement-based (d-b) element Continuous lines = force-based (f-b) element		
 <p>1(a): 1 element</p>	 <p>1(b): d-b ∇ and f-b ∇</p>	 <p>1(c): d-b ∇, f-b ∇</p>
 <p>2(a): 1 element</p>	 <p>2(b): d-b ∧, f-b ∇</p>	 <p>2(c): d-b ∧, f-b ∇</p>
 <p>3(a): 1 element</p>	 <p>3(b): d-b ∧, f-b ∇</p>	 <p>3(c): d-b ∧, f-b ∇</p>
 <p>4(a): 2 elements</p>	 <p>4(b): d-b ∧, f-b ∇</p>	 <p>4(c): d-b ∧, f-b ∇</p>

∇ = numerical solution coincident with the exact one  
 ∧ = numerical solution approximated with respect the exact one

**Table 2.3:** Some comparisons between displacement-based (dotted lines) and force-based approach (continuous line).

These simple examples help in understand the differences between a displacement-based and a force-based element, nevertheless only linear elastic field is considered. In particular, two type of approximations are present in a displacement approach:

- deformed modes are chosen *a priori* and, in general, they represents the correct solution only for some special cases;
- distributed forces are introduced by means of equivalent nodal forces and hence only the correct nodal effects is described.

In contrast, a force-based element gives always the correct solutions.

When we move to nonlinear field, these limitations are accentuated and the superior behavior of flexibility-based element is evident. In the non linear field all the integrals shown in this chapter must be evaluated by numerical integration. Thus, the flexibility approach yields the exact solution within the numerical integration tolerance, since the axial force interpolation function agrees with the exact solution. A discretization error does not arise. By contrast, the shortcomings of the stiffness approach are evident. While the latter satisfies equilibrium in the weighted residual sense, it does not satisfy equilibrium in a strict point-by-point sense.

In conclusion, the superior behavior of the flexibility-based element derives from the fact that it is always straightforward to come up with force interpolation functions that satisfy equilibrium exactly, while it is often impossible to find exact displacement interpolation functions. The consequence is that the finite-element solution with the stiffness based frame element can only be improved by refining the finite-element mesh. By contrast, the numerical accuracy of a flexibility-based approach can be increased by a better numerical integration through either mesh refinement or an increase of the number of integration points in the element.

## 2.8 SHEAR MODELING

---

In the previous, the attention is given to the problem related to normal stresses. In fact, all the expression are referred to the generalized stresses  $N$  and  $M$  and the work due to the shear force  $V$  is not included. In the following, hence, it is recalled how it is possible to include shear in the non linear beam problem by considering both displacement-based and force-based elements.

At first, it is necessary to update the generalized stresses and strains definition, as follow:

$$\mathbf{e}_s = \begin{bmatrix} \varepsilon_0 \\ \gamma_0 \\ \chi_0 \end{bmatrix} \quad \mathbf{f}_s = \begin{bmatrix} N \\ V \\ M \end{bmatrix} \quad (2.53)$$

With respect to before, the generalized shear deformation  $\gamma_0$  and the shear force  $V$  are present.

### 2.8.1 DISPLACEMENT-BASED ELEMENT

The Timoshenko beam finite element with linear interpolation functions of both transverse deflection and rotation is considered:

$$\begin{bmatrix} u_0 \\ v_0 \\ \varphi \end{bmatrix} = \begin{bmatrix} N_1 & 0 & 0 & N_2 & 0 & 0 \\ 0 & N_1 & 0 & 0 & N_2 & 0 \\ 0 & 0 & N_1 & 0 & 0 & N_2 \end{bmatrix} \mathbf{q} = \mathbf{N}(x) \mathbf{q} \quad (2.54)$$

with:

$$N_1 = 1 - \frac{x}{l} \quad N_2 = \frac{x}{l} \quad (2.55)$$



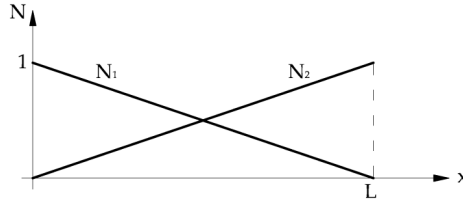


**Figure 2.8:** Shape functions.

By applying the internal compatibility equations, the definition of the generalized stresses is:

$$\begin{bmatrix} \varepsilon_0 \\ \gamma_0 \\ \chi_0 \end{bmatrix} = \begin{bmatrix} N_{1,x} & 0 & 0 & N_{2,x} & 0 & 0 \\ 0 & N_{1,x} & -N_1 & 0 & N_{2,x} & -N_2 \\ 0 & 0 & N_{1,x} & 0 & 0 & N_{2,x} \end{bmatrix} \mathbf{q} = \mathbf{B} \mathbf{q} \quad (2.56)$$

in which the derivatives of the shape functions are present:

$$N_{1,x} = -\frac{1}{l} \quad N_{2,x} = \frac{1}{l} \quad (2.57)$$

Then, by following the same steps exposed before, the restoring forces and element stiffness matrix can be defined.

### 2.8.1.1 SHEAR LOCKING PREVENTION

In order to avoid shear locking effects, the following bubble function is introduced (Auricchio, 2003):

$$N_L = \frac{1}{2} x \left( 1 - \frac{x}{l} \right) \quad (2.58)$$

$$\mathbf{N} = \begin{bmatrix} N_1 & 0 & 0 & N_2 & 0 & 0 \\ 0 & N_1 & N_L & 0 & N_2 & -N_L \\ 0 & 0 & N_1 & 0 & 0 & N_2 \end{bmatrix} \quad (2.59)$$

$$\mathbf{B} = \begin{bmatrix} N_{1,x} & 0 & 0 & N_{2,x} & 0 & 0 \\ 0 & N_{1,x} & N_{L,x} - N_1 & 0 & N_{2,x} & -N_{L,x} - N_2 \\ 0 & 0 & N_{1,x} & 0 & 0 & N_{2,x} \end{bmatrix} \quad (2.60)$$

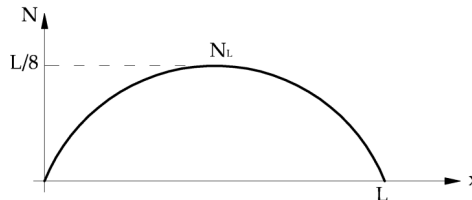


**Figure 2.9:** Bubble shape function.

Then, reduced integration is applied.

### 2.8.2 FORCE-BASED ELEMENT

In a force-based element, since equilibrium interpolating matrices are used, the inclusion of shear modeling is very simple and, in addition, no shear locking phenomena born.

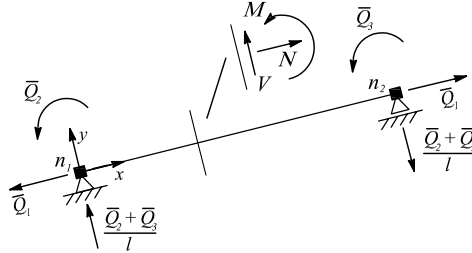


Figure 2.10: Inclusion of shear in a force-based element.

$$\begin{aligned} \begin{bmatrix} N \\ V \\ M \end{bmatrix} &= \begin{bmatrix} 1 & 0 & 0 \\ 0 & -1/l & -1/l \\ 0 & (x/l - 1) & x/l \end{bmatrix} \begin{bmatrix} \bar{Q}_1 \\ \bar{Q}_2 \\ \bar{Q}_3 \end{bmatrix} \\ \mathbf{f}_s(x) &= \mathbf{b}(x) \quad \bar{\mathbf{Q}} \end{aligned} \quad (2.61)$$

### 2.9 CLOSING REMARKS

---

In this chapter, the non linear beam problem has been presented. Particular attention is given to the dual formulations that can be applied in formulating finite beam-column elements. The two strategies have been presented and critically compared, also with respect the description of shear.

As a general conclusion, it can be stated that a force-based element presents a superior behavior, because it satisfy equilibrium in a strict point-by-point sense. In addition, shear locking problems do not arise. However, a displacement-based element is more simple and less computational demanding.

Once again, it must be pointed out that in this chapter only the longitudinal problem is considered, since the section is simply a sub-module of the formulation. Concerning the section, in chapter 3 the State of the Art will be recalled and in chapter 5 two sectional proposals will be given.

# 3

## RC Sectional Models: Problem Statement & State of the Art

*In the previous chapter the non linear beam problem has been presented. Particular attention is given to the dual approaches that can be applied in formulating finite beam-column elements. The so-obtained techniques are generally valid in dealing with geometric and material non linearities. In this chapter, the problem is outlined with respect RC structures.*

### 3.1 DEFINITION OF THE PROBLEM

---

The Finite Element Method (FEM), applied to frame structures discretized with monodimensional models, works through nested modules that goes from the structure to the material point (fibre). In particular, 4 nested states must be evaluated:

1. the state of the *structure*, that is made of elements;
2. the state of the *element*, that is made of sections;
3. the state of the *section*, that is made of fibers;
4. the state of the *fiber*, on which constitutive laws are assumed and/or evaluated by using specific techniques.

The *state of the structure* is obtained by assembling the states of the elements in which it is subdivided. In a global displacement approach, the *state of the element* must be obtained starting from its nodal displacements and the results of this phase, called Element State Determination, are the nodal resisting forces and the element stiffness matrix. Chapter 2 has clearly deal with it, and two dual formulations have been presented: a displacement-based and a force-based formulation. It has been shown that the state of the element is obtained by *weighting* the *state of the sections* that compose it, but no regards are given to the material.

The exposed formulation is hence general, but now it is necessary to specify it to RC frame structures. In doing that, the work must be done only in the definition of the sectional state, that is obtained by integrating the *state of the fibers* that compose it. In RC sections, it's clear that we have to deal with two materials:

(1) the concrete, that is described by a continuum sectional domain, and (2) the reinforcing steels, that is described by discrete quantities arbitrary positioned in the sectional domain.

This chapter, hence, deals with the definition of the state of a RC section, by proposing adequately sectional models that can then applied in formulating finite beam-column elements. As already outlined, this process can be considered straightforward if we deal with the problem of normal stresses, but the same problem in which an high interaction between normal and shear stresses is present is still today an object of several researches. In the following, the main reasons are presented and discussed.

**3.1.1 DEALING WITH NORMAL FORCES**

Since a RC section is composed by two materials, the concrete - that corresponds to a continuum domain - and the reinforcing steel - that corresponds to a union of discrete bars, in order to obtained the sectional state a specific sectional integration strategy is needed. At this end, the most adopted strategy is the so called “fiber approach”, in which the section is subdivide in sub-domains, called fibers (C.E.B., 1996), according to Fig. 3.1. Mathematically speaking, this rule refers to the Riemann Mid-Point Integration Rule, through which the function that has to be integrated is evaluated in the centroid of the fiber and then weighted by its area; doing that for all the fibers, the integral is obtained through the summation of each fiber’s contribution. Other integration techniques can be proposed. Some examples are given in Appendix A, in which a new sectional discretization strategy, having the fibers approach as a simply particular case, is proposed.

If the Navier-Bernoulli (plane section) hypothesis is assumed (see Tab. 3.1(a)), only the uniaxial longitudinal strain  $\varepsilon_x$  is active. Hence, given the strains in all

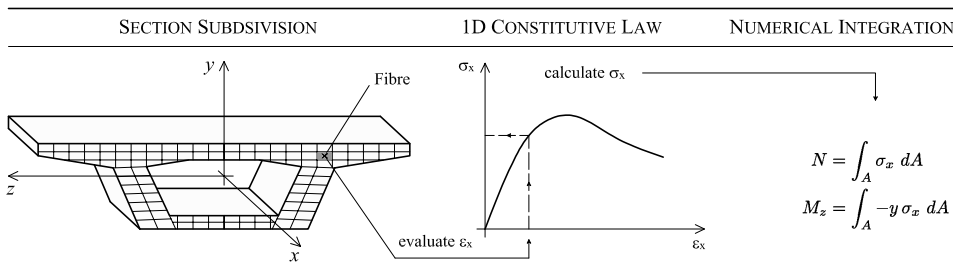


**Figure 3.1:** Fibers Sectional Approach (normal stresses).

the fibers, the longitudinal stresses  $\sigma_x$  can be computed by using a non-linear uniaxial constitutive model. Then, their integral over the sectional domain gives the generalized stresses  $N, M$  as Fig. 3.1 shows.

When fiber sectional discretization is combined with a force-based element, the highest degree of accuracy and stability is obtained in a frame structural model at the current state of knowledge.

If the normal solicitations are dominant in the behavior of the framed structure, plane section hypothesis produce a suitable kinematic constraint, because it has been observed that this hypotheses remains valid for all range of loading (Bairán, 2005).

However, common fiber beam-column elements that neglect shear effects and their interaction with other internal forces are not generally applicable, since it has been recognized that in a beam model the main assumptions, such as the plane section hypothesis, are more important than the details on more specific aspects related to the element's formulation or to the material's behavior.

### 3.1.2 DEALING WITH NORMAL AND TANGENTIAL FORCES

The inclusion of shear effects in these models is not an easy task (Ferreira, 2013). If for uniaxial concrete response is simply to furnish uniaxial constitutive models  $\sigma = \sigma(\varepsilon)$ , the same approach applied to a  $\tau = \tau(\gamma)$  relationship can not be proposed since the high complexity of the shear mechanisms in RC elements, generated along with the strong non linear behavior found in diagonally cracked concrete, that depends not only to the concrete characteristics, but also to the geometry of the section and to the position and the types of reinforcements.

On the contrary, as it will be explained in chapter 4, 2D modeling of shear resistance mechanisms in RC structures is performed since more than thirty years and successfully applied in the non linear analysis for all range off loadings.

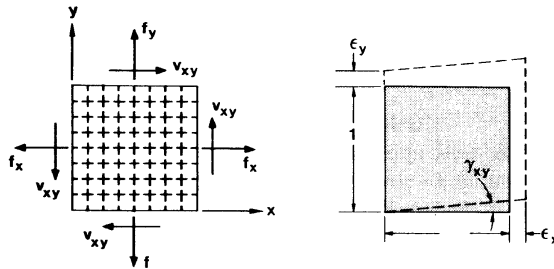


Figure 3.2: Membrane RC element, (Vecchio and Collins, 1986).

Several strategies have been proposed, but in this work the attention is focused on smeared type models (Fig. 3.2) that treat reinforcing concrete as a continuum material with his own state-dependent relationships:

$$\begin{aligned} \begin{bmatrix} \sigma_x \\ \sigma_y \\ \tau_{xy} \end{bmatrix} &= \begin{bmatrix} D_{11} & D_{12} & D_{13} \\ D_{21} & D_{22} & D_{23} \\ D_{31} & D_{32} & D_{33} \end{bmatrix} \begin{bmatrix} \varepsilon_x \\ \varepsilon_y \\ \gamma_{xy} \end{bmatrix} \\ \boldsymbol{\sigma} &= \mathbf{D}(\boldsymbol{\varepsilon}) \quad \boldsymbol{\varepsilon} \end{aligned} \quad (3.1)$$

With this in mind, one objective of this thesis is to investigate the strategies in order to move from bidimensional *towards* monodimensional modeling of RC framed structures, including also shear effects. The effort is to minimize the discrepancies

between 2D and 1D modeling, using concepts based on Continuum Mechanics (Fig. 3.3).

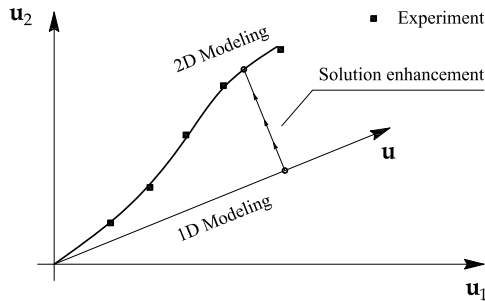


**Figure 3.3:** Enhancement of 1D solution, adapted from (Bairán, 2005).

Once constitutive law are assumed according to eq. (3.1), the stresses as a function of the strains ( $\boldsymbol{\sigma} = \boldsymbol{\sigma}(\boldsymbol{\varepsilon})$ ) can be evaluated at the material (or fiber) level. The goal, now, is understand which structural beam theories can be used in order to do that:

(a) NAVIER-BERNOULLI BEAM THEORY:

in this theory, plane section hypothesis is used and shear deformation is neglected. According to Tab. 3.1(a), only the longitudinal deformation  $\varepsilon_x$  is active. As already said, this implies that uniaxial non-linear constitutive laws can be applied, but finite beam elements based on this sectional kinematic can address only the problem of normal stresses. However, if shear is dominant, this models produce erroneous predictions. In any case, since only  $\varepsilon_x$  is described by this theory, a link with a constitutive law as (3.1) can not be performed.

(b) TIMOSHENKO BEAM THEORY:

once again, plane section hypothesis is chosen, but a constant shear strain distribution is taken into account. Now, two deformations are described by the model ( $\varepsilon_x$  and  $\gamma_{xy}$ ) but the transversal strain  $\varepsilon_y$ , necessary to use the constitutive model, is not present (Tab. 3.1(b)). However, as it will be explained later in details, by introducing some assumptions regarding the strains/stresses patterns, this kinematic can be used in order to formulate shear-flexible beam-column RC elements.

(c) GENERALIZED BEAM THEORY:

in the previous theories, the sectional kinematic is taken fixed and the interpolating matrix  $\mathbf{a}_s$  depends only on the geometry of the section. Here, instead, the sectional kinematic is not only able to describe the total strain's tensor  $\boldsymbol{\varepsilon} = [\varepsilon_x, \varepsilon_y, \gamma_{xy}]^T$ , but it is also *state-dependent* with matrix  $\mathbf{a}_s$  that depends on strains (Tab. 3.1(c)). Clearly, this sectional kinematic presents a very high level of generality and it really addresses the problem of shear modeling in RC framed structures, but the implementation of the so-obtained model is quite challenging due to computational efficient and stability.

SECTIONAL KINEMATIC	FUNDAMENTAL RELATIONS
	$\begin{cases} u(x, y) = u_0(x) - y \cdot v'_0(x) \\ v(x) = v_0(x) \end{cases}$ $\begin{bmatrix} \varepsilon_x \end{bmatrix} = \begin{bmatrix} 1 & -y \end{bmatrix} \begin{bmatrix} \varepsilon_0 \\ \chi_0 \end{bmatrix} = \mathbf{a}_s(y) \mathbf{e}_s$
(a) Navier-Bernoulli kinematic.	
	$\begin{cases} u(x, y) = u_0(x) - y \cdot (v'_0(x) - \gamma_0(x)) \\ v(x) = v_0(x) \end{cases}$ $\begin{bmatrix} \varepsilon_x \\ \gamma_{xy} \end{bmatrix} = \begin{bmatrix} 1 & 0 & -y \\ 0 & 1 & 0 \end{bmatrix} \begin{bmatrix} \varepsilon_0 \\ \gamma_0 \\ \chi_0 \end{bmatrix} = \mathbf{a}_s(y) \mathbf{e}_s$
(b) Timoshenko kinematic.	
	$\mathbf{u}(x, y) = \mathbf{u}^{ps}(x, y) + \mathbf{u}^w(x, y)$ $\begin{bmatrix} \varepsilon_x \\ \varepsilon_y \\ \gamma_{xy} \end{bmatrix} = \begin{bmatrix} \cdot & \cdot & \cdot \\ \cdot & \cdot & \cdot \\ \cdot & \cdot & \cdot \end{bmatrix} \begin{bmatrix} \varepsilon_0 \\ \gamma_0 \\ \chi_0 \end{bmatrix} = \mathbf{a}_s(y, \mathbf{e}_s) \mathbf{e}_s$
(c) Generalized kinematic.	

**Table 3.1:** Navier-Bernoulli, Timoshenko and Generalized sectional kinematic.

3.1.3 SHEAR IN RC SECTIONS: THE MAIN DIFFICULTY

As already exposed, when tangential forces are applied, plane section hypothesis is no longer valid due to the appearance of distortion and the distribution of shear strains and stresses in the cross section is not only more complex, but also *state-dependent*, showing important variations while cracking is developing and when the ultimate state is approached. The problem can be better explained if Jourawski strategy is applied, as outlined in (Ferreira, 2013).

It is known that a variation of the bending moments along the beam's axis is possible thanks to the presence of shear forces. Due to this bending increment, a fiber is submitted to an increment of axial stresses that are equilibrated by out-of-plane stresses, as deduced by Jourawski in 1856, Fig. 3.4.

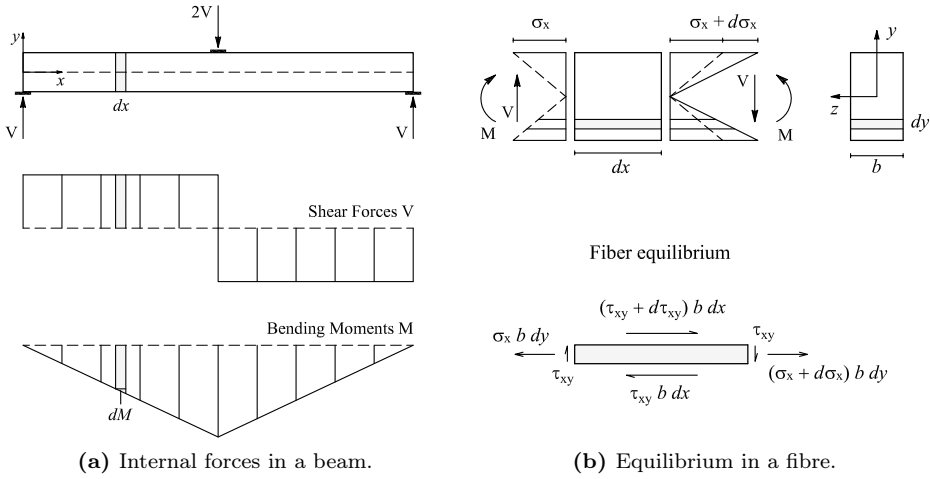


Figure 3.4: In plane shear stresses in a beam deduced by Jourawski (1856).

The equilibrium equation of the fibre is given by:

$$\frac{\partial \sigma_x}{\partial x} + \frac{\partial \tau_{xy}}{\partial y} = 0 \tag{3.2}$$

and the shear stresses can be written as:

$$\tau_{xy}(y) = -\frac{1}{b} \int_0^y \frac{\partial \sigma_x}{\partial x} b \, dy \tag{3.3}$$

In case of isotropic-elastic material, the solution of eq. (3.3) is straightforward:

$$\tau_{xy}(y) = -\frac{1}{b} \int_0^y \frac{V b y}{I} \, dy = \frac{V Q(y)}{I b(y)} \tag{3.4}$$

where  $Q(y)$  is the first moment of area integrated from the bottom of the section to point at quote  $y$  and  $b(y)$  is the width of the cross section at the coordinate  $z$ . Once the shear stress is defined with eq. (3.4), the shear strain can be obtained by means of the elastic tangential modulus  $G$ :

$$\gamma_{xy}(y) = -\frac{1}{G b} \int_0^y \frac{V b y}{I} \, dy = \frac{1}{G} \frac{V Q(y)}{I b(y)} \tag{3.5}$$



However, cracked concrete is no longer elastic, but presents a strong anisotropic behavior, in which coupling of normal and tangential stresses and strains appears. For these reasons, eq. (3.5) is no longer valid, since shear stresses depend not only on the sectional geometry, but also on the state of the material. In other words, in RC section it's not possible to define a corrective shear area, because in the non linear field there is the dependability also from the material and hence it becomes state-dependent. This is the main problematic of the difficulty of modeling nonlinear response of RC sections with the presence of shear forces and, as exposed in (Bairán and Marí, 2007a), finding a solution or approximation for eqs. (3.4) and (3.5) is the basis for a kinematic constraint to model shear on cracked RC sections.

### 3.2 SECTIONAL KINEMATIC APPROACHES CONSIDERING SHEAR EFFECTS

A general review of shear-flexural beam finite elements can be found in (Ceresa *et al.*, 2007). The classification here proposed defines three group of models:

#### 1. *Strut & Tie based Models*

in which independent models for the shear and flexural deformations are superimposed, and where a truss analogy is then employed to take into account the shear deformation and strength. Between them, the following works must be cited:

- Guedes *et al.* (1994), that proposes a two node Timoshenko beam element. The truss is made of two diagonal concrete struts, whose inclination represents the directions of principal stresses and strains, and steel ties in longitudinal and transversal directions. The element has been implemented in CASTEM 2000<sup>(1)</sup>;
- Ranzo and Petrangeli (1998), focused on a 2-D fiber element following a flexibility-based approach. The axial-flexural behavior is a function of section axial deformation and curvature as in the traditional fiber model, while the shear behavior is a function of the section distortion identified with a nonlinear truss model;
- Martinelli (2008), in which the contributions to shear strength due to both the arch action and the inclined thrust-line developing in squat elements are accounted for. Additionally, in shear, the Mörsch's truss is explicitly modeled considering both the tension and compression concrete diagonal.

#### 2. *Inter-Fibre Equilibrium Approaches*

in which shear stress-strain distributions are state-dependent and consequently change during loading. These models, equivalent to force-based sectional models, present a very high accuracy, but also an highly complexity and computational demanding. Between them:

- Vecchio and Collins (1988), that propose the Dual Section Analysis. By defining two control sections, the increment of longitudinal stress is

---

<sup>(1)</sup>CASTEM 2000 is a Finite Element Program developed by CEA (2000).

computed by Finite Differences. This is not a real sectional model but it must be cited because it is the pioneer model of this group;

- [Bentz \(2000\)](#), that improves the Dual Section Analysis by taking the limit of the distance between the two controlled sections. This method, called Longitudinal Stiffness Method, is effectively a sectional model and contains the basis of several more recent approaches. The method is actually implemented in Response-2000<sup>(2)</sup>;
- [Bairán \(2005\)](#), in which a model named TINSA (Total Interaction Non linear Sectional Analysis) is presented. This is the most elegant sectional approach proposed to date. Since a finite element analysis of the cross sections - using 2D concrete elements and 1D steel elements - must be performed, its implementation in a structural program is quite challenging;
- [Mohr \(2011\)](#), that deals with a generalized section kinematic aiming of extending TINSA from the section at the element level. The model addresses the state-dependent problem by using a series of polynomials.

### 3. Fixed Pattern Approaches

where an a priori fixed constraint is assumed in the cross section. These approaches, equivalent to the displacement-based sectional model, estimate the internal shear stress-strain distribution in the cross section by assuming a shear strain or stress pattern that is taken constant during the whole loading process. The inter-fibre equilibrium is not directly verified, as the compatibility in the transversal direction is not guaranteed. These models are however less computational demanding but even less accurate than the previous ones. Between them there are:

- [Güner \(2008\)](#), where shear at the cross section is considered through different options based on Fixed Pattern Approaches. It was concluded that shear-strain-based approaches are less computationally demanding and more stable than shear-stress-based approaches;
- [Ceresa et al. \(2009\)](#), in which a fixed strain approach has been presented and implemented in a 2 nodes Timoshenko beam;
- [Ferreira \(2013\)](#), that presents a hybrid fibre beam-column model based on a fixed stress approach. The so-obtained procedure has been implemented in CONS<sup>(3)</sup> and permits to perform not only analysis of shear critical framed structures, but also to include the time-dependent behavior of RC structures and to study different strengthening scenarios.

Some of these models are detailed in the next.

---

<sup>(2)</sup>Response-2000 is free program developed at University of Toronto by Collins, Vecchio, Bentz and others. Web: <http://www.ecf.utoronto.ca/añbentz/download.htm>.

<sup>(3)</sup>CONS is a Finite Element Program originally developed at University of California (Berkeley) by [Marí \(1984\)](#) and extended at the Universitat Politècnica de Catalunya - BarcelonaTECH (UPC) in [\(Marí, 2000\)](#).

3.2.1 STRUT & TIE BASED MODELS

3.2.1.1 MARTINELLI'S MODELING STRATEGY

Martinelli (2008) developed a fiber column element based on Timoshenko beam theory to model the cyclic response of the end critical zones of bridge piers characterized by a low-to-intermediate shear slenderness. Shear contribution is computed by integration along the element of the shear force acting at the cross-sections. The shear resultant over the cross-section is derived by different resisting mechanisms - the arch action, the truss mechanism, the compression concrete above the neutral axis, and aggregate interlock, each of which studied in independent fashion.

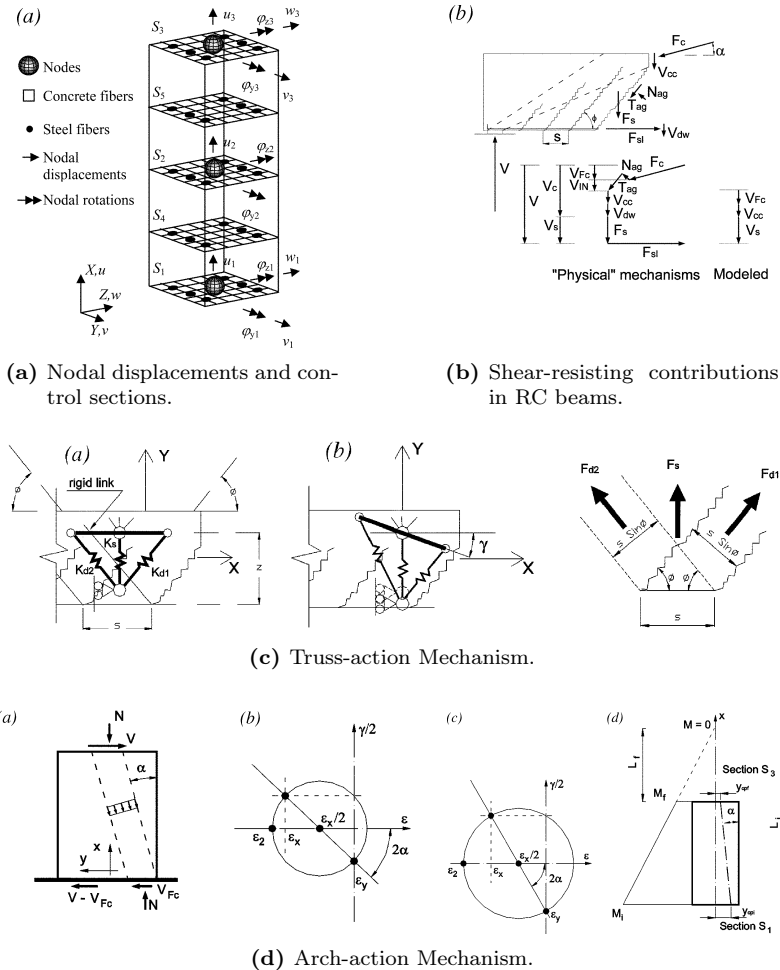


Figure 3.5: Martinelli's Modeling Strategy (Martinelli, 2008).

This model represents the most complete formulation between the strategies in which shear and flexural deformations are superimposed, and where a truss analogy is employed to take into account the shear's effects.

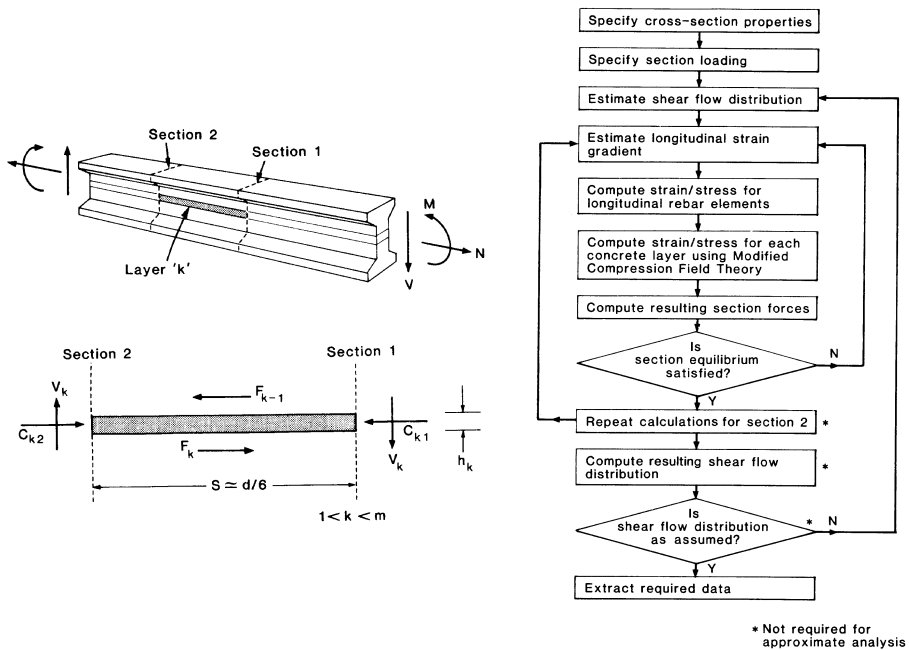
### 3.2.2 INTER-FIBRE EQUILIBRIUM APPROACHES

#### 3.2.2.1 THE DUAL SECTIONAL ANALYSIS

The “Dual Section Analysis” was originally proposed by (Vecchio and Collins, 1988) in order to evaluate the gradient of normal stresses generated by the presence of shear forces. By applying the Finite Difference Method (Fig. 3.6a):

$$\frac{\partial \sigma_x}{\partial x} \approx \frac{\sigma_x(x_2) - \sigma_x(x_1)}{S} \tag{3.6}$$

in which the evaluation of the normal stresses in two different sections separated by a finite distance  $S$  is required. Then, from equilibrium of the two controlled sections, by applying the iterative procedure shown in Fig. 3.6b, the distribution of shear stresses and strains can be determined.



(a) The two controlled sections. (b) Logical scheme.

**Figure 3.6:** The Dual Section Analysis, (Vecchio and Collins, 1988).

It’s clear that this approach used an information that is not well established: the distance between the two control sections  $S$ , besides the value  $S = H/6$  is suggested. This proposal, hence, is not a sectional model as it needs informations outside the section, but it is a rigorous analysis approach where inter-fibre equilibrium is accomplished. However, it is time consuming, has problems of stability and cannot be introduced easily into a FE code as an independent sectional model.

## 3.2.2.2 THE LONGITUDINAL STIFFNESS METHOD

Bentz (2000) improved the Dual Sectional Analysis by taking the limit of the distance between the two control sections. The so-obtain approach is called “Longitudinal Stiffness Method” and it is the base of several more recent approaches.

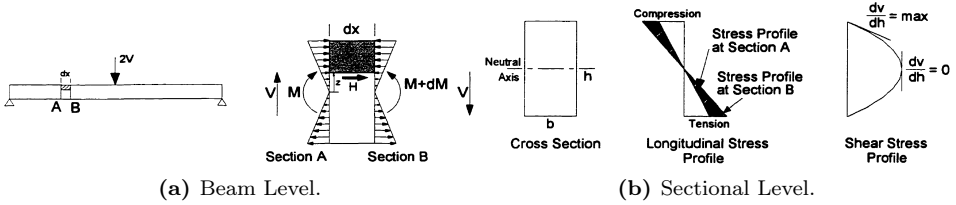


Figure 3.7: Longitudinal Stiffness Method, (Bentz, 2000).

In this method, the chain-rule is used to determine the gradient of normal stresses as the derivatives of the stress with respect of the element’s axis. It requires an initial shear strain pattern as a function of the average sectional shear deformations (that can be assumed as the Jourawski solution Fig.3.7):

$$\gamma_{xy}(y) = F_{\gamma}(x, y)\gamma_0 = \frac{A S_z}{I_z b(y)}\gamma_0 \quad (3.7)$$

where  $A$  is the area of the cross section. This shear strain profile is used for the further load steps. The Bernoulli’s plane section that computes the axial strain is combined with the current strain pattern. In this manner, the strains in each fibre are determined from the axial strain, curvature and average shear strain of the cross section:

$$\begin{bmatrix} \varepsilon_x \\ \gamma_{xy} \end{bmatrix} = \begin{bmatrix} 1 & 0 & -y \\ 0 & F_{\gamma}(x, y) & 0 \end{bmatrix} \begin{bmatrix} \varepsilon_0 \\ \gamma_0 \\ \chi_0 \end{bmatrix} \quad (3.8)$$

$$\boldsymbol{\varepsilon}(y) = \mathbf{B}(y) \mathbf{e}_s$$

and the differential increment of stress is given by:

$$\begin{bmatrix} \sigma_x \\ \sigma_y \\ \tau_{xy} \end{bmatrix} = \mathbf{D}_t \begin{bmatrix} \varepsilon_x \\ \varepsilon_y \\ \gamma_{xy} \end{bmatrix} \quad (3.9)$$

where  $\mathbf{D}_t$  is the tangent stiffness matrix of the fibre.

After static condensation of the terms in the transverse direction, the derivatives of the normal and shear stresses with respect to the  $x$ -axis is computed through the chain-rule:

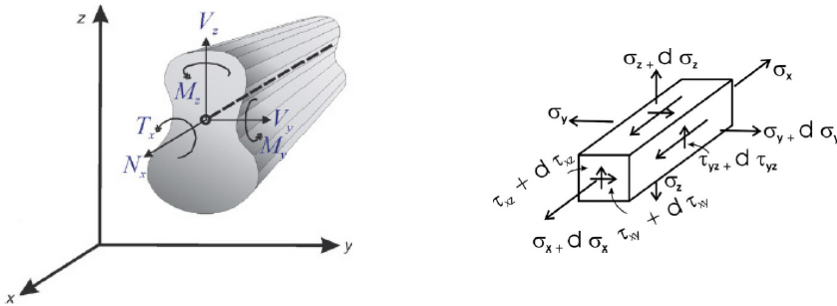
$$\frac{\partial \boldsymbol{\sigma}}{\partial x} = \frac{\partial \boldsymbol{\sigma}}{\partial \boldsymbol{\varepsilon}} \frac{\partial \boldsymbol{\varepsilon}}{\partial \mathbf{e}_s} \frac{\partial \mathbf{e}_s}{\partial x} = \mathbf{D}_t \mathbf{B}(y) \frac{\partial \mathbf{e}_s}{\partial x} \quad (3.10)$$

Hence, in contrast to the Dual Section Analysis, this formulation only requires information from a cross-section of the frame. Only 1D shear flows are considered, and for this reason, its application is limited to in-plane bending and shear.

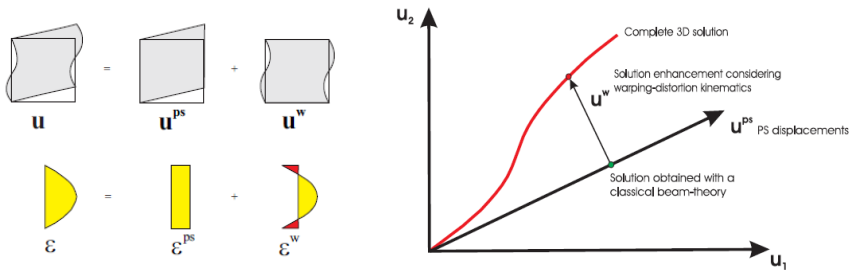
3.2.2.3 THE THEORY OF BAIRÁN-MARÍ

By generalizing the Longitudinal Stiffness Method in 2 dimensions and by applying equations from the theory of continuum solids mechanics, Bairán (2005) proposes a model that solves the problem of the six force interactions at the section level, (Bairán and Marí, 2007a), (Bairán and Marí, 2007b). The model, called TINSA (Total Interaction Nonlinear Sectional Analysis), considers inter-fibre equilibrium without any assumption about the stress or strain distributions that, depending on the state of the section, change continuously.

This is the most elegant and complete sectional model proposed to date. The principal assumption is that sectional displacement field  $\mathbf{u}$  is obtained by enhancing the Bernoulli's plane section theory  $\mathbf{u}^{ps}$  with a three-dimensional warp-distortion field  $\mathbf{u}^w$ , as represented in Fig. 3.8b.



(a) Generalized stresses and infinitesimal equilibrium.



(b) Displacements field decomposition and projections between solutions.

Figure 3.8: TINSA Model, (Bairán, 2005).

It is independent of the constitutive equation, hence any type of 3D model can be used, and as it treats forces and deformations in a single cross section it can be independently implemented in any program of structural analysis, regarding any type of beam element formulation. The model is able to reproduce the force interaction within a cross section, such as coupled normal and tangential forces, for any type and any reinforcement layout. However, its high complexity and computational demanding maxes implementation in structural programs to be quite challenging (Ferreira, 2013).

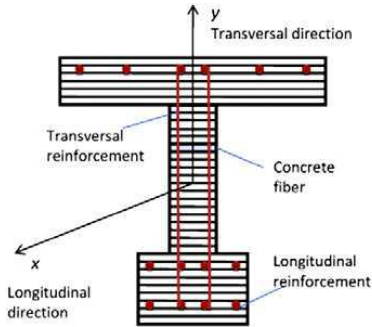
## 3.2.2.4 THE THEORY OF MOHR-BAIRÁN-MARÍ

Motivated by the challenge of extending model TINSÁ from the section to the element level, [Mohr \(2011\)](#) defines shear deformations as a series of polynomials. At the sectional level, this model is more simple with respect to the previous, but it presents a very high level of generality and it considers inter-fibre equilibrium. The same assumption of Bairán's work is taken so that the displacement field  $\mathbf{u}(x, y)$  is due to Bernoulli's plane section theory  $\mathbf{u}^{ps}(x, y)$  plus a warping field  $\mathbf{u}^w(x, y)$  that is expressed as a series of polynomials multiplied by unknown coefficients grouped in vectors  $\mathbf{U}$  and  $\mathbf{V}$ :

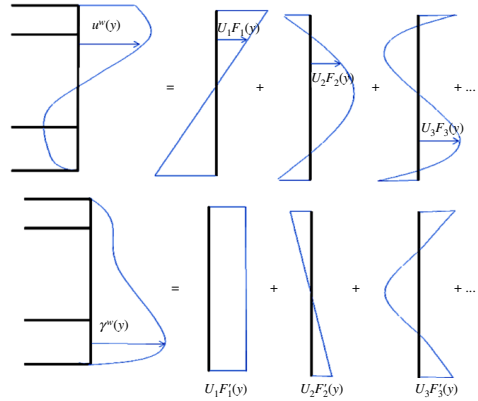
$$\mathbf{u}(x, y) = \mathbf{u}^{ps}(x, y) + \mathbf{u}^w(x, y) \quad (3.11)$$

with:

$$\left\{ \begin{array}{l} u^{ps}(x, y) = u_0 - y \cdot v'_0 \\ v^{ps}(x) = v_0 \end{array} \right. \quad \left\{ \begin{array}{l} u^w(y) = \sum_{i=1}^{n_g} F_{g,i}(y) \cdot u_i = \mathbf{F}_g^T(y) \cdot \mathbf{U} \\ v^w(y) = \sum_{j=1}^{n_e} F_{e,j}(y) \cdot v_j = \mathbf{F}_e^T(y) \cdot \mathbf{V} \end{array} \right. \quad (3.12)$$



(a) Sectional discretization and element nodal displacements.



(b) Deformations as a series of polynomials.

**Figure 3.9:** The Theory of Mohr-Bairán-Marí, ([Mohr et al., 2010](#)).

By using internal compatibility equations, the following expression holds:

$$\begin{bmatrix} \varepsilon_x \\ \varepsilon_y \\ \gamma_{xy} \end{bmatrix} = \begin{bmatrix} \varepsilon_0(x) - y \cdot \chi_0(x) \\ 0 \\ 0 \end{bmatrix} + \begin{bmatrix} 0 \\ \mathbf{F}_e^T(y) \cdot \mathbf{U} \\ \mathbf{F}_g^T(y) \cdot \mathbf{U} \end{bmatrix} \quad (3.13)$$

By introducing the sectional generalized deformations:

$$\mathbf{e}_s = [\varepsilon_0 \quad \gamma_0 \quad \chi_0]^T \quad (3.14)$$

and by taking outside the coefficients  $\mathbf{U}, \mathbf{V}$ , we have:

$$\begin{bmatrix} \varepsilon_x \\ \varepsilon_y \\ \gamma_{xy} \end{bmatrix} = \begin{bmatrix} 1 & 0 & -y \\ 0 & 0 & 0 \\ 0 & 0 & 0 \end{bmatrix} \begin{bmatrix} \varepsilon_0 \\ \gamma_0 \\ \chi_0 \end{bmatrix} + \begin{bmatrix} \mathbf{0}^T & \mathbf{0}^T \\ \mathbf{0}^T & \mathbf{F}'_e{}^T \\ \mathbf{F}'_g{}^T & \mathbf{0}^T \end{bmatrix} \begin{bmatrix} \mathbf{U} \\ \mathbf{V} \end{bmatrix} \quad (3.15)$$

$$\boldsymbol{\varepsilon} = \mathbf{B}^{ps} \mathbf{e}_s + \mathbf{B}^w \mathbf{a}$$

by setting  $\mathbf{a} = [\mathbf{U} \ \mathbf{V}]^T = \mathbf{A} \cdot \mathbf{e}_s$ , the multiaxial strain state in a generic fibre is given by:

$$\boldsymbol{\varepsilon} = \mathbf{B}^{ps} \cdot \mathbf{e}_s + \mathbf{B}^w \cdot \mathbf{A} \cdot \mathbf{e}_s = \boldsymbol{\varepsilon}^{ps} + \boldsymbol{\varepsilon}^w \quad (3.16)$$

where  $\mathbf{B}^{ps}$  is the transformation matrix related with the plane section assumption,  $\mathbf{B}^w$  is the transformation matrix related with the warp-distortion field, and  $\mathbf{A}$  represents the coefficients (unknowns) that modulate the warp-distortion shape functions. Once the values of  $\mathbf{U}$  and  $\mathbf{V}$  are determined (from internal equilibrium considerations), the Virtual Displacement Principle gives the section resisting forces:

$$\begin{aligned} \mathbf{f}_s &= \int_A (\mathbf{B}^{ps} + \mathbf{B}^w \mathbf{A})^T \boldsymbol{\sigma} \, dA = \\ &= \int_A \mathbf{B}^{ps T} \boldsymbol{\sigma} \, dA + \mathbf{A}^T \int_A \mathbf{B}^w T \boldsymbol{\sigma} \, dA \end{aligned} \quad (3.17)$$

whose derivatives gives the section stiffness matrix:

$$\begin{aligned} \mathbf{k}_s &= \int_A (\mathbf{B}^{ps} + \mathbf{B}^w \mathbf{A})^T \mathbf{D}_t (\mathbf{B}^{ps} + \mathbf{B}^w \mathbf{A}) \, dA = \\ &= \int_A \mathbf{B}^{ps T} \mathbf{D}_t \mathbf{B}^{ps} \, dA + \int_A \mathbf{B}^{ps T} \mathbf{D}_t \mathbf{B}^w \, dA \mathbf{A} + \\ &+ \mathbf{A}^T \int_A \mathbf{B}^w T \mathbf{D}_t \mathbf{B}^{ps} \, dA + \mathbf{A}^T \int_A \mathbf{B}^w T \mathbf{D}_t \mathbf{B}^w \, dA \end{aligned} \quad (3.18)$$

By considering different numbers of terms of the series of polynomials different sectional models can be obtained:

- $n_g = 0, n_e = 0$ : Navier Bernoulli beam theory;
- $n_g = 1, n_e = 0$ : Timoshenko beam theory;
- $n_g = 6, n_e = 6$ : Mohr key proposal.

The detailed formulation can be found in (Mohr *et al.*, 2010). This model has been readopted and improved by Le Corvec (2012), in dealing with shear-lag problem in steel beams.



3.2.3 FIXED PATTERN APPROACHES

In this last group of models there are the most direct procedures to estimate the internal shear stress-strain distribution in the cross section. Formally, it is a priori assumed a fixed pattern either for the shear stress or strain and taken it as constant during the whole loading process. Thus, the stress or strain at a point is considered as the value of the assumed pattern multiplied by a generalized quantity of the cross-section state (Bairán, 2005). Two types of Fixed Pattern Approaches are available:

1. the Fixed Strain Approaches:

$$\gamma_{xy}(y) = F_{\gamma}(y) \gamma_0 \quad (3.19)$$

in which the shear response of the cross section is determined by assuming an a priori fixed patter for the tangential strain. This approach has been considered by several authors (Petrangeli *et al.* (1999), Güner (2008), Ceresa *et al.* (2009)), because of its straightforward implementation in a Timoshenko based FE model: the constant distortion of the element is taken as the fixed strain in the cross section.

2. the Fixed Stresses Approaches:

$$\tau_{xy}(y) = F_{\tau}(y) V \quad (3.20)$$

in which the shear response of the cross section is determined by assuming an a priori fixed patter for the tangential stress. This approach is less simple with respect the previous, but in general it gives better results. In (Ferreira, 2013), a Fixed Stress Approach has been proposed.

Although the failure load can be reasonable estimated in some cases with the Fixed Pattern Approaches, the predicted failure mode and the overall non-linear behaviour often do not reflect the real response. In order to compare the accuracy achieved by different models, the result computed by these approximate methods and the more rigorous Dual Section Analysis are presented in Fig. 3.10.

In general, the Fixed Strain Approach underestimates the vertical strains and, hence, predicts lower stresses in the stirrups after the onset of diagonal cracking. In addition, it tends to concentrate the shear stresses in the compressive regions of the section, underestimating the strain in the tension side.

On the contrary, a reasonable chosen Fixed Stress pattern produces a good strain distribution, slightly overestimating the strains and underestimating the stresses.

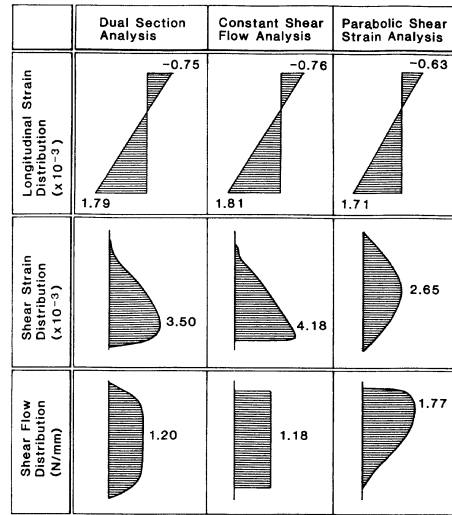


Figure 3.10: Comparisons between shear flow and strain (Vecchio and Collins, 1988).

### 3.3 CLOSING REMARKS

---

Common RC beam-column elements are based on Navier-Bernoulli sectional kinematic that states that (a) section remains plane and (b) shear deformation can be neglected. This leads to monodimensional models with distributed nonlinearity in which the so-called fiber approach is used in order to integrate the material response, that is obtained adopting uniaxial non linear constitutive laws. Such a models address in a very rigorous way only the problem of a RC section subjected to normal forces, such as axial forces and bending moments.

However, if shear acts on the RC section, the Navier-Bernoulli hypothesis is no longer still valid due to the appearance of distortion. As a consequence, common finite beam-column elements based on such a sectional kinematic constraint are no longer applicable and, in order to maintain the model in the 1D domain, improved strategies are needed.

From the presented state of the art, the following observations arise:

- the problem of shear stresses in RC structures is very complex with respect to the problem of normal stresses;
- in Navier-Bernoulli kinematic only the longitudinal strain is active; it's hence clear that if shear's effect has to be account for, classical fiber beam-column elements are not enough;
- since shear in RC structures is not a sectional phenomena, the most intuitive approach is try to model it by using physical models, for instance, the Mörsch's truss analogy;
- in contrast, if we want to use Continuum Mechanic concepts, kinematic must be adequately improved in order to obtained a description not only for the longitudinal strain, but also for the shear and the transversal one, so that a *link* with a 2D constitutive model can be performed.

Several approaches are nowadays existing:

- if the real inter-fiber equilibrium is considered, the highest degree of accuracy is obtained in a frame structural model at the current state of knowledge. The so-obtained models, however, present (a) problems related to numerical instability and (b) a very high computational cost. Since the main goal of a structural theory is to produce synthetic procedures with respect the full 2D numerical approach, it's clear that the implementation of these models in a finite element code is quite challenging;
- it seems hence more convenient the adoption of approximate solutions, based for example on particular strains or stresses patterns, assumed a priori. The so-obtained procedures have, of course, some limitations, but they present higher computational efficiency.

Since shear resistance mechanism in RC elements and the interaction between normal and tangential forces are complex, not clearly defined and not straightforward to model numerically, despite the object of this thesis is to propose a

monodimensional modeling of RC structures, it seems very useful to study at first the problem by bidimensional modeling. Then, by fixing the rules used for 2D and 1D approaches, a complete parallel study can be performed so that the intrinsic approximations of the monodimensional modeling are clearly evident.

In reaching the main object of the thesis - to propose methodologies able to couple the structural analysis with the damage processes and to adequately evaluate the time-evolution of the structural performances by considering environmental hazards - computationally efficiency and stability are strictly required. In this work, hence, two sectional approaches have been considered. The first is a fixed strain approach, in which the strain distribution is assumed a priori, the second is a fixed stress approach, in which an assumed pattern for the shear stress is considered.

Finally, it must be pointed out that, with the framework proposed in this thesis, lifetime predictions can be performed and, to the author's knowledge, the damage effects on shear resistance mechanisms has not been carried out to date.



# 4

## Bidimensional Modeling

*This chapter deals with bidimensional modeling of RC structures. Between the large spectrum of possibilities, smeared type models are chosen. After some historical comments related to shear resistant mechanisms, the Modified Compression Field Theory and the Disturbed Stress Field Model are presented, compared and implemented in a 2D finite element code.*

### 4.1 FROM TRUSSES ANALOGIES TO THE SMEARED APPROACHES

The first model for the description of shear resistant mechanism in reinforced concrete structures (RC) is due to Ritter (1899). Ritter understood that transverse reinforcement introduces a new resisting mechanism, known as “truss-action”, and he proposes a model for the determination of the shear behavior and shear capacity: the so called “truss model”, in which the flow of the stresses is idealized as a series of diagonal concrete struts in compression and tension ties of reinforcement.

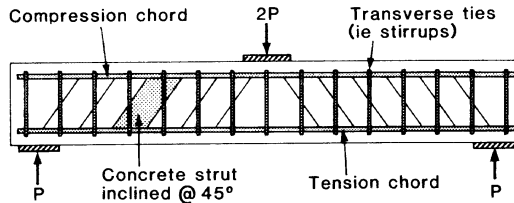


**Figure 4.1:** Truss Analogies Model for concrete beams in shear, adapted from (Vecchio and Collins, 1988).

Mörsch (1902) improved Ritter’s model by substituting the concrete discrete struts with a continuously distributed struts: the so called *compression field*. In addition, he stated that is not possible to find the true crack inclination angle and he proposed the safety value of  $45^\circ$ . This equilibrium-based approach is the basis of the current shear design method.

Some years later, Wagner (1929) proposed the solution to the problem of shear loading of metal beams with very thin web panels. He supposed that after buckling panels are able to support shear forces by a diagonal *tension field*. Wagner was able

to determine the inclination of principal strains and his theory is known as “Tension Field Theory”.

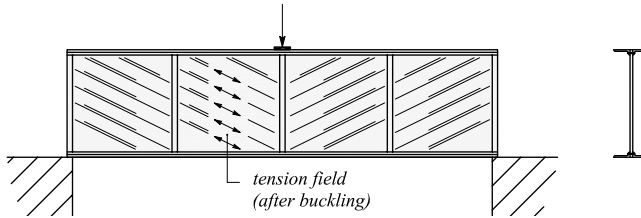


**Figure 4.2:** Metal beam with very thin webs studied by [Wagner \(1929\)](#).

Thirty years later, inspired by Wagner solution, [Kupfer \(1964\)](#), [Baumann \(1970\)](#), [Collins and Lampert \(1973\)](#) solve the problem of determine the crack inclination in RC panels loaded by shear. They worked with linear constitutive laws and by neglecting the concrete tensile strength.

An important effort came from [Robinson and Demorieux \(1968\)](#), who found that concrete compression strength depends on transversal strain: this phenomena is called *compression softening*, Fig. 4.3.

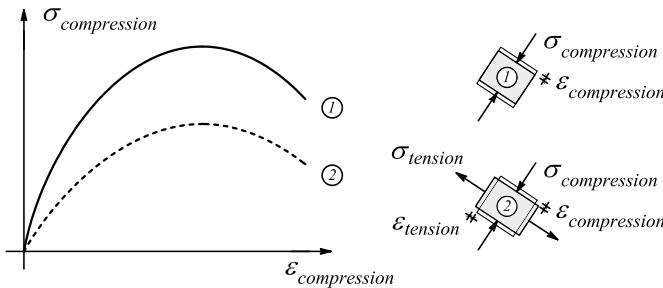


**Figure 4.3:** Compression softening phenomena, ([Robinson and Demorieux, 1968](#)).

By using this last concept, [Collins \(1978\)](#) developed the so-called “Compression Field Theory” - CFT: a smeared model for stress and strains evaluation in RC panels, in which concrete is treated like an anisotropic material with zero tensile strength. The crack inclination angle is taken coincident with the principal compression stress. The theory predicts a shear resistance lower with respect the experimental results. In fact, by neglecting the concrete tensile strength, the aggregate interlock or the dowel action phenomena can’t be described.

An extensive experimental campaign carried out at Toronto University on bidimensional RC panels subjected to plane-stress loading led Vecchio and Collins to the formulation of the so-called “Modified Compression Field Theory” - MCFT, ([Vecchio and Collins, 1986](#)). These tests were carried out on specially build panel-tester, Fig. 4.4.

The MCFT add to the CFT a constitutive law for concrete in tension. In particular, concrete remains linear elastic until the maximum tensile strength is

reached, then a descending branch, representing the interaction between steel and concrete phenomena, is considered.

Parallel to the development of the MCFT, in the University of Houston an experimental campaign on the behavior of RC membranes was carried out by Hsu and his group. As result, a theory named “Rotating-Angle Softened Truss Model” - RA-STM (Hsu, 1998) was developed, differing from the MCFT on the softening model and stress-strain relationships for concrete in compression and tension. The tension-stiffening model in MCFT is referred to the concrete and requires checking the crack state (control of the aggregate interlock), whilst in the RA-STM it is referred to the steel. In this manner, safety check at the crack level is not necessary in the RA-STM, as the stress-strain relation for steel already takes into account the possibility of local yielding at the crack. In addition to this model, the Houston group also proposed the “Fixed-Angle Softened Truss Model” - FA-STM (Pang and Hsu, 1996), which assumes that concrete struts remain with the same inclination as the initial cracks, which can be defined as the principal stress directions in concrete at the onset of cracking (Ferreira, 2013).

In 2000, in order to extend the applicability field of the MCFT and to overcome some critical points highlighted by Hsu, Vecchio proposes the “Disturbed Stress Field Model” - DSFM (Vecchio, 2000b) - (Vecchio, 2001), a sort of intermediate approach between fixed and rotating crack models, in which the principal directions of stresses and strains do not coincide; this difference is taken into account as a shear crack-slip through a strain offset.

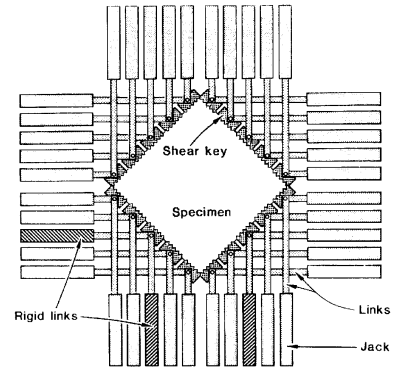


Figure 4.4: Membrane tester.

## 4.2 MODIFIED COMPRESSION FIELD THEORY (MCFT)

---

The Modified Compression Field Theory - MCFT (Vecchio and Collins, 1986) was developed by Vecchio and Collins in 1986 in the context of a wide experimental campaign, as a smeared-crack model with rotating cracks, considering cracked concrete as a material with his own stress-strain relationships.

### 4.2.1 HYPOTHESIS AND SIGN CONVENTIONS

The main assumptions of the MCFT are (Fig. 4.5):

- the reinforcement is considered smeared in concrete;
- cracks are distributed in concrete and are able to rotate continuously;
- loads are applied uniformly in the element;

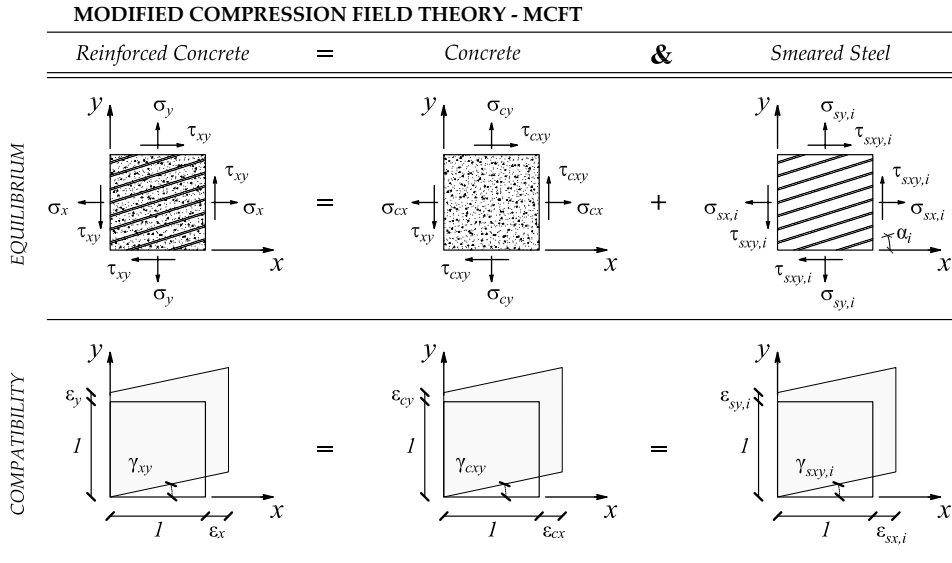


**Figure 4.5:** MCFT: Equilibrium and Compatibility Conditions.

- equilibrium and compatibility equations are evaluated through the average value of the stresses and strains both in the crack plane and in the concrete between cracks;
- local check of the stress state is performed at the crack plane to account for the possible steel yielding;
- principal directions of the stress and strain tensors coincide;
- MCFT is loading history independent;
- it assumes perfect bond between reinforcement and concrete;
- shear stresses in the reinforcement are assumed as null;
- independent constitutive relationships are considered for concrete and steel.

Fig. 4.5 shows the sign convention used for stresses and strains. In addition, it shows the equilibrium and compatibility conditions considered in the theory: for equilibrium, the total stresses in reinforced concrete are given as the sum by stresses in concrete and stresses in smeared reinforcement; instead, due to perfect bond hypothesis, the strains are the same.



### 4.2.2 COMPATIBILITY CONDITIONS

Due to perfect bond between steel and concrete, the following relations hold:

$$\begin{aligned}\varepsilon_x &= \varepsilon_{cx} = \varepsilon_{sx,i} \\ \varepsilon_y &= \varepsilon_{cy} = \varepsilon_{sy,i} \\ \gamma_{xy} &= \gamma_{cxy} = \gamma_{sxy,i}\end{aligned}\quad (4.1)$$

Hence, the kinematic variables of the problem are  $\varepsilon_x$ ,  $\varepsilon_y$  and  $\gamma_{xy}$ .

### 4.2.3 EQUILIBRIUM CONDITIONS

The external actions are taken by concrete and by the  $N$  types of smeared reinforcement; the equilibrium equation in the horizontal direction is:

$$\int_A \sigma_x dA = \int_{A_c} \sigma_{cx} dA + \sum_{i=1}^N \left( \int_{A_{s,i}} \sigma_{sx,i} dA \right) \quad (4.2)$$

By neglecting the reduction in the concrete area due to the presence of steel bars ( $A_c \cong A$ ), the following relation holds:

$$\sigma_x = \sigma_{cx} + \sum_{i=1}^N (\rho_{s,i} \sigma_{sx,i}) \quad (4.3)$$

in which  $\rho_{s,i}$  is the geometric percentage of the  $i$ -th smeared reinforcement. In the same manner, the vertical and rotational equilibrium conditions became:

$$\sigma_y = \sigma_{cy} + \sum_{i=1}^N (\rho_{s,i} \sigma_{sy,i}) \quad (4.4)$$

$$\tau_{xy} = \tau_{cxy} + \sum_{i=1}^N (\rho_{s,i} \tau_{sxy,i}) \quad (4.5)$$

### 4.2.4 CONSTITUTIVE LAWS

Constitutive laws have been calibrated during the extensive experimental campaign carried out at the University of Toronto and involving tests of RC panels subjected to bi-dimensional stress states. 30 square panels, with dimensions  $890\text{ mm} \times 890\text{ mm}$ , width equal to  $70\text{ mm}$ , made of reinforced concrete with two lines of reinforcements, have been tested through a special membrane tester shown in Fig. 4.4.

#### 4.2.4.1 CONCRETE

The concrete constitutive law  $\sigma_c - \varepsilon$  is expressed in the principal strains directions 1, 2. By convention,  $\varepsilon_1 > \varepsilon_2$  with the sign conventions reported in Fig. 4.6. The angle between axis  $y$  and axis 1 is indicated with  $\vartheta$ .

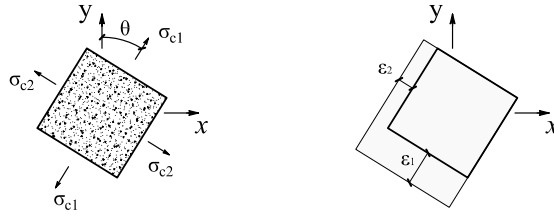


**Figure 4.6:** Convention for average stresses and strains and equilibrium and compatibility conditions.

In compression, the Hognestad parabola is used, as a function of cylindric compression strength  $f'_c$  and strain  $\epsilon'_c$ :

$$\sigma_c = f_{cmax} \left[ 2 \left( \frac{\epsilon}{\epsilon'_c} \right) - \left( \frac{\epsilon}{\epsilon'_c} \right)^2 \right] \quad 2\epsilon'_c \leq \epsilon \leq 0 \quad (4.6)$$

$f_{cmax}$  is a function of the strain  $\epsilon_{\perp}$  in the perpendicular direction. It translates the compression softening effect according to eq. (4.7), as shown in Fig. 4.7:

$$f_{cmax} = \frac{f'_c}{0.8 - 0.34 \epsilon_{\perp} / \epsilon'_c} \leq f'_c \quad (4.7)$$

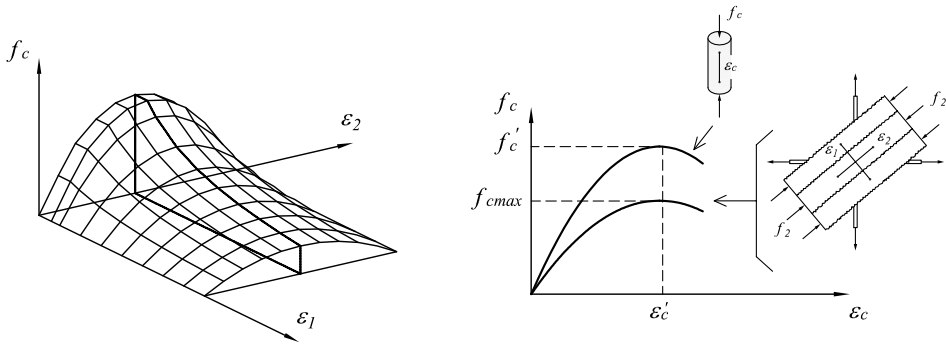


**Figure 4.7:** Compression softening effects in the constitutive laws.

In 2D, the compression softening effects are represented by the dotted curves in Fig. 4.8.

The behavior in tension is described by a linear law until  $f_{cr}$  and then, with discontinuities, with a descending branch that describe an average strength between cracks (tension stiffening effect):

$$\begin{cases} \sigma_c = E_c \epsilon & 0 \leq \epsilon \leq \epsilon_{cr} \\ \sigma_c = \frac{f_{cr}}{1 + \sqrt{200} \epsilon} & 0 \leq \epsilon \leq \epsilon_{cr} \end{cases} \quad (4.8)$$

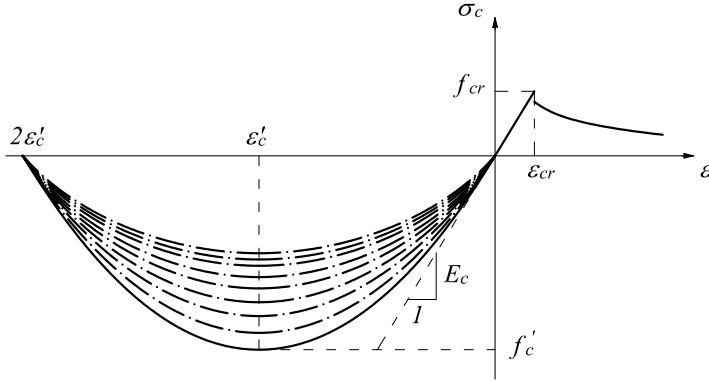


Figure 4.8: Concrete constitutive law.

4.2.4.2 STEEL

The steel constitutive law  $\sigma_{s,i} - \varepsilon$ , for the  $i$ -th smeared line of reinforced, is expressed in the direction defined by the  $i$ -th steel, since it is assumed that steel shear resistance can be neglected. The sign conventions are reported in Fig. 4.9, where  $\alpha_i$  is the angle between the  $x$  axis and the direction of the reinforcement.

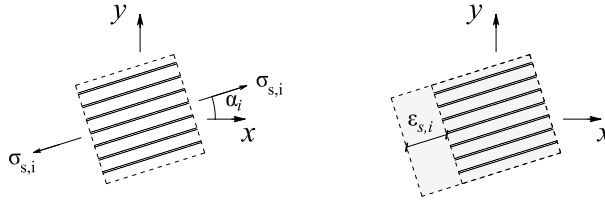


Figure 4.9: Stresses and strains for reinforcement in principal direction.

In relating axial stress to axial strain, the bilinear uniaxial stress-strain relationship shown in Fig. 4.10 is adopted. Thus:

$$\begin{cases} \sigma_{s,i} = E_{s,i} \varepsilon_{s,i} & |\varepsilon_{s,i}| \leq \varepsilon_{y,i} \\ \sigma_{s,i} = \pm f_{y,i} & |\varepsilon_{s,i}| > \varepsilon_{y,i} \end{cases} \quad (4.9)$$

4.2.5 LOADING TRANSMISSION ACROSS THE CRACKS

The stress and strain formulations described deal with average values and do not give information regarding local variations. At a crack, the tensile stresses in the reinforcement will be higher than the average, while midway between cracks they will be lower than the average. The concrete tensile stresses, on the other hand, will be zero at a crack and higher than the average midway between cracks. These local variations are important because the ultimate capacity of a biaxially stressed

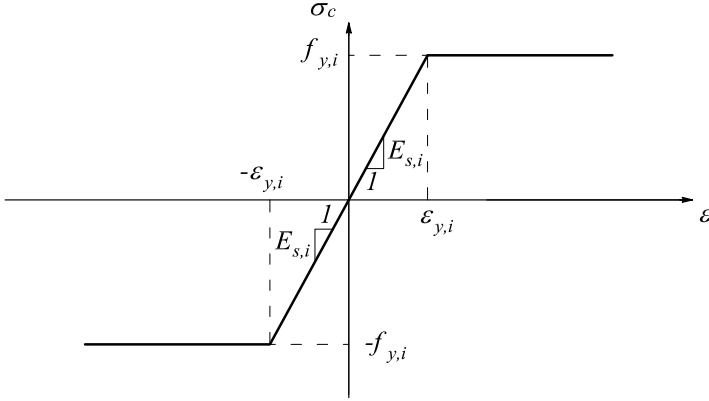


Figure 4.10: Steel constitutive law.

element may be governed by the reinforcement’s ability to transmit tension across the cracks (Vecchio and Collins, 1986).

These aspects can not be considered in the constitutive law and hence a crack check control, between average stresses and stresses across cracks, has been proposed.

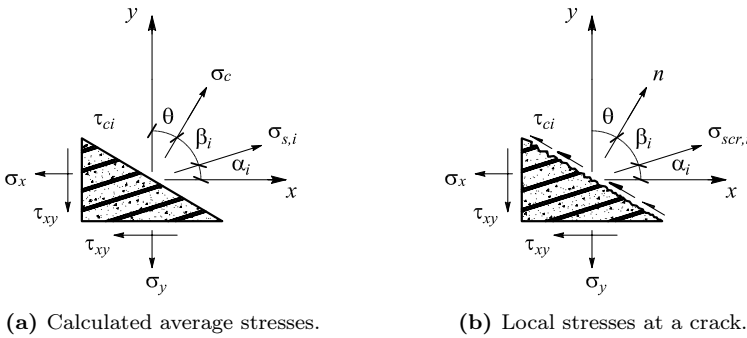


Figure 4.11: Comparisons of local stresses at a crack with calculated average stresses.

With reference to Fig.4.11, the stress in the reinforcement is indicated with  $\sigma_{scr,i}$  and the shear stress due to aggregate interlock with  $\tau_{ci}$ . The static equivalence in normal direction to the crack gives the following expression:

$$\sigma_c = \sum_{i=1}^N (\rho_{s,i} (\sigma_{scr,i} - \sigma_{s,i}) \cos \beta_i^2) \tag{4.10}$$

Since the stress in the reinforcement at a crack cannot exceed the yield strength,

the following limitation holds:

$$\sigma_c \leq \sum_{i=1}^N (\rho_{s,i} (f_{y,i} - \sigma_{s,i}) \cos \beta_i^2) \quad (4.11)$$

The static equivalence of the two systems conduces to the expression:

$$\tau_{ci} = \sum_{i=1}^N (\rho_{s,i} (\sigma_{scr,i} - \sigma_{s,i}) \cos \beta_i \sin \beta_i) \quad (4.12)$$

The shear stress  $\tau_{ci}$  due to aggregate interlock decreases when the crack spacing  $w$  grows and when the maximum aggregate size  $a$  decreases. The original MCFT theory proposes a limitation for  $\tau_{ci}$  on the basis of the aggregate interlock mechanism (Walraven, 1981):

$$\tau_{ci} \leq \frac{\sqrt{f'_c}}{0.31 + 24 w / (a + 26)} \quad (4.13)$$

#### 4.2.6 ADDITIONAL CONDITIONS

In the analysis of adequately reinforced structures, the smeared approach typically provide good results, since the resulting cracks are widely distributed. Instead, several experiences suggest that analysis method based of the smeared rotating crack concept do not adequately model the response of shear-critical concrete beams containing little ( $\rho_s \leq 0.1$ ) or no shear reinforcement (Vecchio, 2000a). In these type of elements, in fact, the crack field is dominated by a limited number of cracks with a spacing that can reach several millimeters. It's clear that this is difficult to describe by a smeared theory with average constitutive laws. In addition, a slip between crack may occur and hence the coincidence between the strains principal axis angle  $\vartheta_\varepsilon$  and the stress one  $\vartheta_\sigma$  is not still valid.

Vecchio proposes two additional controls in order to enhance the original version of the MCFT.

##### 4.2.6.1 CRACK WIDTH LIMIT

In shear critical beam, the formation of a dominant shear crack is localized in a narrow band of elements. In these zones, it is reasonable to discount completely their ability to sustain compressive stresses. Thus, when crack width  $w$  exceeds  $2\text{ mm}$ , the value of the compression stress is limited by using the expressions (Vecchio, 2000a):

$$\begin{aligned} f'_c &= f'_c \left[ 5 - \frac{w}{3} \right] & 2 \leq w \leq 5 \\ f'_c &= 0 & w > 5 \end{aligned} \quad (4.14)$$

##### 4.2.6.2 RESIDUAL TENSION

In the original formulation, the concrete strength after crack is defined by eq. (4.8) and limited through the procedure exposed in par. 4.2.5. However, in members

without shear reinforcement, the latter imposes a compression strength equal to zero (4.11).

In order to avoid this inconvenient problem, the following minimum value is proposed (Vecchio, 2000a):

$$\sigma_c \geq 0.10 f_{cr} \quad (4.15)$$

This additional control produces effects only in element with low amounts of shear reinforcement. In general, it is influential.

### 4.3 DISTURBED STRESS FIELD MODEL (DSFM)

---

Nevertheless it has been proved that Modified Compression Field Theory (MCFT) led generally to good results, some experimental tests show that:

- in the cases of (a) panels with high reinforcement ratio in both directions, (b) panels with high biaxial stresses and (c) panels in which principal inclination angle is limited, MCFT furnishes shear resistance and stiffness generally lower;
- in the case of panels with low reinforcement in one direction, MCFT furnishes shear resistance and stiffness generally higher.

Some examples will be furnished in par. 4.5 on page 74.

The major cause of that discrepancies is due to the hypothesis used about principal direction angle. It is assumed that the principal stresses angle  $\vartheta_\sigma$  is coincident with the principal strains angle  $\vartheta_\varepsilon$ . This hypothesis is generally valid, Fig. 4.12, but since the slip between cracks can not be evaluated, the relative shear stress is not considered and the problems previously exposed born.

In order to extend the applicability field of the MCFT, Vecchio proposes the "Disturbed Stress Field Model" - DSFM (Vecchio, 2000b), a sort of intermediate approach between fixed and rotating crack models, in which the principal directions of stresses and strains do not coincide; this difference is taken into account as a shear crack-slip through a strain offset. In that theory, cracks are perpendicular to the principal tension stress direction, that is not coincident with the principal tension strain direction.

#### 4.3.1 HYPOTHESIS AND SIGN CONVENTIONS

The hypothesis are the same with respect MCFT (see par. 4.2.1 on page 55), with the difference that now the principal direction angle for stresses is not equal to the principal direction angle for strains. Hence, concerning equilibrium the same approach used in MCFT is used, but new compatibility conditions are introduced.

#### 4.3.2 COMPATIBILITY CONDITIONS

The inclusion of the slip between cracks is described by strains superposition:

$$\varepsilon = \varepsilon_c + \varepsilon^s \quad (4.16)$$

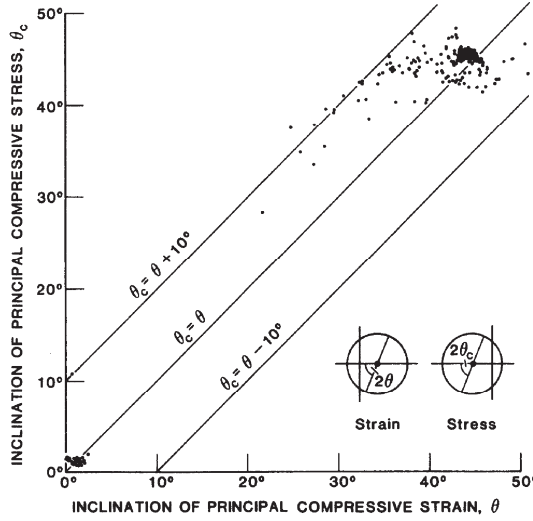


**Figure 4.12:** Comparisons between principal stresses and strains directions, (Vecchio and Collins, 1986).

where  $\varepsilon_c$  is the strain tensor relative to concrete and  $\varepsilon^s$  is the one relative to average crack slip.

From total strains  $\varepsilon$ , Fig. 4.13, the principal strains  $\varepsilon_1$  and  $\varepsilon_2$ , with the relative angle  $\vartheta_\varepsilon$ , can be evaluated using Mohr Circle:

$$\begin{aligned} \varepsilon_{1,2} &= \frac{(\varepsilon_x + \varepsilon_y)}{2} \pm \frac{1}{2} \sqrt{(\varepsilon_x - \varepsilon_y)^2 + \gamma_{xy}^2} \\ \vartheta_\varepsilon &= \frac{1}{2} \arctan \left( \frac{\gamma_{xy}}{\varepsilon_y - \varepsilon_x} \right) \end{aligned} \quad (4.17)$$

In the same manner, from strains  $\varepsilon_c$  the principal strain in concrete  $\varepsilon_{c1}$  and  $\varepsilon_{c2}$  and the relative angle  $\vartheta_\sigma$  are defined as follows:

$$\begin{aligned} \varepsilon_{c1,c2} &= \frac{(\varepsilon_{cx} + \varepsilon_{cy})}{2} \pm \frac{1}{2} \sqrt{(\varepsilon_{cx} - \varepsilon_{cy})^2 + \gamma_{cxy}^2} \\ \vartheta_\sigma &= \frac{1}{2} \arctan \left( \frac{\gamma_{cxy}}{\varepsilon_{cy} - \varepsilon_{cx}} \right) \end{aligned} \quad (4.18)$$

The crack slip  $\delta_s$  (whose expression will be given in par. 4.3.5) is related to an average shear strain  $\gamma^s$ , in direction  $\vartheta_\sigma$ , as Fig. 4.13 shows. By using, once again, Mohr Circle, the corresponding strains  $\varepsilon^s$  in the  $x - y$  reference are:

$$\begin{aligned} \varepsilon_x^s &= -\frac{\gamma^s}{2} \sin 2\vartheta_\sigma \\ \varepsilon_y^s &= +\frac{\gamma^s}{2} \sin 2\vartheta_\sigma \\ \gamma_{xy}^s &= -\gamma^s \cos 2\vartheta_\sigma \end{aligned} \quad (4.19)$$

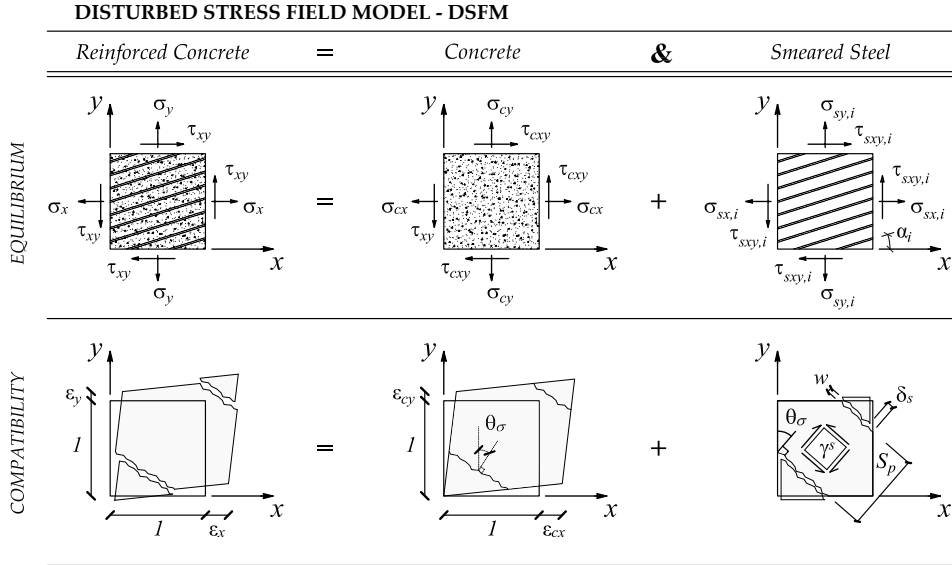


**Figure 4.13:** DSFM: Equilibrium and Compatibility (only for concrete) Conditions.

### 4.3.3 EQUILIBRIUM CONDITIONS

The same equilibrium conditions used in MCFT are considered in the DSFM:

$$\begin{aligned}
 \sigma_x &= \sigma_{cx} + \sum_{i=1}^N (\rho_{s,i} \sigma_{sx,i}) \\
 \sigma_y &= \sigma_{cy} + \sum_{i=1}^N (\rho_{s,i} \sigma_{sy,i}) \\
 \tau_{xy} &= \tau_{cxy} + \sum_{i=1}^N (\rho_{s,i} \tau_{sxy,i})
 \end{aligned} \tag{4.20}$$

### 4.3.4 CONSTITUTIVE LAWS

Constitutive laws have been updated based on new experimental data (Vecchio and Collins, 1993).

#### 4.3.4.1 CONCRETE

The relationship  $\sigma_c - \varepsilon_c$  for concrete is expressed in the principal direction given by  $\varepsilon_c$ , whose inclination is  $\vartheta_\sigma$ . The sign convection is reported in Fig. 4.13 and, as in MCFT, it is considered that  $\varepsilon_1 > \varepsilon_2$ .

Compression softening is described by means of a coefficient  $\beta_d$  that depends



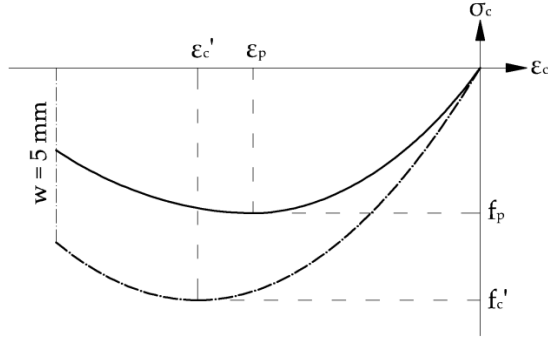


**Figure 4.14:** DSFM: constitutive law for concrete in compression.

on both principal strains and works both on  $f'_c$  and  $\varepsilon'_c$ :

$$\beta_d = \frac{1}{1 + c_s c_d} \leq 1 \quad \text{with:} \quad (4.21)$$

$$c_d = 0.35 \left( -\frac{\varepsilon_{c1}}{\varepsilon_{c2}} - 0.28 \right)^{0.8}$$

$$c_s = 1.00$$

The maximum compression strength and strain are given by:

$$\begin{aligned} f_p &= \beta_d f'_c \\ \varepsilon_p &= \beta_d \varepsilon'_c \end{aligned} \quad (4.22)$$

Concerning compression law, the following relations is proposed:

$$\sigma_{c2} = f_p \frac{n (\varepsilon_{c2}/\varepsilon_p)}{(n-1) (\varepsilon_{c2}/\varepsilon_p)^{nk}} \quad (4.23)$$

where:

$$\begin{aligned} n &= 0.80 - f_p/17 \\ k &= \begin{cases} 1.00 & \varepsilon_p \leq \varepsilon_{c2} \leq 0 \\ 0.67 - f_p/62 & \varepsilon_{c2} \leq \varepsilon_p \end{cases} \end{aligned} \quad (4.24)$$

In tension, concrete constitutive law is equal to that given in eq. (4.8).

#### 4.3.4.2 STEEL

The same constitutive law presented in par. 4.2.4.2 is used.

#### 4.3.5 CRACK SLIP MODELING

The average strains  $\varepsilon^s$  expressed in eq. (4.19) are defined as a function of a smeared deformation  $\gamma_a^s$  that is related to the slip between cracks  $\delta_s$  and to the relative distance  $S_p$  (Fig. 4.13):

$$\gamma_a^s = \frac{\delta_s}{S_p} \quad (4.25)$$

The relative displacement  $\delta_s$  can be written as a function of the cracks width  $w$ , the tangential stresses  $\tau_{ci}$  and the concrete cubic strength resistance  $R_{cm}$  (Walraven, 1981):

$$\delta_s = \frac{\tau_{ci}}{1.8 w^{-0.8} + (0.23 w^{-0.707} - 0.20) R_{cm}} \quad (4.26)$$

The stress  $\tau_{ci}$  that develop trough cracks is evaluated by means of eq. (4.12). However, in case of elements without reinforcement, this approach lead to  $\tau_{ci} = 0$  and so the strain contribution of  $\gamma^s$  is completely neglected. In addition, experimental data have observed that the difference between  $\vartheta_\sigma$  and  $\vartheta_\varepsilon$  (obtained after cracks developing) remains constant until a smeared line of reinforcing yields.

The model, hence, incorporates these aspects by means of the following empirical formulation:

$$\Delta\vartheta_\varepsilon = \vartheta_{ic} - \vartheta_\varepsilon \quad (4.27)$$

$$\begin{cases} \Delta\vartheta_\sigma = \Delta\vartheta_\varepsilon & |\Delta\vartheta_\varepsilon| \leq \vartheta^l \\ \Delta\vartheta_\sigma = \Delta\vartheta_\varepsilon - \vartheta^l & |\Delta\vartheta_\varepsilon| > \vartheta^l \end{cases} \quad (4.28)$$

$$\vartheta_\sigma = \vartheta_{ic} - \Delta\vartheta_\sigma \quad (4.29)$$

where  $\vartheta_{ic}$  is the first crack angle and  $\vartheta^l$  is a constant angle defined as a function of reinforcement's type:

- $\vartheta^l = 5.0^\circ$  if the element is reinforced in both directions;
- $\vartheta^l = 7.5^\circ$  in the other cases.

By using eq. (4.18) and by remembering eq. (4.16), a new deformation  $\gamma_b^s$  due to slip can be obtained:

$$\gamma_b^s = -\gamma_{xy} \cos 2\vartheta_\sigma + (\varepsilon_y - \varepsilon_x) \sin 2\vartheta_\sigma \quad (4.30)$$

The average slip deformation is obtained as follow:

$$\gamma^s = \max[\gamma_a^s, \gamma_b^s] \quad (4.31)$$

It must be pointed out that this hybrid formulation combines the two approaches: for limited stress levels or for elements without reinforcement, the slip deformation is controlled by the constant angle  $\vartheta^l$ ; for high stress levels, the slip deformation is given by the smeared relative displacement  $\delta_s$ .

4.4 REDUCTION OF THE PROBLEM TO ALGEBRAIC FORM

The two theories previously exposed have been implemented in a computer code in which the problem is translated in algebraic form by using standard finite element techniques. In particular, a triangular element is proposed and the numerical approach used to handle the non linearities is based on a secant formulation .

4.4.1 DISPLACEMENT FIELD

Let's consider a solid with volume  $V$  and surface  $S$ , on which the following quantities act:

- volumetric forces  $\mathbf{F}$ ;
- surface forces  $\mathbf{f}$ , acting on  $S_f$ ;
- known displacements  $\mathbf{s}_0$ , acting on  $S_u$ .

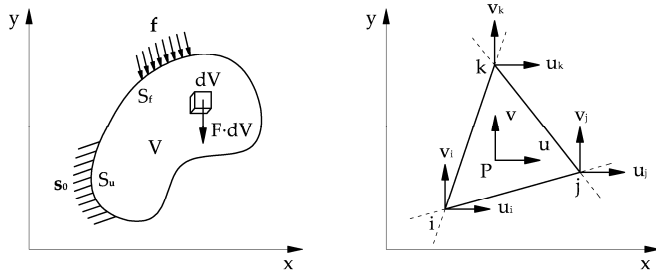


Figure 4.15: Discretization of the continuum domain with a triangular finite element.

Following a displacement-based approach, the continuum solid is divided into finite elements on which displacement shape functions are chosen. By collecting the nodal displacements in the vector  $\mathbf{U}$ :

$$\mathbf{U} = [u_i \ v_i \ u_j \ v_j \ u_k \ v_k]^T \tag{4.32}$$

and by using the linear functions matrix  $\mathbf{N}(x, y)$ :

$$\mathbf{N}(x, y) = \begin{bmatrix} N_1 & 0 & N_2 & 0 & N_3 & 0 \\ 0 & N_1 & 0 & N_2 & 0 & N_3 \end{bmatrix} \tag{4.33}$$

the displacements in the generic  $P$  point of the solid can be written as:

$$\mathbf{u}(x, y) = \begin{bmatrix} u(x, y) \\ v(x, y) \end{bmatrix} = \mathbf{N}(x, y) \mathbf{U} \tag{4.34}$$

Introducing the compatibility equations, the following relation holds:

$$\boldsymbol{\varepsilon} = \begin{bmatrix} \varepsilon_x \\ \varepsilon_y \\ \tau_{xy} \end{bmatrix} = \mathbf{B} \mathbf{U} \tag{4.35}$$

By indicating with  $\mathbf{D}$  the material matrix, the stresses result:

$$\boldsymbol{\sigma} = \begin{bmatrix} \sigma_x \\ \sigma_y \\ \tau_{xy} \end{bmatrix} = \mathbf{D} \boldsymbol{\varepsilon} = \mathbf{D} \mathbf{B} \mathbf{U} \quad (4.36)$$

Clearly, the unknowns of the problem are the nodal displacements  $\mathbf{U}$ .

#### 4.4.2 REFERENCE SYSTEMS

The global unknowns are referred to the global reference system ( $0 - xy$ ) and the constitutive laws are defined in the principal axis reference system ( $0 - 12$ ), Fig. 4.16. In order to determine the stress state of the generic element a coordinate transformation is needed.

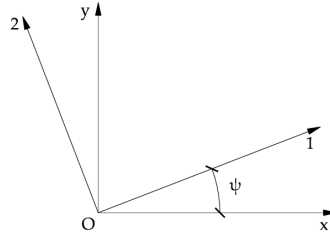


**Figure 4.16:** Global ( $0 - xy$ ) and local ( $0 - 12$ ) reference systems.

By indicating with  $'$  the quantities referred to ( $0 - 12$ ) system, the following relations hold:

$$\begin{aligned} \boldsymbol{\varepsilon}' &= \mathbf{T}_\varepsilon \boldsymbol{\varepsilon} \\ \boldsymbol{\sigma}' &= \mathbf{T}_\sigma \boldsymbol{\sigma} \end{aligned} \quad (4.37)$$

where transformation matrices are ( $c = \cos \Psi$ ,  $s = \sin \Psi$ ):

$$\mathbf{T}_\varepsilon = \begin{bmatrix} c^2 & s^2 & sc \\ s^2 & c^2 & -sc \\ -2sc & 2sc & c^2 - s^2 \end{bmatrix} \quad \mathbf{T}_\sigma = \begin{bmatrix} c^2 & s^2 & 2sc \\ s^2 & c^2 & -2sc \\ -sc & sc & c^2 - s^2 \end{bmatrix} \quad (4.38)$$

for which the following relation holds:

$$\mathbf{T}_\varepsilon^{-1} = \mathbf{T}_\sigma^T \quad (4.39)$$

#### 4.4.3 THE RC TRIANGULAR ELEMENT

As exposed in par. 4.2, the domain of the problem is a RC element with  $n$  smeared types of steel bars. In the following, at first concrete domain and steel domain are separately studied, then they are joined in order to define the state of the element.

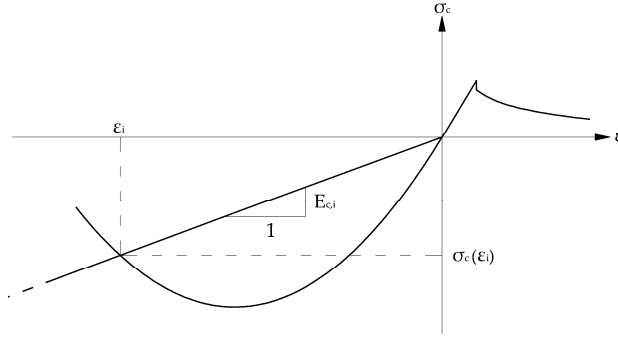


Figure 4.17: Secant concrete modulus.

#### 4.4.3.1 CONCRETE

In the Disturbed Stress Field Model - DSMF - the average deformations  $\varepsilon_c$  in concrete does not coincide with the total deformations  $\varepsilon$ , but they are expressed by using eq. (4.16):

$$\varepsilon_c = \varepsilon - \varepsilon^s \quad (4.40)$$

where the slip deformations  $\varepsilon^s$  are function of the average shear deformation  $\gamma^s$  according to the eqs. reported in par. 4.3.5.

Concrete constitutive laws are expressed in the principal directions, that can be founded as the auto-solutions of the problem:

$$\begin{bmatrix} \varepsilon_{cx} - \varepsilon_i & \gamma_{cxy}/2 \\ \gamma_{cxy}/2 & \varepsilon_{cy} - \varepsilon_i \end{bmatrix} \begin{bmatrix} \cos \vartheta \\ \sin \vartheta \end{bmatrix} = \begin{bmatrix} 0 \\ 0 \end{bmatrix} \quad (4.41)$$

They result:

$$\varepsilon_{c1,c2} = \frac{(\varepsilon_{cx} + \varepsilon_{cy})}{2} \pm \frac{1}{2} \sqrt{(\varepsilon_{cx} - \varepsilon_{cy})^2 + \gamma_{cxy}^2} \quad (4.42)$$

and:

$$\vartheta_\sigma = \vartheta = \begin{cases} \frac{1}{2} \arctan \left( \frac{\gamma_{cxy}}{\varepsilon_{cy} - \varepsilon_{cx}} \right) & \varepsilon_{cy} - \varepsilon_{cx} \geq 0 \\ \frac{\pi}{2} + \frac{1}{2} \arctan \left( \frac{\gamma_{cxy}}{\varepsilon_{cy} - \varepsilon_{cx}} \right) & \varepsilon_{cy} - \varepsilon_{cx} < 0 \end{cases} \quad (4.43)$$

In order to describe the non linear behavior, the secant moduli are used:

$$E_{c1} = \frac{\sigma_c(\varepsilon_{c1})}{\varepsilon_{c1}} \quad E_{c2} = \frac{\sigma_c(\varepsilon_{c2})}{\varepsilon_{c2}} \quad (4.44)$$

whose geometric representation is reported in Fig. 4.17 The tangential modulus, by assuming a Poisson's coefficient  $\nu = 0$  after cracking, can be weighed as follow (Weaver *et al.*, 1984):

$$G_c = \frac{E_{c1} E_{c2}}{E_{c1} + E_{c2}} \quad (4.45)$$

Hence, the stiffness matrix in the principal reference system 0, 12 is:

$$\mathbf{D}'_c = \begin{bmatrix} E_{c1} & 0 & 0 \\ 0 & E_{c2} & 0 \\ 0 & 0 & G_c \end{bmatrix} \quad (4.46)$$

and the stresses are:

$$\boldsymbol{\sigma}'_c = \mathbf{D}'_c \boldsymbol{\varepsilon}'_c \quad (4.47)$$

In order to move from the (0 – 12) reference to the global one, transformation matrices (eq. (4.38)) can be used and the angle  $\Psi$  is:

$$\Psi = \frac{\pi}{2} - \vartheta_\sigma \quad (4.48)$$

By imposing the equality between the internal work in the two reference systems and by remembering eqs. (4.37) the material matrix in the global reference system is obtained:

$$\delta \boldsymbol{\varepsilon}_c^T \boldsymbol{\sigma}_c = \delta \boldsymbol{\varepsilon}'_c{}^T \boldsymbol{\sigma}'_c = \delta \boldsymbol{\varepsilon}'_c{}^T \mathbf{D}'_c \boldsymbol{\varepsilon}'_c = \delta \boldsymbol{\varepsilon}_c^T \mathbf{T}_\varepsilon^T \mathbf{D}'_c \mathbf{T}_\varepsilon \boldsymbol{\varepsilon}_c = \delta \boldsymbol{\varepsilon}_c^T \mathbf{D}_c \boldsymbol{\varepsilon}_c \quad (4.49)$$

hence:

$$\mathbf{D}_c = \mathbf{T}_\varepsilon^T \mathbf{D}'_c \mathbf{T}_\varepsilon \quad (4.50)$$

The stress-strain relationship is finally:

$$\boldsymbol{\sigma}_c = \mathbf{D}_c (\boldsymbol{\varepsilon}_c) \cdot \boldsymbol{\varepsilon}_c \quad (4.51)$$

#### 4.4.3.2 SMEARED STEEL

The constitutive law for the  $i - th$  smeared reinforced steel is expressed in bars direction, because the shear stress due to steel can be neglect. By using, once again, the transformation relationship (4.38) in which:

$$\Psi = \alpha_i \quad (4.52)$$

the following expression holds ( $c = \cos \Psi$ ,  $s = \sin \Psi$ ):

$$\boldsymbol{\varepsilon}_{s,i} = \begin{bmatrix} c^2 & s^2 & cs \end{bmatrix} \begin{bmatrix} \varepsilon_x \\ \varepsilon_y \\ \gamma_{xy} \end{bmatrix} \quad (4.53)$$

Also for the steel a secant modulus is assumed:

$$\bar{E}_{s,i} = \frac{\sigma_{s,i}(\varepsilon_{s,i})}{\varepsilon_{s,i}} \quad (4.54)$$

whose geometric meaning is represented in Fig. 4.18.

Matrix  $\mathbf{D}'_{s,i}$  is:

$$\mathbf{D}'_{s,i} = \begin{bmatrix} E_{s,i} \rho_{s,i} & 0 & 0 \\ 0 & 0 & 0 \\ 0 & 0 & 0 \end{bmatrix} \quad (4.55)$$

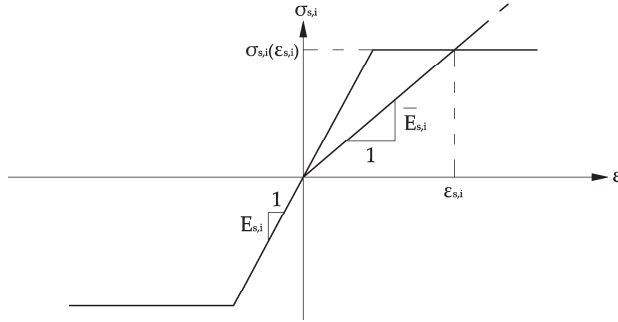


Figure 4.18: Secant steel modulus.

and the constitutive law in the principal reference system is:

$$\boldsymbol{\sigma}'_{s,i} = \begin{bmatrix} \sigma_{s,i} \\ 0 \\ 0 \end{bmatrix} = \begin{bmatrix} E_{s,i} \rho_{s,i} & 0 & 0 \\ 0 & 0 & 0 \\ 0 & 0 & 0 \end{bmatrix} \begin{bmatrix} \varepsilon_{s,i} \\ 0 \\ 0 \end{bmatrix} = \mathbf{D}'_{s,i} \boldsymbol{\varepsilon}'_{s,i} \quad (4.56)$$

In order to move from principal to global reference system, the same procedure exposed for concrete can be used:

$$\boldsymbol{\sigma}_{s,i} = \mathbf{T}_{\varepsilon,i}^T \mathbf{D}'_{s,i} \mathbf{T}_{\varepsilon,i} \boldsymbol{\varepsilon} = \mathbf{D}_{s,i} \boldsymbol{\varepsilon} \quad (4.57)$$

#### 4.4.3.3 REINFORCED CONCRETE: CONCRETE & SMEARED STEEL

In order to obtain the state of the RC element, the solutions related to concrete and steel must be summed, according to the equilibrium equations (4.20). In general,  $n$  type of smeared steel are present:

$$\begin{aligned} \boldsymbol{\sigma} &= \boldsymbol{\sigma}_c + \sum_{i=1}^n \boldsymbol{\sigma}_{s,i} = \mathbf{D}_c \boldsymbol{\varepsilon}_c + \sum_{i=1}^n \mathbf{D}_{s,i} \boldsymbol{\varepsilon} = \mathbf{D}_c (\boldsymbol{\varepsilon} - \boldsymbol{\varepsilon}^s) + \sum_{i=1}^n \mathbf{D}_{s,i} \boldsymbol{\varepsilon} = \\ &= \left( \mathbf{D}_c + \sum_{i=1}^n \mathbf{D}_{s,i} \right) \boldsymbol{\varepsilon} - \mathbf{D}_c \boldsymbol{\varepsilon}^s = \\ &= \mathbf{D} \boldsymbol{\varepsilon} - \mathbf{D}_c \boldsymbol{\varepsilon}^s \end{aligned} \quad (4.58)$$

#### 4.4.3.4 RESISTING FORCES AND ELEMENT STIFFNESS

Resisting forces and element stiffness can be defined through the internal virtual work  $\delta W_i$ :

$$\delta W_i = \int_V \delta \boldsymbol{\varepsilon}^T \boldsymbol{\sigma} dV \quad (4.59)$$

that, according to eq. (4.32) and eq. (4.58), can be written as:

$$\begin{aligned}
 \delta W_i &= \int_V \delta \boldsymbol{\varepsilon}^T \boldsymbol{\sigma} \, dV = \\
 &= \int_V \delta \mathbf{U}^T \mathbf{B}^T (\mathbf{D} \boldsymbol{\varepsilon} - \mathbf{D}_c \boldsymbol{\varepsilon}^s) \, dV = \\
 &= \delta \mathbf{U}^T \left( \int_V \mathbf{B}^T \mathbf{D} \mathbf{B} \, dV \right) \mathbf{U} - \delta \mathbf{U}^T \int_V \mathbf{B}^T \mathbf{D} \boldsymbol{\varepsilon}^s \, dV
 \end{aligned} \tag{4.60}$$

in which  $\mathbf{K}$  is the element stiffness matrix:

$$\mathbf{K} = \int_V \mathbf{B}^T \mathbf{D} \mathbf{B} \, dV \tag{4.61}$$

Adopting a secant approach, the element restoring forces  $\mathbf{F}_{r,e}$  result:

$$\mathbf{F}_{r,e} = \mathbf{K} \mathbf{U} - \int_V \mathbf{B}^T \mathbf{D} \boldsymbol{\varepsilon}^s \, dV = \mathbf{K} \mathbf{U} - \mathbf{F}_e^s \tag{4.62}$$

in which the additional forces  $\mathbf{F}_e^s$  are due to the slip effect accounted for in the DSFM. These forces can be viewed as external forces and, if MCFT is chosen, they result equal to zero since no slip is considered ( $\boldsymbol{\varepsilon}^s = \mathbf{0}$ ).

#### 4.4.4 SECANT SOLUTION AND CONVERGENCE CRITERION

By assembling all the element's contributions given by eq. (4.62), a global system of equilibrium equations can be obtained. Due to non linear material behavior, the system is non linear and requires iterative numerical techniques. It must be pointed out that, in general, not only the stiffness matrix depends from the solution itself, but also the external forces vector due to presence of the slip. We can write:

$$\mathbf{K}_t(\mathbf{s}) = \mathbf{F}_e + \mathbf{F}_e^s(\mathbf{s}) \tag{4.63}$$

where  $\mathbf{K}_t$  is the structure's stiffness matrix,  $\mathbf{F}_e$  is the vector of structural external forces,  $\mathbf{F}_e^s$  is the structural contribution of slip effect and  $\mathbf{s}$  is the global structural displacements vector. The schematic representation of the secant solution scheme is reported in Fig. 4.19. Fig. 4.20 shows the flowchart of the computer code, by putting in evidence the difference between MCFT and DSFM. It must be observed that additional finite elements can be incorporated in the code, just by adding the relative computation of resisting forces and stiffness matrices in the assembling procedure.



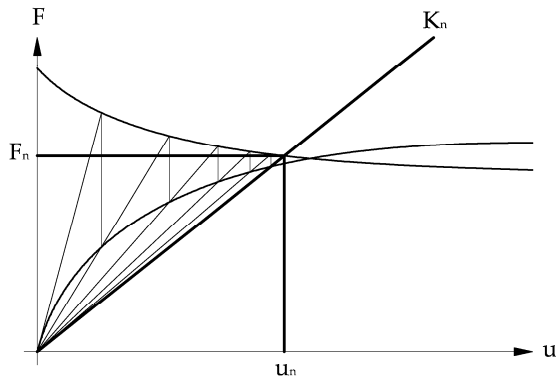
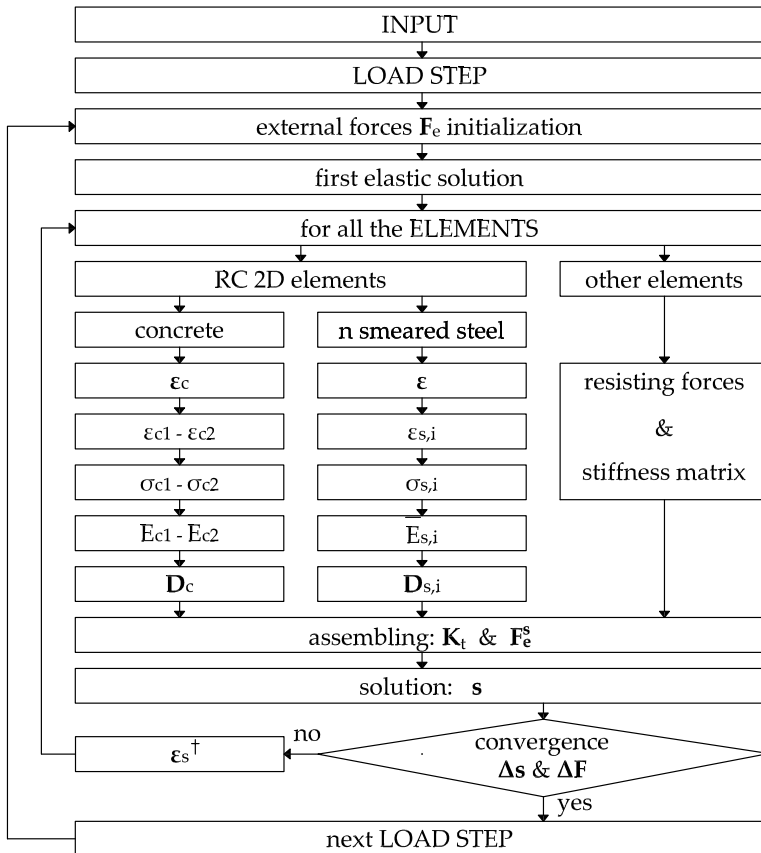


Figure 4.19: Secant solution scheme.



† If MCFT is used:  $\epsilon_s = 0$

Figure 4.20: MCFT & DSFM: flow chart.

## 4.5 VALIDATION AND COMMENTS

Both the theories previous exposed have been implemented in a specific computer code, whose validation is presented now. At first, by focusing the attention on the differences between MCFT and DSFM, some panels used in the definition of the smeared theories are presented. Then, two famous beams in which the collapse is due to shear are considered.

The obtained results show that, in panels, the Disturbed Stress Field Model gives better results with respect the Modified Compression Field Theory, but in more complex structures the differences are very small and, in some case, MCFT gives better results.

### 4.5.1 PV20 PANEL

The first example deals with the PV20 Panel, one of the 30 panels tested for MCFT formulation (Vecchio and Collins, 1986). It is a  $890\text{ mm} \times 890\text{ mm}$  square panel, with a width equal to  $70\text{ mm}$ . The panel is subject by a pure shear action, as Fig. 4.21 shows. The materials characteristics are showed in Tab. 4.1. Concerning the mesh adopted, 4 triangular finite elements are used.

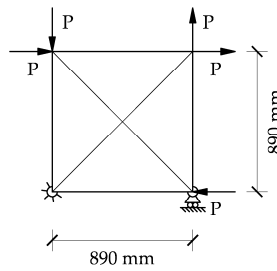


**Figure 4.21:** PV20 Panel: geometry and forces.

$\varepsilon'_c$	$f'_c [MPa]$	$E_c [MPa]$	$f_{cr} [MPa]$	$\varepsilon_{cr}$
$-1.8 \cdot 10^{-3}$	-19.6	21777	1.46	$6.7 \cdot 10^{-5}$

(a) Concrete characteristics.

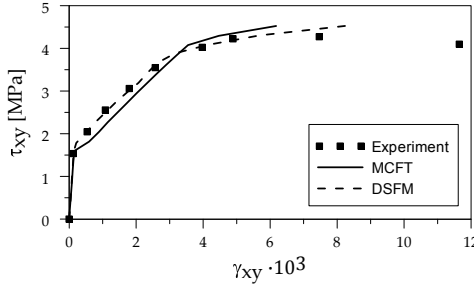
$\alpha [^\circ]$	$f_y [MPa]$	$E_s [MPa]$	$\rho [\%]$
0	460	200000	1.79
90	297	200000	0.89

(b) Reinforcing steel characteristics.

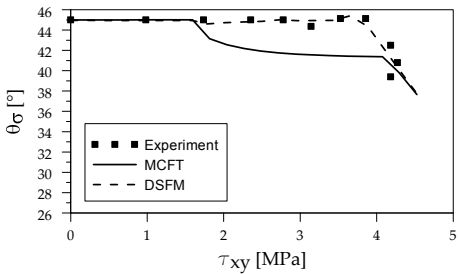
**Table 4.1:** PV20 Panel: materials characteristics.

In Fig. 4.22a, the  $\tau_{xy} - \gamma_{xy}$  curve is presented and a good agreement between experimental and numerical result is observed. Fig. 4.22b and Fig. 4.22c reports,

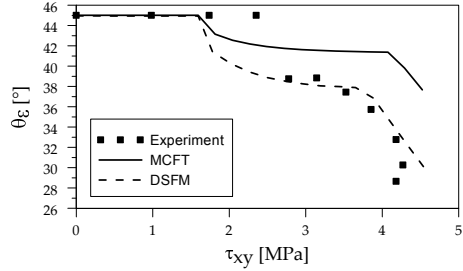
respectively, the  $\vartheta_\sigma - \tau_{xy}$  and the  $\vartheta_\varepsilon - \tau_{xy}$  curves. The conceptual difference between MCFT and DSFM is clearly observed: for MCFT, the two angles are coincident, instead DSFM is able to predict in a more realistic way the experimental result.



(a) Shear stress versus shear strain.



(b) Angle  $\vartheta_\sigma$  versus shear stress.



(c) Angle  $\vartheta_\varepsilon$  versus shear stress.

Figure 4.22: PV20 Panel: comparisons between MCFT and DSFM results.

### 4.5.2 PV23 PANEL

The second validation concerns the PV23 Panel, cited in (Vecchio, 2000b) as typical example in which MCFT predicts both a lower stiffness and a lower ultimate load, due to the contemporaneous presence of shear and biaxial compression state. It is a  $890\text{ mm} \times 890\text{ mm}$  square panel, with a width equal to  $70\text{ mm}$ , Fig. 4.23. Once again, 4 triangular elements are used for the mesh and the materials characteristics are showed in Tab. 4.2.

The  $\tau_{xy} - \gamma_{xy}$  curve is presented in Fig. 4.24, in which a better agreement between experimental result and DSFM is observed.

### 4.5.3 PB20 PANEL

The third example deals with the PB20 Panel, cited in (Vecchio, 2000b) as a typical case in which MCFT predicts both a greater stiffness and a greater ultimate load due to the absence of reinforcing steel in one direction. As Fig. 4.25 shows, it is a  $890\text{ mm} \times 890\text{ mm}$  square panel, with a width equal to  $70\text{ mm}$ . The materials

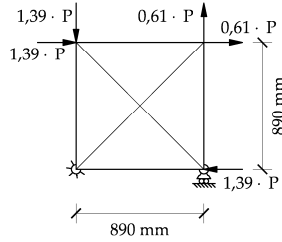


Figure 4.23: PV23 Panel: geometry and forces.

$\varepsilon'_c$	$f'_c [MPa]$	$E_c [MPa]$	$f_{cr} [MPa]$	$\varepsilon_{cr}$
$-2.0 \cdot 10^{-3}$	-20.5	20500	1.76	$8.6 \cdot 10^{-5}$

(a) Concrete characteristics.

$\alpha [^\circ]$	$f_y [MPa]$	$E_s [MPa]$	$\rho [\%]$
0	518	200000	1.79
90	518	200000	1.79

(b) Reinforcing steel characteristics.

Table 4.2: PV23 Panel: materials characteristics.

characteristics are showed in Tab. 4.3; 4 triangular elements are chosen for the structural mesh.

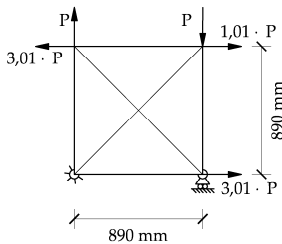
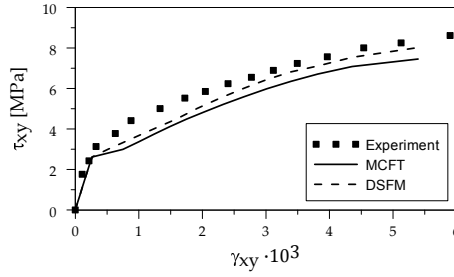


Figure 4.25: PB20 Panel: geometry and forces.

The  $\tau_{xy} - \gamma_{xy}$  curve is presented in Fig. 4.26, in which a better agreement between experimental result and DSFM is observed.

#### 4.5.4 PW3-2 CERVENKA PANEL

The PW3-2 Panel studied in (Cervenka, 1970) is considered. The geometrical characteristics are showed in Fig. 4.27a and the mechanical ones are reported in Tab. 4.4-4.5. The structure has been modeled with 988 triangular finite elements, as Fig. 4.27b shows. It can be observed that both MCFT and DSFM furnish good predictions of the real structural behavior.



**Figure 4.24:** PV23 Panel: shear stress versus shear strain.

$\varepsilon'_c$	$f'_c [MPa]$	$E_c [MPa]$	$f_{cr} [MPa]$	$\varepsilon_{cr}$
$-2.0 \cdot 10^{-3}$	-21.7	21700	1.79	$8.3 \cdot 10^{-5}$

(a) Concrete characteristics.

$\alpha [^\circ]$	$f_y [MPa]$	$E_s [MPa]$	$\rho [\%]$
0	424	200000	2.2

(b) Reinforcing steel characteristics.

**Table 4.3:** PB20 Panel: materials characteristics.

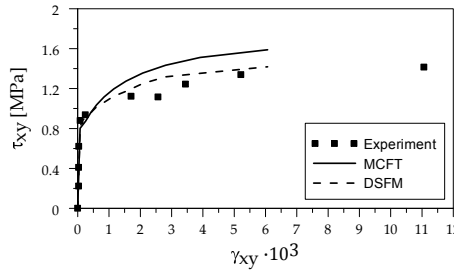


**Figure 4.26:** PB20 Panel: shear stress versus shear strain.

$\varepsilon'_c$	$f'_c [MPa]$	$E_c [MPa]$	$f_{cr} [MPa]$	$\varepsilon_{cr}$
$-1.8 \cdot 10^{-3}$	-26.8	20000	1.71	$8.5 \cdot 10^{-5}$

**Table 4.4:** PW3-2 Cervenka Panel: concrete characteristics.

$\alpha [^\circ]$	$f_y [MPa]$	$E_s [MPa]$	$\rho [\%]$
0 ( <i>inf</i> )	353	190000	1.83
0 ( <i>inf</i> )	353	190000	0.92
90	353	190000	0.92

**Table 4.5:** PW3-2 Cervenka Panel: reinforcing steel characteristics.

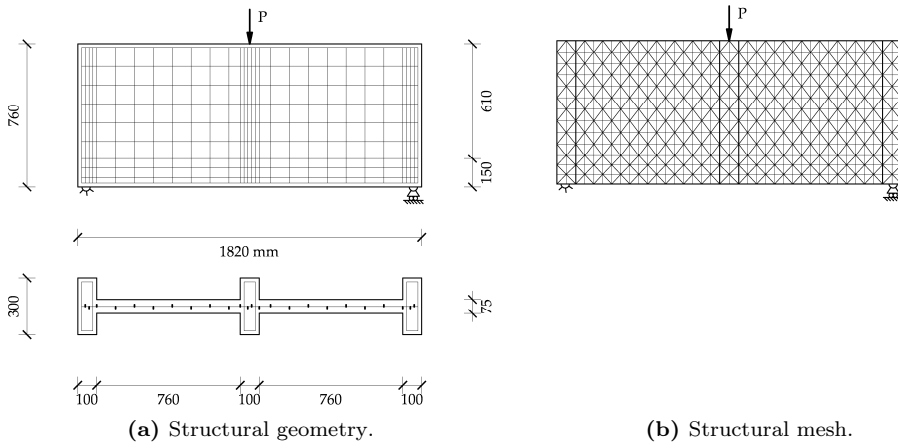


Figure 4.27: PW3-2 Cervenka Panel: geometry and mesh.

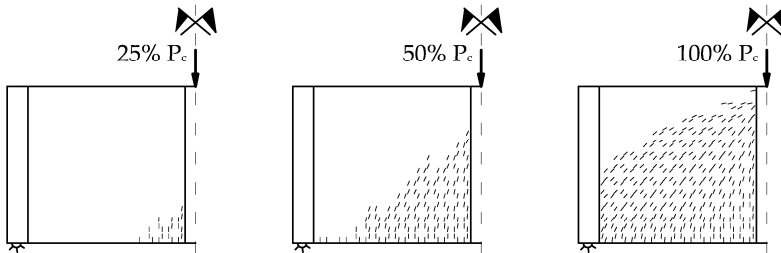


Figure 4.28: PW3-2 Cervenka Panel: numerical crack patterns.

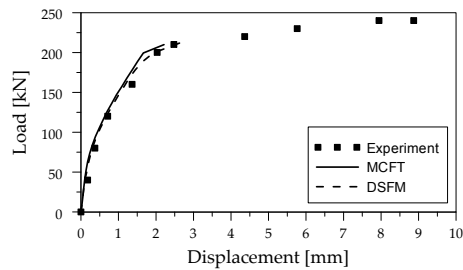
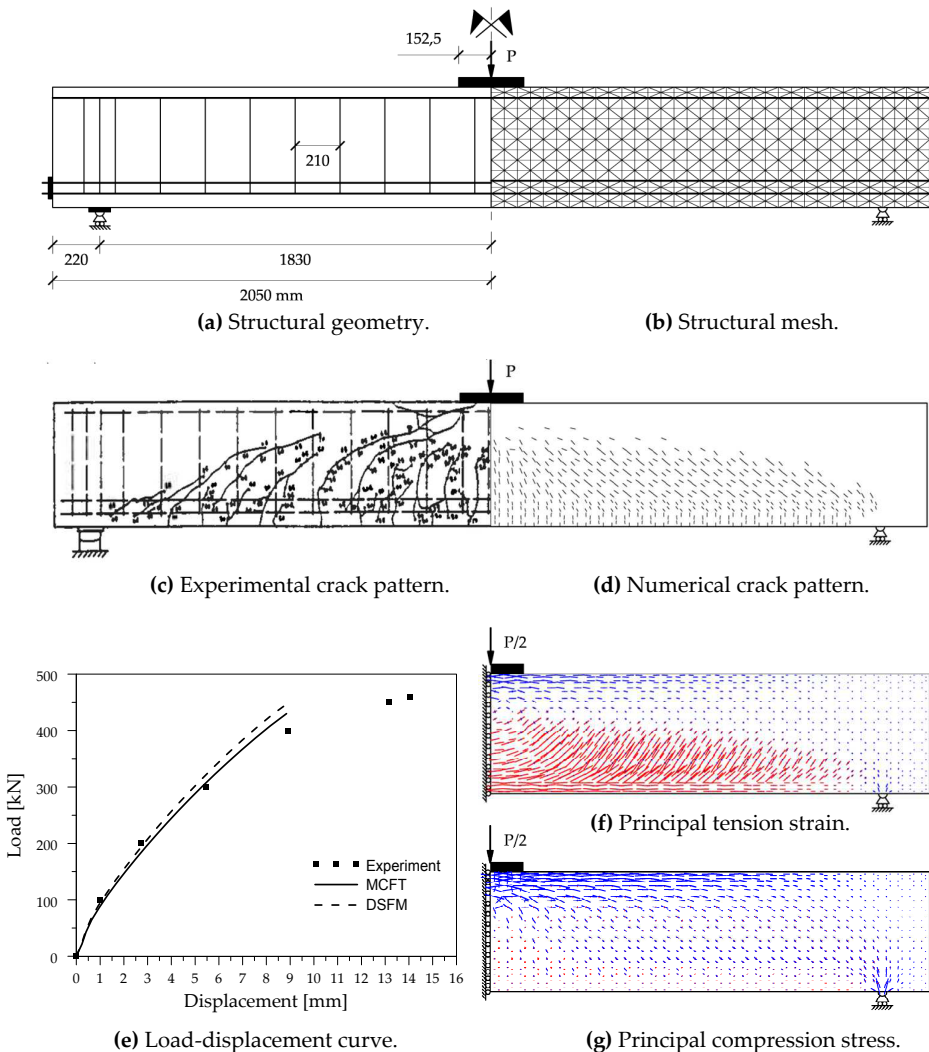


Figure 4.29: PW3-2 Cervenka Panel: force versus displacement.

## 4.5.5 A1 BRESLER &amp; SCORDELIS BEAM

The last example deals with A1 Beam, tested by [Bresler and Scordelis \(1963\)](#). It is a simply supported beam design in order to obtain a shear collapse. The geometry of the structure is reported in Fig. 4.30a and Fig. 4.31, and the mesh used (made of 952 triangular elements) in Fig. 4.30b. The materials characteristics are detailed in Tab. 4.6.



**Figure 4.30:** A1 Bresler & Scordelis Beam: geometry, mesh and results.

By observing (a) the principal deformation pattern, (b) the principal stresses pattern and (c) the crack pattern, the load transfer mechanism can be explained. In fact, it's clear that a smeared compression field is present in the beam's web and the collapse can be described by Mörsh analogy ([Mörsh, 1902](#)) (see par. 4.1).

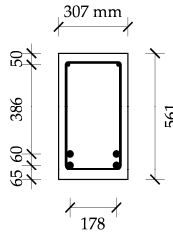


**Figure 4.31:** A1 Bresler & Scordelis Beam: geometry of the section.

$\varepsilon'_c$	$f'_c$ [MPa]	$E_c$ [MPa]	$f_{cr}$ [MPa]	$\varepsilon_{cr}$
$-1.8 \cdot 10^{-3}$	-24.1	26778	1.62	$6.0 \cdot 10^{-5}$

(a) Concrete characteristics.

$\alpha$ [°]	$f_y$ [MPa]	$E_s$ [MPa]	$\rho$ [%]
90	325	190000	0.1

(b) Reinforcing smeared steel.

bars	$f_y$ [MPa]	$E_s$ [MPa]	$\phi$ [mm]
sup.	345	201000	$2\phi 12.7$
inf.	555	218000	$4\phi 28.7$

(c) Reinforcing longitudinal steel.

**Table 4.6:** A1 Bresler & Scordelis Beam: materials characteristics.

## 4.6 CLOSING REMARKS

This chapter presents the bidimensional modeling of RC structures, focusing the attention on smeared type models. Two well know smeared theories have been recalled and compared: the Modified Compression Field Theory (MCFT) and the Disturbed Stress Field Model (DSFM).

MCFT has been presented in 1986. Such a theory presents some intrinsic limitations that can be solved by introducing additional controls, such as a crack check control, a crack limit width, or a residual tension control. However, one of the most restricting hypothesis of MCFT is that the principal stresses angle  $\vartheta_\sigma$  is coincident with the principal strains angle  $\vartheta_\varepsilon$ , and hence crack slip cannot be evaluated.

In order to overcome these intrinsic limitations, an enhanced theory - the DSFM - has been presented in 2000. This theory is a sort of intermediate approach between fixed and rotating crack models, in which cracks are perpendicular to the principal tension stress direction, not coincident with the principal tension strain one.

Both the theories have been implemented in a finite element code and some typical examples have been presented. The main result is that DSFM is effectively able to describe more in detail the structural behavior in dealing with the specific panels in which MCFT clearly exhibits its intrinsic approximations. However, in dealing with more complex structures, the differences decrease and for his simplicity, MCFT can be considered a powerful tool in predicting the structural response of RC beams in shear.



# 5

## Monodimensional Modeling

*This chapter deals with the definition of the state of a generic reinforced concrete section by considering shear's effects, with the aim of formulating shear flexible beam-column elements. Despite several strategies have been proposed until now, this problem leads to a rather complex model, whose numerical implementation is not straightforward as happen in dealing with normal stresses.*

### 5.1 GLOBAL FRAMEWORK

The global structural framework is explained with reference to Fig. 5.1. The real generic structure of Fig. 5.1a is discretized in monodimensional elements as Fig. 5.1b shows.

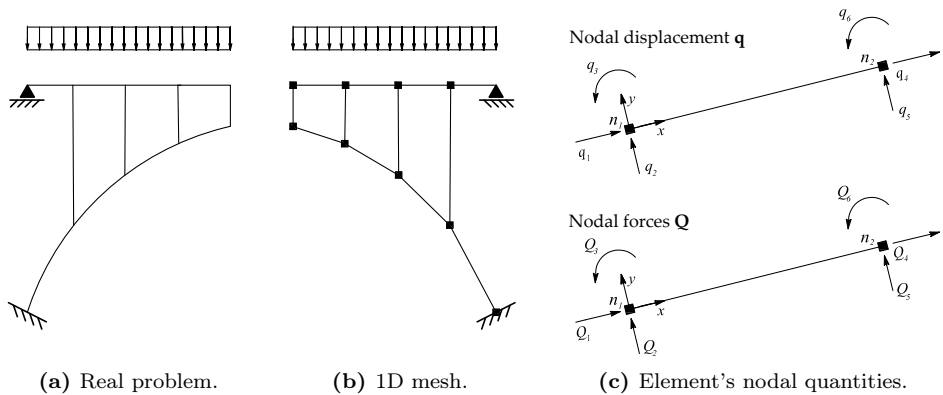


**Figure 5.1:** Global Analysis Framework. Real structure, structural mesh and element's nodal quantities.

By using a global displacement approach, the unknowns of the problem are the global displacements  $\mathbf{s}$ . The external loads acting on the system are transformed in equivalent nodal forces that can be collected in a vector  $\mathbf{F}_e$ . Aim of the finite element analysis is to find the *State of the Structure* so that the resisting structural forces  $\mathbf{F}_r$  are equal to the external ones:

$$\mathbf{F}_r(\mathbf{s}) = \mathbf{F}_s(\mathbf{s}) \quad (5.1)$$

This is, in general, a non linear system of equations since both the external and the resisting forces may depends on the solution itself, represented by the nodal structural displacements  $\mathbf{s}$ .

The system shows in eq. (5.1) is obtained by assembling the state of the elements in which the structure is discretized. The element's nodal quantities are showed in Fig. 5.1c; the element's nodal displacements are collected in vector  $\mathbf{q}$ , as follow:

$$\mathbf{q} = [q_1 \quad q_2 \quad q_3 \quad q_4 \quad q_5 \quad q_6]^T$$

and the element's nodal forces are grouped in vector  $\mathbf{Q}$ :

$$\mathbf{Q} = [Q_1 \quad Q_2 \quad Q_3 \quad Q_4 \quad Q_5 \quad Q_6]^T$$

The element state determination process - evaluate the nodal forces  $\mathbf{Q}$  given the nodal displacement  $\mathbf{q}$  - can be accomplished by the procedures exposed in par. 2.3.1, if the element is displacement-based, or the ones exposed in par. 2.4.2 if a force-based element is considered.

### 5.1.1 ELEMENT: RESISTING FORCES AND STIFFNESS MATRIX

As already explained in Chapter 2, the state of a 1D element with distributed nonlinearities can be obtained by weighting the sectional states with the expressions (2.9) and (2.10) that here are recalled:

$$\mathbf{Q} = \int_0^l \mathbf{B}^T \mathbf{f}_{s,r} dx \quad \mathbf{k} = \int_0^l \mathbf{B}^T \mathbf{k}_s \mathbf{B} dx$$

where  $\mathbf{Q}$  is the already cited vector containing the element's nodal forces,  $\mathbf{k}$  is the element stiffness matrix due to mechanical non linearities only. These quantities are obtained by integrating along the element's axis ( $x$ -axis) the section resisting forces  $\mathbf{f}_{s,r}$  and the section stiffness matrix  $\mathbf{k}_s$  respectively.

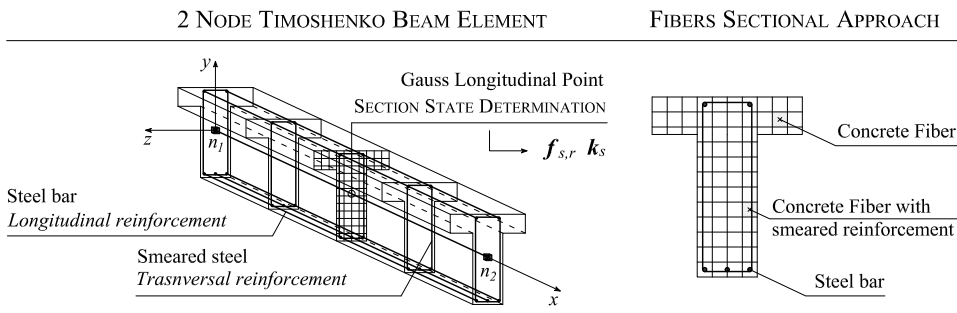


**Figure 5.2:** The 2 Node shear-flexible beam-column element.

The problem of defining the state of the structure is moved, in this way, to the definition of the element, that can be done both with a displacement approach and a flexibility one. Despite the choice adopted, the state of the element requires the definition of the state of the section.

It's clear, hence, that the definition of the structural state is moved, by nested levels, to the definition of the sectional state, that is composed with fibers. In common finite beam-column element, the state of the section is obtained by direct integration of fiber's stresses. Here, instead, aiming of formulate shear-flexible beam-column elements, also the state of the generic fiber must be obtained and, as it will be exposed in the next, it requires the solution of a non linear system of equations.

### 5.1.2 SECTION: RESISTING FORCES AND STIFFNESS MATRIX

As explained, in order to formulate a monodimensional finite element, the Section State Determination process must be performed. If in the Element State Determination process the goal is to find the element resisting forces  $\mathbf{Q}$  and the element stiffness matrix  $\mathbf{k}$ , concerning the section, the goal is to find the section resisting forces  $\mathbf{f}_{s,r}$  and the section stiffness matrix  $\mathbf{k}_s$ .

By considering Timoshenko kinematic, plane section hypothesis is assumed and a mean shear strain  $\gamma_0$  is considered. With reference to Fig. 5.3, a generic point  $P$  moves to point  $P'$ .

By using the small rotations hypothesis, the sectional displacements ( $u$  and  $v$ ) can be written as:

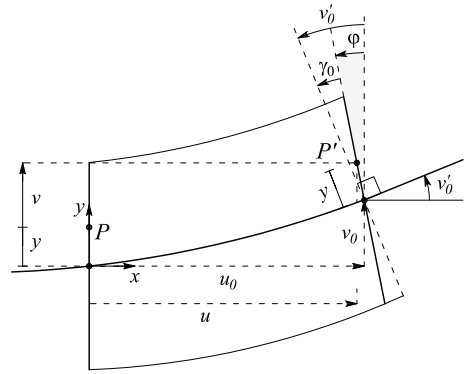


Figure 5.3: Timoshenko's kinematic.

$$\begin{cases} u(x, y) = u_0(x) - y \cdot \varphi(x) \\ v(x) = v_0(x) \end{cases} \quad (5.2)$$

or, in matrix form:

$$\begin{bmatrix} u(x, y) \\ v(x) \end{bmatrix} = \begin{bmatrix} 1 & 0 & -y \\ 0 & 1 & 0 \end{bmatrix} \begin{bmatrix} u_0(x) \\ v_0(x) \\ \varphi(x) \end{bmatrix} \quad (5.3)$$

$$\mathbf{u}(x, y) = \mathbf{a}_s(y) \mathbf{u}_s(x)$$

where  $\mathbf{a}_s$  is the interpolate section matrix that depends only from the geometry of the section ( $y$ ), and  $\mathbf{u}_s$  is the vector containing the generalized sectional displacements that depends on the position of the section ( $x$ ).

By applying the internal compatibility equations, the following strains result:

$$\begin{cases} \varepsilon_x = \frac{\partial u}{\partial x} = \frac{\partial}{\partial x} (u_0 - y \cdot \varphi) = \frac{\partial u_0}{\partial x} - y \frac{\partial \varphi}{\partial x} & \equiv \varepsilon_0 - y \cdot \chi_0 \\ \varepsilon_y = \frac{\partial v}{\partial y} = \frac{\partial}{\partial y} (v_0(x)) & \equiv 0 \\ \gamma_{xy} = \frac{\partial u}{\partial y} + \frac{\partial v}{\partial x} = \frac{\partial}{\partial x} (v_0) + \frac{\partial}{\partial y} (u_0 - y \cdot \varphi) = \frac{\partial v_0}{\partial x} - \varphi & \equiv \gamma_0 \end{cases} \quad (5.4)$$

In Timoshenko kinematic, hence, only two strains can be described and, by using once again a matrix notation, they result as follow:

$$\begin{aligned} \begin{bmatrix} \varepsilon_x(x, y) \\ \gamma_{xy}(x) \end{bmatrix} &= \begin{bmatrix} 1 & 0 & -y \\ 0 & 1 & 0 \end{bmatrix} \begin{bmatrix} \varepsilon_0(x) \\ \gamma_0(x) \\ \chi_0(x) \end{bmatrix} \\ \bar{\boldsymbol{\varepsilon}}(x, y) &= \mathbf{a}_s(y) \mathbf{e}_s(x) \end{aligned} \quad (5.5)$$

where  $\varepsilon_0$  is axial deformation,  $\gamma_0$  is the mean shear strain,  $\chi_0$  is the curvature, that are collected in the section generalized strain vector  $\mathbf{e}_s$ . An over line is used on  $\boldsymbol{\varepsilon}$  in order to indicate that in Timoshenko kinematic we don't deal with the full strain tensor  $\boldsymbol{\varepsilon} = [\varepsilon_x \ \varepsilon_y \ \gamma_{xy}]^T$ , but only with a reduced one  $\bar{\boldsymbol{\varepsilon}} = [\varepsilon_x \ \gamma_{xy}]^T$  in which, according to eq. (5.4),  $\varepsilon_y$  is not present.

The section resisting forces can be defined through the Virtual Displacement Principle, by looking at the internal work:

$$\delta W_i = \int_A \delta \bar{\boldsymbol{\varepsilon}}^T \bar{\boldsymbol{\sigma}} \, dA = \int_A \delta \mathbf{e}_s^T \mathbf{a}_s^T \bar{\boldsymbol{\sigma}} \, dA = \delta \mathbf{e}_s^T \int_A \mathbf{a}_s^T \bar{\boldsymbol{\sigma}} \, dA = \delta \mathbf{e}_s^T \mathbf{f}_{s,r} \quad (5.6)$$

in which also  $\boldsymbol{\sigma}$  is over lined to indicate that we are moving in the reduced Timoshenko domain. The section resisting forces result:

$$\mathbf{f}_{s,r} = \int_A \mathbf{a}_s^T \bar{\boldsymbol{\sigma}} \, dA = \int_A \begin{bmatrix} 1 & 0 \\ 0 & 1 \\ -y & 0 \end{bmatrix} \begin{bmatrix} \sigma_x \\ \tau_{xy} \end{bmatrix} \, dA = \begin{bmatrix} N \\ V \\ M \end{bmatrix} \quad (5.7)$$

The section stiffness matrix can be obtained by using its definition, as follow:

$$\begin{aligned} \mathbf{k}_s &= \frac{\partial \mathbf{f}_{s,r}}{\partial \mathbf{e}_s} = \frac{\partial}{\partial \mathbf{e}_s} \int_A \mathbf{a}_s^T(y) \bar{\boldsymbol{\sigma}}(\bar{\boldsymbol{\varepsilon}}(\mathbf{e}_s)) \, dA = \\ &= \int_A \mathbf{a}_s^T(y) \frac{\partial}{\partial \mathbf{e}_s} (\bar{\boldsymbol{\sigma}}(\bar{\boldsymbol{\varepsilon}}(\mathbf{e}_s))) \, dA = \int_A \mathbf{a}_s^T(y) \frac{\partial \bar{\boldsymbol{\sigma}}}{\partial \bar{\boldsymbol{\varepsilon}}} \frac{\partial \bar{\boldsymbol{\varepsilon}}}{\partial \mathbf{e}_s} \, dA = \\ &= \int_A \mathbf{a}_s^T(y) \frac{\partial \bar{\boldsymbol{\sigma}}}{\partial \bar{\boldsymbol{\varepsilon}}} \frac{\partial}{\partial \mathbf{e}_s} (\mathbf{a}_s(y) \mathbf{e}_s) \, dA = \\ &= \int_A \mathbf{a}_s^T(y) \frac{\partial \bar{\boldsymbol{\sigma}}}{\partial \bar{\boldsymbol{\varepsilon}}} \mathbf{a}_s(y) \, dA = \\ &= \int_A \mathbf{a}_s^T(y) \bar{\mathbf{D}}_t \mathbf{a}_s(y) \, dA \end{aligned} \quad (5.8)$$

in which  $\bar{\mathbf{D}}_t$  is the tangent material matrix. Once again, an over-line is used since in Timoshenko beam theory this matrix has dimension  $[2 \times 2]$  and not  $[3 \times 3]$  as in the case of the complete plane domain. This is due to the fact that the active deformations are only  $\varepsilon_x$  and  $\gamma_{xy}$ , with  $\varepsilon_y$  equal to zero.

Concerning the exposed formulation, it deals with a generically non linear Timoshenko beam. The domain in which this theory moves is a reduction of the real plane domain. It's clear, hence, that in order to link this beam theory with the smeared constitutive law assumed for RC elements and exposed in the previous Chapter, additional considerations are needed as it will be explained in par. 5.2.1.

5.2 SPECIALIZATION TO RC SECTIONS

As exposed, the sectional resisting forces (eq. (5.7)) and the stiffness matrix (eq. (5.8)) are obtained, respectively, by integrating the stresses and the material constitutive matrix over the sectional domain. Clearly, a numerical integration process is needed and, since reinforced concrete is a composite material made of concrete and steel, with reference to Fig. 5.4, the generic section is decomposed in:

1. concrete fibers (with smeared transversal steel);
2. longitudinal bars;

and the sectional resisting forces and stiffness matrix are decompose as:

$$\begin{aligned} \mathbf{f}_{s,r} &= \mathbf{f}_{s,r}^C + \mathbf{f}_{s,r}^S \\ \mathbf{k}_s &= \mathbf{k}_s^C + \mathbf{k}_s^S \end{aligned} \tag{5.9}$$

in which the upper notation <sup>C</sup> is to indicate concrete contribution (with or without smeared transversal steel), and <sup>S</sup> is referred to longitudinal steel only.

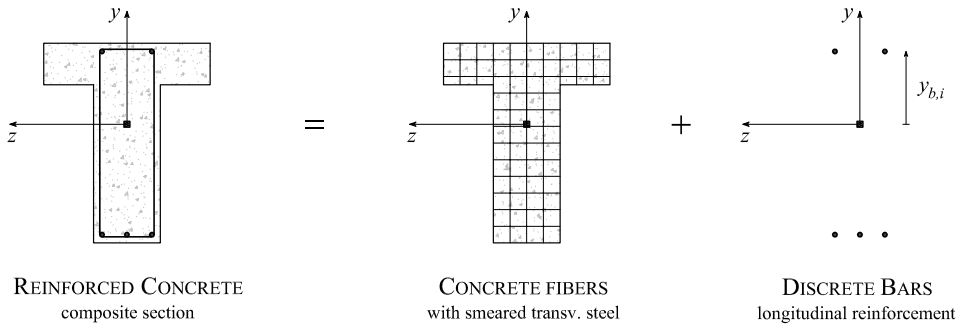


Figure 5.4: RC section: fibers with smeared steel and longitudinal bars.

5.2.1 CONCRETE FIBERS WITH SMEARED TRANSVERSAL STEEL

As clearly highlighted in the previous equations, Timoshenko beam theory works with a sub-part of the problem. In particular, since  $\varepsilon_y \equiv 0$ ,  $\bar{\sigma}$  does not contain  $\sigma_y$  and the dimension of matrix  $\bar{\mathbf{D}}_t$  is not  $[3 \times 3]$ , but  $[2 \times 2]$ . Hence, in order to apply a smeared approach at the fiber level, some additional informations are needed since we have to link the Timoshenko domain with the full plane tensor:

$$\begin{aligned} \begin{bmatrix} \sigma_x \\ \sigma_y \\ \tau_{xy} \end{bmatrix} &= \begin{bmatrix} D_{11} & D_{12} & D_{13} \\ D_{21} & D_{22} & D_{23} \\ D_{31} & D_{32} & D_{33} \end{bmatrix} \begin{bmatrix} \varepsilon_x \\ \varepsilon_y \\ \gamma_{xy} \end{bmatrix} \\ \boldsymbol{\sigma} &= \mathbf{D} \boldsymbol{\varepsilon} \end{aligned} \tag{5.10}$$

Concerning constitutive laws, remember the nature of the problem (see Chapter 3): if we can adequately assume a constitutive uniaxial law for concrete  $\sigma = \sigma(\varepsilon)$ ,

it's not possible to obtain a similar law concerning  $\tau = \tau(\gamma)$ . That is why a link with a plane model, such as the ones presented in Chapter 4, is here performed.

In order to move from the real domain to the reduced one, the condition that the total stress in the concrete must be equilibrated by the transversal steel is used in each fiber, according to (Petrangeli *et al.*, 1999) and (Petrangeli, 1999):

$$\sigma_y = \sigma_{c,y} + \sigma_{s,y} = 0 \quad (5.11)$$

This condition permits to work with the complete domain and to obtain, for each fiber, his matrix  $\mathbf{D}$ . Then, however, a static condensation of  $\varepsilon_y$  must be applied in order to come back in the Timoshenko domain. By expanding eq. (5.11) the following expression is obtained:

$$\sigma_y = D_{21} \cdot \varepsilon_x + D_{22} \cdot \varepsilon_y + D_{23} \cdot \gamma_{xy} = 0 \quad (5.12)$$

and, by solving it with respect  $\varepsilon_y$  the following condition holds:

$$\varepsilon_y = -\frac{D_{21} \cdot \varepsilon_x + D_{23} \cdot \gamma_{xy}}{D_{22}} \quad (5.13)$$

By substituting (5.13) in (5.10), the final form of the condensed fiber matrix is obtained as follow:

$$\begin{aligned} \begin{bmatrix} \sigma_x \\ \tau_{xy} \end{bmatrix} &= \begin{bmatrix} D_{11} - 2 \frac{D_{12}}{D_{22}} & D_{13} - \frac{D_{12} \cdot D_{23}}{D_{22}} \\ D_{13} - \frac{D_{12} \cdot D_{23}}{D_{22}} & D_{33} - 2 \frac{D_{32}}{D_{22}} \end{bmatrix} \begin{bmatrix} \varepsilon_x \\ \gamma_{xy} \end{bmatrix} \\ \bar{\boldsymbol{\sigma}} &= \bar{\mathbf{D}} \bar{\boldsymbol{\varepsilon}} \end{aligned} \quad (5.14)$$

By integrating the material response according to eq. (5.7) and (5.8), concrete and transversal steel contributions to section resisting forces and section stiffness matrix can be obtained as follow:

$$\begin{aligned} \mathbf{f}_{s,r}^C &= \int_A \mathbf{a}_s^T \bar{\boldsymbol{\sigma}} dA \\ \mathbf{k}_s^C &= \int_A \mathbf{a}_s^T(y) \bar{\mathbf{D}}_t \mathbf{a}_s(y) dA \end{aligned} \quad (5.15)$$

### 5.2.2 LONGITUDINAL STEEL

Longitudinal bars contribution can be evaluated in a discrete way, as the summation of all the  $n_b$  single bars states. Only longitudinal strain  $\varepsilon_x$  is considered. By specializing eq. (5.5), the longitudinal strain for each bar can be evaluated as:

$$\varepsilon_{x,i} = \varepsilon_0 - y_{b,i} \cdot \chi_0 \quad (5.16)$$

Hence, the material matrix assumes the following expression:

$$\bar{\mathbf{D}}_{s,i} = \begin{bmatrix} E_{s,i} & 0 \\ 0 & 0 \end{bmatrix} \quad (5.17)$$

and the contribution of longitudinal steel to sectional resisting forces and stiffness matrix is:

$$\mathbf{f}_{s,r}^S = \sum_{i=1}^{n_b} \left( \mathbf{a}_s^T(y_{b,i}) \begin{bmatrix} \sigma_{x,i} \\ 0 \end{bmatrix} \right) A_{s,i}$$

$$\mathbf{k}_s^S = \sum_{i=1}^{n_b} \left( \mathbf{a}_s^T(y_{b,i}) \begin{bmatrix} E_{s,i} & 0 \\ 0 & 0 \end{bmatrix} \mathbf{a}_s(y_{b,i}) \right) A_{s,i}$$
(5.18)

### 5.3 SECTION STATE DETERMINATION

---

At this point, in order to consider different possibilities for determine the state of the section, two Fixed Pattern Approaches as presented. They can be subdivided into two groups: the Fixed *Strain* Approaches and the Fixed *Stress* Approaches.

#### 5.3.1 FIXED STRAIN APPROACHES

A Fixed Strain Approach defines a priori the  $\gamma_{xy}(y)$  pattern, with the condition that the mean value of the so obtained distribution is equal with the shear generalized deformation:

$$\gamma_0 = \frac{\int_h \gamma_{xy}(y) b(y) dy}{A}$$
(5.19)

Two type of distribution has been considered, as Fig. 5.5 shows:

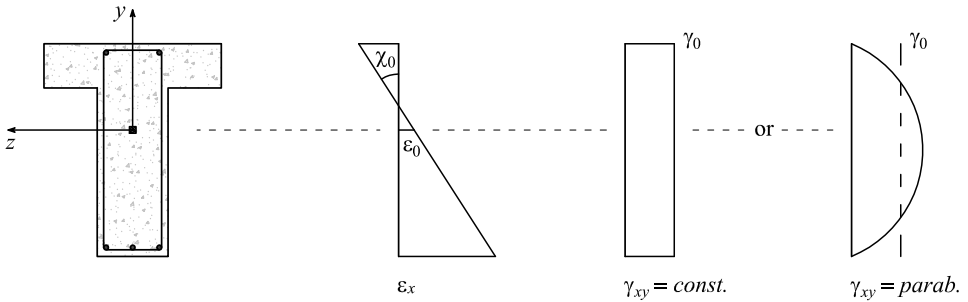


**Figure 5.5:** Fixed Strain Approaches: Input quantities.

The state of the section can be obtained by working with *nested loops* in each fiber. In particular:

- $\epsilon_x$  and  $\gamma_{xy}$  are fixed from sectional kinematic (see Fig. 5.5);
- $\epsilon_y$  is not known, but it can be evaluated by using the condition that the stress in concrete must be equilibrated by the stress in transversal steel (eq. (5.11)) from which eq. (5.13) follows:

$$\epsilon_y = - \frac{D_{21} \cdot \epsilon_x + D_{23} \cdot \gamma_{xy}}{D_{22}}$$

The flow chart of the section state determination is exposed in Fig. 5.7a. For his simplicity, this is the less computational demanding approach, but it tends to concentrate shear resistance in the compression zone of the section (Vecchio and Collins, 1988), with a lower prediction of the stirrups stresses as it will be exposed in par. 5.4.

### 5.3.2 FIXED STRESS APPROACHES

A Fixed Stress Approach defines a priori the  $\tau_{xy}(y)$  pattern, with the condition that the mean value of the obtained distribution for  $\gamma_{xy}(y)$  is equal with the shear generalized deformation:

$$\tau_{xy}^*(y) \parallel \gamma_0 = \frac{\int_h \gamma_{xy}(y) b(y) dy}{A} \quad (5.20)$$

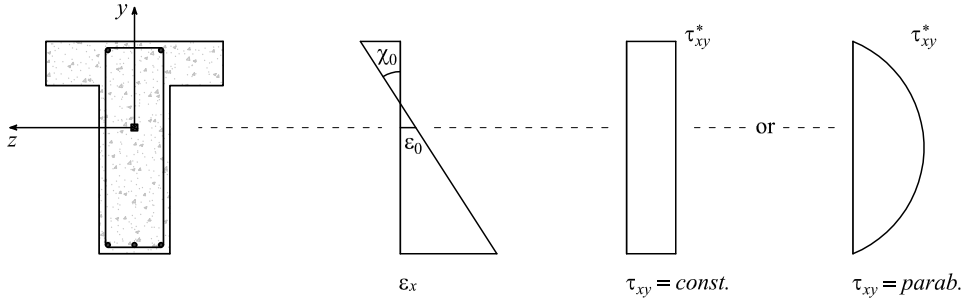


Figure 5.6: Fixed Stress Approaches: Input quantities.

The distribution of  $\tau_{xy}(y)$  can not be imposed a priori, since kinematic variables are needed in order to use a smeared approach (like MCFT). Hence, also in this case the solution is reached in an iterative way, by imposing for each fiber of the section the two conditions:

$$\begin{cases} \sigma_y = 0 \\ \tau_{xy} = \tau_{xy}^* \end{cases} \quad (5.21)$$

By remember eq. (5.10), this system can be rewritten in this form:

$$\begin{cases} D_{21} \cdot \varepsilon_x + D_{22} \cdot \varepsilon_y + D_{23} \cdot \gamma_{xy} = 0 \\ D_{31} \cdot \varepsilon_x + D_{32} \cdot \varepsilon_y + D_{33} \cdot \gamma_{xy} = \tau_{xy}^* \end{cases} \quad (5.22)$$

and can be solved for  $\varepsilon_y$  and  $\gamma_{xy}$ :

$$\begin{cases} \varepsilon_y = -\frac{(D_{23} \cdot D_{31} - D_{21} \cdot D_{33}) \varepsilon_x - D_{23} \cdot \tau_{xy}^*}{D_{22} \cdot D_{33} - D_{23} \cdot D_{32}} \\ \gamma_{xy} = +\frac{D_{22} \cdot \tau_{xy}^* + (D_{21} \cdot D_{32} - D_{22} \cdot D_{31}) \varepsilon_x}{D_{22} \cdot D_{33} - D_{23} \cdot D_{32}} \end{cases} \quad (5.23)$$



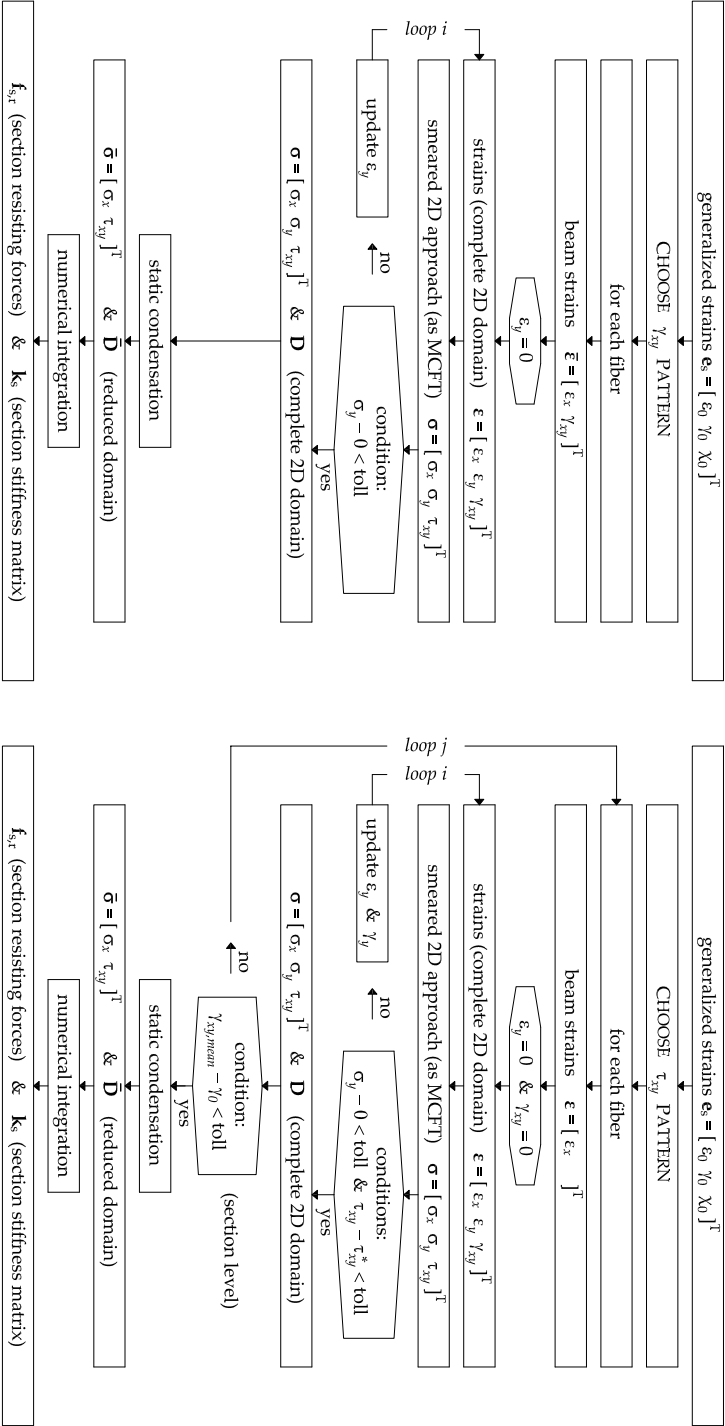
For each fibre, a nested loop solving eq. (5.23) so that (5.21) holds is needed. At the higher level (the sectional level) however, the condition expressed by eq. (5.20) must be satisfied. Hence, an additional sectional loop must be needed, as the flow chart reported in Fig. 5.7b clearly shows.

A similar procedure has been proposed also in (Ferreira, 2013), in which the sectional loop is not performed but a residual shear force is accounted for. According to (Vecchio and Collins, 1988) the imposition of a parabolic pattern for  $\tau_{xy}$  produce a result more close to the real solution.

### 5.3.3 COMPARISON AND FLOW CHARTS

Fig. 5.7 shows the flow charts for the two sectional state determination approaches. It can be observed that:

- *Fixed Strain Approach:*  
with respect a classical RC section that deals with the problem of normal stresses, the inclusion of shear modeling produces a sectional state determination process that is accomplished by an integration of *iterative* fibers. This iteration at the fiber level is request in order to calculate the transversal strain  $\varepsilon_y$  so that  $\sigma_y = 0$  corresponds. We have, hence, a loop  $i$  for each fiber, but the section is not iterative (see Fig. 5.7a) since, in a fixed strain approach, the input are kinematic quantities;
- *Fixed Strain Approach:*  
in this case, the input quantities are not only kinematic because a pattern for the shear stress  $\tau_{xy}$  is imposed. We don't know the effective value, but we just say that the pattern is, for example, constant or parabolic. In this case, hence, in addition to  $\varepsilon_y$  as before, we have also  $\gamma_{xy}$  as unknown. As a consequence, the state of the section is obtained with an *iterative* section, made of *iterative* fibers as Fig. 5.7b shows. With respect a fixed strain approach this procedure is more computational involving.



(a) Fixed Strain Approach: non iterative section.

Figure 5.7: Flow chart of the two proposed Section State Determination.

(b) Fixed Stress Approach: iterative section.

### 5.4 VALIDATION: THE “STUTTGART SHEAR TEST”

All the numerical procedures previous exposed are now validated and compared with the well know shear beam tests carried out in Stuttgart and reported in (Leonhardt and Walther, 1962) - (Leonhardt, 1965). 4 simple supported beams (ET1, ET2, ET3, ET4) have been considered, with same length and same longitudinal and transversal reinforcement. They differ only for the transversal section, in which web widths present the variations:  $0.30\text{ m}$ ,  $0.15\text{ m}$ ,  $0.10\text{ m}$ ,  $0.05\text{ m}$  (see Fig. 5.9). The goal of this test was to examine the influence of the web width on the shear strength of the beams. Comparisons deal with:

1. load displacement curves;
2. crack patterns;
3. collapse types;
4. stresses in transversal stirrups.

Concerning the constitutive laws adopted, the relationships of the original MCFT formulation are considered (Vecchio and Collins, 1986), both for concrete and for steel. See par. 4.2.4 for details.

All the beams are studied both with bidimensional and monodimensional models. The corresponding structural meshes are reported in Fig. 5.8.

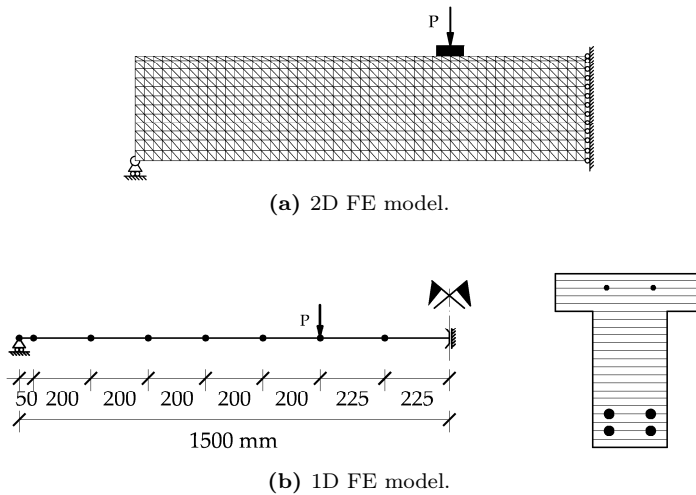
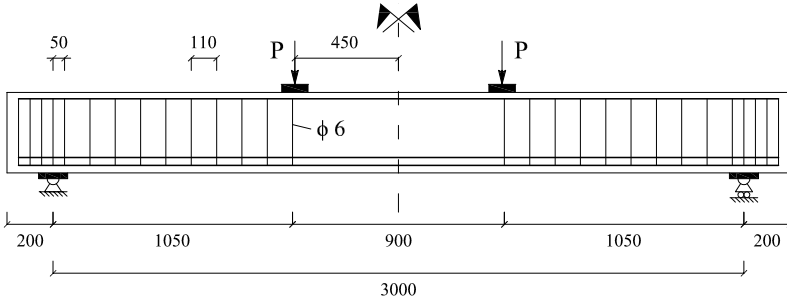
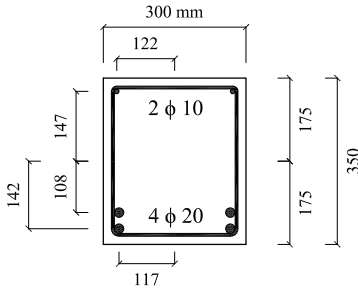


**Figure 5.8:** Stuttgart Shear Test: meshes of the two numerical models used.

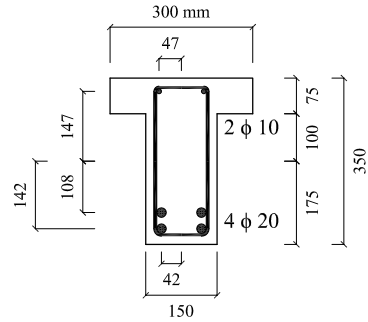
The results of 2D modeling are shown in Fig. 5.10. In particular, for all the beams, the principal tension strain is plotted in correspondence of the collapse load. It can be observed that in ET1 beam, the higher strains interest the central bottom part of the beam. This happens in a flexural-type collapse. Then, by moving from ET1 to ET4 beam, there is a migration of the principal strains in the web of the beam, as happens in a shear-type collapse.



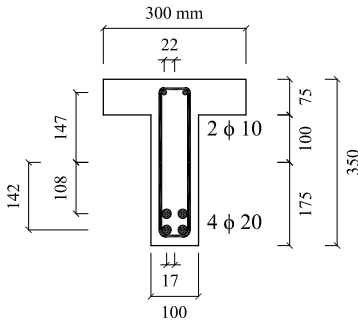
(a) Geometry of the beams [mm].



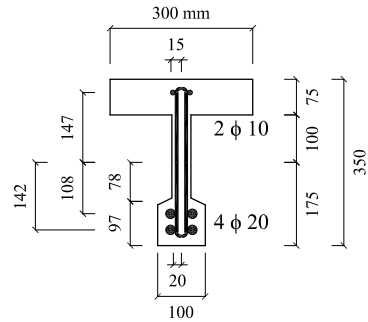
(b) ET1 beam.



(c) ET2 beam.



(d) ET3 beam.



(e) ET4 beam.

$\epsilon'_c$	$f'_c$ [MPa]	$E_c$ [MPa]	$f_{cr}$ [MPa]	$\epsilon_{cr}$
$-2.4 \cdot 10^{-3}$	28.5	23800	2.8	$1.18 \cdot 10^{-4}$

(f) Concrete mechanical properties.

Bars	$f_y$ [MPa]	$E_s$ [MPa]	$\phi$ [mm]
top	420	210000	10
bottom	420	210000	20
transversal	320	200000	6

(g) Steel mechanical properties.

Figure 5.9: Stuttgart Shear Test: geometry, sections and material's properties.

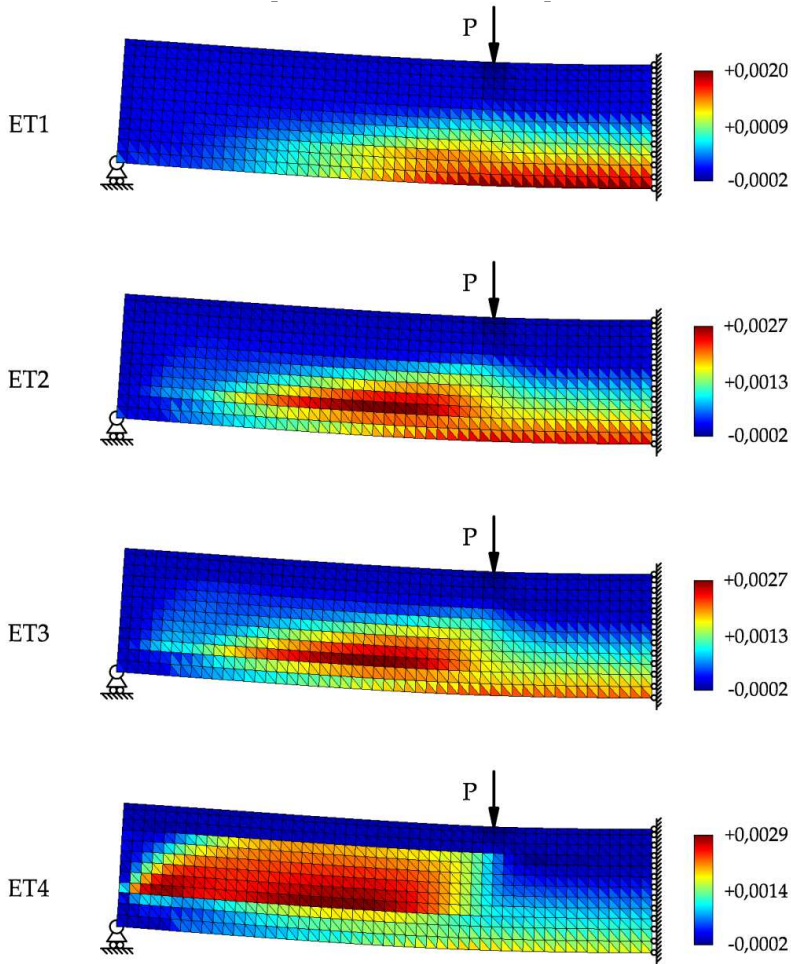


Figure 5.10: Stuttgart Shear Test: comparisons between principal tension strains.

Fig. 5.11 shows the load-displacement curves and the evolution of the stresses in the stirrups, for all the beams and for all the numerical analysis considered. All the numerical procedures exposed in this thesis have been used. In particular, comparisons deal with:

- experimental results;
- 2D modeling;
- 1D modeling with the shear flexible beam-column element;
- 1D modeling with a common beam-column element based on Navier-Bernoulli kinematic.

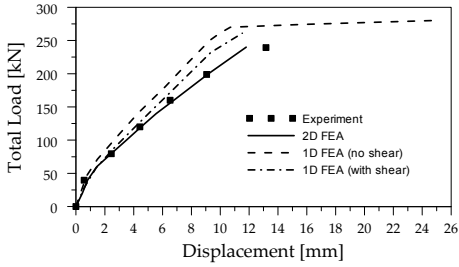
The following comments arise (see Fig. 5.11):

1. bidimensional modeling (based on MCFT):  
it is able to predict the nature of the problem, concerning both the load-displacement curves and the evolution of the stresses in the stirrups, for all the 4 tested beams;
2. monodimensional modeling based on Navier-Bernoulli kinematic:  
in this case, stirrups are not directly modeled and hence the relative stresses can not be evaluated. The loads-displacement curves can not be considered adequate since an overestimation of the collapse load and of the structural ductility are present. In addition, by comparing the 4 beams, it can be observed that all the curves are, more or less, the same. This is due to the fact the neutral axis belong to the upper part of the section and, since the width variations interest the bottom parts, this 1D model is not able to catch the differences between the beams;
3. monodimensional modeling with the shear-flexible beam-column element:  
here, the same constitutive laws assumed for the bidimensional modeling are considered. The result is that, now, the beam element is able to describe better the structural behavior: the ultimate load is adequately captured, with a stiffness that is however higher with respect the 2D modeling. In addition, the stresses in the stirrups can be evaluated:
  - if a fixed strain approach is considered, the shear resistance is concentrated in the compression zone of the section and a lower prediction of the stirrups stresses descends;
  - if a fixed stress approach is used, a better representation of the stresses in the stirrups is generally obtained.

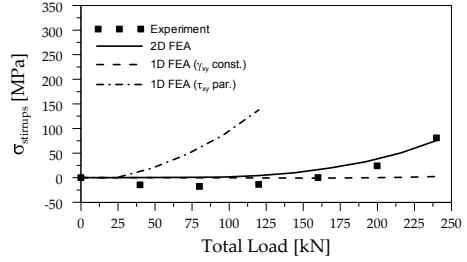
Fig. 5.12 deals with the crack pattern, by comparing the experiment, the bidimensional modeling and the monodimensional model. Concerning the representation in the 2D model, a crack is plotted in the finite element if the cracking stress is reached. The direction of the crack is given by the principal stresses inclination angle. In the 1D model, instead, the procedure used in order to produce the crack pattern is as follow:

- in each element, the mid section is considered;
- in each fiber of that section, it is control if the cracking stress is reached and, if yes, the relative crack inclination is saved;
- by smearing such a results in all the element's length, a conventional crack can be obtained.

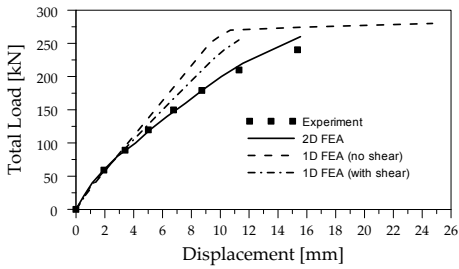
As clearly Fig. 5.12 shows, in the central part of the beam cracks are vertically oriented since, here, only bending moment is present. A more general representation of concrete cracking pattern can be found in (Ferreira, 2013).



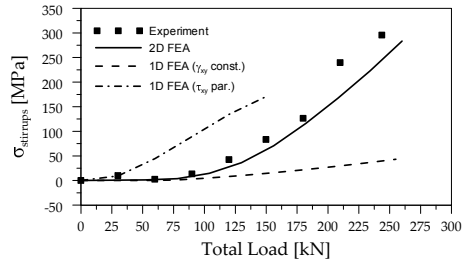
(a) ET1: load-displacement curve.



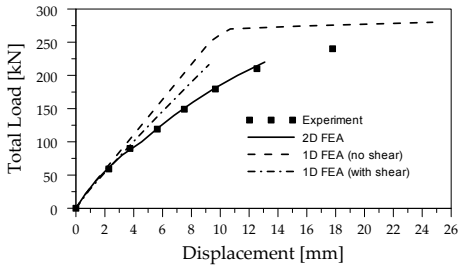
(b) ET1: stresses in the stirrups.



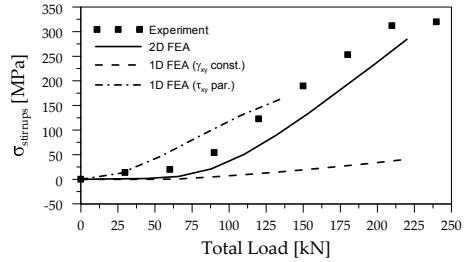
(c) ET2: load-displacement curve.



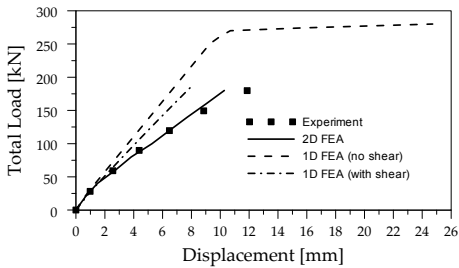
(d) ET2: stresses in the stirrups.



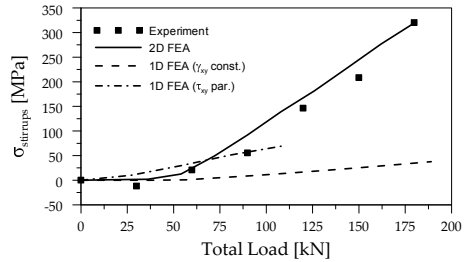
(e) ET3: load-displacement curve.



(f) ET3: stresses in the stirrups.

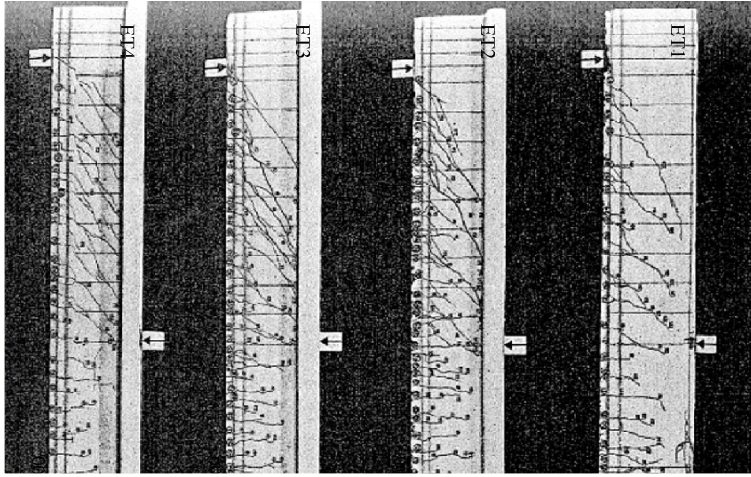


(g) ET4: load-displacement curve.

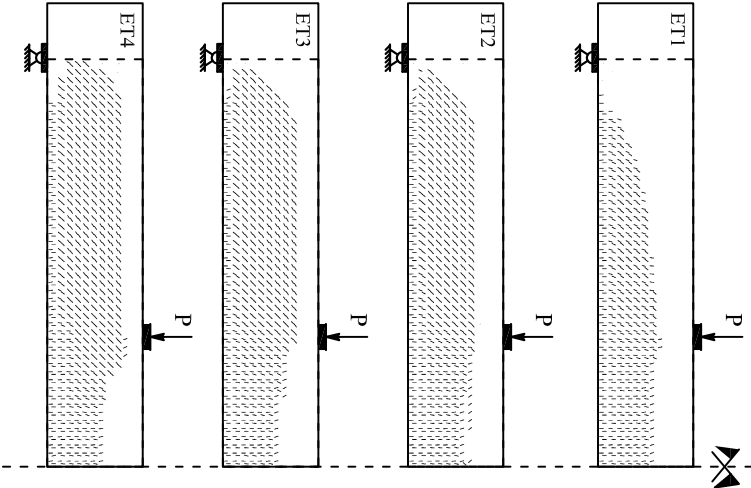


(h) ET4: stresses in the stirrups.

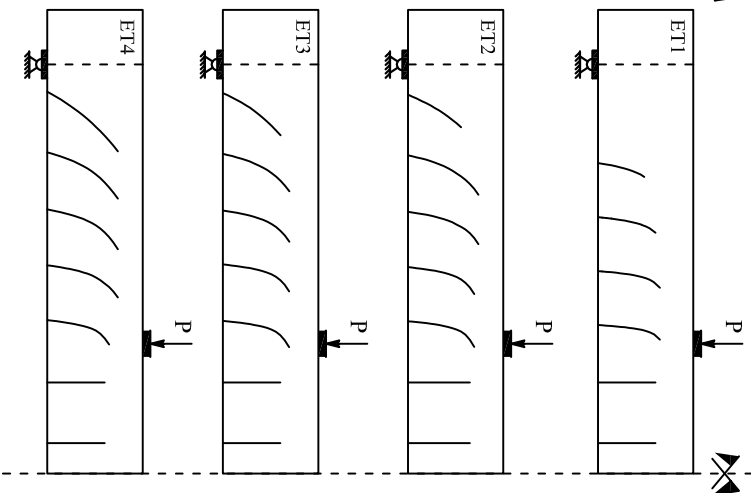
Figure 5.11: Stuttgart Shear Test: comparisons of load-displacement curves and stresses in the stirrups.



(a) Experimental Results.



(b) NL-CST (2D Modeling).



(c) Shear-flexible beam (1D Modeling).

Figure 5.12: Stuttgart Shear Test: comparisons between crack patterns.



## 5.5 CONCLUDING REMARKS

---

In this chapter, some possibilities of the so-called fixed pattern approaches have been considered and, in particular, a 2 node Timoshenko beam has been presented and validated.

At first, the global framework is exposed. The generic structure is subdivided into monodimensional finite beam-column elements. Each beam element is composed by sections and each section is composed by fibers. In a nested way, the problem of determine the state of the structure is moved to the determination of the state of the generic fiber. In order to describe the complex shear behavior and its interaction with normal stresses, a link with a 2D constitutive model is needed. the Modified Compression Field Theory (MCFT) is hence adopted at the fiber level. Transversal reinforcing steels are smeared in the concrete domain.

Then, two section state determinations are presented and compared. The first is a fixed strain approach, with a set of kinematic variables as input. The so obtained sectional state requires a numerical integration of iterative fibers. The second is a fixed stress approach, with both kinematic and static variables as input. The descending sectional state is represented by an iterative section, made of iterative fibers.

All the numerical procedures have been validated on a well know shear beam test. The main conclusion is that only 2D modeling is able to describe the total complex structural behavior. Between the two monodimensional models proposed in this chapter (that differ only in the section state determination process), best results have been obtained with the iterative section in which a parabolic distribution of shear stresses is considered.

Several improvements of the proposed numerical approached are possible. In particular, the main problem of a fixed pattern approach is the choice of the pattern itself. It's clear that, in dealing with sections with arbitrary shape or arbitrary position of reinforcements, such a choice is not straightforward and specific extensions of the formulation are required.



II

---

DAMAGED RC STRUCTURES



# 6

## Damage modeling in RC structures exposed to corrosion

*A general method able to predict the structural lifetime performance of RC structures is presented. The diffusion process is modeled by using Cellular Automata and by including the reduction of cross-sectional areas of corroded bars, the reduction of ductility of reinforcing steel, the deterioration of concrete strength and the spalling of the concrete cover.*

### 6.1 INTRODUCTION

---

Concrete structures exposed to aggressive environments are subjected to lifetime degradation induced by the kinetic process of diffusion of chemical components, such as sulphates and chlorides, driven by concentration gradients inside the material volume (Glicksman, 2000). Sulphates contained in soil or water can contaminate the cement paste causing a progressive loss of concrete strength. Chlorides beyond a threshold value in carbonated concrete can lead to the corrosion of reinforcing steel (Castellani and Coronelli, 1999), (Bertolini *et al.*, 2013). Chlorides are critical in a marine environment, where they diffuse into concrete as airborne chlorides and/or by direct contact with seawater, but they can also come from the application of deicing salts on bridge decks (C.E.B., 1992). In general, for concrete structures, damage scenarios are more critical for bridges than for buildings, since usually the entire structure is directly exposed to the aggressive atmosphere without protection, (Biondini *et al.*, 2013).

In ordinary condition, reinforcing steel bars embedded in sound concrete are protected by a thin protective oxide film that prevents corrosion initiation. In fact, the alkaline solution contained in the pores of the hydrated cement paste promotes the passivation of steel. However, corrosion can take place when the passive film is removed or locally damaged due to carbonation of concrete or to chloride penetration (Sgambi *et al.*, 2012). Based on that, the service life of reinforced concrete structures can be divided in two distinct phases (Fig. 6.1). The first phase is the initiation of corrosion, in which the reinforcement is passive but carbonation and/or chloride penetration take place leading to the progressive loss of passivity. The second phase is propagation of corrosion, that begins when steel is depassivated

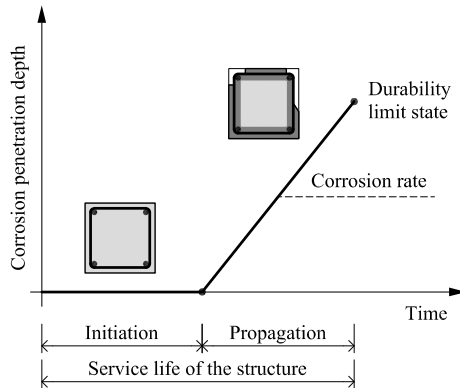


**Figure 6.1:** Initiation and propagation periods for corrosion in RC structures.

and finishes when a limit state is reached beyond which consequences of corrosion cannot be further tolerated.

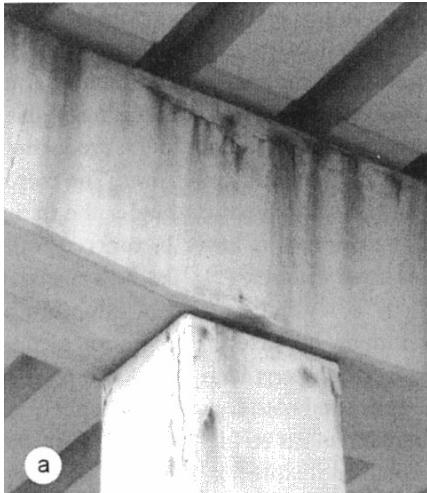
### 6.1.1 INITIATION PHASE

During the initiation phase, aggressive substances that can depassivate steel penetrate from the surface into the inner layers of concrete. Carbonation begins at the surface of concrete and moves gradually towards the inner zones, neutralizing concrete alkalinity by the ingress of carbon dioxide from the atmosphere. As far as chloride attack, chloride ions can penetrate into concrete and reach the reinforcement, destroying the protective layer if their concentration on steel surface reaches a critical level (Camnasio, 2013). The duration of the initiation phase depends mainly on the cover depth and the penetration rate of the aggressive agents as well as on the concentration necessary to depassivate the steel bars. Design codes define cover depths according to the expected environmental class (EN-206-1, 2001). The rate of ingress of the aggressive agents depends on concrete quality, i.e. porosity and permeability, and on the microclimate on concrete surface. Using protective measures that prolong the initiation phase is an effective way to improve concrete durability.

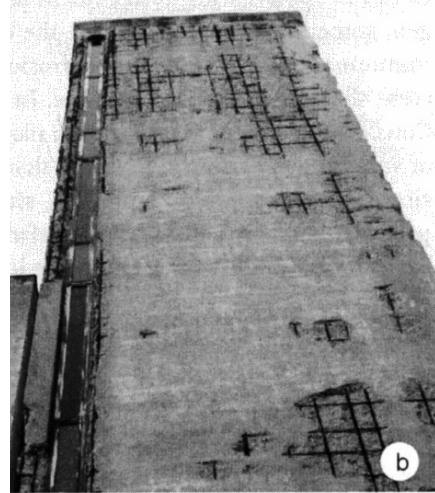
### 6.1.2 PROPAGATION PHASE

When the steel protective layer is destroyed, corrosion starts if water and oxygen are present on the surface of the reinforcement. The corrosion rate greatly depends on temperature and humidity and determines the time it takes to reach the minimally acceptable state of the structure, i.e. the durability failure criterion. Corrosion induced by carbonation is generally uniform on steel surface, since carbonated concrete leads to complete dissolution of the protective layer (Fig. 6.2a-6.2b). In presence of high chlorides content, corrosion tends to be localized, with penetrated attacks of limited area (pits) surrounded by non-corroded areas. This is called pitting corrosion (Fig. 6.2c). Sometimes, when very high levels of chlorides are

present, the passive film is destroyed over wide areas, thus causing a generalized corrosion. Moreover, hydrogen embrittlement can occur on high-strength steel used in prestressed concrete, under particular environmental, mechanical loading and electrochemical conditions, leading to the brittle failure of the material (Fig. 6.2d).



(a) Cracking of columns and cross beam.



(b) Spalling and delamination.



(c) Pitting corrosion.



(d) Brittle failures of prestressing tendons.

**Figure 6.2:** Examples of consequences of corrosion of steel in concrete (Bertolini, 2006).

In the following, a general method able to predict the structural lifetime performances is presented. At first, the aggressive agent penetration is dealt with. Such a problem requires the solution of a partial differential equation and, in order to consider arbitrary geometries and arbitrary positions of reinforcements, a special evolutionary computational technique is applied: the cellular automata. Once chlorides concentration is known in all the RC domain and in time, the reduction of cross-sectional areas, of ductility of reinforcing steel, the deterioration of concrete strength and the spalling of the concrete cover will be modeled by presenting special damage indexes.

## 6.2 DIFFUSION PROCESSES AND CELLULAR AUTOMATA

Corrosion is a complex phenomenon, involving different mechanisms and depending on many parameters. In literature different studies can be found, in order to understand the fundamental factors. Both experimental tests and numerical simulations have been carried out, with the purpose to investigate the effects on a local and a global level, and also to develop analytical models (Titi, 2012). Among different aggressive agents, the presence of chlorides plays a fundamental role (Stewart, 2009). Hence, the attention is concentrated on chlorides induced corrosion.

### 6.2.1 MODELING OF DIFFUSION PROCESSES

The hypothesis of a diffusion mechanism can be acceptable if an effective diffusion coefficient  $D_e$  is introduced. The simplest model, hence, is the Fick's first law, which assumes a linear relationship between the mass flow and the concentration gradient. The combination of the Fick's model with the mass conservation principle leads to the Fick's second law. Assuming an isotropic media, the problem is described by the following second-order partial differential equation (Glicksman, 2000):

$$-\nabla \cdot (-D_e \nabla C) = \frac{\partial C}{\partial t} \quad (6.1)$$

where  $C = C(\mathbf{x}, t)$  is the mass concentration of the component at point  $\mathbf{x} = (x, y, z)$  in the  $t$  time, and  $\nabla C = \mathbf{grad}C$ . Since  $D_e$  is an effective diffusion coefficient, the described model can be enhanced by considering the anisotropy of the media, more diffusion components and particular chemical reactions or stresses effects.

In reinforced concrete structures, the effective diffusion coefficient  $D_e$  depends on relative humidity, on temperature and on the internal stress field. Hence, Fick's law must be improved by considering both the thermal effects and the material constitutive laws in a full coupled physical-mechanical process (C.E.B. (1992), Saetta *et al.* (1999), Xi and Bazant (1999), Xi *et al.* (2000)).

However, the so-obtained models are at first too complex, but secondly they need a wide calibration process that seems too far from the nature of the problem that, in addition, is not so certain.

For these reasons, in lifetime structural assessment, it seems more convenient the adoption of a *macroscopic* approach that neglects all the above mentioned interaction processes but that, for its simplicity, can be easily extended in the non-deterministic field.

In the following, it is hence assumed that Fick's law holds with an effective diffusion coefficient  $D_e$  that is constant in time. Eq. (6.1) can be rewritten as:

$$D \nabla^2 C = \frac{\partial C}{\partial t} \quad (6.2)$$

Despite eq. (6.2) is a linear partial differential equation, its solution exists only for a limited number of classical cases. For that reason, typically the problem of the penetration of chlorides into concrete cross-sections is studied in a uni-dimensional form (C.E.B., 1992) and the solution of eq. (6.2) is expressed as:

$$C(x, t) = C_s \left[ 1 - \operatorname{erf} \left( \frac{x}{2\sqrt{D_e t}} \right) \right] \quad (6.3)$$



However, such a 1D approach is applicable for simple sections, but in general, due to different geometric domains or different positions of steel bars or different attack scenarios, a numerical solution of eq. (6.2) is needed. Inspired to (Biondini *et al.*, 2004b) and (Titi, 2012), in order to solve the diffusion process, a special evolutionary computation technique is used: the *cellular automata*.

### 6.2.2 AN INTRODUCTION TO CELLULAR AUTOMATA

A cellular automata is a dynamic system where space, time and states are discrete. Cellular automata were firstly introduced by von Neumann and Ulam in 1948-1950 (Von Neumann *et al.*, 1966) and subsequently developed by other researchers in many fields of science (see for reviews: Toffoli and Margolus (1987), Adami (1998), Wolfram (2002)). Originally related to the study of self-replication problems on the Turing's machine, cellular automata left laboratories in the 1970s and became popular in the academic circles with the now famous Game of Life invented by Conway (Gardner, 1970). Basically, they represent simple mathematical idealizations of physical systems in which space and time are discrete, and physical quantities are taken from a finite set of discrete values. In fact, any physical system satisfying differential equations may be approximated as a cellular automaton by introducing discrete coordinates and variables, as well as discrete time steps. Properly speaking, therefore, models based on cellular automata provide an alternative and more general approach to physical modeling rather than an approximation; they show a complex behavior analogous to that associated with complex differential equations, but in this case complexity emerges from the interaction of simple entities following simple rules (Biondini *et al.*, 2004b).

The definition of a cellular automata must consider two fundamental characteristics:

1. *uniformity*: the automata's elements are equal in all the domain;
2. *locality*: each element has a state that depends only on what happen around it.

In its basic form, a cellular automaton consists of a regular uniform grid of sites or cells, theoretically having infinite extension, with a discrete variable in each cell which can take on a finite number of states. The state of the cellular automaton is then completely specified by the values  $s_i = s_i(t)$  of the variables at each cell  $i$ . During time, cellular automata evolve in discrete time steps according to a parallel state transition determined by a set of local rules: the variables  $s_i^{k+1} = s_i(t_{k+1})$  at each site  $i$  at time  $t_{k+1}$  are updated synchronously based on the values of the variables  $s_n^k$  in their "neighborhood"  $n$  at the preceding time instant  $t_k$ . The neighborhood  $n$  of a cell  $i$  is typically taken to be the cell itself and a set of adjacent cells within a given radius  $r$ , or  $i - r \leq n \leq i + r$ . Thus, the dynamics of a cellular automaton can be formally represented as:

$$s_i^{k+1} = \phi(s_i^k; s_n^k) \quad i - r \leq n \leq i + r \quad (6.4)$$

where function  $\phi$  is the *evolutionary rule* of the automaton.

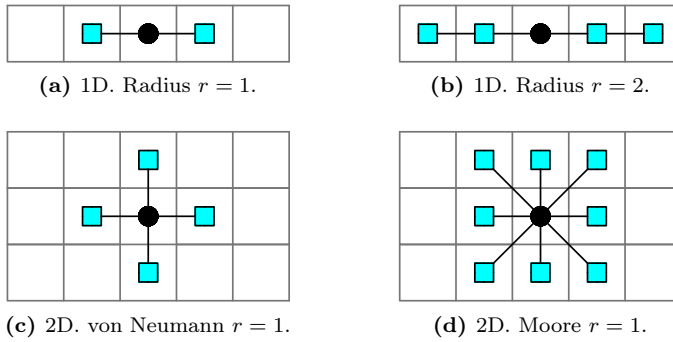


**Figure 6.3:** Typical neighborhoods for 1D and 2D cellular automata.

Clearly, a proper choice of the neighborhood cells  $n$  plays a crucial role in determining the effectiveness of such a rule. Fig. 6.3 shows an example of typical neighborhoods for one and two dimensional cellular automata, but patterns of higher complexity can be also proposed.

### 6.2.3 CELLULAR AUTOMATA SOLUTION OF DIFFUSION EQUATIONS

One of the most effective applications of cellular automata is the simulation of diffusion processes, since their dynamics can accurately reproduce linear or nonlinear flows with complex boundary conditions (Whitney, 1990). This result is easily achieved through a proper selection of both the neighborhood  $n$  and the rule  $\phi$ . As reported in (Biondini *et al.*, 2004b), the diffusion process described by Fick's laws in  $d$  dimensions  $d = 1, 2, 3$  can be effectively simulated by adopting a von Neumann neighborhood (Fig. 6.3c) with radius  $r = 1$  and the following rule of evolution:

$$C_i^{k+1} = \phi_0 C_i^k + \sum_{j=1}^d \phi_j^- C_{j-1}^k + \phi_j^+ C_{j+1}^k \quad (6.5)$$

where the discrete variable  $s_i^k = C_i^k = C(\mathbf{x}_i, t_k)$  represents the concentration of the component in the cell  $i$  at time  $t_k$ . The values of the evolutionary coefficients  $\phi_0(d)$ ,  $\phi_j^-(d)$  e  $\phi_j^+(d)$  must verify the following normality rule:

$$\phi_0 + \sum_{j=1}^d \phi_j^- + \phi_j^+ = 1 \quad (6.6)$$

as required by the mass conservation law.

In addition, for isotropic media, in order to avoid directionality effects, the following symmetric condition must be satisfy:

$$\phi_j^-(d) = \phi_j^+(d) = \phi_1^+(d) \quad (6.7)$$

It is possible to prove the equivalence by the cellular automata rule adopted and the diffusive partial equation.

By considering the one-dimensional case, eq. (6.5) can be rewritten as:

$$\begin{aligned} C(x, t + \Delta t) &= \phi_0 C(x, t) + \phi_1 [C(x - \Delta x, t) + C(x + \Delta x, t)] = \\ &= \phi_0 C(x, t) + \frac{1 - \phi_0}{2} [C(x - \Delta x, t) + C(x + \Delta x, t)] \end{aligned} \quad (6.8)$$

where  $\Delta x$  is the grid dimension and  $\Delta t$  the step time increment. By subtracting in both terms  $C(x, t)$  and by dividing for  $\Delta t$ , the following relation holds:

$$\frac{C(x, t + \Delta t) - C(x, t)}{\Delta t} = \frac{1 - \phi_0}{2} \frac{1}{\Delta t} [C(x - \Delta x, t) + C(x + \Delta x, t) - 2C(x, t)] \quad (6.9)$$

that can be rewritten as:

$$\frac{C(x, t + \Delta t) - C(x, t)}{\Delta t} = \frac{1 - \phi_0}{2} \frac{\Delta x^2}{\Delta t} \frac{[C(x - \Delta x, t) + C(x + \Delta x, t) - 2C(x, t)]}{\Delta x^2} \quad (6.10)$$

By defining:

$$D = \frac{1 - \phi_0}{2} \frac{\Delta x^2}{\Delta t} \quad (6.11)$$

and taking the limit  $\Delta x \rightarrow 0$  and  $\Delta t \rightarrow 0$ , the expression of the second Fick's law is obtained:

$$\frac{\partial C(x, t)}{\partial t} = D \frac{\partial^2 C(x, t)}{\partial x^2} \quad (6.12)$$

In conclusion, given a  $D$  value, the diffusion process can be dealt with by choosing two values  $\Delta x$ ,  $\Delta t$  so that eq. (6.11) holds.

The same procedure can be generalized in  $d$  dimensions. In particular eq. (6.11) becomes:

$$D = \frac{1 - \phi_0}{2d} \frac{\Delta x^2}{\Delta t} = \phi_1 \frac{\Delta x^2}{\Delta t} \quad (6.13)$$

Usually a deterministic value  $\phi_0 = 1/2$  is related to a good accuracy in the results (Titi, 2012). In the present investigation a deterministic definition for the evolutionary coefficient is used; however, in order to consider stochastic effects in the diffusion process, a probabilistic formulation of the cellular automata can be applied.

### 6.3 FROM DIFFUSION PROCESS TO DAMAGE INDEXES

---

Once the diffusion process has been solved, the mechanical damage can be evaluated by introducing suitable material degradation laws. In order to consider (a) the reduction of cross sectional area of corroded bars, (b) the reduction of ductility of reinforcing steel, (c) the deterioration of concrete strength due to development of longitudinal cracks induced by the corrosion products and (d) the spalling of the concrete cover, different damage indexes are proposed. In the following, it will be show that all these damage indexes can be written as a function of a dimensionless damage index  $\delta_s$ , that will be correlated to the diffusion process described before.

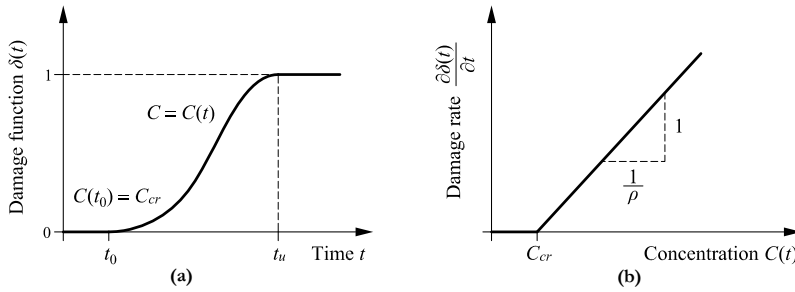


**Figure 6.4:** Modeling of mechanical damage: (a) time evolution of damage indices during diffusion process; (b) linear relationship between rate of damage and concentration of aggressive agent.

### 6.3.1 DEFINITION OF THE DIMENSIONLESS DAMAGE INDEX $\delta_s$

Structural damage can be viewed as a degradation of the mechanical properties which makes the structural system less able to withstand the applied actions. The effects of corrosion damage can be described in the structural model through damage indexes and corrosion can selectively be applied to damaged structural elements with a different level of penetration in each reinforcing bar and a different deterioration for concrete parts, in order to consider prescribed damage patterns and corrosion levels (Camnasio, 2013).

Several formulations has been presented to date in order to correlate the rate of damage and the concentration of the aggressive agent. A critical comparisons will be show in par. 6.4. In this thesis, the formulation proposed in (Biondini *et al.*, 2004b) will be used. In such an approach, a linear relationship between the rate of damage and the concentration of the aggressive agent after the reaching of a concentration threshold  $C_{cr}$  is assumed, so that the following relationship holds (see Fig. 6.4):

$$\frac{\partial \delta_s}{\partial t} = \frac{C(\mathbf{x}, t)}{C_s \Delta t_s} = \rho C(\mathbf{x}, t) \quad (6.14)$$

where  $C_s$  represents the value of constant concentration  $C(\mathbf{x}, t)$ , in a certain position and at a specified time instant, which lead to a complete damage of the materials after the time periods  $\Delta t_s$ .

Concerning the damage's effects, the formulation has been here enhanced by considering all the chlorides corrosion effects in reinforced concrete. In particular, four damage's effects will be presented:

1. the reduction of cross-section of reinforcing bars;
2. the reduction of ductility of reinforcing steel;
3. the reduction of concrete strength;
4. the spalling of the concrete cover.

It will be show that all these effects can be derive as a functions of the dimensionless damage index  $\delta_s$ .

6.3.2 REDUCTION OF THE CROSS-SECTION OF REINFORCING BARS

The most relevant effect of corrosion is the reduction of the cross-section of the reinforcing steel bars. Depending on the source of corrosion, different models can be applied in order to simulate it, Fig. 6.5.

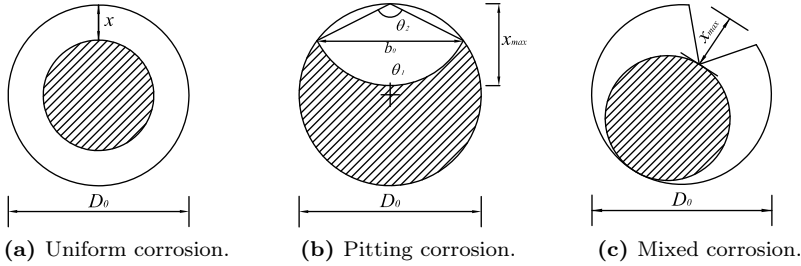


Figure 6.5: Modeling of cross section reduction of a steel bar, adapted from (Titi, 2012).

By denoting  $p$  the corrosion penetration depth, it is useful to introduce a dimensionless corrosion penetration index  $\delta \in [0, 1]$  defined as:

$$\delta = \frac{p}{D_0} \tag{6.15}$$

where  $D_0$  is the original diameter of the bar. Finally, the area of the corroded steel can be represented by a function of corrosion penetration index, depending on type of corrosion:

$$A_s(\delta) = [1 - \delta_s(\delta)] A_{s0} \tag{6.16}$$

where  $A_{s0} = \pi D_0^2/4$  is the area of the undamaged bar and  $\delta_s = \delta_s(\delta)$  is the dimensionless damage index for reinforcing steel.

6.3.2.1 UNIFORM CORROSION

In carbonated concrete, without a significant presence of chlorides, corrosion tends to develop in a uniform way around steel bars, Fig. 6.5a. In this case the penetration depth is  $p = 2x$ , and the damage function  $\delta_s$  has the following expression:

$$\delta_s = \delta(2 - \delta) \tag{6.17}$$

Exploiting eq. (6.16), the uniform reduction of area is:

$$A_s(t) = \pi \left[ \frac{D_0}{2} - x(t_p) \right]^2 \tag{6.18}$$

where  $t_p$  is the time in which corrosion begins.

### 6.3.2.2 LOCALIZED CORROSION

If concrete is contaminated by chlorides, reduction of steel area is not uniform but tend to localize (pit), Fig. 6.5b; the model presented above is therefore not suitable. From measures of current intensity it is possible to obtain a mean value of penetration depth; however, due to the localization of the damage, the maximum depth  $x_{max}$  in correspondence of the pit is significant higher. One solution is to define the pitting factor  $R$ , defined as:

$$R = \frac{x(t)_{max}}{x(t)_{mean}} \quad (6.19)$$

Indicative values for the pitting factor  $R$  can be found in (Gonzalez *et al.*, 1995).

### 6.3.3 REDUCTION OF DUCTILITY OF REINFORCING STEEL

Pitting corrosion may involve a significant reduction of steel ductility. Tensile tests on corroded bars show that for a quite limited mass loss (about 13%) steel behavior may become brittle (Almusallam, 2001). The results of experimental tests reported in (Apostolopoulos and Papadakis, 2008) indicate that ductility reduction is a function of the cross-section loss. Based on this results, the  $\varepsilon_{su}$  can be related to the damage index  $\delta_s = \delta_s(\delta)$  as indicated in (Biondini and Vergani, 2012):

$$\varepsilon_{su}(t) = \begin{cases} \varepsilon_{su0} & 0 \leq \delta_s \leq 0.016 \\ 0.1521 \cdot \delta_s^{-0.4583} \varepsilon_{su0} & 0.016 < \delta_s \leq 1 \end{cases} \quad (6.20)$$

where  $\varepsilon_{su0}$  is the steel ultimate strain of the undamaged bar.

### 6.3.4 EFFECTS OF CORROSION ON CONCRETE

Effects of corrosion are not limited to damage of reinforcing steel bars. In fact, in case of uniform corrosion with low penetration rate, the formation of oxidation products may led to propagation of longitudinal cracks and concrete cover spalling. The effects are presented in Fig. 6.6.

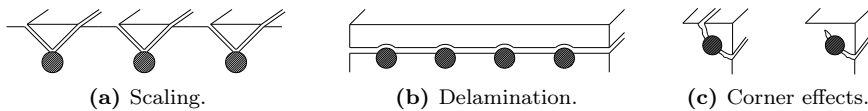


Figure 6.6: Corrosion effects on concrete cracking.

Concrete degradation can be taken into account by modeling the reduction of concrete compression strength  $f_c$  due to cover cracking:

$$f_c = [1 - \delta_c(\delta)] f_{c0} \quad (6.21)$$

where  $f_{c0}$  is the strength of undamaged concrete. The reduced concrete strength  $f_c$  can be evaluated as follows (Coronelli and Gambarova, 2004):

$$f_c(t) = \frac{f_{c0}}{1 + \kappa \frac{\varepsilon_{\perp}(t)}{\varepsilon_{c0}}} \quad (6.22)$$

where  $\kappa$  is a coefficient related to bar diameter and roughness ( $\kappa = 0.1$  for medium-diameter ribber bars),  $\varepsilon_{c0}$  is the strain at peak stress in compression, and  $\varepsilon_{\perp}$  is an average (smeared) value of the tensile strain in cracked concrete at right angles to the direction of the applied stress. The transversal strain  $\varepsilon_{\perp}$  is evaluated by means of the following relationship:

$$\varepsilon_{\perp}(t) = \frac{b_f(t) - b_i}{b_i} = \frac{\Delta b(t)}{b_i} \quad (6.23)$$

where  $b_i$  is the width of the undamaged concrete cross-section and  $b_f$  is the width after corrosion cracking. The increase  $\Delta b$  of the beam width is estimated as follows:

$$b_f - b_i = w_{tot}(t) \quad (6.24)$$

and hence:

$$\varepsilon_{\perp}(t) = \frac{w_{tot}(t)}{b_i} \quad (6.25)$$

where  $w_{tot}(t) = \sum w_i(t)$  is the sum of the mean opening cracks of all the bars.

Several relationships are proposed in literature to evaluate the crack opening  $w$ . The following empirical model is assumed in (Vidal *et al.*, 2004):

$$w = \kappa_w (\delta_s(t) - \delta_{s0}) A_{s0} \quad (6.26)$$

where  $\kappa_w = 0,0575 \text{ mm}^{-1}$  and  $\delta_{s0}$  is the amount of steel damage necessary for cracking initiation. This damage threshold is evaluated as follow:

$$\delta_{s0} = 1 - \left[ 1 - \frac{R}{D_0} \left( 7,53 + 9,32 \frac{c}{D_0} \right) \times 10^{-3} \right]^2 \quad (6.27)$$

where  $c$  is the concrete cover. The crack opening increases with the expansion of corrosion products up to a critical width, conventionally sets to  $1 \text{ mm}$ . The *spalling of concrete cover* is assumed to occur when this threshold is reached.

According to (Biondini and Vergani, 2012), the reduction of concrete strength is not applied to the entire concrete cover, but it is limited to the zones adjacent to reinforcing bars. Fig. 6.7 shows a model where the reduction of concrete strength is applied to a portion of concrete cover surrounding the corroded bars within a radius equal to the cover thickness. Through such an approach, both the mechanisms of *spalling* of the concrete cover and *delamination* phenomena can be dealt with.

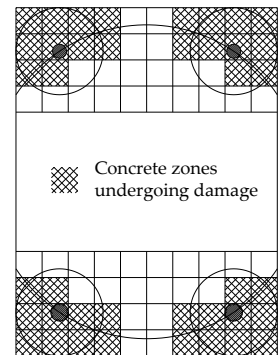


Figure 6.7: Model.

6.4 CRITICAL COMPARISON

As shown, damage modeling needs at first the solution of the diffusion process so that the concentration of the aggressive agent over the sectional domain is known in time ( $C = C(\mathbf{x}, t)$ ); secondly, the evaluation of the dimensionless damage index  $\delta_s = \delta_s(\mathbf{x}, t)$  is required and, once this index is known, the time-evolution of the material characteristics can be evaluated with the previous explained relationships. It's clear that a proper evaluation of  $\delta_s$  plays an important role.

The formulation previously exposed enhances the proposal given in (Biondini *et al.*, 2004b) and assumes a linear relationship between the rate of damage and the concentration of the aggressive agent. Other approaches can be used. In particular, in (Vergani, 2010) and in (Camnasio, 2013) the damage indexes are expressed as a function of the corrosion rate  $r_{corr}$ , that can be assumed according to Fig. 6.8.

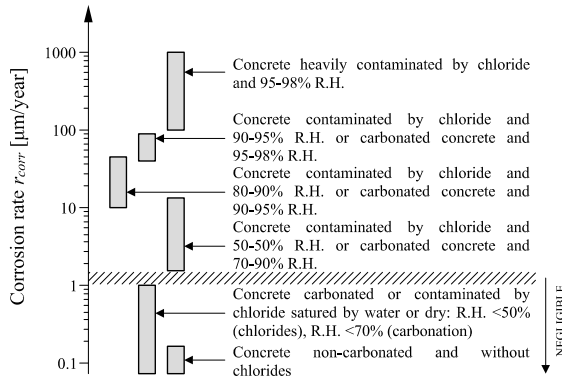


Figure 6.8: Schematic representation of corrosion rate of steel in different concretes and exposure conditions (Camnasio, 2013).

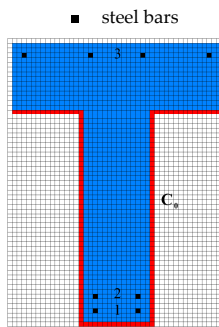


Figure 6.9: Cellular automata grid and steel bars sampling points position.

The different formulations are now compared on the RC section reported in Fig. 6.9. Steel bar's diameter in position 1 is equal to 14 mm and in position 2 and 3 is equal to 12 mm. On the bottom edges of the section (red edges), a chlorides concentration with  $C_0 = 1.5\%$  (mass chlorides percentage over mass cement) acts. The following data are assumed:  $\Delta t_s = 40 \text{ years}$ ,  $\rho = 0.025/C_0$  and  $C_{cr} = 0.6\%$ .



Once the boundary conditions are defined, the diffusion process is simulated by cellular automata, with a diffusion coefficient  $D = 10 \times 10^{-12} \text{ m}^2/\text{s}$ , a grid dimension  $\Delta x = 10 \text{ mm}$  and a time step  $\Delta t = 0.04 \text{ years}$ . The obtained concentration maps of the aggressive agent in time are reported in Fig. 6.10.

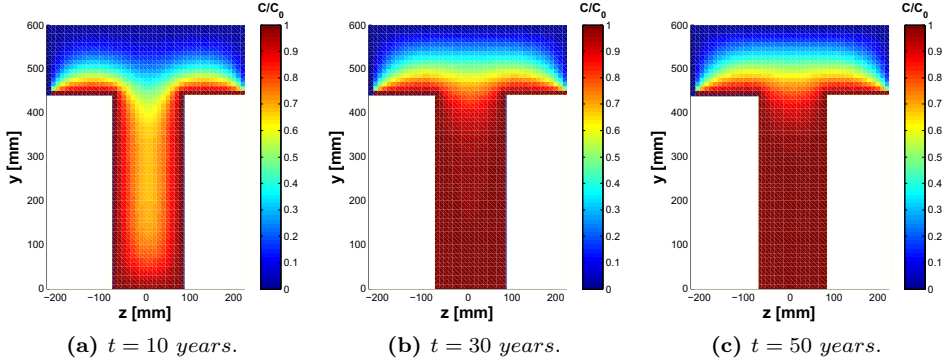


Figure 6.10: Normalized concentration maps in time.

The dimensionless damage index  $\delta_s$  is reported, for all the considered formulations, in Fig. 6.11. In particular, Fig. 6.11a refers to steel bars in position 1 and Fig. 6.11b to steel bars in position 2.

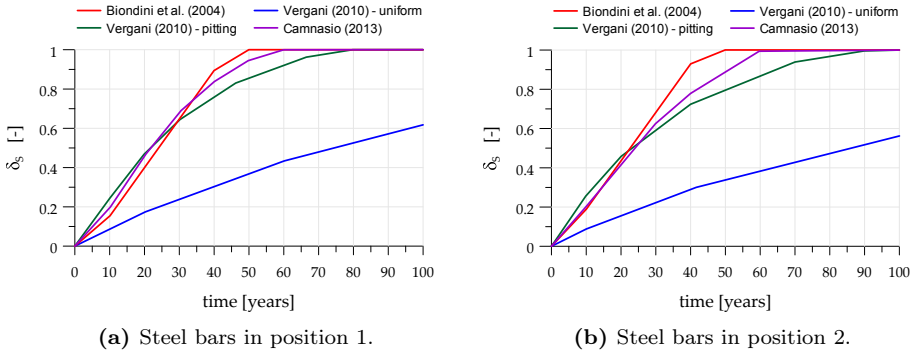


Figure 6.11: Comparisons between different formulations for the dimensionless damage index  $\delta_s$ .

The following comments arise:

- the formulations given in (Biondini *et al.*, 2004b) and (Camnasio, 2013) are very similar. In addition, they produce more safety evaluations, because worst values for the dimensionless damage index  $\delta_s$  are obtained;
- (Vergani, 2010): if a uniform corrosion is considered, wrong predictions of the damage level can be obtained. Better results are obtained if the pitting factor  $R$  is introduced, as  $R = 6$ .

For these reasons, in this thesis the formulation presented in (Biondini *et al.*, 2004b) will be considered. It is worth noting, however, that not only the reduction of steel bars areas is here modeled, but also the reduction of steel ductility, the reduction of concrete strength and the spalling of the concrete cover. All these effects are directly linked with the diffusion process, through the dimensionless damage index  $\delta_s$ .

## 6.5 CLOSING REMARKS

---

Among different aggressive agents interesting RC structures, the presence of chlorides plays a fundamental role. For this reason, the effects of chlorides induced corrosion have been presented. Since corrosion is a complex phenomenon, involving different mechanisms and depending on many parameters, in lifetime structural assessments, seems convenient the adoption of a macroscopic approach that, for its simplicity, can be easily extended in the non deterministic field.

It has been hence assumed that Fick's law holds with an effective diffusion coefficient constant in time. The so-obtained governing equation is a linear partial differential equation whose solution, however, exists only for a limited number of classical cases. In particular, in several European codes the solution is based on a 1D diffusion model. Such a model can be applied in dealing with compact sections, but in general a procedure that considers the real sectional domain is needed. The approach here proposed is based on cellular automata and presents a high level of generality, being able to deal with arbitrary shaped sections and with arbitrary position of reinforcements.

Once the solution of the diffusive process is known in the sectional domain and in time, several damage indexes can be evaluated. In this chapter, four chloride corrosion effects have been presented:

1. the reduction of cross-section of reinforcing bars;
2. the reduction of ductility of reinforcing steel;
3. the reduction of concrete strength;
4. the spalling of the concrete cover.

With the so-obtained procedure, lifetime structural assessments can be performed. It is sufficient to couple the damage model, here exposed, with the structural models presented in Part I. The structural analysis became in this way a sub-module of the damage analysis and the structural behavior can be evaluated not only when the RC structure is *sound*, but also in time, when the structure is progressively *damaged*.

The flow chart of the complete procedure proposed in this thesis is exposed in Fig. 6.12, that clearly shows how the structural analysis is inserted in a loop in the time domain. The logic flow is specialized to a monodimensional modeling with RC beam-column elements, using a tangent approach. However, other solution schemes and other structural models can be used and nested in the damage's model. The proposed procedure is hence very general.

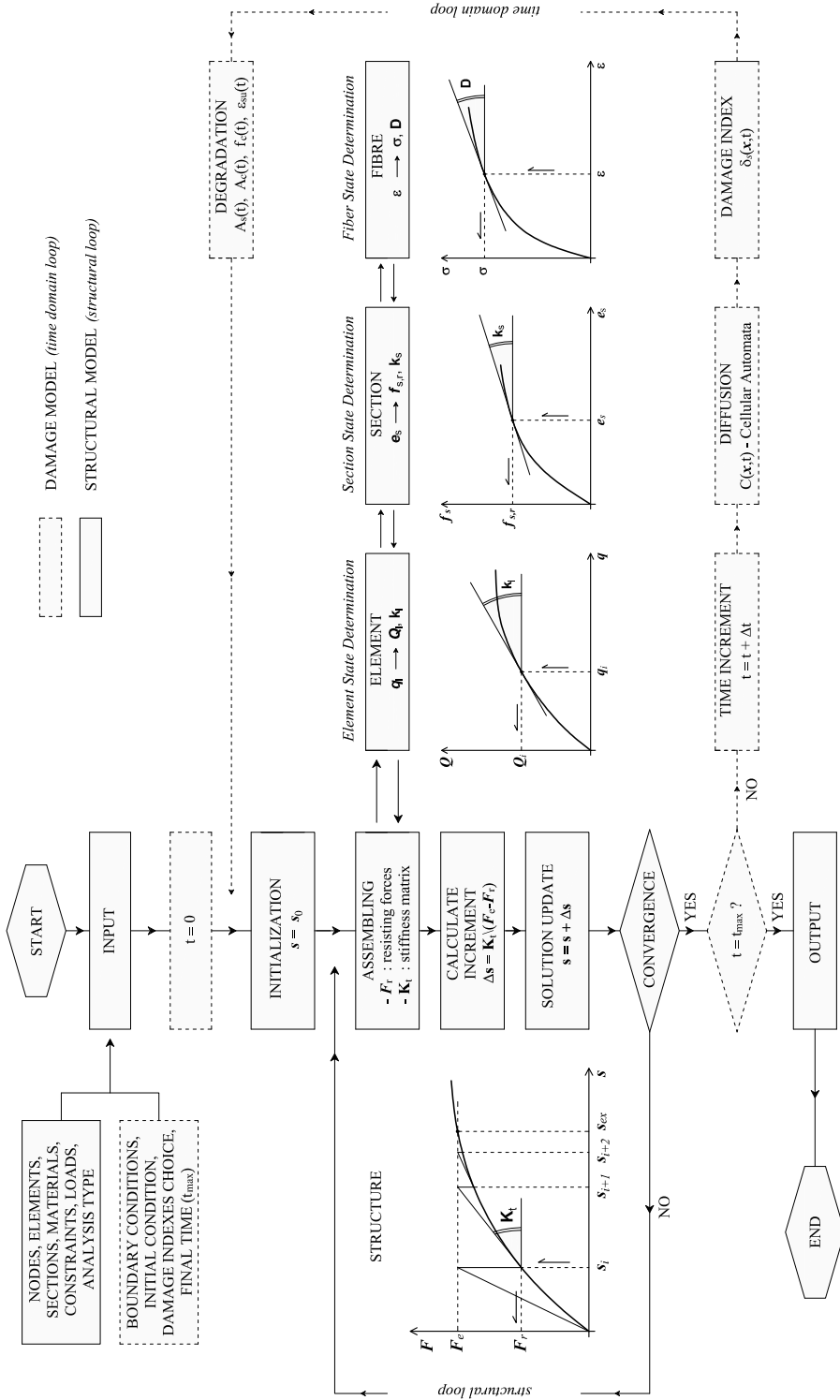


Figure 6.12: Flow chart of the proposed procedure. The structural models are nested in a loop that deals with damage in the time domain.



# III

---

## APPLICATIONS



# 7

## Damage Effects on Structural Performances of Bridges

*This chapter deals with the study of sound and damaged RC bridges. The damage's effects are coupled with the structural performances in order to consider time-variant capacity accounting for environmental hazards. The structural behavior is carried out by a complete parallel study between Non Linear and Limit Analysis.*

### 7.1 INTRODUCTION

---

The structural performances of two bridges - a Cable Stayed Harp Bridge and an Arch Bridge - are presented. The main aim is to understand which are the damage's effects on the structural behaviors. The formulation exposed in chapter 6 consents to evaluate the effects of corrosion at the material level, by considering the reduction of steel bars areas, the reduction of steel ductility, and the reduction of concrete strength until the spalling of the concrete cover occurs. The procedure, based on cellular automata, deals with RC sections with arbitrary shape and with arbitrary reinforcing positions. Once the damage's effects at the material level are known, the corresponding effects at the sectional level and, then, at the structural level can be obtained by computational structural analysis techniques. In order to deeply investigate the time-variant capacity accounting for environmental hazards, different approaches are considered.

At first, Non Linear Analysis are performed. Non Linear Analysis presents a high level of generality and permits to take into account not only the mechanical non linearities, but also the geometric effects due to configuration's change (see par. 2.6).

Secondly, Limit Analysis are presented. It must be emphasized that the applicability of Limit Analysis to RC structures can be reasonably acceptable if an *effectiveness factor* is considered, as exposed in par. B.1. Since the evaluation of this factor is based on theoretical/empirical/experimental observations, in this context a different choice is adopted and *no correction factors are used*. It follows, of course, that Limit Analysis results are not consistent because concrete is treated as a material with infinite ductility, an assumption too far from reality. However, the so-obtained not consistent results can be compared with Non Linear Analysis

ones that give, instead, a more realistic collapse load without requiring effectiveness factor definitions. In this way, a sort of *structural effectiveness factor* can be numerically obtained.

Since Limit Analysis described in this thesis do not considered shear's effects, but only bending moment - axial forces interactions, Non Linear Analysis is performed with the common RC beam finite element presented in par. 2.3 - 2.4.

All these comparisons are performed both for *sound and damaged* bridges, so that the structural performances can be evaluated not only at the age of construction but, by using the technique exposed in chapter 6, also in time.

### 7.2 SOUND CABLE STAYED BRIDGE

The cable stayed harp bridge presented in (Seif and Dilger, 1990) and (Bontempi *et al.*, 1995a) is considered. The geometry of the structure, the different section's types and the different levels of prestress in the deck are reported in Fig. 7.1. Fig. 7.2 reports the geometry of the sections and the reinforcing steel positions. The sectional characteristics and the different levels of prestress are reported in Tab. 7.1.

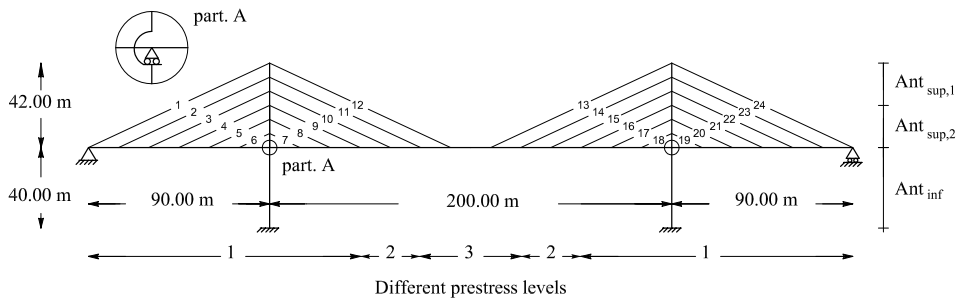


Figure 7.1: Cable Stayed Harp Bridge: geometry, sections and prestress levels.

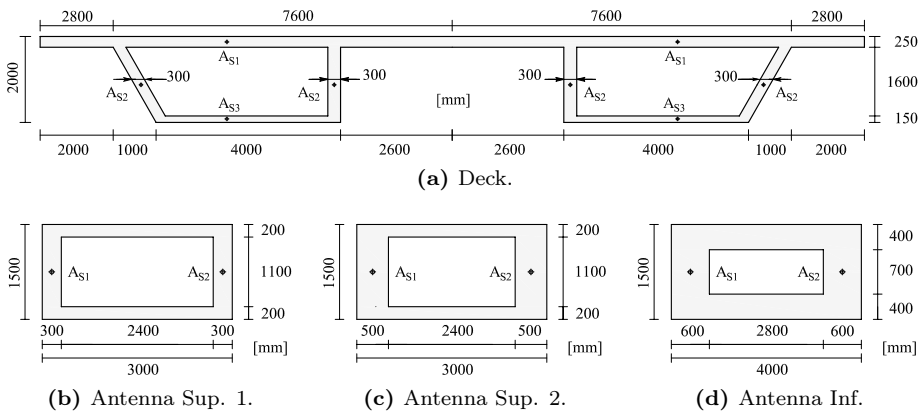


Figure 7.2: Cable Stayed Harp Bridge: geometry of the sections.

The loads acting on the bridge are:



1. the death weight  $q$ , introduced by a uniform distributed load on the deck with intensity equal to  $q = 100 \text{ kN/m}$ ;
2. the prestressing forces in the bridge's deck  $F_{P0}$ , introduced by equivalent nodal forces according to Tab. 7.1;
3. the pretensioning forces  $T_{i=1:24}$  in the cables, evaluated so that the deck, under the self weight  $q$ , presents zero displacements in correspondence of the stays.

	$A_{cls} [m^2]$	$A_{s1} [cm^2]$	$A_{s2} [cm^2]$	$A_{s3} [cm^2]$	$A_p [cm^2]$	$F_{P0} [kN]$
Deck 1	3.96	150	50	150	80	9600
Deck 2	3.96	150	50	150	160	19200
Deck 3	3.96	150	50	150	240	28800
Ant. Inf	4.04	202	202		0	0
Ant. Sup 2	2.30	131	131		0	0
Ant. Sup 1	1.86	130	130		0	0

(a) Geometrical characteristics.

Concrete	$f'_c = -34 \text{ MPa}$	$\varepsilon_{c0} = -0.002$	$\varepsilon_{cu} = -0.0035$
Normal steel	$f_{sy} = 400 \text{ MPa}$	$E_s = 200000 \text{ MPa}$	$\varepsilon_{sy} = 0.02$
Prestressing steel	$f_{spsy} = 1680 \text{ MPa}$	$E_{sp} = 190000 \text{ MPa}$	$\varepsilon_{spy} = 0.0088$

(b) Mechanical characteristics.

**Table 7.1:** Cable Stayed Harp Bridge: geometrical/mechanical characteristics and prestressing levels.

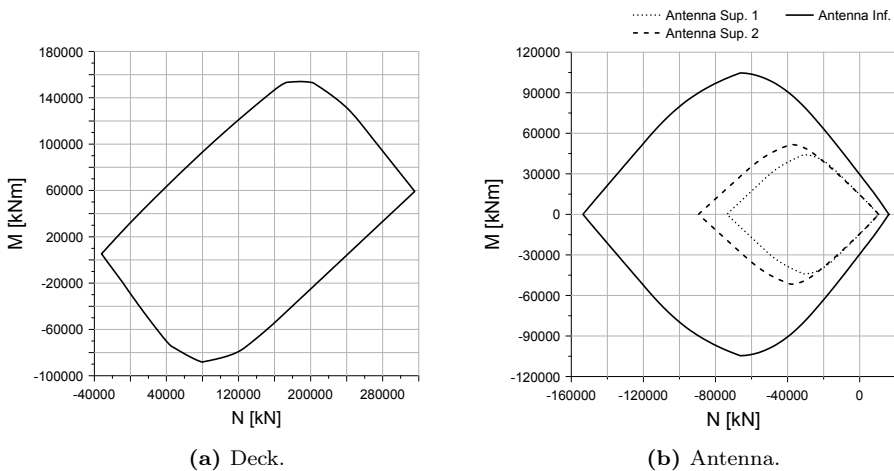


**Figure 7.3:** Cable Stayed Harp Bridge: Axial Force-Bending Moment Resistance Diagrams.

7.2.1 CABLE PRESTRESSING FORCES EVALUATION

The 24 prestressing forces in the cables are evaluated so that, under the self weight  $q$ :

- in all the anchorages stay-deck, the vertical displacements are equal to zero (22 conditions);
- the horizontal displacements at the top of the antennas are equal to zero (2 conditions).

With reference to Fig. 7.1, the following system of equations can be generated:

$$\mathbf{M} \cdot \mathbf{t} = \mathbf{s}_0 \tag{7.1}$$

where matrix  $\mathbf{M}$  contains the displacements due to unitary prestressing forces in the cables,  $\mathbf{t}$  is the unknown prestressing forces vector and  $\mathbf{s}_0$  is the vector containing the displacements due to the self weight  $q$ . In explicit form, the system (7.1) became:

$$\begin{bmatrix} s_1^1 & s_1^2 & s_1^3 & s_1^4 & s_1^5 & \dots & s_1^{23} & s_1^{24} \\ s_2^1 & s_2^2 & s_2^3 & s_2^4 & s_2^5 & \dots & s_2^{23} & s_2^{24} \\ s_3^1 & s_3^2 & s_3^3 & s_3^4 & s_3^5 & \dots & s_3^{23} & s_3^{24} \\ s_4^1 & s_4^2 & s_4^3 & s_4^4 & s_4^5 & \dots & s_4^{23} & s_4^{24} \\ s_5^1 & s_5^2 & s_5^3 & s_5^4 & s_5^5 & \dots & s_5^{23} & s_5^{24} \\ \dots & \dots & \dots & \dots & \dots & \dots & \dots & \dots \\ s_{23}^1 & s_{23}^2 & s_{23}^3 & s_{23}^4 & s_{23}^5 & \dots & s_{23}^{23} & s_{23}^{24} \\ s_{24}^1 & s_{24}^2 & s_{24}^3 & s_{24}^4 & s_{24}^5 & \dots & s_{24}^{23} & s_{24}^{24} \end{bmatrix} \cdot \begin{bmatrix} T_1 \\ T_2 \\ T_3 \\ T_3 \\ T_4 \\ T_5 \\ \dots \\ T_{23} \\ T_{24} \end{bmatrix} = \begin{bmatrix} s_1^0 \\ s_2^0 \\ s_3^0 \\ s_3^0 \\ s_4^0 \\ s_5^0 \\ \dots \\ s_{23}^0 \\ s_{24}^0 \end{bmatrix} \tag{7.2}$$

whose solution is reported in the histogram in Fig. 7.4. The so obtained prestress distribution is not symmetric since the constraints acting on the bridge are not symmetric (an hinge in the left support and a roller in the right one).

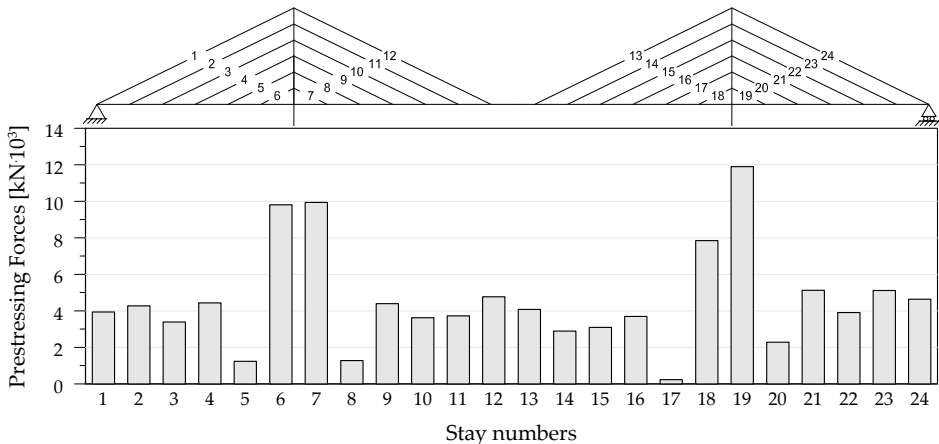


Figure 7.4: Histogram of the prestressing forces in the cables.

## 7.2.2 NON LINEAR ANALYSIS

Non Linear Analysis results are reported in Fig. 7.5 - 7.6 for three different values of the load  $q$  acting on the deck.  $q = 381 \text{ kN/m}$  is the collapse load obtained by considering both mechanical and geometrical non linearities. Instead, the collapse load due to mechanical non linearities only is equal to  $q = 420 \text{ kN/m}$  (see Tab. 7.2).

Analysis	N.L.G.	N.L.M.	Collapse load	Load Factor
(1)	✓	✓	$381 \text{ kN/m}$	3.81
(2)	-	✓	$420 \text{ kN/m}$	4.20

**Table 7.2:** Different analysis for the Cable Stayed Bridge. N.L.G. = Non Linear Geometry, N.L.M. = Non Linear Mechanics.

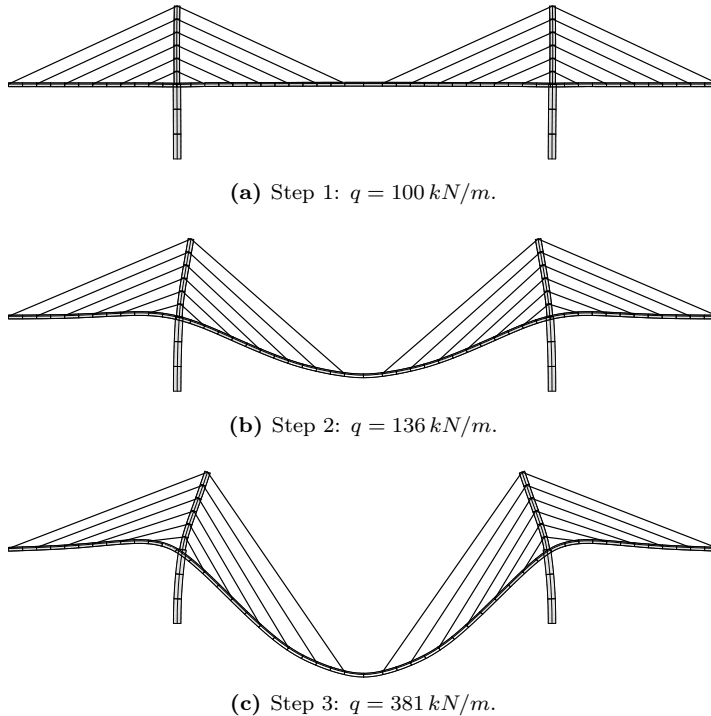
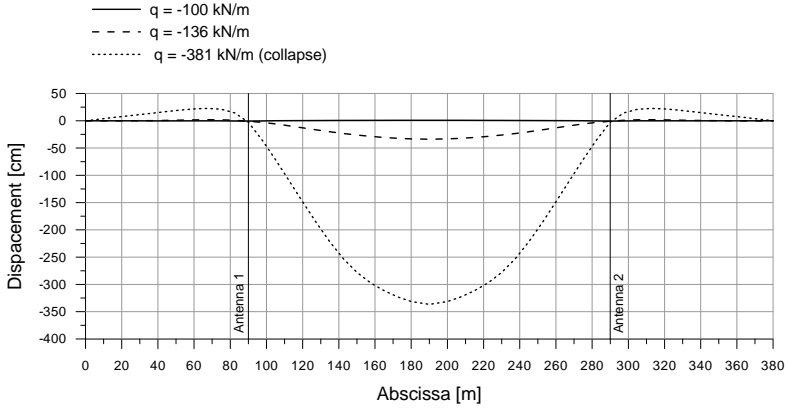
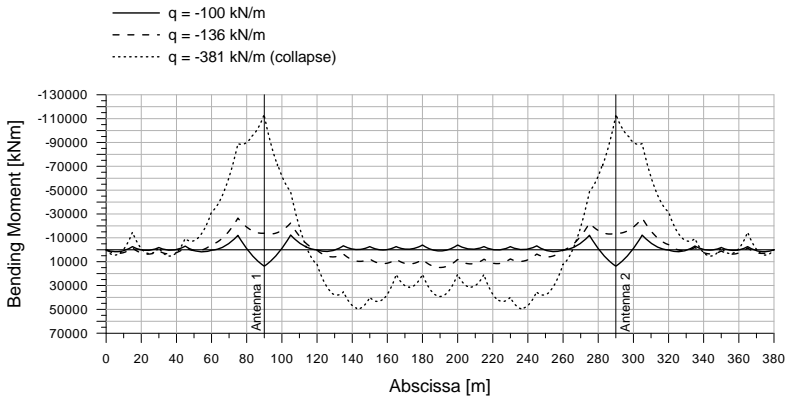


**Figure 7.5:** Cable Stayed Harp Bridge: deformed configurations until collapse.

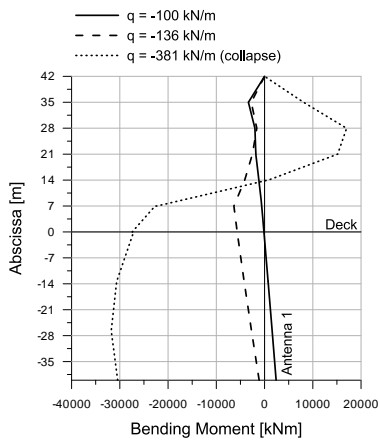
The displacements and the bending moments in the deck, with the bending moments in the pylons are reported in Fig. 7.6, for the three different values of the load  $q$  acting on the deck. It can be observed that, under  $q = 100 \text{ kN/m}$ , the deck's displacements are practically coincident with zero, since this load combination has been chosen in order to design the prestressing forces in the stays.



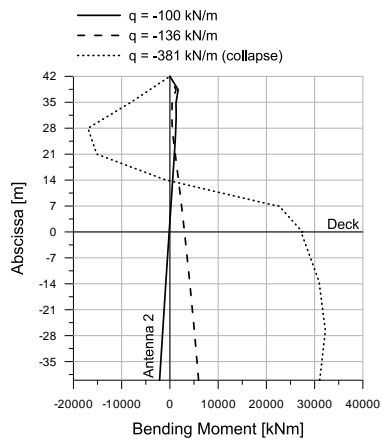
(a) Displacements in the deck.



(b) Bending moments in the deck.



(c) Bending moments in left pylon.



(d) Bending moments in right pylon.

Figure 7.6: Cable Stayed Harp Bridge: displacements and bending moments in the deck and bending moments in the pylons.

7.2.3 LIMIT ANALYSIS AND COMPARISONS

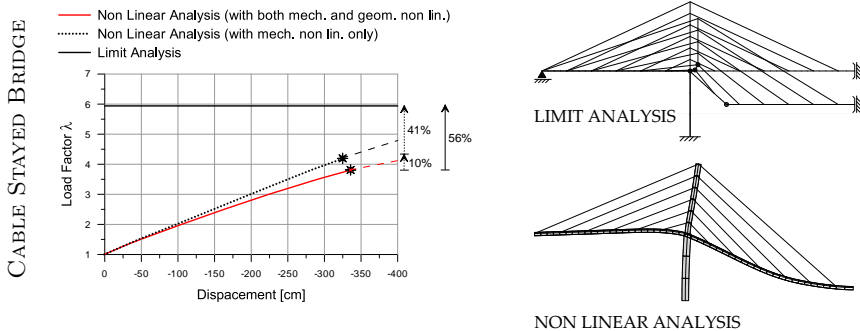
Limit Analysis requires the definition of the interaction domains for all the sections of the bridge. Concerning the pylon and the deck, the domain used in the analysis are reported Fig.7.3. The stays, instead, are considered infinitely resisting. The collapse load obtained by Limit Analysis is equal to  $q = 594 \text{ kN/m}$  and the relative mechanism is show in Tab.7.3. By comparing Non Linear Analysis and Limit Analysis, the following observations arise, Tab. 7.3:

- Limit and Non Linear Analysis results are not equal. By comparing the collapse load due to Limit Analysis and the one due to Non Linear Analysis without geometrical effects there is a difference that can be used in order to determine a sort of *numerical structural effectiveness factor*  $\nu_e$ :

$$\nu_e = \frac{\lambda_{NLA}}{\lambda_{LA}} = \frac{420}{594} = 0.71$$

- the geometrical effects on the collapse load can be estimated with a percentage that is approximately equal to 10 %;
- despite the results are different, both the analyses identify as critical structural part the bottom of the antenna. In particular, Non Linear Analysis predict here a large concentration of deformations; Limit Analysis, instead, predicts the formation of three plastic hinges as the collapse mechanism shown.

	Collapse Load	Load Factor
An. (1)	381 $\text{kN/m}$	3.81
An. (2)	420 $\text{kN/m}$	4.20
An. (3)	594 $\text{kN/m}$	5.94

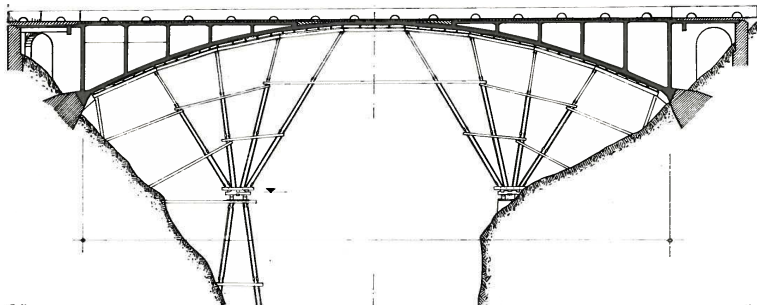


An. (1)	Non Linear Analysis (with both mechanical and geometrical non linearities)
An. (2)	Non Linear Analysis (with mechanical non linearities only)
An. (3)	Limit Analysis

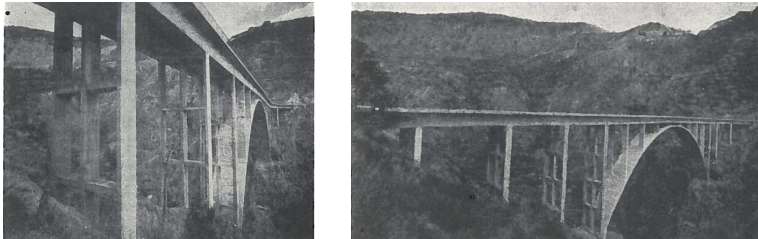
Table 7.3: Cable Stayed Harp Bridge: Non Linear Versus Limit Analysis.

### 7.3 SOUND ARCH BRIDGE (CORACE RIVER, CALABRIA, ITALY)

Following the same procedures adopted for the cable stayed bridge of the previous section, Non Linear Analysis and Limit Analysis are now compared with reference to the reinforced concrete arch bridge over the Corace river in Italy (Fig. 7.7). The bridge, designed by Galli and Franciosi (1955), presents a span equal to 80 m and a dept equal to 26.10. The bridge is more than half a century old.



(a) Construction process.



(b) View of the bridge.

**Figure 7.7:** Corace Bridge (Calabria, Italy), (Franciosi, 1959).

The structural model refers to the data presented in (Galli and Franciosi, 1955) and (Ronca and Cohn, 1979b). The beam has a two-cellular cross-section with main nominal dimensions  $6.00\text{ m} \times 2.00\text{ m}$ . The distribution of the reinforcements along the beam refers to the subdivision shown in Fig. 7.8 and is given in Tab. 7.4c. The arch has a  $6.00\text{ m} \times 0.57\text{ m}$  rectangular cross-section and it is reinforced with  $45 + 45 = 90$  steel bars, each having a nominal diameter  $\phi = 28\text{ mm}$  (see Tab. 7.4d and Fig. 7.9b).

With reference to Fig. 7.8, two types of loads are considered:

(1) dead load:

- an uniform distributed load on the beam:  $g_0 = 102.9\text{ kN/m}$ ;
- an uniform distributed load on the arch:  $g_1 = 85.0\text{ kN/m}$ ;

(2) live load:

- an uniform distributed load acting on the half span of the beam:  
 $p = 53.3\text{ kN/m}$ .

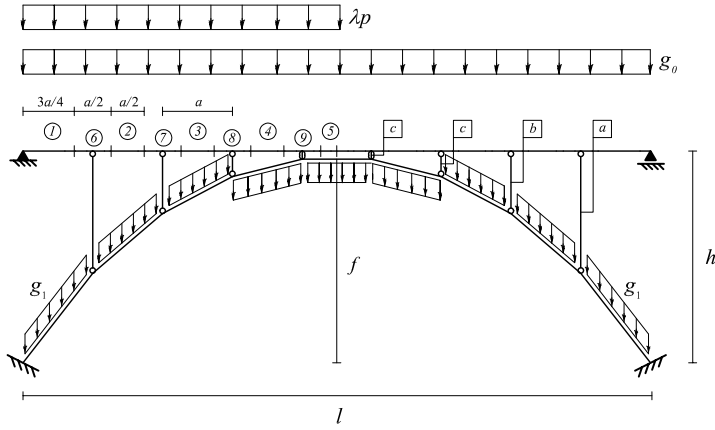


Figure 7.8: Geometry of the bridge.

$x$ [m]	$y$ [m]
0.00	0.00
8.89	11.43
17.80	19.04
26.70	23.76
35.60	25.98
40.00	26.10

(a) Arch Shape.

Data		
$l$	80.00	m
$f$	26.10	m
$h$	27.00	m
$g_0$	102.90	kN/m
$g_1$	85.00	kN/m
$g_0$	53.30	kN/m

(b) Geometric data.

Beam	1	2	3	4	5	6	7	8	9
$A'_s$	21 $\phi$ 28	48 $\phi$ 28	42 $\phi$ 28	30 $\phi$ 28	24 $\phi$ 8	48 $\phi$ 8	48 $\phi$ 8	45 $\phi$ 8	33 $\phi$ 8
	130 $\phi$ 8	130 $\phi$ 8	130 $\phi$ 8	130 $\phi$ 8	130 $\phi$ 8	130 $\phi$ 8	130 $\phi$ 8	130 $\phi$ 8	130 $\phi$ 8
$A_s$	21 $\phi$ 28	30 $\phi$ 28	42 $\phi$ 28	24 $\phi$ 28	24 $\phi$ 28	21 $\phi$ 28	36 $\phi$ 28	27 $\phi$ 28	24 $\phi$ 28

(c) Distribution of the top  $A'_s$  and bottom  $A_s$  reinforcement along the beam.  $n\phi d = n$  steel bars with diameter  $d$  [mm].

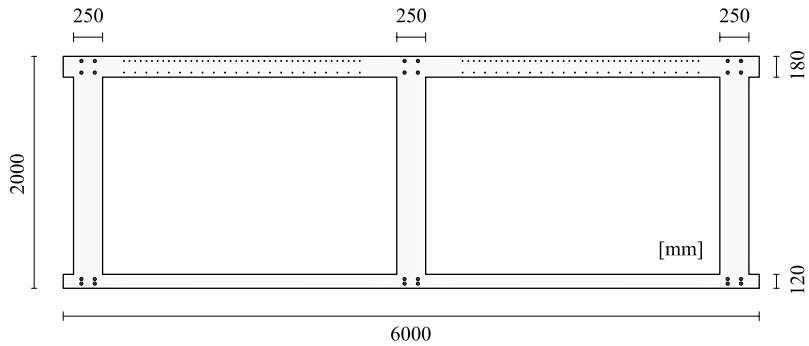
Element	$A'_s$	$A_s$
Arch	45 $\phi$ 28	45 $\phi$ 28
Supp. Walls - Type (a)	12 $\phi$ 18	12 $\phi$ 18
Supp. Walls - Type (b)	12 $\phi$ 18	12 $\phi$ 18
Supp. Walls - Type (c)	12 $\phi$ 18	12 $\phi$ 18

(d) Reinforcement distribution in the arch and supporting walls.

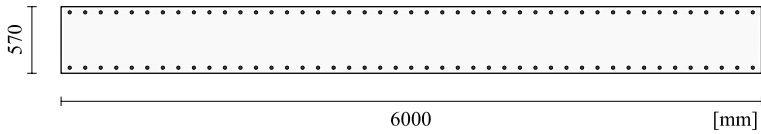
Concrete	$f_c$	= -30 MPa	$\epsilon_{cu}$	= -0.0035	$\epsilon_{c0}$	= -0.002
Steel	$f_{sy}$	= 300 MPa	$E_s$	= 206000 MPa	$\epsilon_{sy}$	= 0.0014563

(e) Material's characteristics.

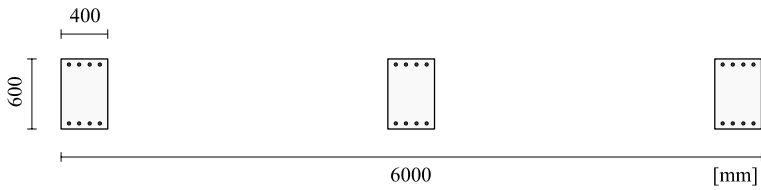
Table 7.4: Corace Bridge: reinforcing steel and material's characteristics.



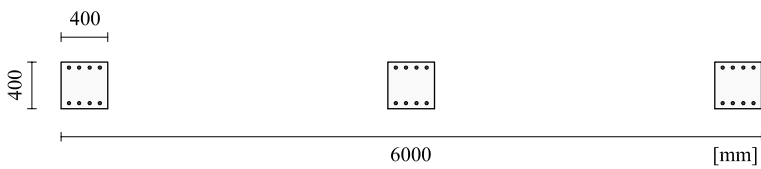
(a) Beam's section.



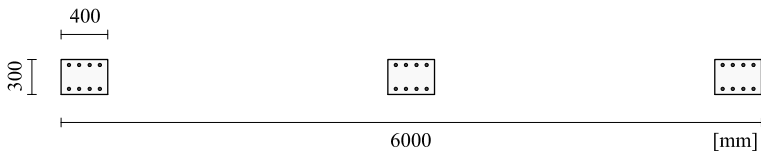
(b) Arch section.



(c) Column - Type (a) section.



(d) Column - Type (b) section.



(e) Column - Type (c) section.

**Figure 7.9:** Corace Bridge: geometry of the sections and reinforcement positions.



The bridge is analyzed with different type of analysis, not only with the aim of compare them, but principally in order to understand the structural behavior:

- Non Linear Analysis:
  - with mechanical and geometric non linearities;
  - with mechanical non linearities only;
- Limit Analysis:
  - without considering geometric non linearities and without applying effectiveness factor.

It is recalled that with Limit Analysis only informations related to the collapse are obtained. Since no effectiveness factor are used, limit analysis results are not consistent. In contrast, with Non Linear Analysis we can follow the real structural behavior for all the range of loadings and the definition of effectiveness factor is not required. Hence, by comparing Non Linear with Limit results, a sort of numerical structural effectiveness factor can be obtained.

### 7.3.1 NON LINEAR ANALYSIS

Non Linear Analysis results are reported in Fig. 7.10 for two different values of the load  $p$  acting on the deck.  $p = 112 \text{ kN/m}$  is the collapse load obtained by considering both mechanical and geometrical non linearities. Instead, the collapse load due to mechanical non linearities only is equal to  $p = 157 \text{ kN/m}$  (see Tab. 7.5).

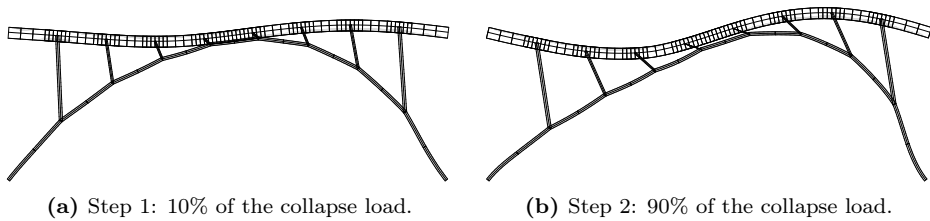


**Figure 7.10:** Non Linear Analysis: deformed configuration until collapse.

Analysis	N.L.G.	N.L.M.	Collapse load	Load Factor
(1)	✓	✓	$112 \text{ kN/m}$	2.10
(2)	-	✓	$157 \text{ kN/m}$	2.95

**Table 7.5:** Different analysis for the Corace Bridge. N.L.G. = Non Linear Geometry, N.L.M. = Non Linear Mechanics.

7.3.2 LIMIT ANALYSIS AND COMPARISONS

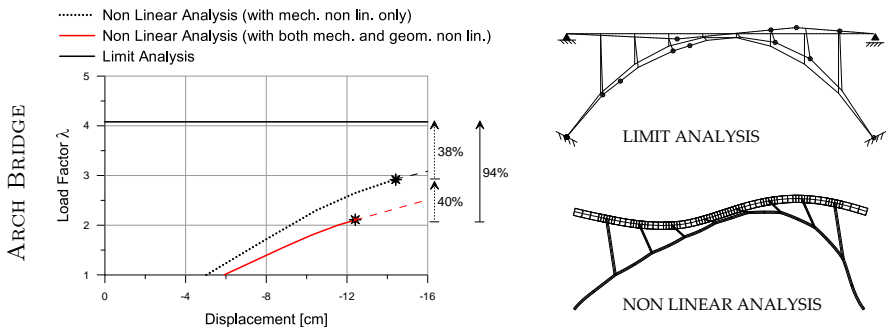
Limit Analysis requires the definition of the interaction domains for all the sections of the bridge. Concerning the arch and the beam, the domain used in the analysis are reported, also for sound conditions, in Fig. 7.17. Since the supporting walls are only compressed, they are assumed infinitely resisting. The collapse load obtained by Limit Analysis is equal to  $p = 217\text{ kN/m}$  and the relative mechanism is show in Tab. 7.6. By comparing Non Linear Analysis and Limit Analysis, the following observations arise (Tab. 7.6):

- Limit and Non Linear Analysis results are not equal. By comparing the collapse load due to Limit Analysis and the one due to Non Linear Analysis without geometrical effects there is a difference that can be used in order to determine a sort of *numerical structural effectiveness factor*  $\nu_e$ :

$$\nu_e = \frac{\lambda_{NLA}}{\lambda_{LA}} = \frac{157}{217} = 0.72$$

- the geometrical effects on the collapse load can be estimated with a percentage that is approximately equal to 40%;
- despite the results are different, both the analyses identify the same critical structural parts (see the comparisons between deformed configuration obtained with Non Linear Analysis and the mechanism obtained with Limit Analysis in Tab. 7.6).

	Collapse Load	Load Factor
An.(1)	112 kN/m	2.10
An.(2)	157 kN/m	2.95
An.(3)	217 kN/m	4.08



An. (1)	Non Linear Analysis (with both mechanical and geometrical non linearities)
An. (2)	Non Linear Analysis (with mechanical non linearities only)
An. (3)	Limit Analysis

Table 7.6: Arch Bridge: Non Linear Versus Limit Analysis.

## 7.4 DAMAGED ARCH BRIDGE (CORACE RIVER, CALABRIA, ITALY)

As already said, the Corace Bridge studied in the previous section is more than an half century old. For this reason, the lifetime behavior of the bridge is now presented and, by considering different scenarios, the damage effects on the structural performances are outlined and discussed.

The same structure has been studied also in (Biondini and Frangopol, 2008), in a probabilistic limit context. However, the effects considered here are not only due to the *reduction of steel bars areas*, but also to the *reduction of steel ductility*, the to *reduction of concrete strength* and to the *concrete spalling*, according to the formulation presented in chapter 6. In addition, Non Linear and Limit Analysis are compared in order to understand the *evolution of the effectiveness factor* in time.

### 7.4.1 CORROSION SCENARIOS

In order to perform lifetime predictions, the informations about types, position, and intensities of the aggressive agents are required. In the following, three types of chlorides-corrosion scenarios are considered according to Fig. 7.11:

1. only arch is interested by corrosion, in the adjacent zones to the supporting walls (Fig. 7.11a);
2. only beam is interested by corrosion, in the zones highlighted by Fig. 7.11b;
3. both arch and beam are interested by corrosion, according to Fig. 7.11c;

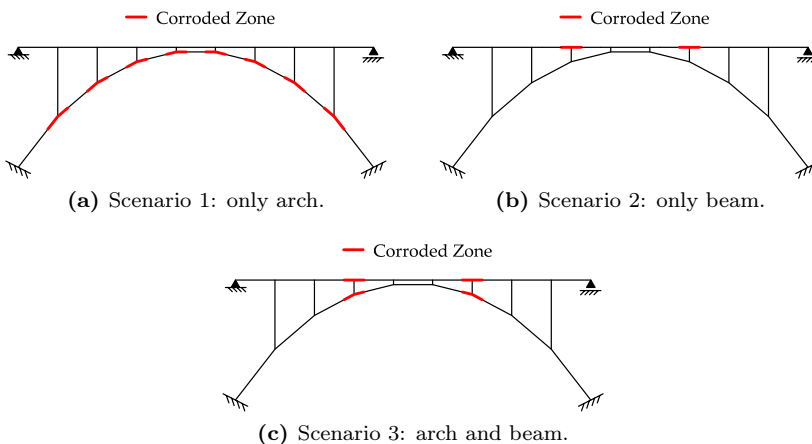


**Figure 7.11:** Corrosion scenarios: longitudinal distribution of the aggressive agent.

In addition to the longitudinal position of the corroded zones, the local sectional distributions are needed. Concerning the beam, it is reasonable to assume that chlorides attack interests only the lateral and the bottom parts of the section; concerning the arch, since it is completely exposed, all the 4 external parts of the section are considered attacked. The so obtained sectional corrosion scenarios are reported in Fig. 7.12.

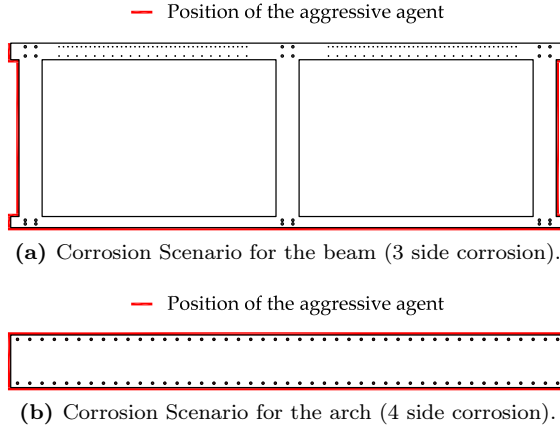


**Figure 7.12:** Corrosion scenarios: sectional distribution of the aggressive agent.

**7.4.2 SOLUTION OF THE DIFFUSION PROCESS**

With reference to Fig. 7.12, the diffusion process is dealt with cellular automata. By considering a nominal diffusivity coefficient  $D = 10^{-11} m^2/s$ , the cellular automaton is defined by a grid dimension  $\Delta x = 10 mm$  and a time step  $\Delta t = 0.16 year$ . Damage rates are assumed to be defined by the values  $C_0 = 3\%$ .

The diffusion process is highlighted in Fig. 7.13 and 7.14, where the maps of concentration  $C(\mathbf{x}, t)/C_0$  of the aggressive agent at different time instants are shown in the arch and the beam respectively.

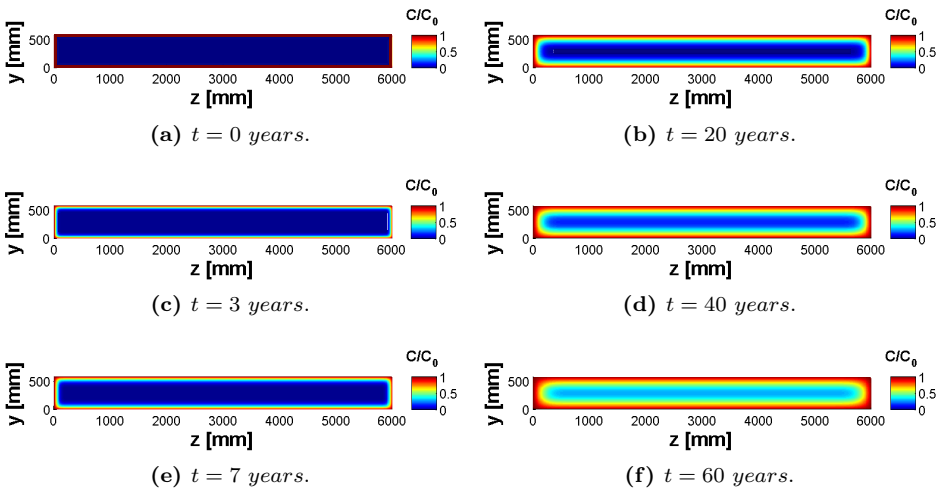


**Figure 7.13:** Evolution in time of the normalized concentration maps for the arch.

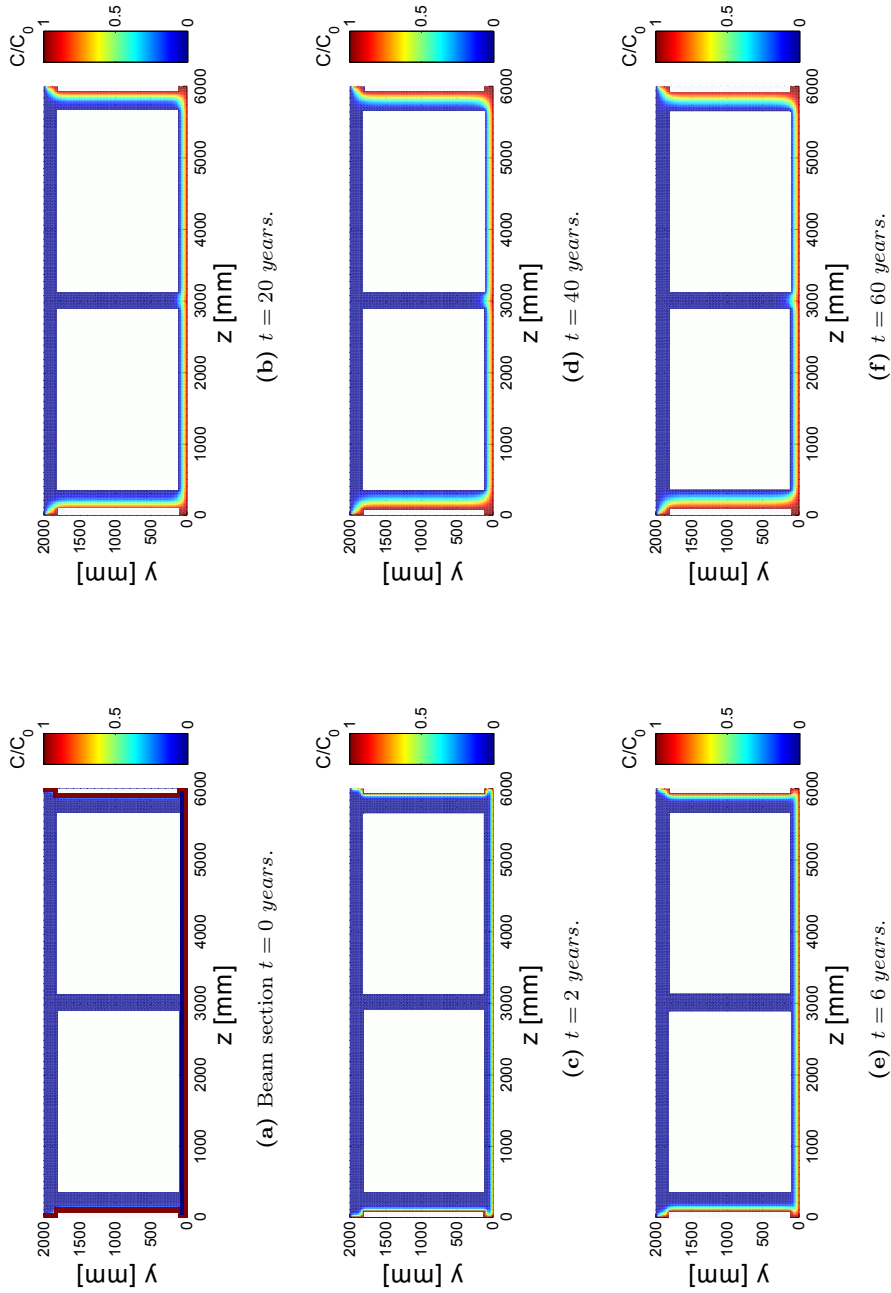


**Figure 7.14:** Evolution in time of the normalized concentration maps for the beam.

### 7.4.3 MECHANICAL DAMAGE INDUCED BY CORROSION

Once the diffusion process has been solved, damage indexes can be computed in all the points of the cross-section, for all the materials, and for all the time instants. Several damage's effects are here considered:

1. reduction of steel bars areas;
2. reduction of steel ductility;
3. reduction of concrete strength;
4. spalling of the concrete cover.

According to what exposed in section 6.3.4, that not all the parts of the section are interested by effects 3 – 4, but only the zones adjacent to reinforcing bars. In this way, both local effects and delamination phenomena can be dealt with.

The obtained corrosion effects on the cross-sections are reported in Fig. 7.15-7.16, which show the concrete parts interested by spalling. It can be observed that in the beam, due to the position of reinforcing steel and to the choice of the aggressive scenario (the upper part is not interested by corrosion), spalling interests three *local* zones at the bottom. Instead, in the arch, spalling interests all the external parts of the cross-section (*delamination*). In the same Figs., specific evolutions of geometrical and mechanical parameters are showed in time:

- in the beam, Fig. 7.15, the damage effects in the central upper part of the section are equal to zero. Instead, the maximum values of corrosion are obtained in the external corners at the bottom. This clearly depends not only on the geometry of the section, but also on the corrosion scenario considered (in this case, only the two lateral and the bottom parts of the section are attacked by the aggressive agent);
- in the arch, Fig. 7.16, the same reductions are obtained in the upper and the bottom parts, due to the symmetry of the corrosion scenario that interests all the 4 sides of the section.

All these considerations concern the time effects of damage on the materials and on the relative distributions in the sectional domain. In order to understand the damage effects on the section's performances, the time evolution of the resistance curves  $f(N, M) = 0$  are reported in Fig. 7.17. It can be observed that we have a reduction in time and the spalling of the concrete cover acts like a discontinuity (cyan area). In the beam, spalling's effect is very limited, in the arch, instead, spalling produces a big reduction of the sectional resistance.

In the following, aiming to describe the effects of damage at the structural level, two types of evaluations are presented:

1. the damage effects on the *service* performance of the bridge, where Non Linear Analysis is used;
2. the damage effects on the *ultimate* performance of the bridge, where Non Linear Analysis is compared, in time, with Limit Analysis.

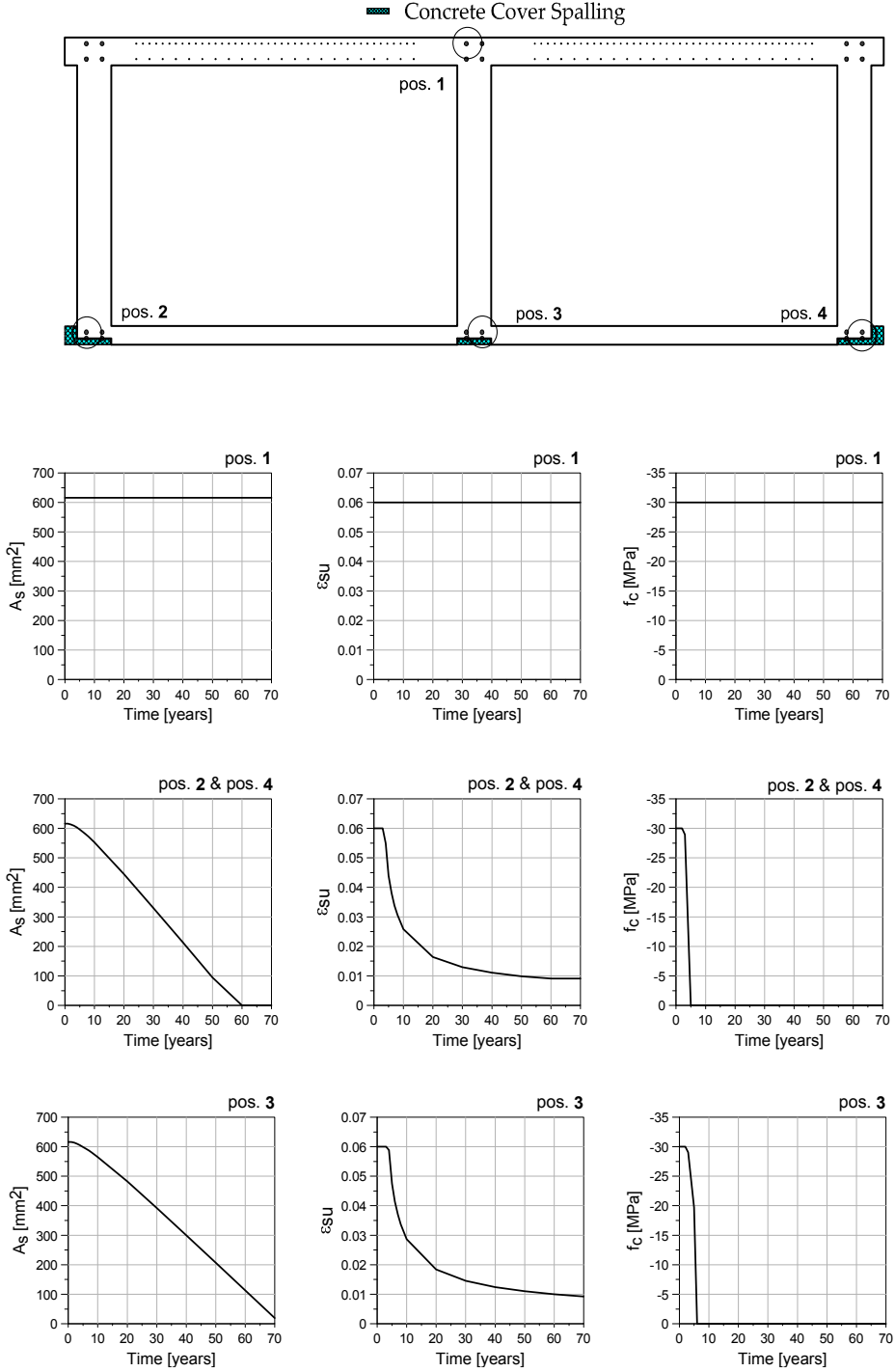


Figure 7.15: Damage effects on the section of the beam.

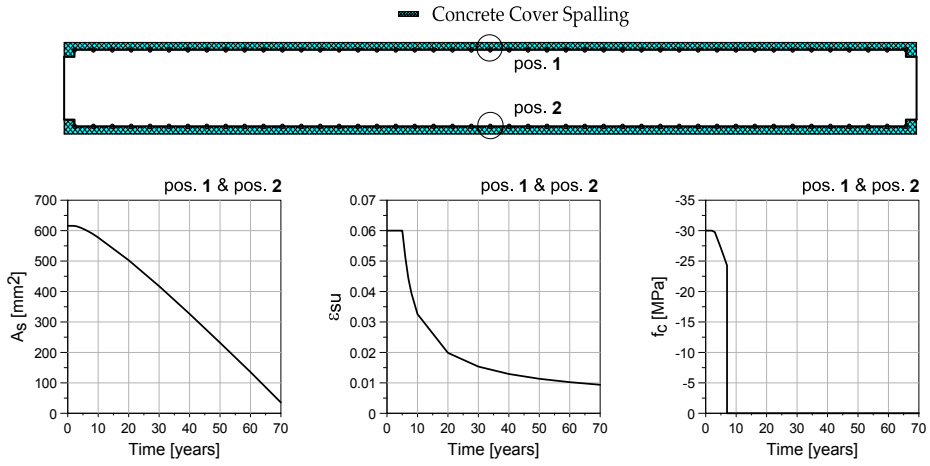


Figure 7.16: Damage effects on the section of the arch.

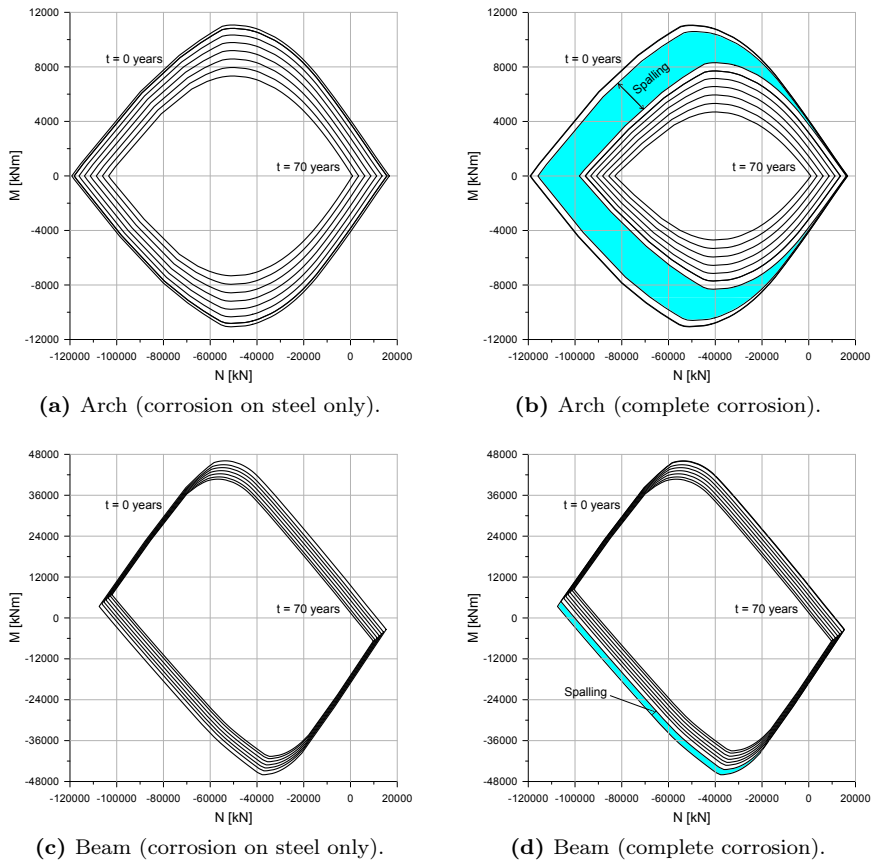


Figure 7.17: Axial Force-Bending Moment Resistance Diagrams.



7.4.4 EFFECTS ON SERVICE PERFORMANCE

In order to understand the damage effects on the service performances of the bridge, the influence line of the vertical displacement in the mid-span of the beam, due to a moving 30 tons truck, is presented in time. As clearly Fig. 7.18 shows, the damage effects cannot be catch by observing the displacements due to normal load conditions. All the influence lines results in fact coincident and very small variations can be observed at  $t = 40\text{ years}$  and  $t = 60\text{ years}$ .

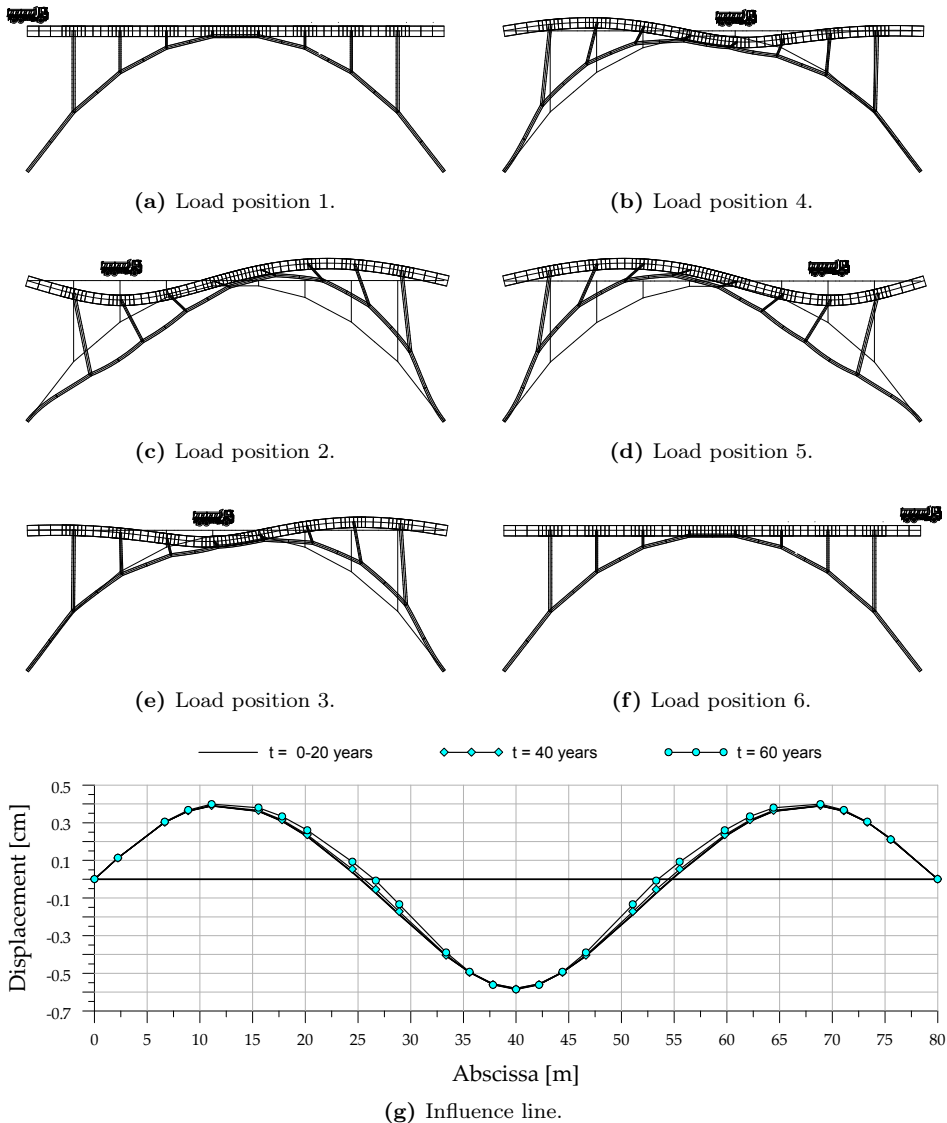


Figure 7.18: Corace Bridge: influence line of the vertical displacement in the mid-span of the beam due to a moving load with intensity equal to 30 tons.

7.4.5 EFFECTS ON ULTIMATE PERFORMANCE

The ultimate performances are now considered and studied both with Non Linear and with Limit Analysis. The time-evolutions of the so obtained collapse multipliers are reported in Fig. 7.19 for the different damage scenarios chosen (see Fig. 7.11):

1. corrosion acts only on the arch. Two sub-cases are considered: (1) only steel is interested by corrosion, Fig. 7.19a; (2) both steel and concrete are interested by corrosion (complete corrosion), Fig. 7.19b;
2. corrosion acts only on the beam, Fig. 7.19c;
3. corrosion acts both on arch and on beam, Fig. 7.19d;

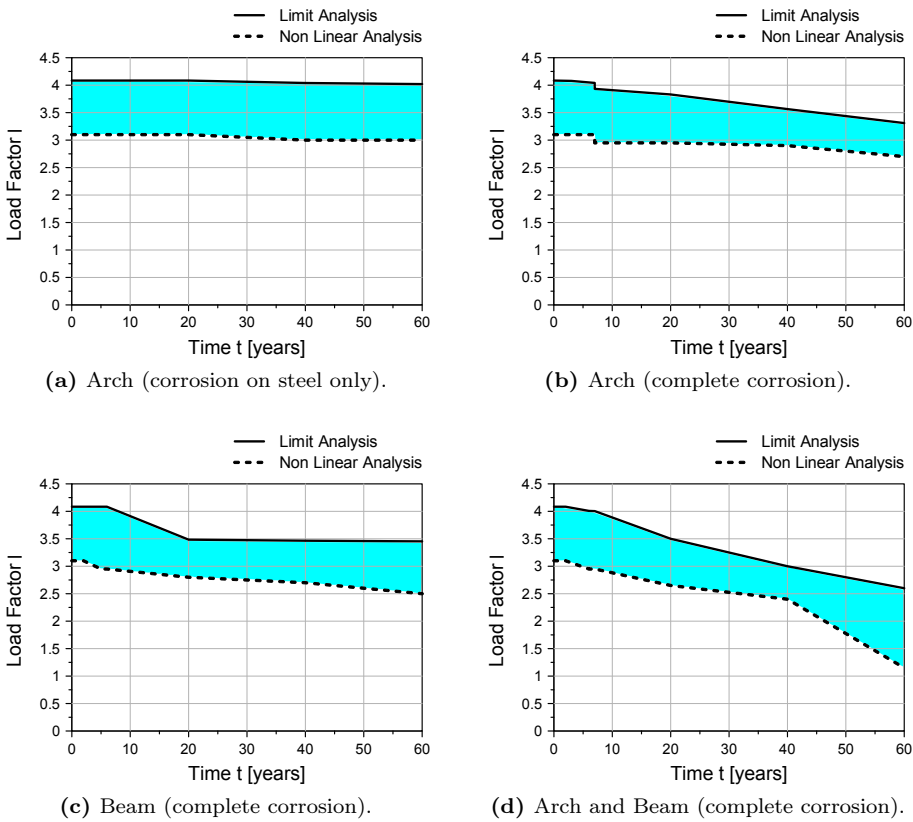


Figure 7.19: Time evolution of the collapse multiplier.

As clearly highlighted in Fig. 7.19a, if corrosion interests only the reinforcements of the arch, significant reductions of the collapse load are not observed. The arch, in fact, works prevalently in compression and hence its behavior depends principally on concrete. However, when a full corrosion is considered as in Fig. 7.19b, the spalling of the concrete cover produce a significant reduction of the arch sectional resisting area; as a consequence, the reduction of the collapse multiplier is higher.

It is interesting to observe the trends between Limit and Non Linear Analysis results. In particular, when corrosion interests the arch, the difference between the two curves is decreasing in time; when corrosion interests the beam, instead, the trend is contrary, with the difference between the two curves that increase in time. Since what we have in the middle is a sort of numerical effectiveness factor at the structural level, defined as:

$$\nu_e = \frac{\lambda_{NLA}}{\lambda_{LA}}$$

it's clear that:

- in the case of arch corrosion, the effectiveness factor is increasing in time and, after 60 *years*, it is equal to  $2.7/3.3 = 0.82$  (see Fig. 7.19b);
- in the case of beam corrosion, the effectiveness factor is decreasing in time and, after 60 *years*, it is equal to  $2.5/3.5 = 0.71$  (see Fig. 7.19c).

The conclusion is that, in the first case, the collapse is governed by reinforcing steel, that presents high ductility; in the second case, instead, the collapse is governed by concrete, for which the assumption of infinite ductility used in Limit Analysis is too far from reality and a more high effectiveness factor is needed.

Such a conclusion is confirmed also by the diagrams in Tab. 7.7 - 7.8 - 7.9, where the time evolutions of the internal forces (axial forces and bending moments) and the collapse mechanisms are given for the three corrosion scenarios.

From Tab. 7.7, it can be observed that a corrosion scenario in the arch produces a redistribution of solicitations that is moved from the arch, damaged, to the beam, that is sound. This happens until a flexural collapse (hence with high ductility) affects the beam.

In Tab. 7.8, instead, the opposite behavior is outlined: if the beam is damaged, the forces progressively moves to the arch, until a collapse due to compression (hence with low ductility) is obtained.

When a mixed scenario is considered as in Tab. 7.8, an intermediate behavior can be observed.

These conclusion are very important in the study of damaged RC structures, because we can directly see which parts of the structure are damaged, but this is not sufficient in order to design a repair intervention since the structure maybe has varied its behavior in time, with a flow of forces that progressively is moved from the damaged parts to the sound ones. A more specific attention is hence required, and a coupling between damage's effects and global structural performances is needed.

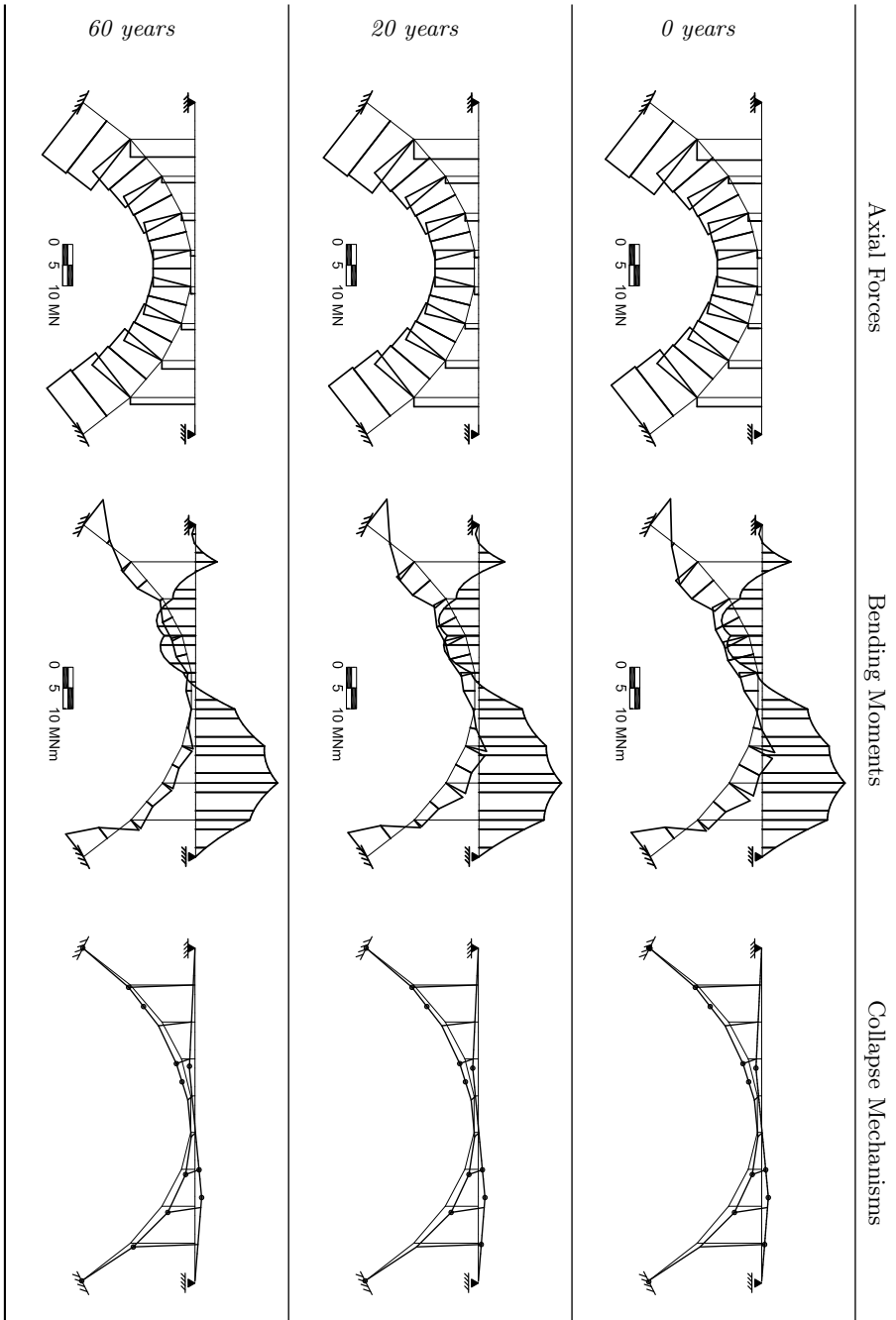


**Table 7.7:** Arch corrosion scenario: axial forces, bending moments and collapse mechanisms in time.

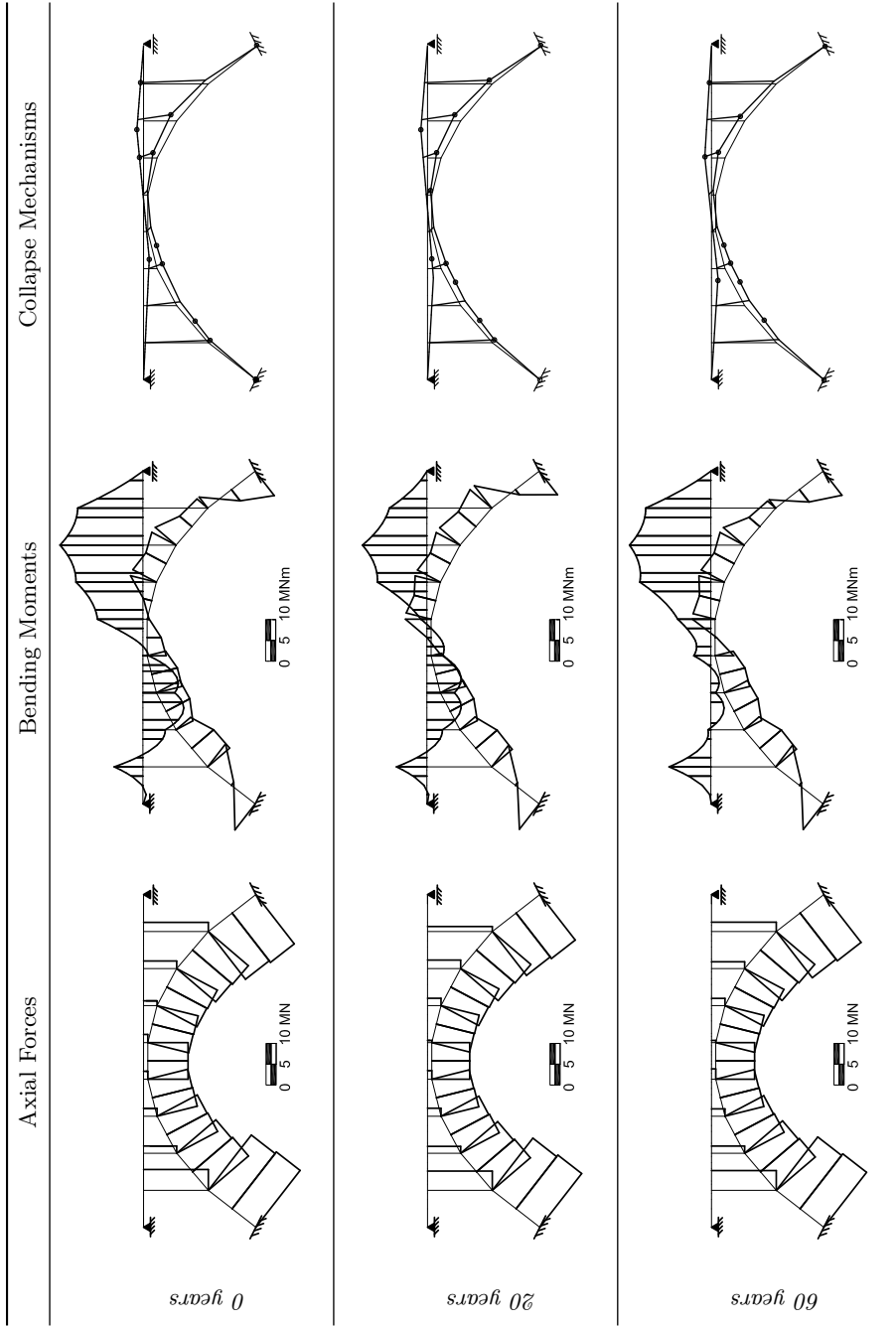
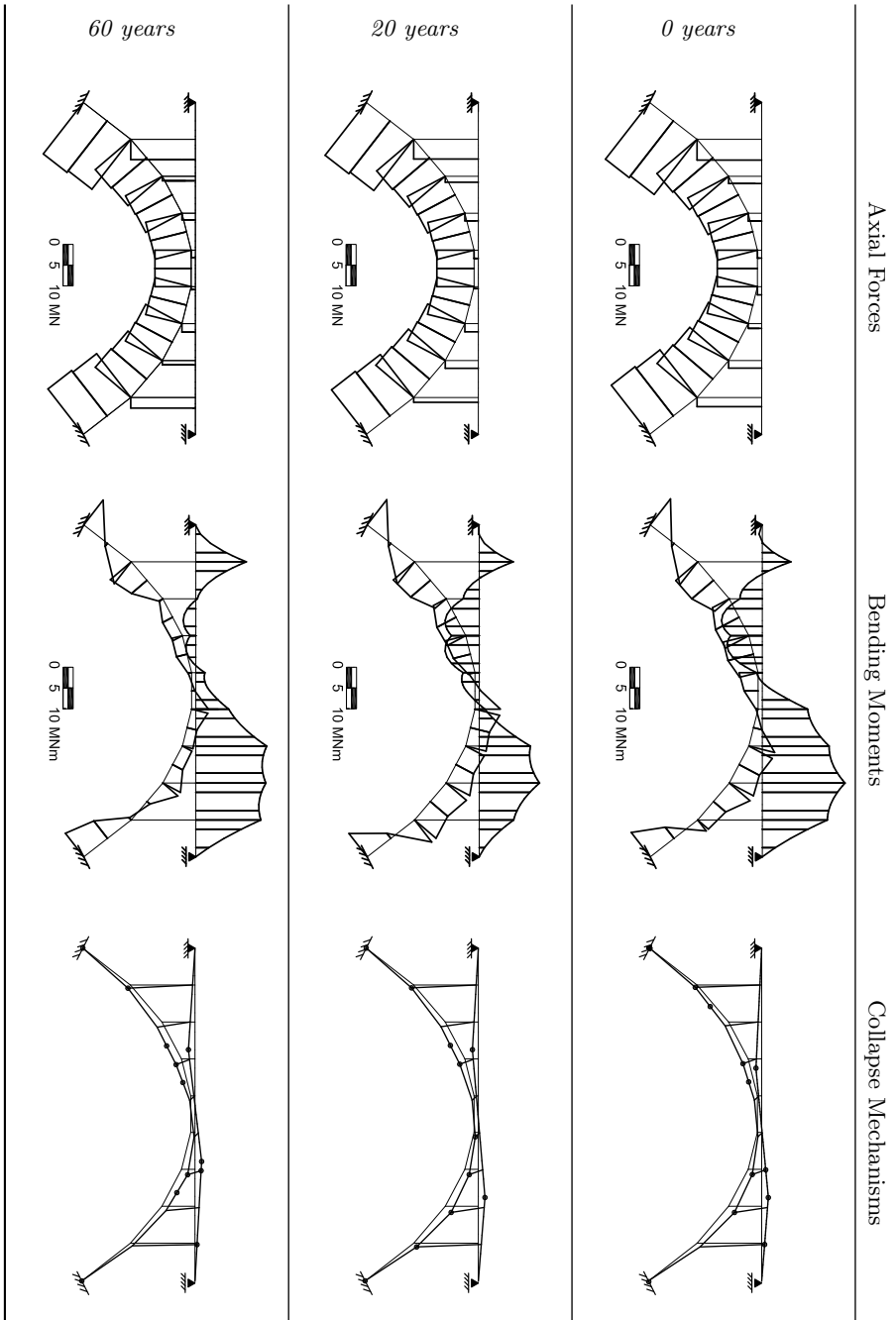


Table 7.8: Beam corrosion scenario: axial forces, bending moments and collapse mechanisms in time.



**Table 7.9:** Arch and Beam corrosion scenario: axial forces, bending moments and collapse mechanisms in time.

## 7.5 CONCLUDING COMMENTS

---

In this chapter, the structural performances of two bridges - a Cable Stayed Harp Bridge and an Arch Bridge - have been presented. The damage's effects are coupled with the structural performances in order to consider time-variant capacity accounting for environmental hazards. The structural behavior is carried out by a complete parallel study between Non Linear and Limit Analysis.

Between the most important conclusions:

- Non Linear Analysis presents an high level of generality and permits to take into account not only the mechanical non linearities, but also the geometric effects due to configuration's changes. However, despite based on the most synthetic formulation (monodimensional modeling with beam-column finite elements), the interpretation of the obtained results requires some considerations. If, for instance, we are searching the causes of the collapse, a lot of data and informations must be checked, aiming to find where a large amount of strains occur, or where instable behaviors have been obtained, etc.
- in contrast, Limit Analysis is the most immediate tool in order to understand the structural behavior but, since concrete is not a perfectly plastic material, it can be applicable to RC structures only if an adequate effectiveness factor is considered. And here a problem arises: what about an adequate choice of such a factor? If the collapse is governed by the steel, a correct evaluation of the effectiveness factor can be obtained, but in general, the definition of such a factor is based on theoretical/empirical/experimental observations. The main suggestion is to use prudential values. For these reasons, a complete different choice has been done: no effectiveness factor are used. It follow, of course, that Limit Analysis results are not consistent because concrete is treated as a material with infinite ductility, assumption too far from reality. However, the so-obtained not consistent results can be compared with Non Linear Analysis ones that give, instead, a more realistic collapse load without requiring effectiveness factor definitions. In this way, a sort of *structural effectiveness factor* has been numerically obtained.
- the obtained value for the effectiveness factor are in the range  $0.70 \div 0.85$ . The lower bond identifies a collapse governed by concrete, the upper value a collapse governed by steel.
- all these considerations have been outlined not only when the structure is sound, but also when it is damaged. At first, the damage's effects are deeply exposed at the material level, then they are moved at the sectional level, and at the structural level. It has been obtained that, despite localized corrosion scenarios have been considered, the structural performances can varying in time in a non-straightforward way. In particular, since a real structure is statically undetermined, if corrosion acts in a section, here we have a decrease of the structural stiffness and the consequence is that the solicitations move in time towards the sections in which the stiffness is higher, so towards the sound sections.

- hence, the most important practical conclusion is that damage produce not only the reduction of the local capacity, but also a redistribution of the solicitations towards the sound structural parts. For these reasons, in design repair interventions, it is not sufficient to repair the damaged parts, but it is more important to check if the sound structural components have sufficient resistance to contrast time-variant solicitations.

Since current design is based on the Lower Bond Theorem, it's seems very useful try to enhance also Limit Analysis by considering axial force - bending moment - shear force interaction, so that the complete structural behavior can be dealt with. This is one the possible improvement of this thesis.



# 8

## Damage Effects on Shear Resisting Mechanisms

*Structural performances can vary in time due to environmental hazards. In the previous chapter, particular attention is given to the global response. In this chapter, instead, the effects of damage on shear resistance mechanisms are presented and discussed. The structural models are coupled with the damage ones in order to study the time-variant structural behavior.*

### 8.1 PROBLEM STATEMENT AND DIFFUSIVE PROCESS

The Stuttgart Beams (Leonhardt and Walther, 1962) presented in par. 5.4 are considered. The beams, simply supported with a span equal to 3000 mm, are loaded by two equal concentrate loads  $P$  as sketched in Fig. 8.1. This figure also shows the reinforcement layout.

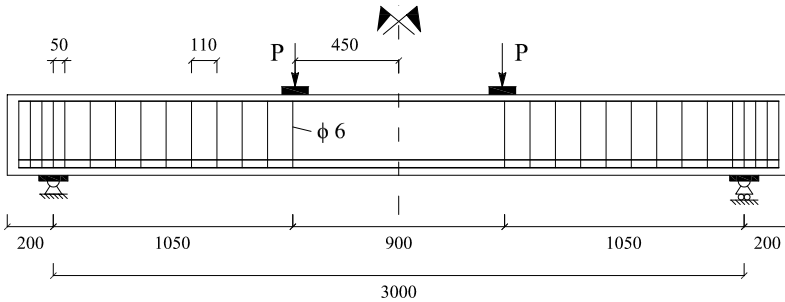


**Figure 8.1:** Geometry of the beams [mm].

The element's depth, flange width and reinforcements are taken fixed, while web thickness varied in order to investigate its influence on the overall response. Four variations of the web thickness has been created in order to produce four specimens called ET1, ET2, ET3 and ET4.

All the beams have been studied in par. 5.4, both with a bidimensional and a monodimensional modeling. Accordingly to the numerical results, all beams failed by crushing of concrete in the web. However, in the first beam this happens after

extensive yielding of longitudinal bars instead, in other three cases, after yielding of stirrups, with an importance that progressively grows by moving from ET2 towards ET4 beam. The general conclusion is that ET1 fails in bending, ET2 presents a mixed shear-bending failure, ET3 and ET4 fail in shear.

For these reasons, since this chapter aim to understand the damage effects on the resisting mechanisms, only the first two beams (ET1 and ET2) are now considered, Fig. 8.2. With respect to the previous analysis, however, their structural behavior is not only studied in sound conditions, but it is also evaluated in time.

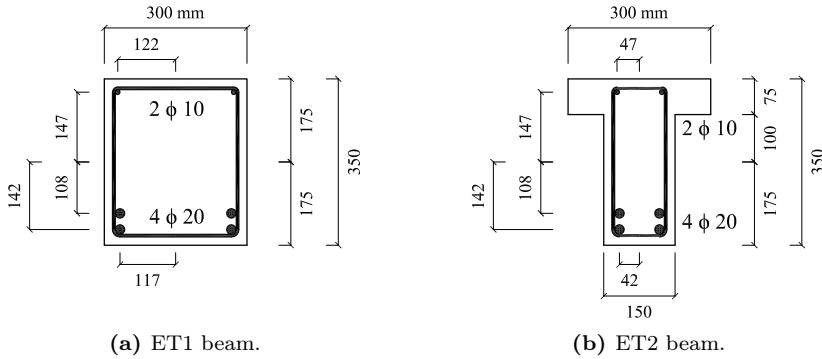


Figure 8.2: Geometry of the sections ET1-ET2.

8.1.1 CORROSION SCENARIO

Concerning the corrosion scenario, a chlorides corrosion attacks is considered. The distribution of such a scenario is as follow:

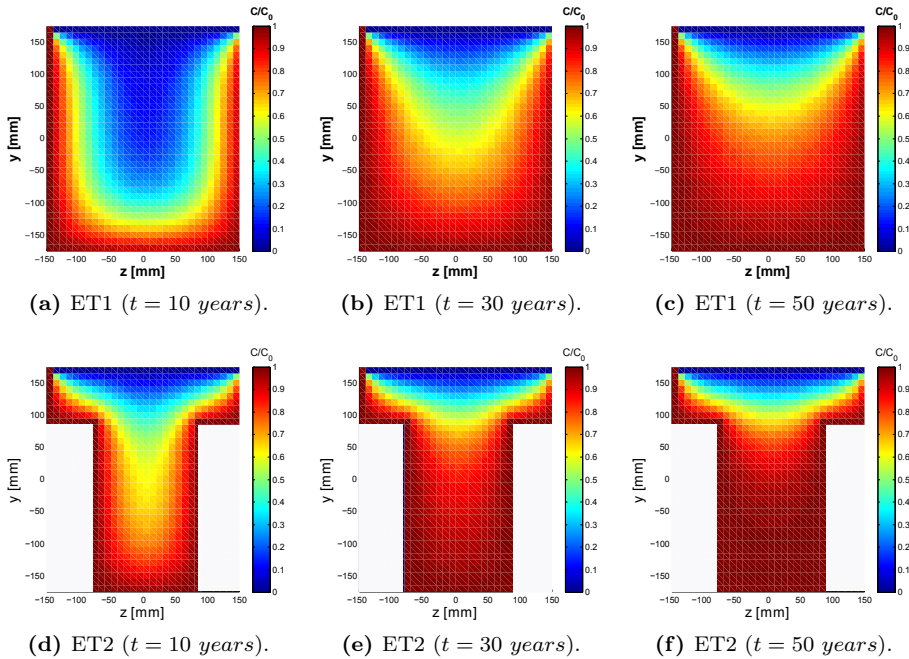
- the longitudinal distribution of corrosion is uniform and interests the entire beams;
- the sectional distribution of corrosion is assumed to be located along the two laterals and the bottom sides of the cross-sections, with a concentration  $C_0 = 3\%$ , as Fig. 8.3 shows.



Figure 8.3: ET1-ET2 corrosion scenario: sectional position of the aggressive agent.

## 8.1.2 CELLULAR AUTOMATA SOLUTION OF THE DIFFUSION PROCESS

Once the corrosion scenario has been defined, the diffusion problem must be solved both in the sectional domain and in time. The cellular automata technique is hence applied (see chapter 6), with a diffusivity coefficient  $D = 10^{-11} m^2/s$ , a grid dimension  $\Delta x = 10 mm$  and a time step  $\Delta t = 0.04 year$ . The results are the concentration maps, in time, for the two considered cross-sections, Fig. 8.4.



**Figure 8.4:** Time evolution of the normalized concentration maps for the cross-sections.

Despite the corrosion scenario is the same for the two cross-sections, the two penetration paths are different. This is the shape's effect and, if the problem is handle with 1D diffusion models, as suggested in (C.E.B., 1992), wrong predictions can be obtained. These 1D models can be applied in dealing with compact sections, but in general a procedure that considers the real sectional domain is needed. The approach here proposed, instead, presents an high level of generality and is able to deal with arbitrary shaped sections and with arbitrary position of reinforcements.

## 8.2 TIME VARIANT STRUCTURAL ANALYSIS

The structural behavior can be studied in time by coupling the diffusion process with the structural analysis. At each time instant, from the concentration in a generic point of the section ( $C = C(\mathbf{x}, t)$ ), it is possible to compute all the damages indexes exposed in chapter 6. For the sake of simplicity, despite the proposed procedure is able to consider also the reduction of steel ductility, the reduction of concrete strength and the concrete cover spalling, only the reduction of steel bars areas is taken into account.

Hence, starting from the results obtained in par. 5.4, where the beams are in sound conditions, their structural behavior is now studied in time. Tab. 8.1 shows the time evolution of the principal tension strain. It can be observed that:

- in ET1 beam, damage process does not produce large effects. It seems that the collapse mechanism remains a flexural-type mechanism also in time (see the first column of Tab. 8.1);
- in ET2 beam, instead, we can observe that strains are moving towards the beam’s web, like happens in a shear-type mechanism (see the second column of Tab. 8.1).

It is interesting to check also the evolution in time of the stresses in the stirrups and in the longitudinal bars, Tab. 8.2. The following comments arise:

- ET1 beam (first column of Tab. 8.2):  
the greater stresses interest the longitudinal bars and this happens for all the studied time instants;
- ET2 beam (second column of Tab. 8.2):  
when the beam is sound, collapse is reached with yielded longitudinal bars, but with not-yielded stirrups, despite an high stress is present. In time, however, such a trend vary and after 50 *years* of corrosion, stirrups are yielded before longitudinal bars. For these reasons, strains are moving towards the web and the beam’s collapse became clearly a shear-type mechanism.

These comments have been outlined by considering both load and time as a variables. However, the conclusion became very simple if we fix the acting load and consider only time variations. Fig. 8.5 shows the time evolution of the stresses (normalized with respect to yielding) in the stirrups and in the longitudinal bars, for an acting total load equal to 240 *kN*. It is evident that in the ET1 beam the greater stresses are measured in longitudinal bars. This holds also for ET2 beam, but only from 0 to 25 *years* circa; then there is a switch and the greater stresses are measure in the stirrups. The effects of damage, hence, produce a switch between collapse mechanisms. When the beam is sound, a mixed shear-bending failure occurs, but in time the collapse is moved clearly towards a shear failure.

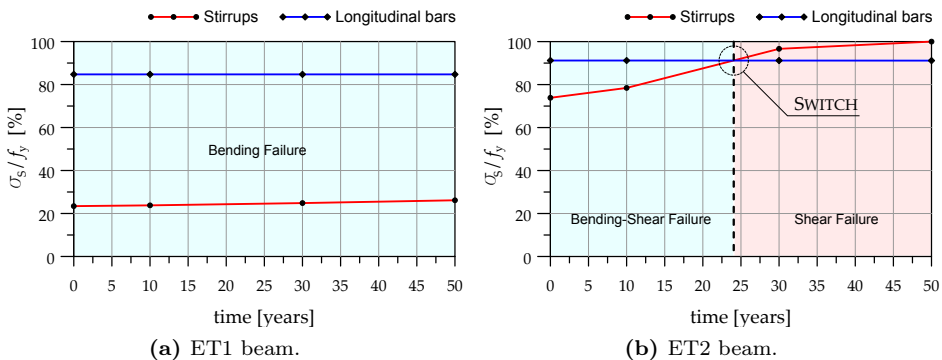


Figure 8.5: Evolution in time of the stresses for a constant total load equal to 240 *kN*.

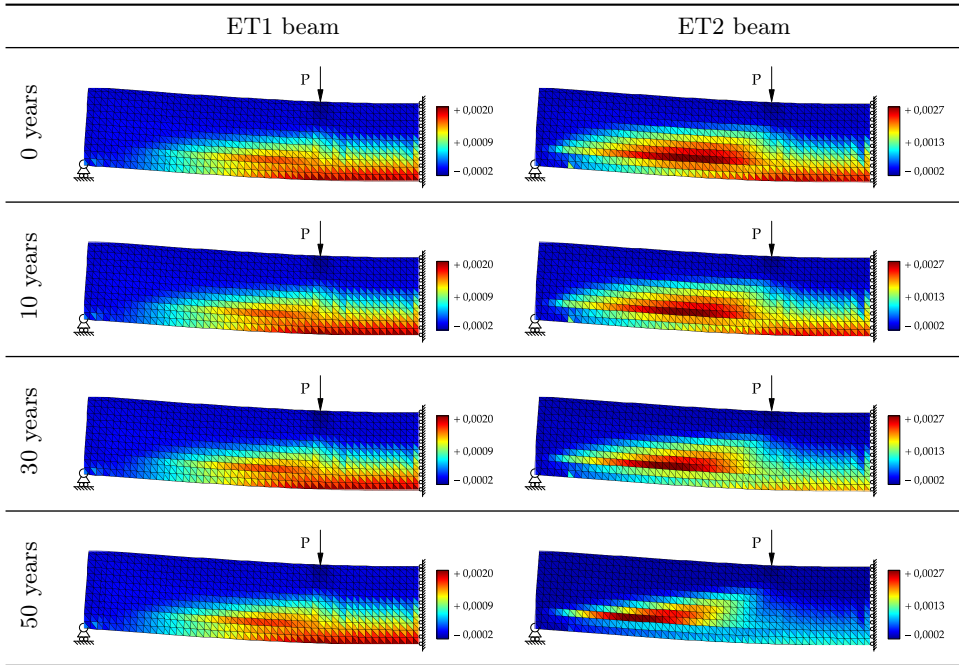


Table 8.1: Time evolution of the principal tension strain for ET1 and ET2 beams.

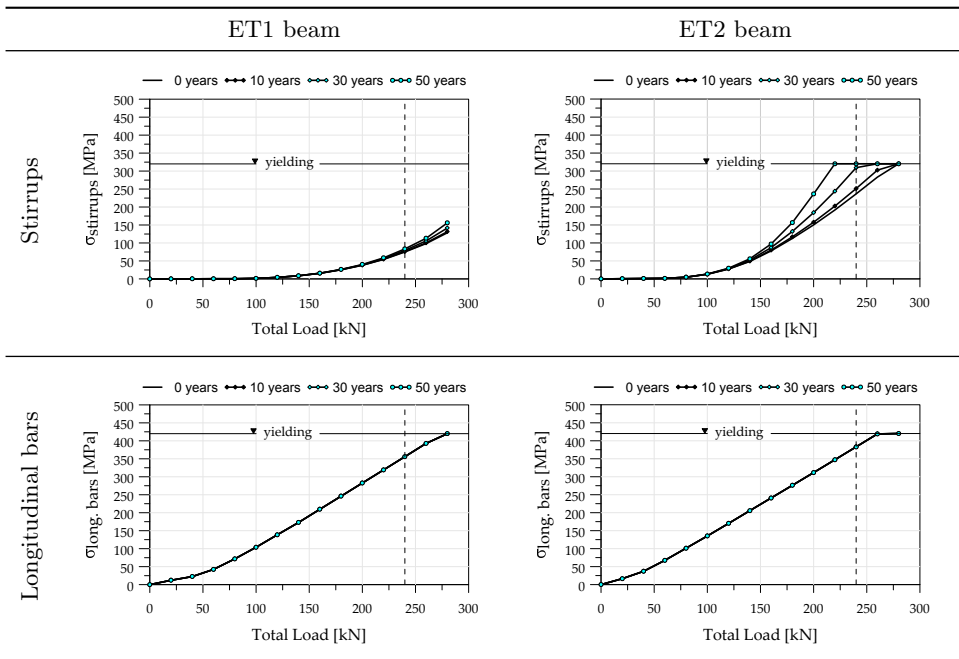


Table 8.2: Time evolution of the maximum stresses in longitudinal bars and stirrups.

### 8.3 CLOSING REMARKS

---

This chapter has dealt with a specific problem: the effects of damage on the resisting mechanisms in RC beams. The problem is not only important from a theoretical point of view, but also from a practical point of view, since today the majority of RC structures are reaching their ultimate lifetime.

In order to accomplish such a problem, the FE models exposed in part I have been coupled with the damage models detailed in part II, and lifetime predictions have been performed. Concerning corrosion scenarios, a chloride induced corrosion has been considered, with a given distribution along the cross-section's edges.

In particular, the diffusion process has been solved through cellular automata at first. The boundary conditions, the diffusion parameters and the size of the automaton have been detailed; secondly, the evolution of the concentration maps in time has been given. Starting to these results, the structural analysis are then performed in time and the damage's effects on the structural performances have been finally obtained.

The main conclusion of these investigations is that the effects of damage can produce a variation in the failure modes. Due to the complexity of the RC mechanisms, this conclusion can not be taken as a general statement, for these reasons:

- RC mechanism depends not only on the ratio of transverse reinforcements, but also on the shape of the section. Since the worst damage's effect in RC elements is the reduction of steel bars areas, it's clear that if a beam can transfer the load mainly through concrete contribution, a reduction of transversal steel does not produce effects on the ultimate behavior. This is the case of ET1 beam in which, thanks to the compact section's shape, the load can be transfer by inclined compression stresses acting on concrete that creates a smeared compression field;
- on the contrary, if the load transfer flow is based also to concrete-steel interactions, it's clear that a reduction of steel areas can produce dangerous effects. This is the case of ET2 beam. In sound condition, its failure mode can be classified as a bending-shear type collapse mechanism, with a concrete crushing in the web anticipated by the yielding of the longitudinal steel. Stirrups are not yielded, but they present an high stress level. If the structural behavior is studied in time, a switch between longitudinal and transversal steel roles has been obtained after 25 *years* of corrosion. After that time, the collapse of the beam can be classified as a shear-critical collapse mechanism.

Finally, it must be observed that the proposed methodology is able to predicts all these complex behaviors and, by coupling the structural analysis with the damage's models, is able to account for environmental hazards. Hence, it can be very useful in a general life-cycle approach.

# IV

---

---

## OTHER ITEMS SUGGESTED & FURTHER IMPROVEMENTS





# A

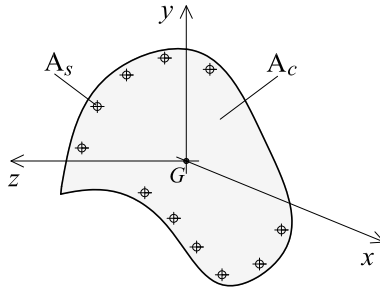
## A sectional parametric subdomains discretization

*A methodology handling the integrals that define the state of a generic R.C. section is presented. The section is divided in subdomains that are parametrically transformed in the same square parent domain on which integration rules refer. In this way, several combinations of integration strategies can be performed, with the widely used “fibers method” as particular case.*

### A.1 INTRODUCTION

---

Lets' consider the section domain, referred to a right handed reference system  $(0, x, y, z)$  with the origin placed in the centroid of the concrete domain. The  $x - axis$  is normal to the sectional plane and oriented along the element, Fig. A.1.

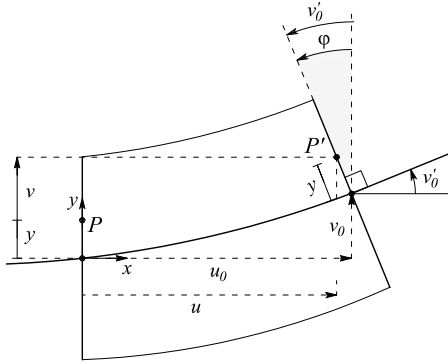
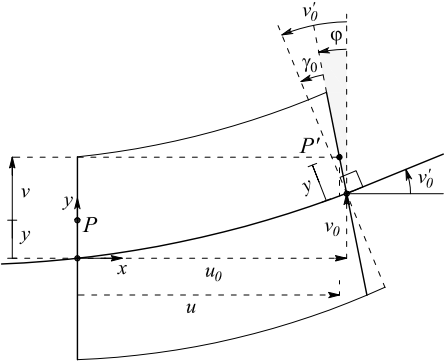


**Figure A.1:** A generic RC section and his reference system.

Once suitable constitutive laws are assumed, so that the stresses  $\boldsymbol{\sigma}$  in a generic point of the section can be evaluated from the strains  $\boldsymbol{\varepsilon}$ , and once a suitable interpolating matrix  $\mathbf{a}_s$  is defined, the generalized stresses  $\mathbf{f}_s$  can be evaluated by direct integration of the local stresses over the section domain. Such an integral is given in the following equation:

$$\mathbf{f}_s = \int_A \mathbf{a}_s(y, z, \boldsymbol{\varepsilon}) \boldsymbol{\sigma}(\boldsymbol{\varepsilon}) dA \quad (\text{A.1})$$

This problem always arise at the sectional level, despite the formulation adopted for the finite beam-column element. In common sectional kinematic assumptions such as Navier-Bernoulli or Timoshenko, matrix  $\mathbf{a}_s$  does not depend from  $\varepsilon$ , but only to  $(y, z)$  (see Tab. A.1). Instead, in beam theories with a more high kinematic level, the interpolating matrix can be state-dependent.

NAVIER-BERNOULLI	TIMOSHENKO
	
$\varepsilon_x = \begin{bmatrix} 1 & -y \end{bmatrix} \begin{bmatrix} \varepsilon_0 \\ \chi_0 \end{bmatrix} = \mathbf{a}_s \mathbf{e}_s$	$\begin{bmatrix} \varepsilon_x \\ \gamma_{xy} \end{bmatrix} = \begin{bmatrix} 1 & 0 & -y \\ 0 & 1 & 0 \end{bmatrix} \begin{bmatrix} \varepsilon_0 \\ \gamma_0 \\ \chi_0 \end{bmatrix} = \mathbf{a}_s \mathbf{e}_s$

**Table A.1:** Navier-Bernoulli and Timoshenko sectional kinematics.

In any case, since the arise stresses on the section are not linear, the evaluation of the integral (A.1) must be performed numerically. Actually, the most used numerical approach that deals with sectional numerical integration is the so-called “fibers approach” (C.E.B., 1996), through which the section is subdivided in sub-domains called “fibers” and the integral is evaluated with the Riemann Mid-Point Integration Rule, Fig. A.2.

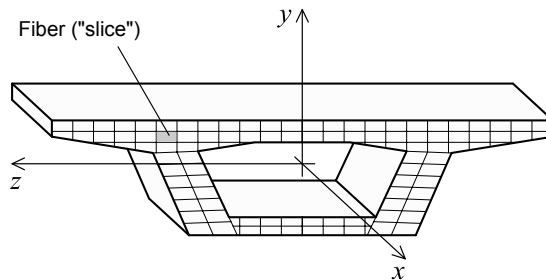


**Figure A.2:** Fibers Approach (Riemann Mid-Point Integration Rule).

In the following, instead, a special numerical integration technique is presented. The strategy has been proposed in (Malerba, 1984); in this context, a contribution that deals with circular or circular/hollow sections is proposed. The classical fibers approach is simply a *particular case* of the present more general approach.

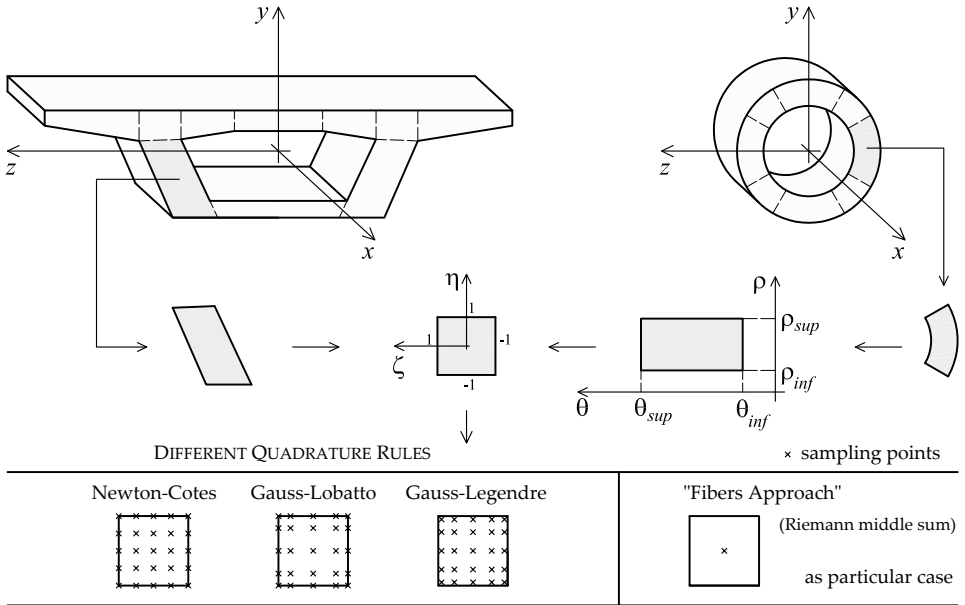


**Figure A.3:** Integration strategies. The section is divided into sub-domains and the integration works sampling in a parent domain by using parametric transformations. The so called fibers approach is a particular case of these integration procedures.

**A.2 NUMERICAL INTEGRATION BY PARAMETRIC TRANSFORMATIONS**

In order to deal with sections of arbitrary shape, the numerical integration is based on parametric transformations. The section is divided into sub-domains and the actual geometry of each sub-domain is transformed into a parent geometry by using parametric equations (Malerba, 1984), (Bontempi, 1992). In this way, sampling points refer to the parent domain and the relation with the reference to the actual geometry is ruled by Jacobian of the transformation. We set the integral form as follows:

$$I = \int_A f(z, y) dA \tag{A.2}$$

and we consider the section subdivided with these two types of sub-domains:

1. quadrilateral sub-domains;
2. circle or semicircle or circular ring sub-domains.

Obviously, sections composed by both can be dealt with. The application fields of such discretization choices are shown in Fig. A.3. In case 1, only one parametric transformation is needed. In case 2, two different transformations are required.

### A.2.1 QUADRILATERAL SUB-DOMAIN

In this case, the transformation from the given quadrilateral sub-domain to the square parent domain (Fig. A.4) is ruled by the well-known bilinear interpolation function (Bathe, 1996):

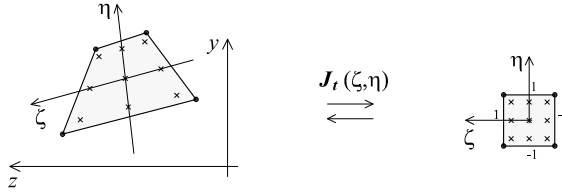


**Figure A.4:** Transformation between real quadrilateral sub-domain and square parent domain.

$$N_i = \frac{(1 + \zeta \cdot \zeta_i)(1 + \eta \cdot \eta_i)}{4}, \quad i = 1, 2, 3, 4 \quad (\text{A.3})$$

which, ordered in matrix form, results:

$$\mathbf{x} = \begin{bmatrix} z \\ y \end{bmatrix} = \mathbf{N} \cdot \mathbf{c} \quad (\text{A.4})$$

with

$$\mathbf{N} = \begin{bmatrix} N_1 & 0 & N_2 & 0 & N_3 & 0 & N_4 & 0 \\ 0 & N_1 & 0 & N_2 & 0 & N_3 & 0 & N_4 \end{bmatrix} \quad (\text{A.5})$$

$$\mathbf{c} = [z_1 \quad y_1 \quad z_2 \quad y_2 \quad z_3 \quad y_3 \quad z_4 \quad y_4]^T \quad (\text{A.6})$$

The corresponding determinant of the Jacobian matrix is:

$$\det(\mathbf{J}_t) = \frac{1}{8} [(z_{24} \cdot y_{13} - z_{13} \cdot y_{24}) + (z_{14} \cdot y_{23} - z_{23} \cdot y_{14}) \zeta + (z_{12} \cdot y_{34} - z_{34} \cdot y_{12}) \eta] \\ z_{ij} = z_i - z_j, \quad y_{ij} = y_i - y_j \quad (\text{A.7})$$

### A.2.2 CIRCULAR SECTORIAL SUB-DOMAIN

In this second case, two transformations are needed (Fig. A.5). The first one uses polar coordinates to transform the sector in a rectangular domain by using the relationships:

$$\begin{cases} z = \rho \cdot \sin \theta \\ y = \rho \cdot \cos \theta \end{cases} \quad (\text{A.8})$$

The relative Jacobian of the polar transformation is:

$$\det(\mathbf{J}_p) = \rho \quad (\text{A.9})$$

Then, a second step transforms the rectangular sub-domain in the usual square parent domain.

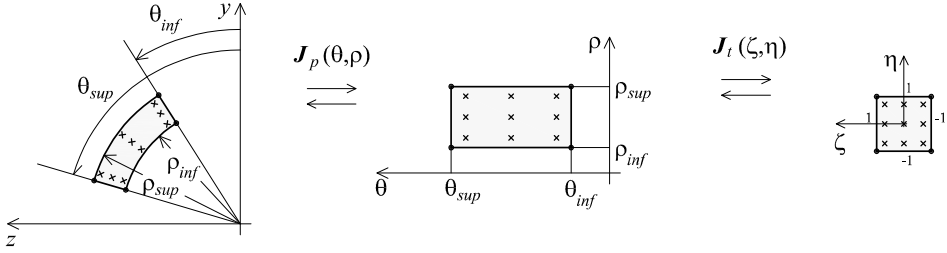


Figure A.5: From a quadratic shape to a circular sector: a double transformation.

### A.2.3 INTEGRATION RULES

Through the transformations previously exposed, the generic integral is written with reference to the basic square parent domain. The differential must contain the corresponding Jacobian matrix.

$$I = \int_A f(z, y) dA = \int_{-1}^1 \int_{-1}^1 f(\zeta, \eta) \det(\mathbf{J}(\zeta, \eta)) d\zeta d\eta \quad (\text{A.10})$$

The problem is reduced to algebraic form through sums, which for the quadrilateral sub-domain, are:

$$I \approx \sum_{i=1}^n \sum_{j=1}^n f(\zeta_i, \eta_j) \det(\mathbf{J}_t(\zeta_i, \eta_j)) \cdot w_i \cdot w_j \quad (\text{A.11})$$

and for the circular sector sub-domain are:

$$I \approx \sum_{i=1}^n \sum_{j=1}^n f(\zeta_i, \eta_j) \det(\mathbf{J}_t(\zeta_i, \eta_j)) \det(\mathbf{J}_p) w_i \cdot w_j \quad (\text{A.12})$$

As shown, in this second case two Jacobian matrices are involved. The sampling points location and the relative weights depend on the quadrature rule adopted (Abramowitz and Stegun, 1964).

For the sake of comparison, in this work, three type of quadratures rules and different numbers of sampling points  $n$  have been considered.

- Newton-Cotes rule, that integrates exactly polynomials of grade  $n - 1$ ;
- Gauss-Legendre rule, that integrates exactly polynomials of grade  $2n - 1$ ;
- Gauss-Lobatto rule, that integrates exactly polynomials of grade  $2n - 3$ .

We remember that we are dealing with problems concerning reinforced concrete sections. In this field the most used integration strategy discretizes the section into fibers (C.E.B., 1996), that in fact are sub-domains with only one sampling point. Such an integration rule (midpoint integration rule) is the simplest possible and corresponds to what proposed in this work just putting  $n = 1$ . On the other side, working with R.C. sectional problems, we know that the maximum strains lie on the boundaries, so it seems more effective adopt Gauss-Lobatto rule, which choses sampling points on the frontier of the domain.

A.2.4 SAMPLING POINTS AND WEIGHTS FACTORS

Sampling points location and relative weights can be find in specific book of Numerical Analysis. For example, Fig. A.6 and A.7 report the sampling given in (Abramowitz and Stegun, 1964).

Table 2.5.4 ABSCISSAS AND WEIGHT FACTORS FOR GAUSSIAN INTEGRATION

$$\int_{-1}^{+1} f(x) dx \approx \sum_{i=1}^n w_i f(x_i)$$

Abscissas= $\pm x_i$ (Zeros of Legendre Polynomials)			Weight Factors= $w_i$		
$\pm x_i$	$w_i$		$\pm x_i$	$w_i$	
$n=2$			$n=8$		
0.57735 02691 89626	1.00000 00000 00000		0.18343 46424 95650	0.36268 37833 78362	
			0.52553 24099 16329	0.31370 66458 77887	
			0.79666 64774 13627	0.22238 10344 53374	
			0.96028 98564 97536	0.10122 85362 90376	
$n=3$			$n=9$		
0.00000 00000 00000	0.88888 88888 88889		0.00000 00000 00000	0.33023 93550 01260	
0.77459 66692 41483	0.55555 55555 55556		0.32425 34234 03809	0.31234 70770 40003	
			0.61337 14327 00590	0.26061 06964 02935	
			0.83603 11073 26636	0.18064 81606 94857	
			0.96816 02395 07626	0.08127 43883 61574	
$n=4$			$n=10$		
0.33998 10435 84856	0.65214 51548 62546		0.14887 43389 81631	0.29552 42247 14753	
0.86113 63115 94053	0.34785 48451 37454		0.43339 53941 29247	0.26926 67193 09996	
			0.67940 95682 99024	0.21908 63625 15982	
			0.86506 33666 88985	0.14945 13491 50581	
			0.97390 65285 17172	0.06667 13443 08688	
$n=5$			$n=12$		
0.00000 00000 00000	0.56888 88888 88889		0.12523 34085 11469	0.24914 70458 13403	
0.53846 93101 05683	0.47862 86704 99366		0.36783 14989 98180	0.23349 25365 38355	
0.90617 98459 38664	0.23692 68850 56189		0.58731 79542 86617	0.20316 74267 23066	
			0.76990 26741 94305	0.16007 83285 43346	
			0.90411 72563 70475	0.10693 93259 95318	
			0.98156 06342 46719	0.04717 53363 86512	
$n=6$			$n=7$		
0.23861 91860 83197	0.46791 39345 72691		0.41795 91836 73469		
0.66120 93864 66265	0.36076 15730 48139		0.38183 05005 05119		
0.93246 95142 03152	0.17132 44923 79170		0.27970 53914 89277		
			0.12948 49661 68870		

Figure A.6: Gauss-Legendre quadrature, (Abramowitz and Stegun, 1964).

Table 2.5.6 ABSCISSAS AND WEIGHT FACTORS FOR LOBATTO INTEGRATION

$$\int_{-1}^{+1} f(x) dx \approx w_1 f(-1) + \sum_{i=2}^{n-1} w_i f(x_i) + w_n f(1)$$

Abscissas= $\pm x_i$			Weight Factors= $w_i$		
$n$	$\pm x_i$	$w_i$	$n$	$\pm x_i$	$w_i$
3	1.00000 000	0.33333 333	7	1.00000 000	0.04761 904
	0.00000 000	1.33333 333		0.83022 390	0.27682 604
				0.46884 879	0.43174 538
				0.00000 000	0.48761 904
4	1.00000 000	0.16666 667	8	1.00000 000	0.03571 428
	0.44721 360	0.83333 333		0.87174 015	0.21070 422
5	1.00000 000	0.10000 000	9	1.00000 00000	0.02777 77778
	0.65465 367	0.54444 444		0.89975 79954	0.16549 53616
	0.00000 000	0.71111 111		0.67718 62795	0.27453 87126
				0.36311 74638	0.34642 85110
6	1.00000 000	0.06666 667	10	1.00000 00000	0.02222 22222
	0.76505 532	0.37847 496		0.91953 39082	0.13330 59908
	0.28523 152	0.55485 838		0.73877 38651	0.22488 93420
				0.47792 49498	0.29204 26836
			0.16527 89577	0.32753 97612	

Figure A.7: Gauss-Lobatto quadrature, (Abramowitz and Stegun, 1964).

In the following tables, the sampling points and weights are furnish for  $n = 1, 2, \dots, 12$ , divided in the three quadrature rules previously exposed (see Tab. A.2, A.3, A.4). These quadrature rules are used in the code developed in this thesis not only at the sectional level, but also at the element level.

NEWTON-COTES					
n	$x_i$	$\alpha_i$	n	$x_i$	$\alpha_i$
1	0.0000000000000000 -	2.0000000000000000 -	2	-1.0000000000000000 1.0000000000000000	1.0000000000000000 1.0000000000000000
3	-1.0000000000000000 0.0000000000000000 1.0000000000000000 -	0.3333333333333333 1.3333333333333330 0.3333333333333333 -	4	-1.0000000000000000 -0.3333333333333333 0.3333333333333333 1.0000000000000000	0.2500000000000000 0.7500000000000000 0.7500000000000000 0.2500000000000000
5	-1.0000000000000000 -0.5000000000000000 0.0000000000000000 0.5000000000000000 1.0000000000000000 -	0.1555555555555556 0.7111111111111111 0.2666666666666667 0.7111111111111111 0.1555555555555556 -	6	-1.0000000000000000 -0.6000000000000000 -0.2000000000000000 0.2000000000000000 0.6000000000000000 1.0000000000000000	0.1319444444444444 0.5208333333333333 0.3472222222222222 0.3472222222222222 0.5208333333333333 0.1319444444444444
7	-1.0000000000000000 -0.6666666666666667 -0.3333333333333333 0.0000000000000000 0.3333333333333333 0.6666666666666667 1.0000000000000000 -	0.097619047619048 0.514285714285714 0.064285714285714 0.647619047619048 0.064285714285714 0.514285714285714 0.097619047619048 -	8	-1.0000000000000000 -0.714285714285714 -0.428571428571429 -0.142857142857143 0.142857142857143 0.428571428571429 0.714285714285714 1.0000000000000000	0.086921296296296 0.414004629629630 0.153125000000000 0.345949074074074 0.345949074074074 0.153125000000000 0.414004629629630 0.086921296296296
9	-1.0000000000000000 -0.7500000000000000 -0.5000000000000000 -0.2500000000000000 0.0000000000000000 0.2500000000000000 0.5000000000000000 0.7500000000000000 1.0000000000000000 -	0.069770723104056 0.415379188712522 -0.065467372134039 0.740458553791887 -0.320282186948854 0.740458553791887 -0.065467372134039 0.415379188712522 0.069770723104056 -	10	-1.0000000000000000 -0.7777777777777778 -0.555555555555556 -0.3333333333333333 -0.1111111111111111 0.1111111111111111 0.3333333333333333 0.555555555555556 0.7777777777777778 1.0000000000000000	0.063772321428571 0.351361607142857 0.024107142857143 0.431785714285714 0.128973214285714 0.128973214285714 0.431785714285714 0.024107142857143 0.351361607142857 0.063772321428571
11	-1.0000000000000000 -0.8000000000000000 -0.6000000000000000 -0.4000000000000000 -0.2000000000000000 0.0000000000000000 0.2000000000000000 0.4000000000000000 0.6000000000000000 0.8000000000000000 1.0000000000000000 -	0.053668296723852 0.355071882849661 -0.162087141253808 0.909892576559243 -0.870310245310245 1.427529260862590 -0.870310245310245 0.909892576559243 -0.162087141253808 0.355071882849661 0.053668296723852 -	12	-1.0000000000000000 -0.818181818181818 -0.636363636363636 -0.454545454545455 -0.272727272727273 -0.090909090909091 0.090909090909091 0.272727272727273 0.454545454545455 0.636363636363636 0.818181818181818 1.0000000000000000	0.049866461823927 0.309710717041446 -0.074338463587596 0.579316509589947 -0.220356178350970 0.355800953483245 0.355800953483245 -0.220356178350970 0.579316509589947 -0.074338463587596 0.309710717041446 0.049866461823927

Table A.2: Newton-Cotes Quadrature Rule: sampling points and weight factors.

GAUSS-LEGENDRE					
n	$x_i$	$\alpha_i$	n	$x_i$	$\alpha_i$
1	0.0000000000000000 -	2.0000000000000000 -	2	-0.577350269189626 0.577350269189626	1.0000000000000000 1.0000000000000000
3	-0.774596669241483 0.0000000000000000 0.774596669241483 -	0.5555555555555556 0.8888888888888889 0.5555555555555556 -	4	-0.861136311594054 -0.339981043584857 0.339981043584856 0.861136311594053	0.347854845137453 0.652145154862547 0.652145154862547 0.347854845137453
5	-0.906179845938664 -0.538469310105683 0.0000000000000000 0.538469310105683 0.906179845938664 -	0.236926885056189 0.478628670499367 0.5688888888888889 0.478628670499366 0.236926885056189 -	6	-0.932469514203153 -0.661209386466264 -0.238619186083197 0.238619186083197 0.661209386466263 0.932469514203154	0.171324492379169 0.360761573048140 0.467913934572692 0.467913934572688 0.360761573048142 0.171324492379169
7	-0.949107912342760 -0.741531185599394 -0.405845151377397 0.0000000000000000 0.405845151377397 0.741531185599394 0.949107912342760 -	0.129484966168868 0.279705391489280 0.381830050505115 0.417959183673472 0.381830050505116 0.279705391489280 0.129484966168868 -	8	-0.960289856497539 -0.796666477413624 -0.525532409916329 -0.183434642495650 0.183434642495650 0.525532409916330 0.796666477413623 0.960289856497541	0.101228536290375 0.222381034453380 0.313706645877883 0.362683783378361 0.362683783378367 0.313706645877877 0.222381034453384 0.101228536290372
9	-0.968160239507627 -0.836031107326636 -0.613371432700590 -0.324253423403809 0.0000000000000000 0.324253423403809 0.613371432700590 0.836031107326635 0.968160239507625 -	0.081274388361574 0.180648160694859 0.260610696402935 0.312347077040002 0.330239355001260 0.312347077040002 0.260610696402936 0.180648160694856 0.081274388361576 -	10	-0.973906528517184 -0.865063366688974 -0.679409568299027 -0.433395394129248 -0.148874338981631 0.148874338981631 0.433395394129247 0.679409568299026 0.865063366688971 0.973906528517182	0.066671344308679 0.149451349150606 0.219086362515955 0.269266719310012 0.295524224714749 0.295524224714748 0.269266719310012 0.219086362515954 0.149451349150604 0.066671344308682
11	-0.978228658146072 -0.887062599768073 -0.730152005574058 -0.519096129206811 -0.269543155952345 0.0000000000000000 0.269543155952345 0.519096129206813 0.730152005574051 0.887062599768080 0.978228658146071 -	0.055668567116165 0.125580369464943 0.186290210927675 0.233193764592044 0.262804544510203 0.272925086777940 0.262804544510209 0.233193764592032 0.186290210927684 0.125580369464944 0.055668567116162 -	12	-0.981560634246719 -0.904117256370479 -0.769902674194298 -0.587317954286623 -0.367831498998179 -0.125233408511469 0.125233408511469 0.367831498998180 0.587317954286623 0.769902674194297 0.904117256370483 0.981560634246718	0.047175336386509 0.106939325995323 0.160078328543347 0.203167426723058 0.233492536538362 0.249147045813402 0.249147045813397 0.233492536538368 0.203167426723051 0.160078328543355 0.106939325995318 0.047175336386509

**Table A.3:** Gauss-Legendre Quadrature Rule: sampling points and weight factors.



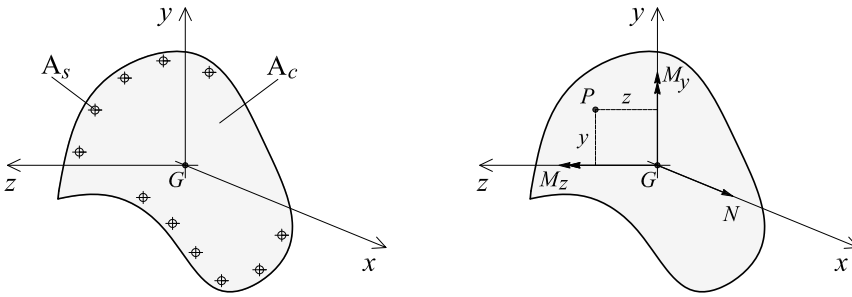
GAUSS-LOBATTO					
n	$x_i$	$\alpha_i$	n	$x_i$	$\alpha_i$
1	0.000000000000000 -	2.000000000000000 -	2	-1.000000000000000 1.000000000000000	1.000000000000000 1.000000000000000
3	-1.000000000000000 0.000000000000000 1.000000000000000 -	0.333333333333333 1.333333333333330 0.333333333333333 -	4	-1.000000000000000 -0.447213595499958 0.447213595499958 1.000000000000000	0.166666666666667 0.833333333333333 0.833333333333333 0.166666666666667
5	-1.000000000000000 -0.654653670707977 0.000000000000000 0.654653670707977 1.000000000000000 -	0.100000000000000 0.544444444444445 0.711111111111111 0.544444444444444 0.100000000000000 -	6	-1.000000000000000 -0.765055323929465 -0.285231516480645 0.285231516480645 0.765055323929466 1.000000000000000	0.066666666666666 0.378474956297847 0.554858377035486 0.554858377035487 0.378474956297847 0.066666666666666
7	-1.000000000000000 -0.830223896278567 -0.468848793470714 0.000000000000000 0.468848793470714 0.830223896278567 1.000000000000000 -	0.047619047619048 0.276826047361566 0.431745381209862 0.487619047619047 0.431745381209863 0.276826047361566 0.047619047619048 -	8	-1.000000000000000 -0.871740148509606 -0.591700181433143 -0.209299217902479 0.209299217902479 0.591700181433144 0.871740148509606 1.000000000000000	0.035714285714286 0.210704227143505 0.341122692483504 0.412458794658704 0.412458794658705 0.341122692483504 0.210704227143505 0.035714285714287
9	-1.000000000000000 -0.899757995411461 -0.677186279510739 -0.363117463826178 0.000000000000000 0.363117463826178 0.677186279510738 0.899757995411461 1.000000000000000 -	0.027777777777778 0.165495361560804 0.274538712500162 0.346428510973048 0.371519274376416 0.346428510973047 0.274538712500162 0.165495361560805 0.027777777777778 -	10	-1.000000000000000 -0.919533908166462 -0.738773865105502 -0.477924949810446 -0.165278957666387 0.165278957666387 0.477924949810445 0.738773865105504 0.919533908166459 1.000000000000000	0.022222222222219 0.133305990851074 0.224889342063127 0.292042683679680 0.327539761183900 0.327539761183896 0.292042683679684 0.224889342063124 0.133305990851073 0.022222222222222
11	-1.000000000000000 -0.934001430408055 -0.784483473663149 -0.565235326996204 -0.295758135586939 0.000000000000000 0.295758135586939 0.565235326996203 0.784483473663149 0.934001430408056 1.000000000000000 -	0.018181818181822 0.109612273266991 0.187169881780302 0.248048104264036 0.286879124779002 0.300217595455696 0.286879124779002 0.248048104264035 0.187169881780303 0.109612273266991 0.018181818181821 -	12	-1.000000000000000 -0.944899272222886 -0.819279321644002 -0.632876153031862 -0.399530940965349 -0.136552932854928 0.136552932854928 0.399530940965349 0.632876153031864 0.819279321643999 0.944899272222888 1.000000000000000	0.015151515151508 0.091684517413205 0.157974705564372 0.212508417761012 0.251275603199208 0.271405240910697 0.271405240910697 0.251275603199208 0.212508417761012 0.157974705564372 0.091684517413205 0.015151515151508

Table A.4: Gauss-Lobatto Quadrature Rule: sampling points and weight factors.

### A.3 RC SECTION BASED ON NAVIER-BERNOULLI KINEMATIC

In order to compare the sectional discretization strategy here proposed with the fibers approach, the State of a RC Section based on Navier-Bernoulli kinematic is presented. By using such an assumption, it's clear that only the problem related with normal stresses can be dealt with. However, this is the most common approach used in reinforced concrete and consent to determine, for example, Moment-Curvature Diagrams or Interaction Domains. In addition, the state of the so obtained section can be used in the formulation of beam-column finite elements in which shear's effect is not directly considered. The following hypotheses are hence assumed:

- (a) plane sections remain plane after deformations;
- (b) shear deformation is not considered;
- (c) perfect bond holds between steel and concrete.



**Figure A.8:** RC section and generalized normal stresses.

According to these hypotheses, in a deformed configuration, the normal displacement at a generic point P (Fig. A.8) of the section is given by:

$$w_p(x, y, z) = w_0(x) - y \cdot \phi_z(x) + z \cdot \phi_y(x) \quad (\text{A.13})$$

where  $w_0$  is the displacement at the origin and  $\phi_z$ ,  $\phi_y(x)$  are, respectively, the rotations around the  $z$  and  $y$  axes. The corresponding normal strain at point P (Fig. A.8) is given by:

$$\varepsilon_p(x, y, z) = \frac{\partial w_p(x, y, z)}{\partial x} = \varepsilon_0(x) - y \cdot \chi_z(x) + z \cdot \chi_y(x) \quad (\text{A.14})$$

where  $\varepsilon_0$  is the normal strain at the origin and  $\chi_z$ ,  $\chi_y$  are, respectively, the curvatures around the  $z$  and  $y$  axes. The kinematic variables can be grouped by introducing the sectional displacement vector  $\mathbf{s}(x)$  and the sectional deformation vector  $\mathbf{e}_s(x)$ :

$$\mathbf{s}(x) = [w_0 \quad \phi_z \quad \phi_y]^T \quad (\text{A.15})$$

$$\mathbf{e}_s(x) = [\varepsilon_0 \quad \chi_z \quad \chi_y]^T \quad (\text{A.16})$$

Through the operator:

$$\mathbf{a}_s(z, y) = [1 \quad -y \quad z] \quad (\text{A.17})$$

eqs. (A.13) and (A.14) can be put in the matrix form:

$$w_p(x, y, z) = \mathbf{a}_s(z, y) \cdot \mathbf{s}(x) \quad (\text{A.18})$$

$$\varepsilon_p(x, y, z) = \mathbf{a}_s(z, y) \cdot \mathbf{e}_s(x) \quad (\text{A.19})$$

With reference to a section belonging to a beam element, eqs. (A.18) and (A.19) decompose the kinematic field into the product of a function  $\mathbf{a}_s(z, y)$ , depending on the coordinates on the section, by a function of the coordinate  $x$  of the section along the beam axis.

### A.3.1 SECTION EQUILIBRIUM

The sectional equilibrium equations are derived through the Principle of Virtual Displacements, by equating the work done by the static quantities of the actual equilibrated field and the kinematic quantities of a virtual kinematic field. The section is considered belonging to a unitary length segment of the beam.

$$\delta W_i = \delta W_e \quad (\text{A.20})$$

The external and internal works are, respectively:

$$\delta W_e = \delta \mathbf{e}_s(x)^T \cdot \mathbf{f}_{s,e}(x) \quad (\text{A.21})$$

$$\delta W_i = \int_A \delta \varepsilon_p(x, y, z) \sigma_p(x, y, z) dA \quad (\text{A.22})$$

By substituting in Eq. (A.22) the expression of  $\varepsilon_p$  given by (A.19), it follows that:

$$\delta \mathbf{e}_s(x)^T \cdot \mathbf{f}_{s,e}(x) = \delta \mathbf{e}_s(x)^T \cdot \int_A \mathbf{a}_s(z, y)^T \sigma_p(x, y, z) dA \quad \forall \delta \mathbf{e}_s \quad (\text{A.23})$$

Doing such an equation be valid for any virtual  $\delta \mathbf{e}_s$ , the following relationship must hold:

$$\mathbf{f}_{s,e}(x) = \int_A \mathbf{a}_s(z, y)^T \sigma_p(x, y, z) dA = \int_A \begin{bmatrix} 1 \\ -y \\ z \end{bmatrix} \sigma_p(x, y, z) dA \quad (\text{A.24})$$

This equation defines the generalized section stresses  $N$ ,  $M_z$ ,  $M_y$  which equilibrate the distribution of the internal uniaxial stresses  $\sigma_x$ :

$$\mathbf{f}_{s,r}(x) = \begin{bmatrix} N(x) \\ M_z(x) \\ M_y(x) \end{bmatrix} = \int_A \begin{bmatrix} 1 \\ -y \\ z \end{bmatrix} \sigma_p(x, y, z) dA \quad (\text{A.25})$$

and can be rewritten as:

$$\begin{aligned}
 N(x) &= \int_A \sigma_p(x, y, z) \, dA \\
 M_z(x) &= \int_A -y \cdot \sigma_p(x, y, z) \, dA \\
 M_y(x) &= \int_A z \cdot \sigma_p(x, y, z) \, dA
 \end{aligned} \tag{A.26}$$

Clearly, the integrals are meant extended to all the materials composing the section. These integrals will be continuous over the concrete domain and discrete sums on the reinforcing bars.

### A.3.2 THE TWO TYPES OF SECTION PROBLEMS

The stress  $\sigma_p(x, y, z)$  in Eq. (A.25) is given as function of the strain  $\varepsilon_p(x, y, z)$  by an assumed uniaxial constitutive law. The most known stress-strain relationships are those proposed by (Kent and Park, 1971) and (Mander *et al.*, 1988).

$$\mathbf{f}_{s,r}(x) = \int_A \mathbf{a}_s(z, y)^T \sigma_p(\mathbf{e}_s(x)) \, dA \tag{A.27}$$

Eq. (A.27), strictly speaking, is an equilibrium equation. Its use in the design practice and in finite element analysis can be associated to the following two types of problems:

- given a strain state (the sectional strains)  $\mathbf{e}_s$ , determine the stress state (the resultant section forces)  $\mathbf{f}_{s,r}$ ; this happen in a displacement based element and the problem is in a direct form;
- given a stress state  $\mathbf{f}_{s,e}$ , determine the sectional strain state  $\mathbf{e}_s$ ; this happen in a flexibility based element and the problem is a indirect form.

#### A.3.2.1 TYPE 1 PROBLEM

The first problem is formulated in a direct way. In fact, given the section deformations  $\mathbf{e}_s$ , the section stresses in any point are directly given by the assumed constitutive law. The integral of the stresses over the section domain gives the section forces  $\mathbf{f}_{s,r}$ . Hence Problem 1 requires a suitable integration strategy only.

#### A.3.2.2 TYPE 2 PROBLEM

The second problem can't have a direct solution. It involves the solution of a system of nonlinear equations and can be stated as follow: for an assigned vector of section forces  $\mathbf{f}_{s,e}$ , reckon the section deformations  $\mathbf{e}_s$  giving corresponding internal forces  $\mathbf{f}_{s,r}$  (resisting or restoring forces) equal to  $\mathbf{f}_{s,e}$ . The internal forces are computed through the integration of the stress distribution over the section domain:

$$\mathbf{f}_{s,r}(\mathbf{e}_s) = \int_A \mathbf{a}_s(z, y)^T \sigma_p(\mathbf{e}_s) \, dA \tag{A.28}$$

The equilibrium condition states that:

$$\mathbf{f}_{s,e} = \mathbf{f}_{s,r}(\mathbf{e}_s) \quad (\text{A.29})$$

Such a condition is written in homogeneous form as follows:

$$\mathbf{g}(\mathbf{e}_s) = \mathbf{f}_{s,e} - \mathbf{f}_{s,r}(\mathbf{e}_s) = \mathbf{0} \quad (\text{A.30})$$

and solved by Newton-Raphson (NR) method. The main steps of the NR solution are:

1. choice of an initial solution  $\mathbf{e}_{s0}$ .
2. linearization of the problem as follows:

$$\mathbf{g}(\mathbf{e}_s) \cong \mathbf{g}(\mathbf{e}_{s0}) + \mathbf{J}(\mathbf{e}_{s0}) \cdot (\mathbf{e}_s - \mathbf{e}_{s0}) = \mathbf{0} \quad (\text{A.31})$$

where  $\mathbf{J}(\mathbf{e}_{s0})$  is the Jacobian matrix evaluated in  $\mathbf{e}_{s0}$ .

3. search for a new solution, by solving Eq. (A.32):

$$\mathbf{e}_{s1} = \mathbf{e}_{s0} - [\mathbf{J}(\mathbf{e}_{s0})]^{-1} \cdot \mathbf{g}(\mathbf{e}_{s0}) \quad (\text{A.32})$$

4. iteration until convergence.

In a more explicit form, the Jacobian matrix is given by the Equation:

$$\begin{aligned} \mathbf{J}(\mathbf{e}_s) &= \frac{\partial \mathbf{g}(\mathbf{e}_s)}{\partial \mathbf{e}_s} = \frac{\partial (\mathbf{f}_{s,e} - \mathbf{f}_{s,r}(\mathbf{e}_s))}{\partial \mathbf{e}_s} \\ &= - \frac{\partial \mathbf{f}_{s,r}(\mathbf{e}_s)}{\partial \mathbf{e}_s} \end{aligned} \quad (\text{A.33})$$

which shows how  $\mathbf{J}(\mathbf{e}_s)$  equals the derivatives of the resisting forces  $\mathbf{f}_{s,r}(\mathbf{e}_s)$  with respect to  $\mathbf{e}_s$ . By expanding Eq. (A.33) we have:

$$\begin{aligned} \frac{\partial \mathbf{f}_{s,r}(\mathbf{e}_s)}{\partial \mathbf{e}_s} &= \frac{\partial}{\partial \mathbf{e}_s} \int_A \mathbf{a}_s^T \sigma_p(\mathbf{e}_s) dA = \int_A \frac{\partial (\mathbf{a}_s^T \sigma_p(\mathbf{e}_s))}{\partial \mathbf{e}_s} dA = \int_A \mathbf{a}_s^T \frac{\partial (\sigma_p(\mathbf{e}_s))}{\partial \mathbf{e}_s} dA = \\ &= \int_A \mathbf{a}_s^T \frac{\partial \sigma_p}{\partial \varepsilon_p} \cdot \frac{\partial \varepsilon_p}{\partial \mathbf{e}_s} dA = \int_A \mathbf{a}_s^T \frac{\partial \sigma_p}{\partial \varepsilon_p} \cdot \frac{\partial (\mathbf{a}_s \cdot \mathbf{e}_s)}{\partial \mathbf{e}_s} dA = \int_A \mathbf{a}_s^T \frac{\partial \sigma_p}{\partial \varepsilon_p} \cdot \mathbf{a}_s dA = \\ &= \int_A \mathbf{a}_s^T E_{tan} \mathbf{a}_s dA \cong \mathbf{k}_s \end{aligned} \quad (\text{A.34})$$

where  $E_{tan}$  is the tangent modulus and  $\mathbf{k}_s$  is the tangent sectional stiffness matrix. The following relationship between Jacobian matrix and tangent stiffness matrix holds:

$$\mathbf{J}(\mathbf{e}_s) = -\mathbf{k}_s \quad (\text{A.35})$$

The recursive equation of the NR solution results:

$$\mathbf{e}_{s,i+1} = \mathbf{e}_{s,i} + [\mathbf{k}_s(\mathbf{e}_{s,i})]^{-1} \cdot \mathbf{g}(\mathbf{e}_{s,i}) = \mathbf{e}_{s,i} + \Delta \mathbf{e}_i \quad (\text{A.36})$$

and will be iterated until convergence.

### A.3.3 REMARKS ON THE SECTION STIFFNESS MATRIX

For a linear elastic material, the expanded form of the sectional stiffness matrix  $\mathbf{k}_s$  is:

$$\mathbf{k}_s = \int_A \mathbf{a}_s^T E_{tan} \mathbf{a}_s dA = \int_A E_{tan} \begin{bmatrix} 1 & -y & z \\ -y & y^2 & -yz \\ z & -yz & z^2 \end{bmatrix} dA \quad (\text{A.37})$$

The stress-strain relationship is simply  $\sigma = E\varepsilon$  and  $\partial\sigma_p/\partial\varepsilon_p = E$ , where  $E$  is the Young's modulus. For the special case of homogeneous sections, Eq. (A.37) can be rewritten as:

$$\mathbf{k}_s = E \int_A \mathbf{a}_s^T \mathbf{a}_s dA = E \int_A \begin{bmatrix} 1 & -y & z \\ -y & y^2 & -yz \\ z & -yz & z^2 \end{bmatrix} dA \quad (\text{A.38})$$

If the system  $(y, z)$  coincides with that of the principal axis of the section, the first order moments equal zero and the two flexural components uncouple, so that Eq. (A.38) becomes:

$$\mathbf{k}_s = E \begin{bmatrix} A & 0 & 0 \\ 0 & I_z & 0 \\ 0 & 0 & I_y \end{bmatrix} \quad (\text{A.39})$$

For a non linear stress strain relationship and non homogeneous sections, the tangent modulus varies with the sampling point P on the section. Further complications arise if the section is non homogeneous (made of concrete and reinforcing bars). In this case there isn't a reference system more effective than another. The simplest way is to assume the origin in the centroid of the concrete section. As a consequence, the tangent stiffness matrix is always full (Ciampi and Di Carlo, 1977).

In conclusion, two types of problems arise in dealing with the section state. The first one is written in an explicit way, the second one requires a numerical strategy for solving systems of nonlinear equations. In *both of them*, clearly, numerical integration over the section must be performed.

### A.3.4 INTERACTION DOMAINS

We refer to a generic reinforced concrete section. The interaction domain is a volume which contains all the states  $[N, M_z, M_y]$  acceptable within certain limits, stated according to given hypotheses. Its frontier is the locus of the points corresponding to an ultimate sectional state. In such a surface frontier lie the points having as coordinates the triplets of values  $[N, M_z, M_y]$  which lead a fiber of concrete or a bar of steel to reach its ultimate strain. In this paragraph we deal with the problem to define such a surface. The problem may be solved both in the space of the deformations  $\mathbf{e}_s(x)$  as well as in the space of the forces  $\mathbf{f}_s$ . In the first case we have to solve an ordinate succession of problems Type 1 (direct problems). The succession will explore all the deformative states corresponding to an ultimate value of the material strains. In the second case, working in the space of forces, we have to solve problems Type 2, involving repeated solutions of nonlinear equations.

This second way is time consuming, but more effective from a practical point of view, because it works defining the 3D domain  $N, M_z, M_y$  as a succession of 2D domains  $\bar{N}, M_z, M_y$ , reckoned for a constant value of the axial force.

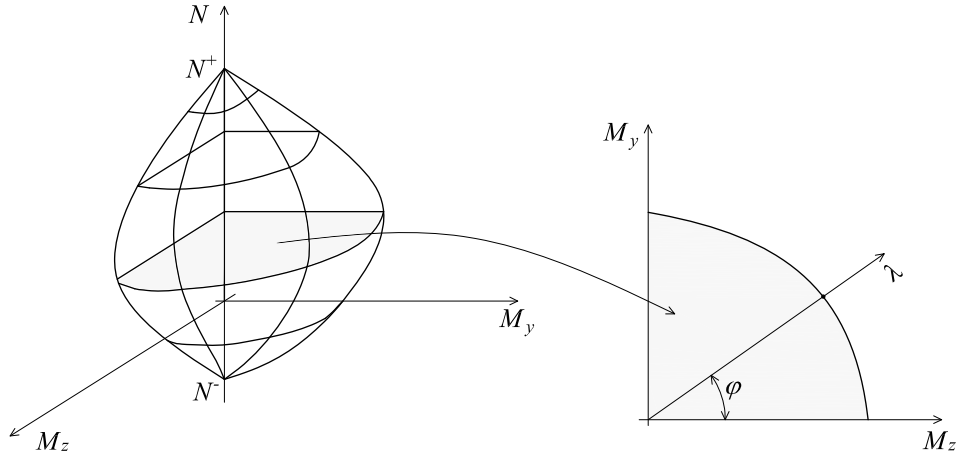


**Figure A.9:** Generic 3D Interaction Domain.

According to (Bontempi, 1992), we work through the following steps, Fig. A.9:

1. we chose a value  $\bar{N} = N \in [N^+; N^-]$ ;
2. in the plane  $\bar{N}, M_z, M_y$  we have to find the points associated to an ultimate limit state. To this purpose:
  - we chose at first an angle  $\varphi = 0 \div 2\pi$ ;
  - this angle gives a line on which we define a local variable  $\lambda$  so that:

$$\begin{aligned} M_z &= \lambda \cdot \cos \varphi \\ M_y &= \lambda \cdot \sin \varphi \end{aligned} \tag{A.40}$$

- with the bisection method we find the value of  $\lambda$  to which correspond the forces producing an ultimate state;

By repeating this search for a discrete set of angles  $\varphi$  and axial forces  $\bar{N}$  the surface frontier is built point wise. The same approach is applicable to the definition of 2D domains ( $M - N$  moment-axial force).

---

#### A.4 VALIDATION AND APPLICATIONS

The three reinforced concrete sections shown in Fig. A.10 are now considered: the first one is a square section reinforced with symmetrical bars, the second is a L shaped section, with distributed bars and the third is an hollow circular section with distributed bars. As already explained the first and the second sections need only one transformation while the third involves two parametric transformations.

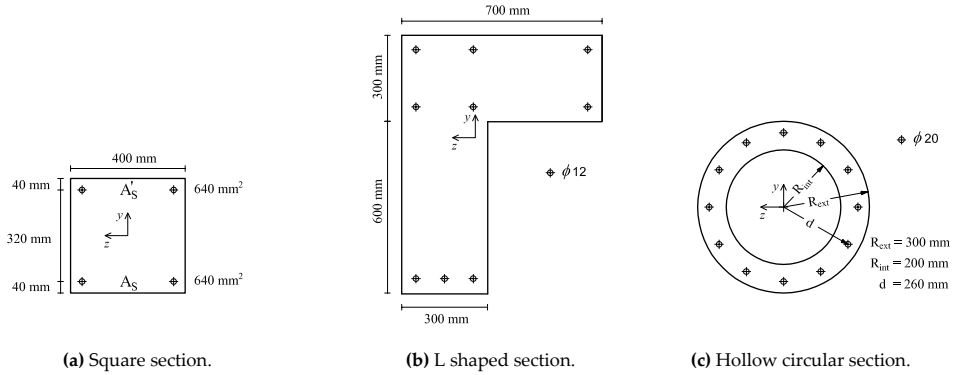


Figure A.10: R.C. sections considered for benchmarking.

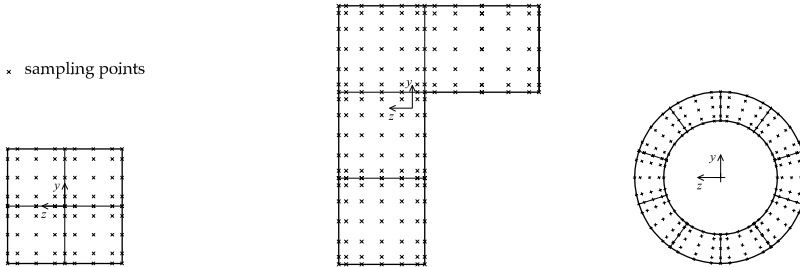


Figure A.11: Example of sub-domains discretization and sampling points position.

In order to compare the results with those of other Authors, for concrete the stress-strain parabola-rectangle relationship has been used. The steel is assumed having an elastic perfectly plastic behavior. The strength and ultimate strains parameters are listed in Tab. A.5.

Concrete	Steel
$f_c = -15 \text{ MPa}$	$f_y = 375 \text{ MPa}$
$\epsilon_{c0} = -0.0020$	$\epsilon_y = 0.0020$
$\epsilon_{cu} = -0.0035$	$\epsilon_y = 0.0100$

Table A.5: Material characteristics.

### Benchmark organization

- Square RC Section: reckoning of moment-curvature diagrams, with comparisons among different discretizations and different grids of sampling points. The fiber discretization method is also used. The results are compared in term of moment-curvature diagrams and assigned and approximate stress distributions;
- Square, L-shaped and hollow circular sections: construction of the multiaxial interaction domains.



**A.4.1 SQUARE SECTION. COMPARISONS AMONG DIFFERENT DISCRETIZATIONS**

The square reinforced concrete section of Fig. A.10(a), loaded by three different axial forces  $N = -240 - 1200 - 1680 \text{ kN}$ , is considered. The section is subdivided into 30 sub-domains and in each sub-domain a Gauss-Lobatto integration scheme with  $n=3$  sampling points is used. The corresponding moment-curvature diagrams are shown in Fig. A.12. The results obtained with this fine discretization agree with those reported in (C.E.B., 1978) and will be considered in the following as the reference solution.

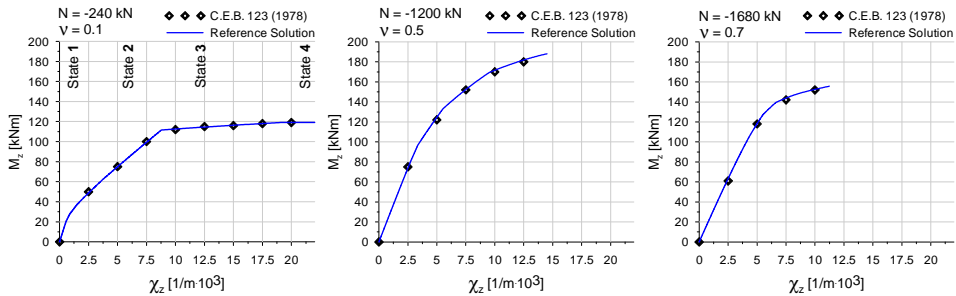


**Figure A.12:** Moment-curvature diagrams for different axial forces.

Fig. A.13 shows the stress distributions for different states of the moment-curvature diagram for the case with  $N = -240 \text{ kN}$ . One can observe how the neutral axis is moving upward and how at the final stage the points on the upper border catch the maximum compressive stress equal to  $15 \text{ MPa}$ .

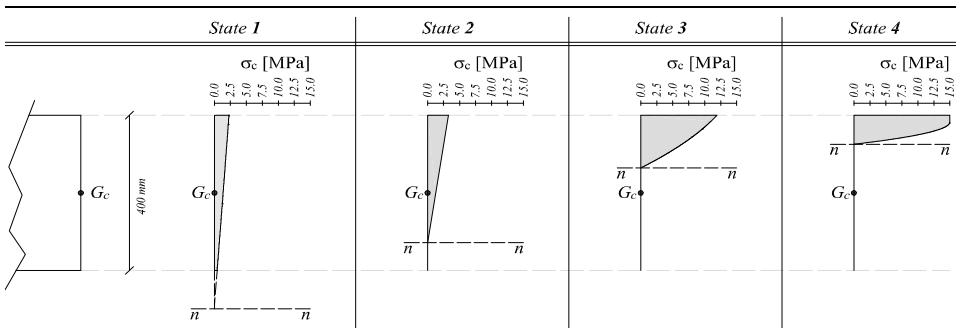


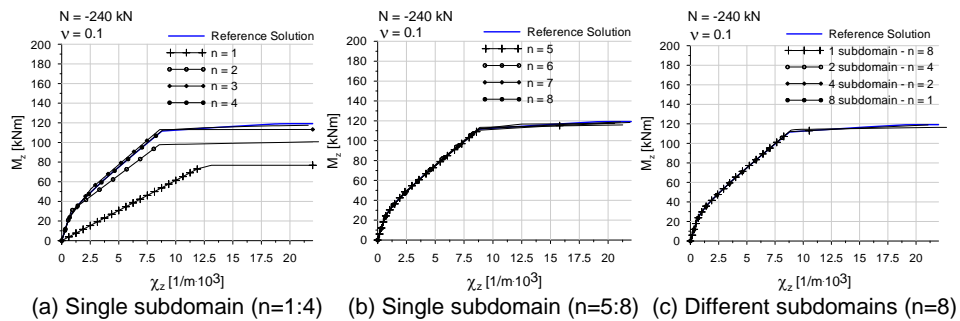
**Figure A.13:** Stresses in the concrete at different states ( $N = -240 \text{ kN}$ ).

Tensile stresses are null below the neutral axis, so we have to deal with the integration of a function that presents discontinuities whose position is state-dependent. On the other hand the interpolation functions associated to the integration rules are continuous.

In order to deal with the local discontinuity, three possible ways are explored and compared:

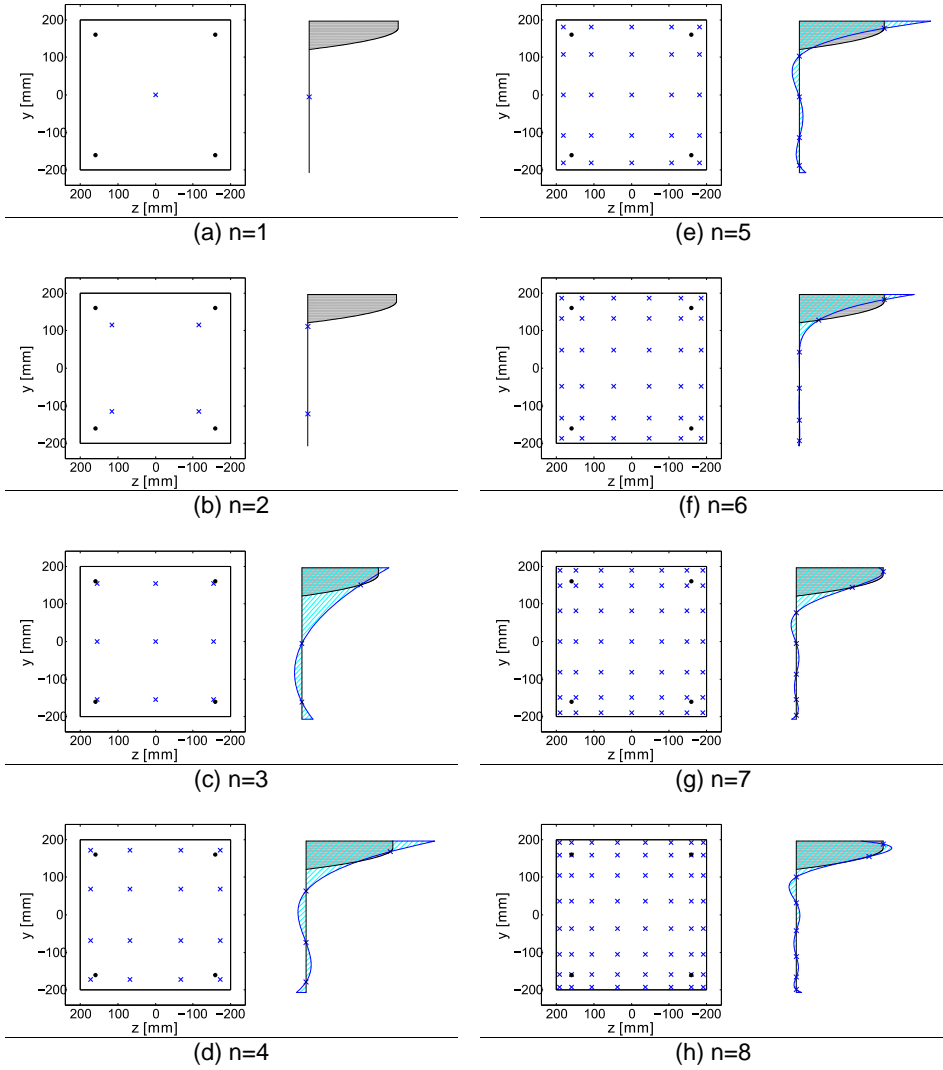
1. by fixing the dimension of the sub-domains and improving the integration by changing or the quadrature rule or the number of the sampling points;
2. by fixing the quadrature rule and increasing the number of sub-domains in order to increase the possibility to catch the stress discontinuity;
3. a combination of the two previous cases.

Fig. A.14 shows the moment-curvature diagram for the square R.C. section with  $N = -240 \text{ kN}$ . One can observe that by increasing the number of the sampling points the accuracy increases. From  $n \geq 5$ , no practical differences are observed in the results. Considering now the case with  $n = 8$  sampling points. By working with strategy 2 we use different sub-domain discretizations, taking always  $n = 8$ . The results are reported in Fig. A.14(c). No practical differences are observed in the results.



**Figure A.14:** Moment-curvature diagrams for different sectional discretizations.

Fig. A.15 and Fig. A.16 report the results for different discretizations and different numbers of sampling points. With reference to the ultimate states, these figures compare the stress distribution, associated to the assumed constitutive law, and the stress distributions as interpolated according to the integration rule. Even though the final results globally agree with the equilibrium condition, we observe that the interpolated stresses may have shapes quite different with respect the given one and that, in particular, they have non-null values below the neutral axis. Numerical convergence is reached through the balance of positive and negative areas, which tends to sum zero. As a consequence of these first results, it appears more convenient deal with to a so marked discontinuity, by adopting more small sub-domains. In fact, the well known fiber approach works with many fibers and uses a single sampling point.



**Figure A.15:** First discretization strategy. Real (black) and approximated (blue) distributions of stresses at the final state of moment-curvature curve. Comparison between the exact resultant of stresses (grey area) and approximate distribution (cyan area).

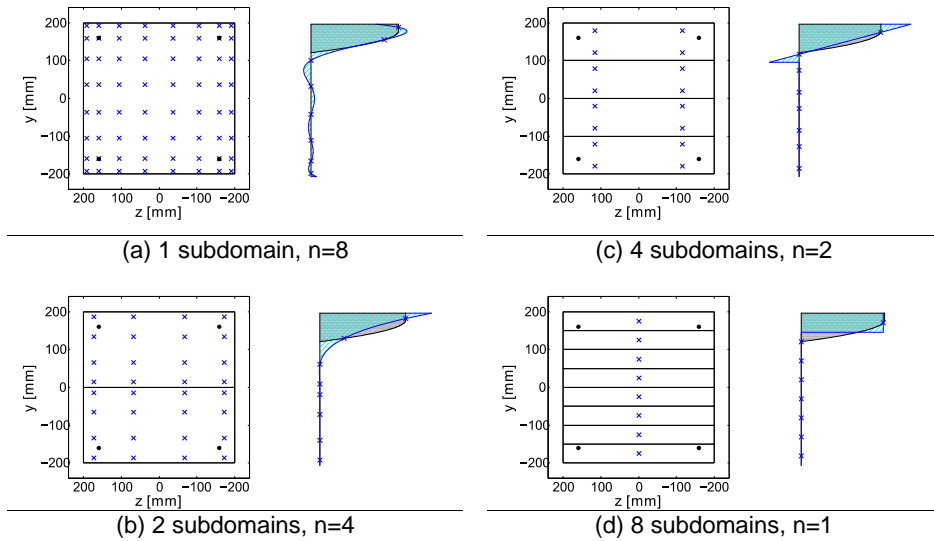


**Figure A.16:** Second discretization strategy. Real (black) and approximated (blue) distributions of stresses at the final state of moment-curvature curve. Comparison between the exact resultant of stresses (grey area) and approximate distribution (cyan area).

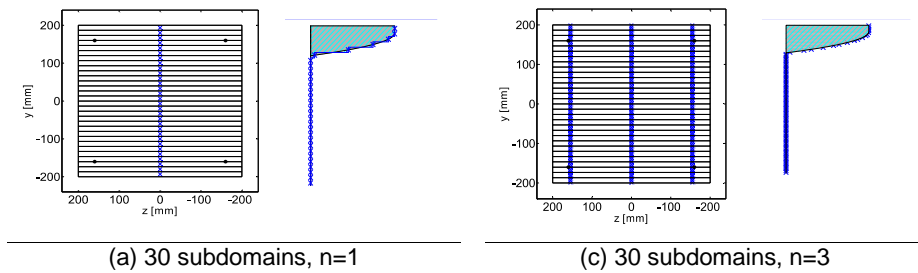


**Figure A.17:** Dense discretization. Real (black) and approximated (blue) distributions of stresses at the final state of moment-curvature curve. Comparison between the exact resultant of stresses (grey area) and approximate distribution (cyan area).

A.4.2 MULTIAXIAL INTERACTION DOMAINS

For the three R.C. sections shown in Fig. A.10, the multiaxial interaction domains are exposed in the next.

A.4.2.1 A SQUARE R.C. SECTION

The first example concerns the square R.C. section reported in Fig. A.10(a). The section has been subdivided in 4 sub-domains and the Gauss-Lobatto rule with 5 sampling points has been used in each of them. Fig. A.18(a) shows the 3D interaction domain. The relative bottom, top and lateral view are reported in Fig. A.18(c-d-e).

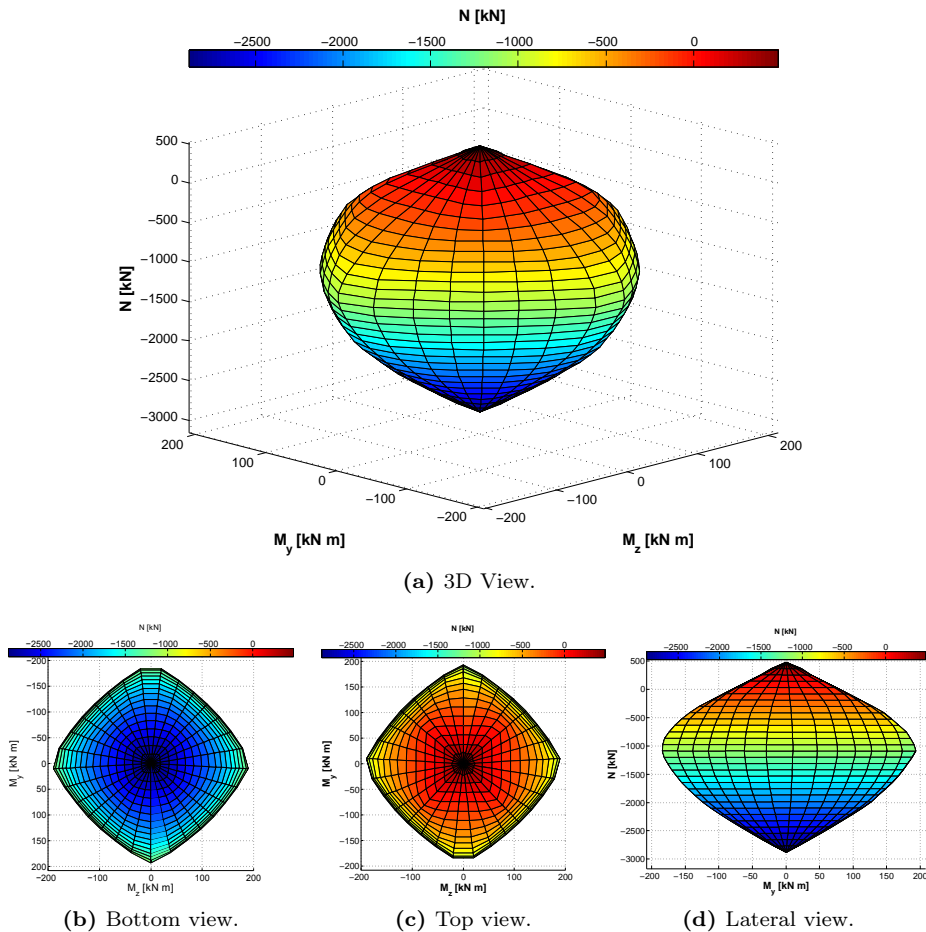


Figure A.18: Interaction domain for the square section of Fig. A.10(a).

## A.4.2.2 AN L SHAPED R.C. SECTION

The second example concerns the L-shaped R.C. section reported in Fig. A.10(b). The section has been subdivided in 4 sub-domains and the Gauss-Lobatto rule with 7 sampling points has been used in each of them. Fig. A.19(a) shows the 3D interaction domain. The relative bottom, top and lateral view are reported in Fig. A.19(c-d-e).

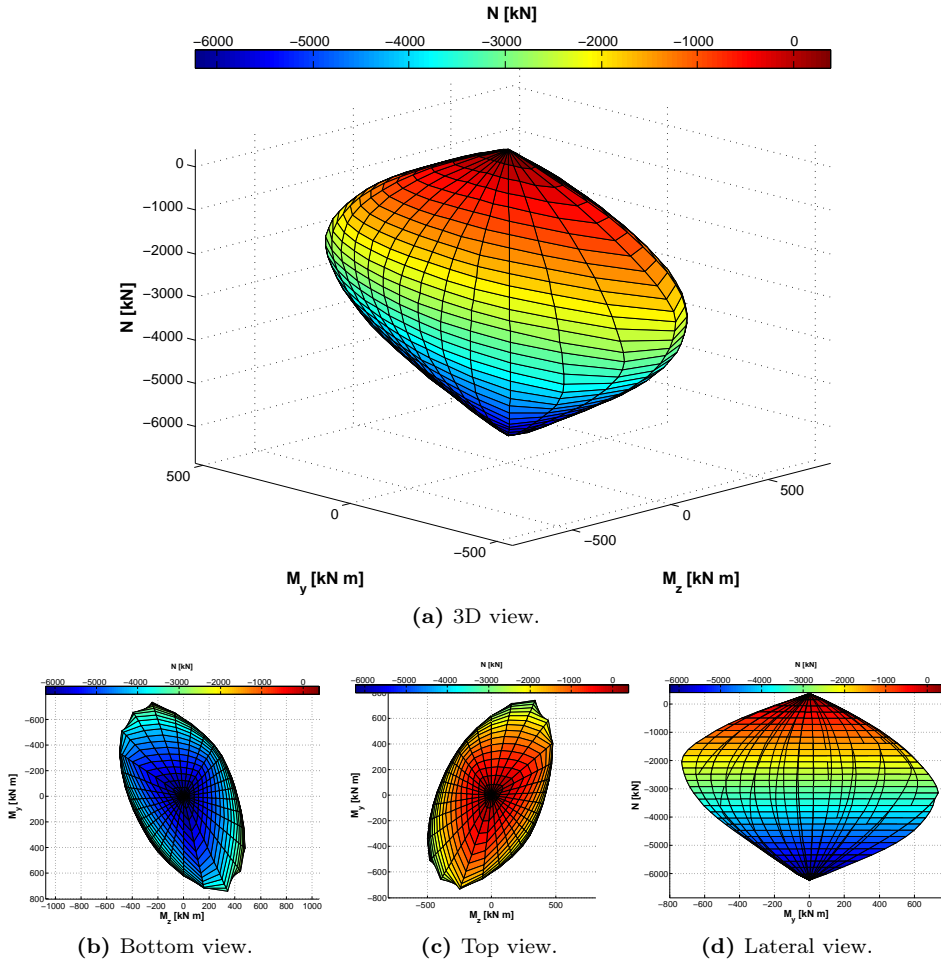


Figure A.19: Interaction domain for the L shaped section of Fig. A.10(b).

A.4.2.3 AN HOLLOW CIRCULAR R.C. SECTION

The third example concerns the circular hollow R.C. section reported in Fig. A.10(c). The section has been subdivided in 10 sub-domains and the Gauss-Lobatto rule with 5 sampling points has been used in each of them. Fig. A.20(a) shows the 3D interaction domain. The relative bottom, top and lateral view are reported in Fig. A.20(c-d-e).

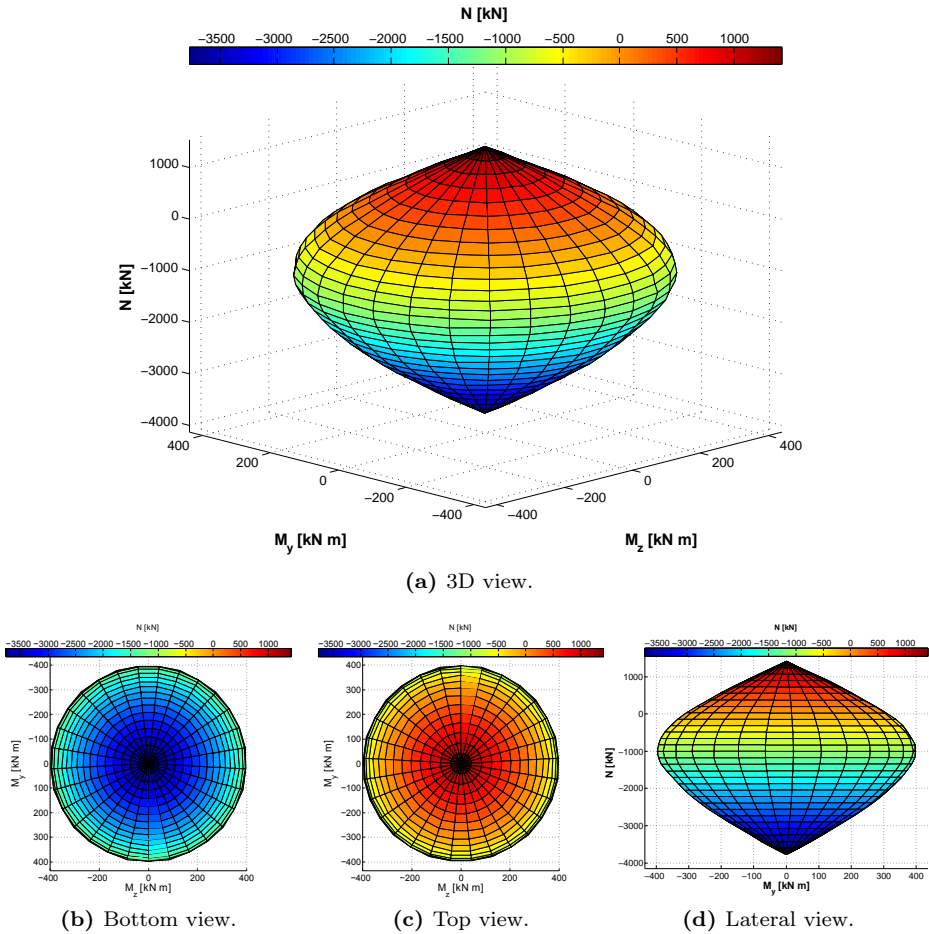


Figure A.20: Interaction domain for the circular hollow section of Fig. A.10(c).





# B | Limit analysis

*A systematic approach to the limit analysis of framed structures, which considers axial force and bending moment interaction, is presented. Following the general theory for limit analysis, the complete solution of the problem (i.e. the collapse loads, a stress distribution at the incipient collapse and a collapse mechanism) is obtained by linear programming.*

## B.1 INTRODUCTION AND BASIC HYPOTHESIS

---

The theory dealing with the determination of the load-carrying capacity of structures made of perfectly plastic materials is called *limit analysis*. A general formulation of a complete theory for perfectly plastic materials was given by Gvozdev (1938), but his work was not known in the Western world until the 1950s, where previously, mainly in works of Prager while at Brown University (Drucker *et al.* (1952) and Prager (1952)), a very similar theory had been developed (Nielsen and Hoang, 2011). One of the most important improvements in the development of the plastic theory was undoubtedly the establishment of the *upper* and *lower* bound theorems that, when the first computer based calculations became possible, can be translated in linear mathematical programming problems. Some of the first works in that direction has been done by De Donato and Maier (1972) and Maier (1973), in which also the geometrical non linearities are considered.

In many cases, the ultimate limit state of structural collapse can be adequately evaluated by assuming perfectly plastic behavior and neglecting second order effects, which make the general theory of limit analysis applicable to steel structures. Instead, since concrete is not a perfectly plastic material, the application of limit analysis to reinforced concrete structures requires some preliminary considerations.

Since reinforced concrete is a composite material, made of concrete and reinforcing steel, the use of a plastic approach is acceptable in cases where the strength is governed mainly by the reinforcement, e.g., flexure of beams and slabs. Also in this case, however, concrete properties can modify the ultimate structural behavior. If it is simple to assume that the tensile strength of concrete can be neglected, concerning the compression strength is much more difficult to propose reasonable assumptions, since concrete exhibits a significant strain softening. In addition, local mechanical properties can be influenced by cracks phenomena or interaction mechanisms between steel and concrete.

For that reasons, limit analysis seems not generally applicable to reinforced concrete structures. However, several experiences suggest that limit analysis can be successfully applicable to RC problems if (Biondini, 1999):

- concrete tensile strength is neglected;
- concrete compression strength is modify trough a coefficient  $\nu_e$  called *effectiveness factor*:

$$f_c^* = \nu_e f_c \quad \text{with } \nu_e \in [0; 1] \quad (\text{B.1})$$

Of course, adequate values for  $\nu_e$  are required. Exner (1979) proposes the evaluation of the effectiveness factor by using the energy equivalence reported in Fig. B.1. However, it must be pointed out that concrete properties alone cannot define such a coefficient, because several informations must be considered, e.g., properties and position of reinforcing steel, structural geometry, support conditions, structural forces flow and load conditions. For these reasons, prudential values has been proposed, such as  $\nu_e = 0.60$  suggested in (Marti, 1985) and (Rogowsky and MacGregor, 1986).

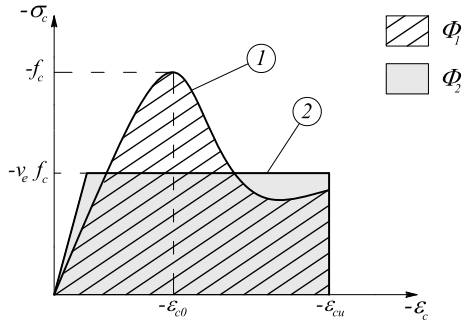


Figure B.1: Effectiveness factor.

Several applications of limit analysis by mathematical programming can be found in (Cocchetti and Maier, 2003), (Ardito, 2004), (Ardito *et al.*, 2008), in which also softening plastic-hinge models are considered in the elastic-plastic analyses of frames and critical thresholds on deformations are introduced by solving a nonconvex nonsmooth constrained optimization problem usually referred to in the literature as “mathematical program under equilibrium constraints” (Ardito *et al.*, 2010).

The approach here proposed neglects shear failures and considers axial force  $N$  and bending moment  $M$  as interacting generalized plastic stresses. A rigid perfectly-plastic constitutive law is adopted to relate these stresses to the correlative generalized plastic strains, represented by the cross-sectional axial elongation  $\Delta l$  and bending rotation  $\vartheta$ , respectively. In this way, the behavior of the discrete cross-sections where the plastic strains tend to develop can be represented by a generalized plastic hinge that allows a free axial-bending kinematic behavior and, at the same time, fully transfers the corresponding plastic values of the axial force and bending moment. The plastic collapse is reached when the set of generalized plastic hinges is able to activate a kinematic mechanism for which the equilibrium can no longer be satisfied, (Biondini and Frangopol, 2008).

The hypothesis used are: (1) small displacements; (2) rigid perfectly-plastic behavior; (3) only axial force and bending moment active and interacting (Fig. B.2); (4) ultimate axial forces and bending moments described by the interaction domain, that can be linearized as Fig. B.3 shows; (5) the formation of plastic hinges is limited at the extreme of the elements. This approximation produces limitations that can be overcome by increasing the elements number of the mesh.

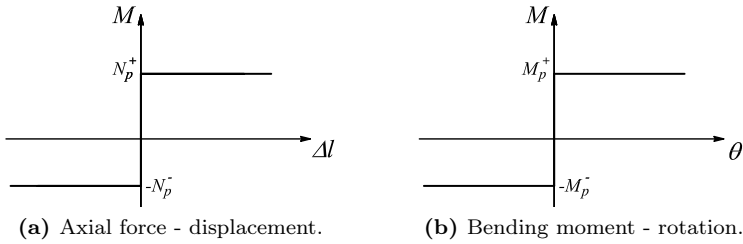


Figure B.2: Rigid perfectly-plastic behavior.

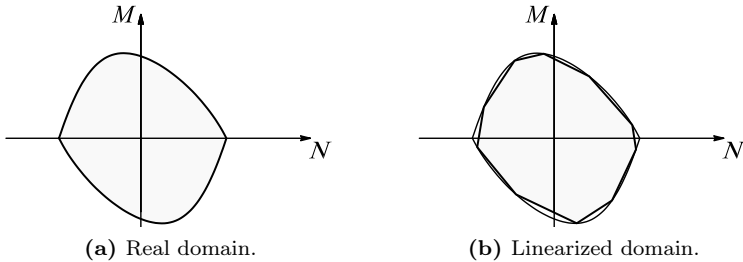


Figure B.3: Limit Interaction Domains.

B.2 GLOBAL EQUILIBRIUM AND COMPATIBILITY EQUATIONS

In order to apply the Limit Analysis Theorems, global equilibrium and compatibility equations must be formulated. At this end, the generic structure is subdivided in finite elements as Fig. B.4 shown. Forces and generalized stresses are assumed in accordance with the conventions and with the reference systems shown in Fig. B.4c.

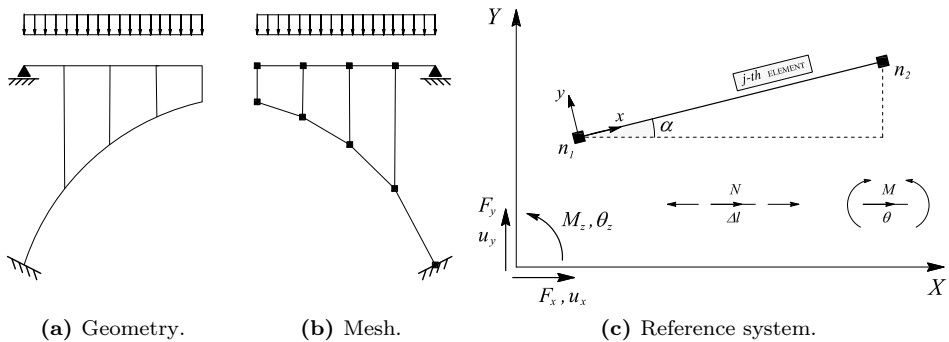
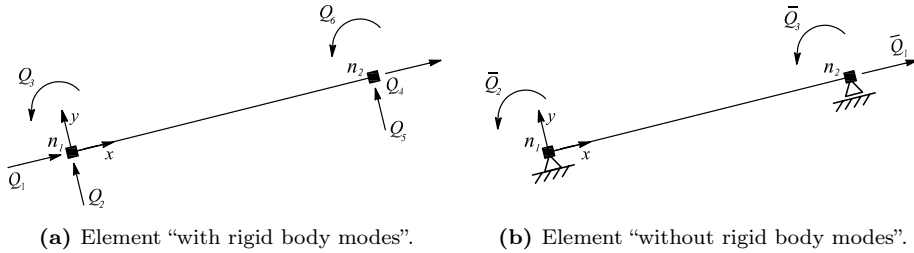


Figure B.4: Limit analysis: structural geometry, structural mesh and reference system.

Since it is reasonable to replace a distributed load with statically equivalent concentrated loads in an appropriate number of cross-sections, no distributed loads are considered acting on the element. In these cases, an additional subdivision of the mesh can be introduced in order to increase accuracy.

### B.2.1 EQUILIBRIUM EQUATIONS

Let's considered the generic  $j$ -th element of a structure. The equilibrium equations can be obtained by following the steps used for a force-based element (see par. 2.4).



**Figure B.5:** Static field: element with and without rigid body modes.

In particular, by removing the rigid body motions, the following relation holds:

$$\mathbf{Q}_j = \mathbf{h}_l^T \bar{\mathbf{Q}}_j \quad (\text{B.2})$$

The nodal forces in the global reference system  $\mathbf{Q}_{g,j}$  can be obtained from the local ones  $\mathbf{Q}_j$  through the transformation matrix  $\mathbf{T}_\alpha$ :

$$\mathbf{T}_\alpha = \begin{bmatrix} \mathbf{T}_0 & \mathbf{0} \\ \mathbf{0} & \mathbf{T}_0 \end{bmatrix} \quad \text{with} \quad \mathbf{T}_0 = \begin{bmatrix} \cos \alpha & -\sin \alpha & 0 \\ \sin \alpha & \cos \alpha & 0 \\ 0 & 0 & 1 \end{bmatrix} \quad (\text{B.3})$$

so that:

$$\mathbf{Q}_{g,j} = \mathbf{T}_\alpha \mathbf{Q}_j \quad (\text{B.4})$$

By substituting in (B.4) eq. (B.2), the following relation holds:

$$\begin{aligned} \mathbf{Q}_{g,j} &= (\mathbf{T}_\alpha \mathbf{h}_l) \bar{\mathbf{Q}}_j \\ &= \mathbf{H}_{g,j} \bar{\mathbf{Q}}_j \end{aligned} \quad (\text{B.5})$$

where  $\mathbf{H}_g$  is the element equilibrium matrix.

Finally, by assembling all the  $ne$  elements, the nodal equilibrium equations for the whole structure result as follows:

$$\begin{aligned} \mathbf{F}_e &= \sum_{j=1}^{ne} \mathcal{A}(\mathbf{Q}_{g,j}) \\ &= \sum_{j=1}^{ne} \mathcal{A}(\mathbf{H}_{g,j} \cdot \bar{\mathbf{Q}}_j) \end{aligned} \quad (\text{B.6})$$

that, in matrix form, becomes:

$$\mathbf{F}_e = \mathbf{H} \cdot \mathbf{Q}_t \quad (\text{B.7})$$

where  $\mathbf{F}_e$  is the external nodal forces vector,  $\mathbf{H}$  is the *equilibrium matrix* of the structure and  $\mathbf{Q}_t$  is the vector that contain all the basic forces of the elements.

**B.2.2 COMPATIBILITY EQUATIONS**

Fig. B.6 shows the kinematic quantities in the reference system “with rigid body modes” and in the one “without rigid body modes”. The same quantities are used in a force-based element.

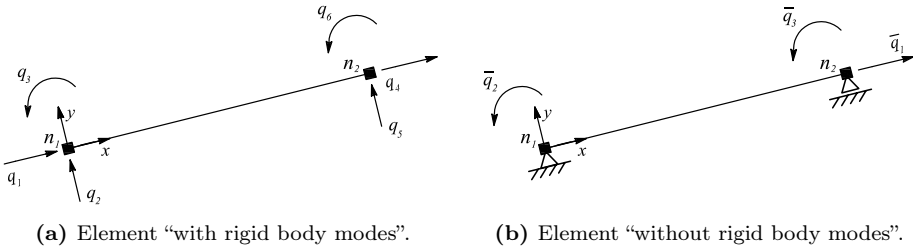


**Figure B.6:** Kinematic field: element with and without rigid body modes.

Compatibility conditions for the whole structure can be obtained by using a dual approach with respect equilibrium, in which the Virtual Force Principle is applied. The external and the internal works are:

$$\delta W_e = \delta \mathbf{F}^T \mathbf{s} \qquad \delta W_i = \delta \mathbf{Q}_t^T \mathbf{q}_t \qquad (\text{B.8})$$

and the Principle of Virtual Forces states that:

$$\delta W_i = \delta W_e \quad \Rightarrow \quad \delta \mathbf{F}^T \mathbf{s} = \delta \mathbf{Q}_t^T \mathbf{q}_t \qquad (\text{B.9})$$

For the static field the following equilibrium equation holds:

$$\delta \mathbf{F} = \mathbf{H} \delta \mathbf{Q}_t \qquad (\text{B.10})$$

By substituting eq. (B.10) in eq. (B.9) the following relation is obtained:

$$\delta \mathbf{Q}_t^T \mathbf{H}^T \mathbf{s} = \delta \mathbf{Q}_t^T \mathbf{q}_t \qquad (\text{B.11})$$

Since such an equation is valid for any choice of  $\delta \mathbf{Q}_t^T$ , the following compatibility equations are finally obtained:

$$\mathbf{q}_t = \mathbf{H}^T \mathbf{s} \qquad (\text{B.12})$$

where matrix  $\mathbf{H}^T$  is the *compatibility matrix* of the structure and it is the transpose of the equilibrium matrix.

**B.2.3 ABOUT EQUILIBRIUM AND COMPATIBILITY MATRICES**

It has been show that the equilibrium matrix is the transpose of the compatibility matrix. Such a results can be used in order to classify a structure:

- if matrix  $\mathbf{H}$  has full rank, with equilibrium equations we can find the vector of basic forces and hence the internal forces: this is the case of a *statically determined structure*;

- if matrix  $\mathbf{H}$  has more columns than rows, equilibrium states that infinite solutions can be possible. This is the case of a *statically undetermined structure*;
- if matrix  $\mathbf{H}$  has more rows than columns, equilibrium states that there are not solutions. This is the case of a *kinematic undetermined structure*.

### B.3 MATERIAL CONSTITUTIVE MODELS

According to the hypothesis of the rigid perfectly-plastic constitutive law, (a) the yielding criterion, which defines the stress state corresponding to the start of the plastic flow, is convex, and (b) the flow rule, through which the increments of the plastic strains are correlated to the stress state, is associated with the yielding surface (normality rule).

#### B.3.1 YIELD CONDITION

By assuming the normal force  $N_i$  and the bending moment  $M_i$  as the only active generalized plastic stresses (Fig. B.7), the yielding criterion for the  $i$ -th generic critical cross-section can be written as:

$$f_i(N_i, M_i) = 0 \tag{B.13}$$

Such a criterion defines, in the  $N - M$  plane, a domain that can be reasonably idealized by a stepwise approximation which is, for the sake of safety, inscribed within the convex yielding criterion:

$$f_i(N_i, M_i) \leq 0 \tag{B.14}$$

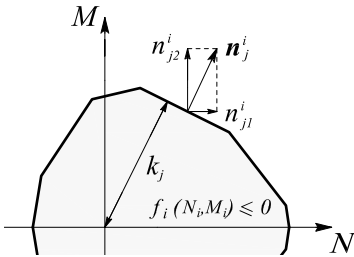


**Figure B.7:** Yielding criterion. By assuming a stepwise linearization with  $q$  sides for each  $i$ -th plastic domain, with reference to Fig. B.7 we can define:

- a matrix  $\mathbf{N}_i$ , in which each row contains the components with respect the axis of the normal vector  $\mathbf{n}_j^i$  to the  $j$ -th side of the curve ( $n_{j1}^i, n_{j2}^i$ );
- a vector  $\mathbf{k}_i$ , with inside the  $k_j$  distance between the side of the domain and the origin of the axis.

The dimension of these quantities depends on the quality of the stepwise linearization chosen. Matrix  $\mathbf{N}_i$  and vector  $\mathbf{k}_i$  have this expression:

$$\mathbf{N}_i = \begin{bmatrix} n_{11}^i & n_{12}^i \\ n_{21}^i & n_{22}^i \\ \dots & \dots \\ n_{j1}^i & n_{j2}^i \\ \dots & \dots \\ n_{q1}^i & n_{q2}^i \end{bmatrix} \quad \mathbf{k}_i = \begin{bmatrix} k_1^i \\ k_2^i \\ \dots \\ k_j^i \\ \dots \\ k_q^i \end{bmatrix} \tag{B.15}$$

Therefore, the yielding criterion for each  $i$ -th critical cross-section can be rewritten in matrix form as:

$$\Theta_i = \mathbf{N}_i \mathbf{r}_i - \mathbf{k}_i \leq 0 \tag{B.16}$$

where  $\mathbf{r}_i$  is the vector whose components are the generalized stresses acting in the  $i - th$  section:

$$\mathbf{r}_i = \begin{bmatrix} N_i \\ M_i \end{bmatrix} \quad (\text{B.17})$$

and  $\Theta_i$  is the *plastic potential vector*, whose components give a measure of the distance between the point and the  $j - th$  side of the limit domain:

$$\Theta_i = [\Theta_1^i \quad \Theta_2^i \quad \dots \quad \Theta_j^i \quad \dots \quad \Theta_q^i]^T \quad (\text{B.18})$$

The internal forces  $\mathbf{r}_i$  in a generic section of the element can be evaluated from the basic forces  $\bar{\mathbf{Q}}$  by using the equilibrium equation:

$$\begin{bmatrix} N \\ M \end{bmatrix} = \begin{bmatrix} 1 & 0 & 0 \\ 0 & (x/l - 1) & x/l \end{bmatrix} \begin{bmatrix} \bar{Q}_1 \\ \bar{Q}_2 \\ \bar{Q}_3 \end{bmatrix} \quad (\text{B.19})$$

In this formulation, only the extreme sections of the element are controlled and hence:

$$\mathbf{r}_{n1} = \begin{bmatrix} N \\ M \end{bmatrix} = \begin{bmatrix} 1 & 0 & 0 \\ 0 & -1 & 0 \end{bmatrix} \begin{bmatrix} \bar{Q}_1 \\ \bar{Q}_2 \\ \bar{Q}_3 \end{bmatrix} \quad \mathbf{r}_{n2} = \begin{bmatrix} N \\ M \end{bmatrix} = \begin{bmatrix} 1 & 0 & 0 \\ 0 & 0 & 1 \end{bmatrix} \begin{bmatrix} \bar{Q}_1 \\ \bar{Q}_2 \\ \bar{Q}_3 \end{bmatrix} \quad (\text{B.20})$$

For each element, the yielding criterion becomes:

$$\Theta_i = \mathbf{N}_i \bar{\mathbf{Q}} - \mathbf{k}_i \leq 0 \quad (\text{B.21})$$

By assembling all the elements, it is possible to set the *structural yielding criterion* as follows:

$$\begin{aligned} \Theta_t &= \sum_{j=1}^{ne} \mathcal{A}(\Theta_j) \leq 0 \\ &= \sum_{j=1}^{ne} \mathcal{A}(\mathbf{N}_j \bar{\mathbf{Q}}_t - \mathbf{k}_j) \leq 0 \\ &= \mathbf{N} \bar{\mathbf{Q}}_t - \mathbf{k} \leq 0 \end{aligned} \quad (\text{B.22})$$

In (Olsen, 1998) the influence of the linearization of the yield surface on the load-bearing capacity is detailed.

### B.3.2 FLOW RULE

The associated flow rule for each  $i - th$  critical cross-section is given by:

$$\mathbf{d}_i = \begin{cases} \Delta l_i & = \mu_i \frac{\partial f_i}{\partial N_i} \\ \theta_i & = \mu_i \frac{\partial f_i}{\partial M_i} \end{cases} \quad (\text{B.23})$$

with the multiplier  $\mu_i$  that allows plastic flows only for the points lying on the yielding curve along the outside normal (Fig. B.7):

$$\begin{cases} \mu_i = 0 & \text{if } f_i(N_i, M_i) < 0 \\ \mu_i > 0 & \text{if } f_i(N_i, M_i) = 0 \end{cases} \quad (\text{B.24})$$

or, in compact form:

$$\mu_i \cdot f_i(N_i, M_i) = 0 \quad (\text{B.25})$$

For the linearized case, the following matrix notation can be introduced:

$$\mathbf{d}_i = \mathbf{N}_i^T \cdot \boldsymbol{\mu}_i \quad (\text{B.26})$$

with

$$\begin{cases} \mu_j^i \cdot \phi_j^i = 0 & j = 1, \dots, q \\ \mu_i \geq 0 \end{cases} \quad (\text{B.27})$$

where vector  $\boldsymbol{\mu}_i$  contains the terms  $\mu_j^i$  relative to each side of the linearized domain:

$$\boldsymbol{\mu}_i = [\mu_1^i \quad \mu_2^i \quad \dots \quad \mu_1^j \quad \dots \quad \mu_q^i]^T \quad (\text{B.28})$$

As before, the flow rule can be written for the generic element by connecting the vector of plastic deformation  $\mathbf{d}_i$  with the vector of basic displacement  $\bar{\mathbf{q}}$ :

$$\bar{\mathbf{q}} = \mathbf{N}_i^T \boldsymbol{\mu}_i \quad (\text{B.29})$$

By assembling all the element, the *structural flow rule* becomes:

$$\mathbf{q} = \sum_{j=1}^{ne} \mathcal{A}(\bar{\mathbf{q}}_j) = \sum_{j=1}^{ne} \mathcal{A}(\mathbf{N}_j^T \boldsymbol{\mu}_j) = \mathbf{N}^T \boldsymbol{\mu} \quad (\text{B.30})$$

with

$$\begin{cases} \mu_j^i \cdot \phi_j^i = 0 & j = 1, \dots, q \\ \boldsymbol{\mu} > 0 \end{cases} \quad (\text{B.31})$$

#### B.4 STATIC AND KINEMATIC APPROACH (DUALITY)

---

Let  $\mathbf{P}_0$  be a vector of constant loads and  $\mathbf{P}$  a vector of loads whose intensity is proportional to a given scalar multiplier  $\lambda \geq 0$ . By assuming that the structure is safe for  $\lambda = 0$ , the collapse multiplier  $\lambda_c$  associated with its failure is derived from the *two fundamental theorems* of limit analysis.

The *lower bound theorem* states that  $\lambda_c$  is the maximum of the multipliers associated with stress fields that satisfy both the equilibrium conditions and the yielding criterion. In mathematical terms:

$$\lambda_c = \max \{ \lambda \mid \lambda \mathbf{P} - \mathbf{H} \mathbf{Q}_t = -\mathbf{P}_0, \quad \mathbf{N} \mathbf{Q}_t \leq \mathbf{k}, \quad \lambda \geq 0 \} \quad (\text{B.32})$$



THEOREM		INPUT		OUTPUT
Lower Bond	<b>H</b>	equilibrium matrix	$\lambda_c$	collapse multiplier
	<b>N</b>	yielding criterion matrix	<b>Q</b>	basic forces
	<b>k</b>	yielding distance vector		
Upper Bond	<b>H<sup>T</sup></b>	compatibility matrix	$\lambda_c$	collapse multiplier
	<b>N</b>	yielding criterion matrix	<b>s</b>	nodal displacements
	<b>k</b>	yielding distance vector	<b><math>\mu</math></b>	flow parameters vector

**Table B.1:** Limit Analysis Theorem: Input & Output variables.

The *upper bound theorem* states that  $\lambda_c$  is the minimum of the multipliers associated with plastic flows that satisfy both compatibility conditions and flow rule. In mathematical terms:

$$\lambda_c = \min \{ \mathbf{k}^T \boldsymbol{\mu} - \mathbf{P}_0^T \mathbf{s} \mid \mathbf{N}^T \boldsymbol{\mu} - \mathbf{H}^T \mathbf{s} = \mathbf{0}, \mathbf{P}^T \mathbf{s} = 1, \boldsymbol{\mu} \geq 0 \} \quad (\text{B.33})$$

Therefore the fundamental theorems of the limit analysis can be translated into dual linear constrained optimization problems: the first one requires to find a maximum, while the second one a minimum. It is worth noting that in the second case, the minimum condition is related to the work done by the proportional loads **P** for the displacements **s** associated with the collapse mechanism. Since this mechanism is associated with an arbitrary multiplier, it results in being univocally identified by the condition  $\mathbf{P}^T \mathbf{s} = 1$ . The solution of the previous dual linear programs leads to the complete solution of the problem, i.e. the collapse multiplier, the stress distribution at the incipient collapse and the collapse mechanism. As it is the separator of two sets,  $\lambda_c$  is unique. However, the uniqueness of  $\lambda_c$  does not necessarily mean the uniqueness of the collapse mechanism, or that of the stress field at collapse.

Finally, it must be pointed out that computationally speaking the two theorems are not equal. In fact, in the case of the lower bond theorem, the solution is a search in the space defined by equilibrium, on which the yielding criterion acts like a constrain: the unknowns of the problem are  $\lambda_c$  and the basic forces  $\mathbf{Q}_i$  in all the elements. Instead, in the case of the upper bond theorem, the solution is a search in the space defined by compatibility, but the flow rule and, in particular, the vector  $\boldsymbol{\mu}$  enter in the definition of the space: the unknowns of the problem are  $\lambda_c$ , the displacement vector **s** and vector  $\boldsymbol{\mu}$ . Since the last has a dimension that depends on the number of stepwise linearization used for domains, it is clear that the upper bond theorem is more computational demanding with respect the lower bond one.

Limit analysis procedure previously exposed has been implemented in a specific computer code. The optimization problem has been solved by the *simplex method*.

**B.5 BENCHMARKS**

In the following, three benchmarks with increasing complexity are presented:

1. a portal frame with two variable concentrate loads (Dell’Acqua, 1994);
2. a clamped RC arch (Ceradini and Gavarini, 1965);
3. a collaborating beam-arch system (Ronca and Cohn, 1979a).

**B.5.1 A PORTAL FRAME**

The portal frame shows in Fig. B.8 is considered. It is supposed that the bending moment is the only active generalized plastic stresses. The resisting bending moment of the beam is double with respect the columns. The geometry of the structure, the external supports, the loads acting and the mesh used are reported in Fig. B.8a. Limit analysis gives the combinations of  $(\lambda_1, \lambda_2)$  that produce the collapse of the portal frame. The results are shown in Fig. B.8b.

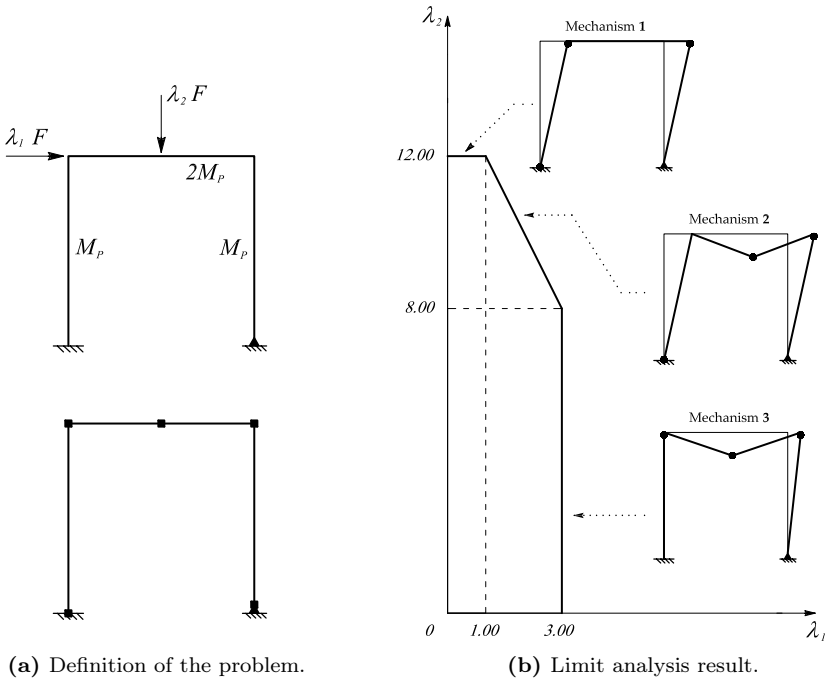


**Figure B.8:** Portal frame with two variable concentrate loads.

In the first mechanism, there is a plastic hinge in the fixed support at the left and two plastic hinges at the top of the columns. In the second mechanism, there is a plastic hinge in the fixed support at the left, a plastic hinge in the middle of the beam and a plastic hinge at the top of the right column. In the third mechanism, two plastic hinges at the top of the columns and a plastic hinge in the middle of the beam are present.

B.5.2 A CLAMPED RC ARCH

The clamped arch subdivided in 28 elements and shown in Fig. B.9 is analyzed.

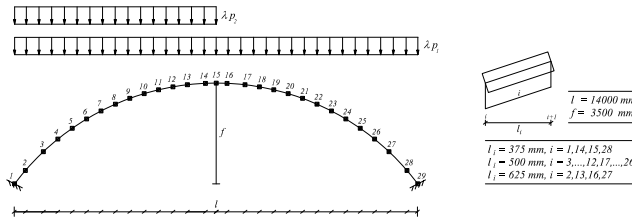
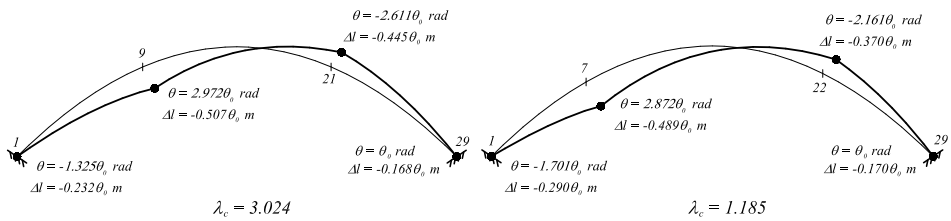


Figure B.9: Clamped RC arch. Geometry and discretization.

Two load combinations (with same multiplier  $\lambda$ ) are considered:

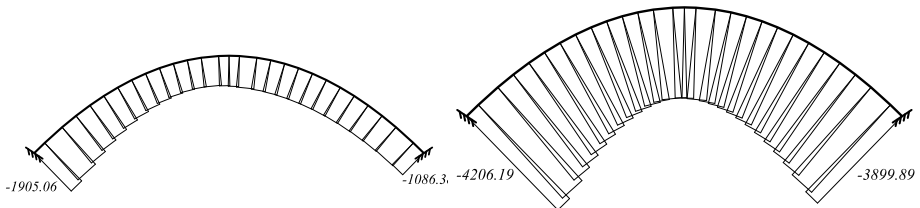
1. Case 1:  $p_1 = 0.0 \text{ N/mm}$  and  $p_2 = 100 \text{ N/mm}$ ;
2. Case 2:  $p_1 = 300 \text{ N/mm}$  and  $p_2 = 100 \text{ N/mm}$ .

For both, Fig. B.10 reports the collapse mechanisms and the relative internal forces.



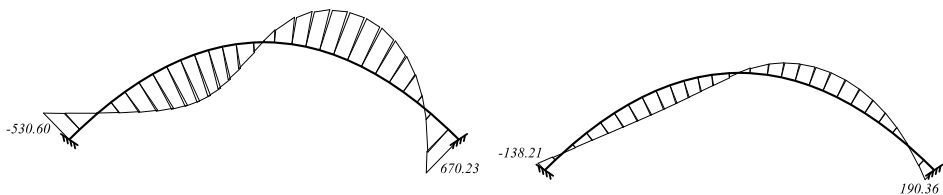
(a) Case 1: collapse mechanism.

(b) Case 2: collapse mechanism.



(c) Case 1: axial forces [kN].

(d) Case 2: axial forces [kN].



(e) Case 1: bending moments [kNm].

(f) Case 2: bending moments [kNm].

Figure B.10: Clamped RC arch: limit analysis results.

Fig. B.11 shows the positions of the generalized plastic hinges in the interaction domains.

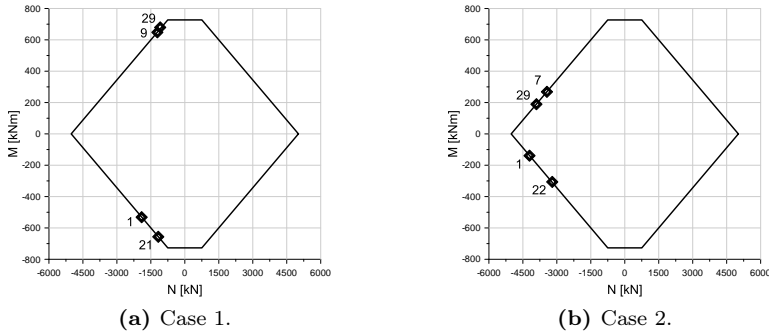


Figure B.11: Clamped RC arch: plastic hinges position in the interaction domains.

Finally, the obtained results are compared with the ones gives in (Ceradini and Gavarini, 1965), in order to control the validity of the proposed computer code.

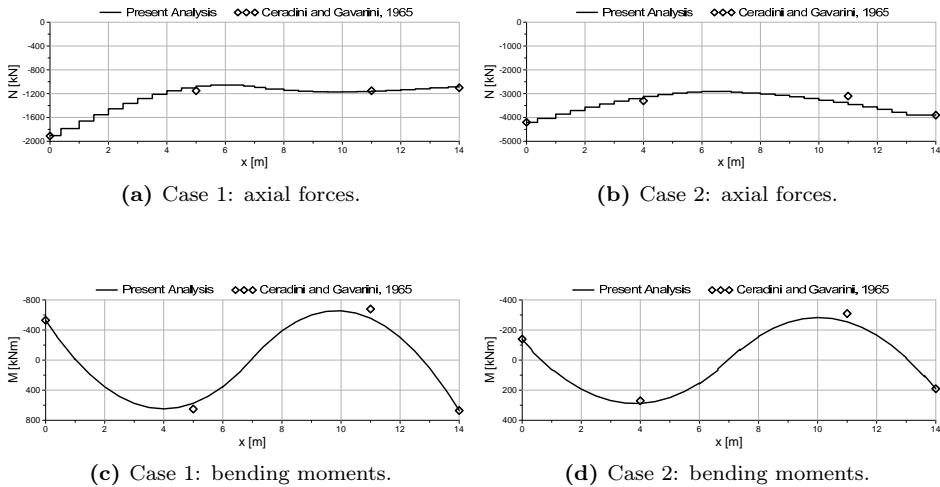
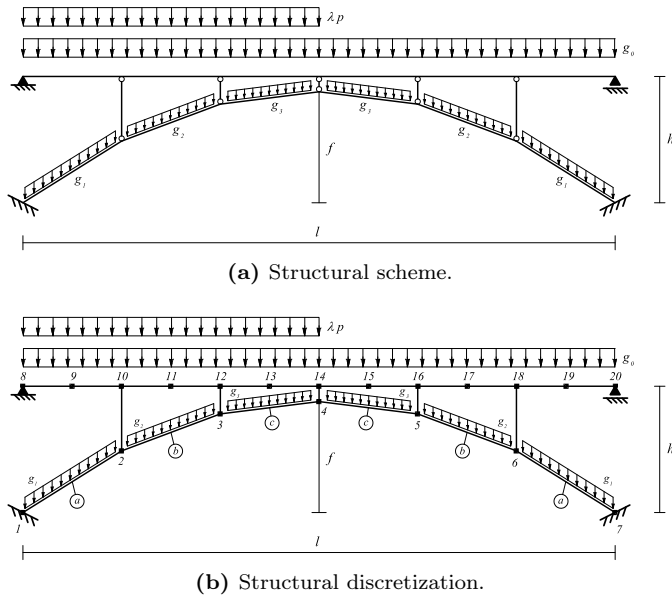


Figure B.12: Clamped RC arch: comparisons with the solution obtained by (Ceradini and Gavarini, 1965).

**B.5.3 A COLLABORATING BEAM-ARCH SYSTEM**

The collaborating beam-arch system shown in Fig. B.13a is considered. For geometry and loads:  $l = 4000\text{ mm}$ ,  $f = 750\text{ mm}$ ,  $h = 800\text{ mm}$ ;  $g_0 = 1.87\text{ N/mm}$ ,  $g_0 = 1.87\text{ N/mm}$ ,  $g_1 = 1.18\text{ N/mm}$ ,  $g_2 = 0.90\text{ N/mm}$ ,  $g_3 = 0.56\text{ N/mm}$ ,  $p = 10.00\text{ N/mm}$ . For the beam, a resisting bending moment equal to  $M_p = 6\text{ kNm}$  is considered. For the arch, the three interaction domains shown in Fig. B.14 are used. The connections between beam and arch are considered as infinitely resisting.



**Figure B.13:** Geometry and loads of the beam-arch system.

Fig. B.14 shows the position of plastic hinges in the interaction domains. The limit solution is show in Fig. B.15, where in addition the comparisons with (Ronca and Cohn, 1979a) are reported.

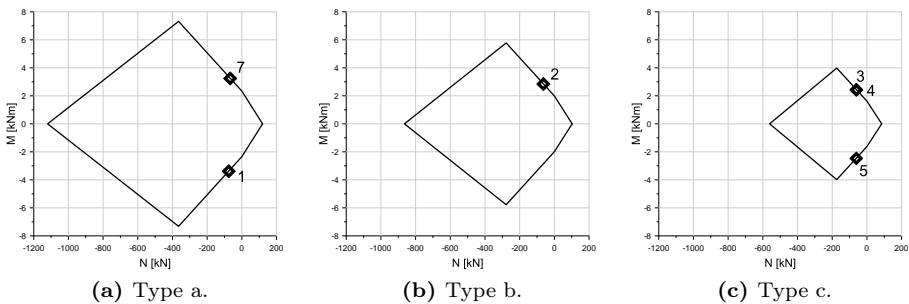
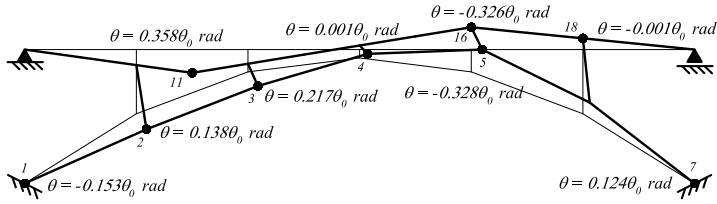
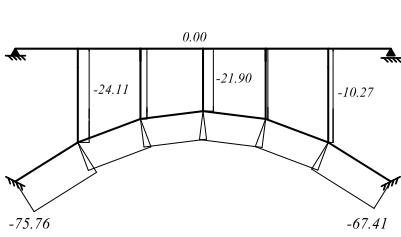


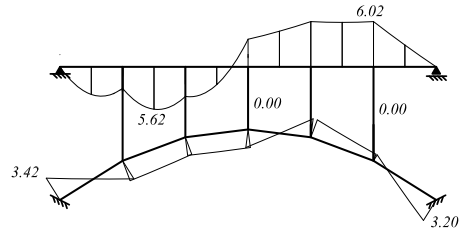
**Figure B.14:** Collaborating beam-arch system: plastic hinge positions.



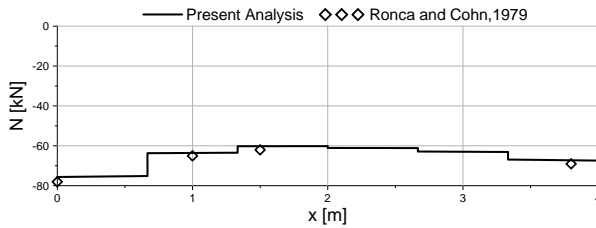
(a) Collapse mechanism.



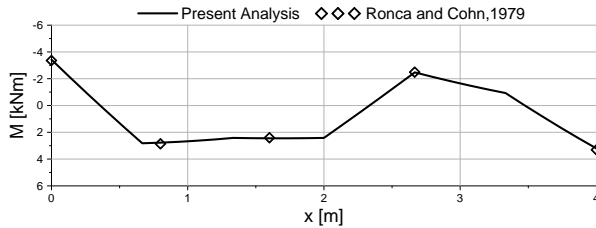
(b) Axial forces [kN].



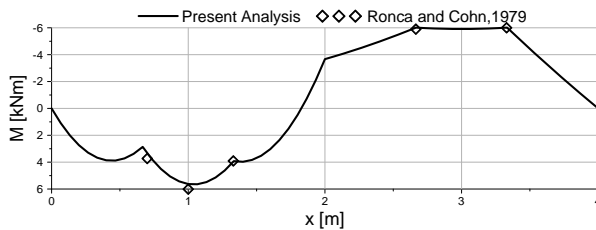
(c) Bending moments [kNm].



(d) Axial forces in the arch.



(e) Bending moments in the arch.



(f) Bending moments in the beam.

**Figure B.15:** Collaborating beam-arch system: limit analysis solution and comparisons (Ronca and Cohn, 1979a).  $\lambda_c = 3.835$ .

---

---

## CONCLUSIONS





# Conclusions

## OUTLINE & GENERAL CONCLUSIONS

---

A robust methodology for the assessment of reinforced concrete structures based on time-variant capacity has been presented. Structural analyses have been coupled with the damage processes in order to evaluate the time-evolution of the structural performances accounting for environmental hazards.

The thesis is composed of four parts:

- Part **I** concerns the methods of structural analysis suitable to deal with the non-linear behavior of RC structures. The main aim of this part is to propose a shear sensitive beam element;
- Part **II** extends theories and methods previously developed to damaged RC structures modeling;
- Part **III** studies cable stayed and arch bridges and presents a coherent set of applications involving one or more of the aforementioned problems, as well as significant comparisons with other approaches to the structural analysis of R.C. structures (non linear analysis versus limit analysis). In addition, the damage effects on resisting mechanisms are outlined and discussed;
- Part **IV** contains two appendices, collecting notes, comments and deepening emerged in developing the theoretical formulations and in setting up the numerical algorithms.

### PART I

Chapter 1 frames the argument of the thesis, outlines the research significance and presents its aims. In Chapter 2, after a short recall of the Principle of Virtual Work, the basic characteristics of non-linear beam elements are derived by using both a displacement-based and a force-based approach (dual formulation). In particular, it is shown how a force-based beam element is suitable to represent, for any distributed applied load, the exact internal forces distribution, while a displacement-based element is constrained by the assumed shape functions. Chapter 3 distinguishes the different and nested levels of analysis (structure, element, section, fiber). With reference to the infinitesimal beam element, the evolution of the sectional kinematic from the Navier-Bernoulli, to Timoshenko and to the generalized beam theory is analyzed, showing how each new grade of refinement

requires necessarily a more refined stress-strain relationship (linear or non linear too):

- for the Navier-Bernoulli beam only normal strains and normal stresses are involved, hence a mono-dimensional stress-strain relationship (linear or non linear) is sufficient;
- for the Timoshenko beam, in the elastic field only the normal and tangential elasticity modulus of elasticity are needed, but the same model is not suitable to deal with non linear material, because for such an extension we cannot simply superimpose two elementary behavior (behavior under the normal strains and, separately, that under the shear strains), but a coupling between normal and tangential stresses is required;
- hence, a non linear shear beam element necessarily involves a more rich kinematic field, with all the term of the strain tensor, and, as a consequence, a corresponding fully bi-dimensional stress-strain constitutive laws.

In the same Chapter the main approaches proposed until now are presented and shortly discussed:

- Strut & Tie based Models;
- Inter-fiber equilibrium model;
- Fixed Pattern based Approaches.

Due to the necessity of a bi-dimensional stress-strain relationships, in Chapter 4 two known and widely used Theories are examined: the Modified Compression Field Theory (MCFT) and the Disturbed Stress Field Theory (DSFT). Both Theories are discussed and tested with an original code and with reference to panels and beams having shear critical behaviors. Results and methods are compared and widely discussed in order to choice the most effective for the formulation of a shear sensitive beam element.

A finite element beam suitable to deal a with the shear effects is then proposed and developed in Chapter 5 both with a fixed strain approach and a fixed stress approach. The difference between these two approaches depends on the type of the additional condition to be imposed in order to make the problem determinate. The element formulation is accomplished with proposal that allows to compute the stresses in the stirrups and of a proposal of conventional representation of the crack pattern in the web of the beam. The model has been validated with reference to beams of the Stuttgart series ET1, ET2, ET3, ET4. These beams have been analyzed through (I) 2D CST-F.E. analyses and MCFT Theory, (II) with no shear 1D beam elements and (III) with 1D shear sensitive beam elements.

The comparisons have been made with respect to the load-displacement curves, the crack patterns, the collapse mechanism and the stresses in the stirrups. The general agreement is good. The differences among some results have been discussed and motivated.

## PART II

The damage diffusion process and its modeling through the diffusivity equation is presented. The diffusion problem is solved through the Cellular Automata algorithm. Introductory examples show the effectiveness of such a numerical approach. The effects of the damage are then specialized to Reinforced Concrete Elements. New damage indexes, concerning both steel and concrete, are introduced and then tested for different reinforcement assemblies.

## PART III

This part studies cable stayed and arch bridges and presents a coherent set of applications involving one or more of the aforementioned problems. In particular, significant comparisons are made between non-linear analyses and limit analyses results, that led to introduce an efficiency factor that takes into account the different nature of these two approaches, as well as the different criteria to model the material properties with respect to the ultimate behavior.

## PART IV

Two appendices, collecting notes, comments and deepening emerged in developing the theoretical formulations and in setting up the numerical algorithms are exposed. A set of notes on the so called fibre method outline some hidden aspects associated to the numerical integration of section properties. A concise recall of the limit analysis theory and a set of basic as well as actual applications put in evidence the powerful and also the care to be adopted in using this type of analysis.

## ORIGINAL CONTRIBUTIONS

---

In developing the theoretical formulations and in setting up the numerical algorithms, several original contributions has been carried out.

Concerning the structural model, the main contribution is the development of the shear sensitive beam element, based on two different sectional approaches depending on the type of the condition to be imposed. In particular, a new section state determination process, effectively efficient and stable, has been presented. In order to reach such a result, an important effort comes from the fact that also bidimensional modeling has been developed and coded in a finite element based program. It has been shown that such a computational technique can be successfully applied in dealing with the non linear behavior of RC structures for all range off loadings. Clearly, since a structural 1D theory contains some intrinsic approximations with respect the complete 2D problem, such a strategic choice has permitted to obtained critical suggestions in order to move the formulation from bidimensional towards monodimensional modeling.

Concerning the damage model, a general computational approach based on the Cellular Automata algorithm has been formulated in dealing with damage processes affecting RC structures. Through such an approach, it is possible to deal with: (a) the reduction of steel bars areas, (b) the reduction of steel ductility, (c) the reduction of concrete strength until (d) the spalling of concrete cover occurs.

Due to his generality, the so-obtained damage model can be linked with any structural model. Hence, a general method aiming to assess the life cycle performances of a generic RC structures has been obtained. This is the most important and practical contribution of this work.

Two others marginal contributions are the following.

In coding beam-column elements, specific numerical integrations strategies are required both at the element level and at the sectional level. In the last case, the most used approach is the so-called fibers approach, through which the section is divided in sub-domains, called fibers, and the integral is evaluated with the Riemann Mid-Point Integration Rule. In this work, a more general numerical integration strategy, able to deal with arbitrary quadrilateral-circular shaped sections, has been proposed. The section is divided, once again, in sub-domains that now are parametrically transformed in the same square parent domain on which integration rules refers. In this way, several combinations of integration strategies can be performed, with the widely used fiber method as particular case.

In developing the applications, a complete parallel study between limit and non linear analysis has been carried out. Through such a parallelism, a proposal for the evaluation of the so-called effectiveness factor has been given, not only when the structural system is sound, but also in time, when the structure is progressively interested by damage.

## FINAL CONCLUSIONS

---

The main aim of this work is to consider the possibilities of shear-flexible beam column elements in the study of RC structures, both in sound and in damaged conditions. In order to reach this result the basic methods of non linear structural analysis, two renowned RC membrane theories have been reviewed, developed and compared with reference to shear critical panels and beams. A finite element beam suitable to deal with the shear effects is then proposed and developed two different approaches depending on the type of the additional condition to be imposed. The model has been validated with reference to beams of the Stuttgart series ET1-ET4. The comparisons have been made with respect to the load-displacement curves, the crack patterns, the collapse mechanism and the stresses in the stirrups. The general agreement is good. These theories and methods have been then extended to model damaged RC Structures. New damage indexes, concerning both steel and concrete, have been introduced and then tested for different reinforcement assemblies. A wide set of applications confirm the soundness of both of theoretic proposals and of the algorithms used to reduce the problems to algebraic forms. The types of application stand out the effectiveness of the model in dealing with actual and complex structures. Particular interesting are the effects of damage on shear resistance mechanisms.

In concluding, this thesis proposes a general and versatile methodology that deals with the time-evolution of RC structural performances accounting for environmental hazards. The proposed procedure can be applied also as a general life-cycle approach.

## FURTHER DEVELOPMENTS

---

Based on the achieved results, several future developments of this work are possible:

- the shear-flexible beam-column element:  
the formulation proposed in this thesis is based on fixed pattern approaches. Despite different types of patterns are considered, it's clear that this choice contains some intrinsic approximations. The main difficulty in formulating beam-column elements sensible to shear is the definition of a consistent section state determination process. Since shear mechanism in RC elements is not a sectional phenomena, it's clear that this step is not straightforward. A very important improvement of the beam formulation must be reckoned in the so-called generalized beam theory, in which the kinematic of the section is state dependent. A lot of work in this field has been already carried out and the most elegant approaches have been recalled in Chapter 5;
- concerning limit analysis:  
it has been shown that limit analysis is the most synthetic approach. If small displacement hypothesis is assumed, the solution of the problem (i.e. the collapse load, a stress distribution at the incipient collapse and a collapse mechanism) is obtained by linear programming. In the formulation exposed in the thesis, only axial force and bending moment interaction is considered. In the plane, however, three are the interacting generalized stresses: the axial force  $N$ , the shear force  $V$  and the bending moment  $M$ . If an adequate resistance criterion, that consider  $N - V - M$  interaction, is proposed, then limit analysis can be extended also in the study of shear collapse mechanisms. Since current design criterion are based on the lower bound theorem, this is a very practical and useful development of this work;
- dealing also with seismic performances:  
an important development concerns the extension of the presented procedures also in the dynamic field, so that also the time-variant seismic performances can be evaluated considering different environmental hazards;
- extension to the non deterministic field:  
it has been shown that the phenomena involved in damage processes are not so clear and, in addition, not so certain due to dependability on aleatory quantities such as the chlorides content, the position of the corrosion scenarios and so on. A natural development of this work is to extend the proposed procedure in the non deterministic field, in order to deal with the intrinsic uncertainties affecting the considered phenomena.

As shown, several and not directly linked improvements can be possible. This is due to the methodology adopted in carrying out this research, that is obtained as a nested summation on independent theoretical and computational parts.



# References

- AAS-JAKOBSEN, K. and GRENACHER, M. (1974), «Analysis of Slender Reinforced Concrete Frames», *Bericht nr. 50 Institut fur Baustatik ETH Zurich*, vol. 50.
- ABRAMOWITZ, M. and STEGUN, I. (1964), *Handbook of mathematical functions with formulas, graphs, and mathematical tables*, Dover publications.
- ADAMI, C. (1998), *Introduction to artificial life*, Springer.
- ALMUSALLAM, A. A. (2001), «Effect of degree of corrosion on the properties of reinforcing steel bars», *Construction and Building Materials*, vol. 15 (8), p. 361–368.
- APOSTOLOPOULOS, C. and PAPADAKIS, V. (2008), «Consequences of steel corrosion on the ductility properties of reinforcement bar», *Construction and Building Materials*, vol. 22 (12), p. 2316–2324.
- ARDITO, R. (2004), *Diagnostic and Limit State Analyses of Concrete Dams by Optimization Methods*, PhD Thesis, Supervisor: Prof. G. Maier, Politecnico di Milano, Milan, Italy.
- ARDITO, R., COCCHETTI, G. and MAIER, G. (2008), «On structural safety assessment by load factor maximization in piecewise linear plasticity», *European Journal of Mechanics-A/Solids*, vol. 27 (5), p. 859–881.
- ARDITO, R., COCCHETTI, G. and MAIER, G. (2010), «Generalized limit analysis in poroplasticity by mathematical programming», *Archive of Applied Mechanics*, vol. 80 (1), p. 57–72.
- AURICCHIO, F. (2003), «Nonlinear finite element analysis.», *Class Notes, ROSE School, Pavia, Italy.*, vol. 1 (1), p. 1–124.
- BAIRÁN, J. (2005), *A non-linear coupled model for the analysis of reinforced concrete sections under bending, shear, torsion and axial forces*, PhD Thesis, Supervisor: Prof. A.R. Mari, Technical University of Catalonia, Barcelona, Spain.
- BAIRÁN, J. and MARÍ, A. (2006a), «Coupled model for the non-linear analysis of anisotropic sections subjected to general 3D loading. Part 1: Theoretical formulation», *Computers & structures*, vol. 84 (31), p. 2254–2263.

- BAIRÁN, J. and MARÍ, A. (2006b), «Coupled model for the nonlinear analysis of sections made of anisotropic materials, subjected to general 3D loading. Part 2: Implementation and validation», *Computers & structures*, vol. 84 (31), p. 2264–2276.
- BAIRÁN, J. and MARÍ, A. (2007a), «Multiaxial-coupled analysis of RC cross-sections subjected to combined forces», *Engineering structures*, vol. 29 (8), p. 1722–1738.
- BAIRÁN, J. and MARÍ, A. (2007b), «Shear-bending-torsion interaction in structural concrete members: a nonlinear coupled sectional approach», *Archives of Computational Methods in Engineering*, vol. 14 (3), p. 249–278.
- BATHE, K.-J. (1996), *Finite element procedures*, Prentice hall Englewood Cliffs.
- BAUMANN, T. (1970), «Versuche zum Studium der Verdubelungswirkung der Biegezugbewehrung eines Stahlbetonbalkens», *Heft 210, Berlin, Deutscher Ausschuss für Stahlbeton*.
- BELLUZZI, O. (1969), *Scienza delle costruzioni, vol. I, II e III*, Zanichelli, Bologna.
- BENTZ, E. C. (2000), *Sectional analysis of reinforced concrete members*, PhD Thesis, Supervisor: Prof. M.P. Collins, University of Toronto, Canada.
- BERTOLINI, L. (2006), «Materiali da costruzione-Volume II: Degrado, prevenzione, diagnosi, restauro», *Città Studi Edizioni, Milano*.
- BERTOLINI, L., ELSENER, B., PEDEFERRI, P., REDAELLI, E. and POLDER, R. B. (2013), *Corrosion of steel in concrete: prevention, diagnosis, repair*, Wiley. com.
- BIONDINI, F. (1999), «Il Fattore di Efficienza della Modellazione Strut-and-Tie di Elementi in Cemento Armato», *Aicap '99, Lo sviluppo del cemento armato e del precompresso in Italia e la lezione di questo secolo*, vol. 1, p. 129–138.
- BIONDINI, F., BONTEMPI, F. and MALERBA, P. (2004a), «Fuzzy reliability analysis of concrete structures», *Computers & structures*, vol. 82 (13), p. 1033–1052.
- BIONDINI, F., CAMNASIO, E. and PALERMO, A. (2013), «Lifetime seismic performance of concrete bridges exposed to corrosion», *Structure and Infrastructure Engineering*, vol. 1 (1), p. 1–21.
- BIONDINI, F. and FRANGOPOL, D. M. (2008), «Probabilistic limit analysis and lifetime prediction of concrete structures», *Structure and Infrastructure Engineering*, vol. 4 (5), p. 399–412.
- BIONDINI, F. and GARAVAGLIA, E. (2005), «Probabilistic service life prediction and maintenance planning of deteriorating structures», in «International Conference on Structural Safety and Reliability (ICOSSAR 2005), Rome, Italy», p. 19–22.



- BIONDINI, F. and VERGANI, M. (2012), «Damage modeling and nonlinear analysis of concrete bridges under corrosion», in «Proceedings of the Sixth International Conference on Bridge Maintenance, Safety and Management (IABMAS 2012), Stresa, Italy, July», p. 8–12.
- BIONDINI, F., BONTEMPI, F., FRANGOPOL, D. and MALERBA, P. (2002), «Durability analysis of deteriorating concrete structures due to diffusion processes: Application to box-girder bridges», in «Proc., 6th Int. Conf. on Short and Medium Span Bridges», vol. 2, p. 745–752.
- BIONDINI, F., BONTEMPI, F., FRANGOPOL, D. M. and MALERBA, P. G. (2004b), «Cellular automata approach to durability analysis of concrete structures in aggressive environments», *Journal of Structural Engineering*, vol. 130 (11), p. 1724–1737.
- BONTEMPI, F. (1992), «Sulla costruzione dei domini di rottura di sezioni in C.A. e C.A.P. soggette a pressoflessione deviata.», *Studi e ricerche - Politecnico di Milano. Scuola di specializzazione in costruzioni in cemento armato.*, vol. 13 (1), p. 261–277.
- BONTEMPI, F., MALERBA, P. and CICCONE, F. (1995a), «Sull’analisi non lineare dei ponti strallati precompressi», *Studi e ricerche - Politecnico di Milano. Scuola di specializzazione in costruzioni in cemento armato.*, vol. 16 (1), p. 289–320.
- BONTEMPI, F., MALERBA, P. and ROMANO, L. (1995b), «Formulazione diretta secante dell’analisi non lineare di telai in CA/CAP», *Studi e ricerche - Politecnico di Milano. Scuola di specializzazione in costruzioni in cemento armato.*, vol. 16, p. 351–386.
- BONTEMPI, F. and MALERBA, P. G. (1997), «The role of softening in the numerical analysis of RC framed structures», *Structural Engineering and Mechanics*, vol. 5 (6), p. 785–801.
- BRELSER, B. and SCORDELIS, A. (1963), «Shear strength of reinforced concrete beams», *ACI Journal Proceedings*, vol. 60 (1).
- CAMNASIO, E. (2013), *Lifetime performance and seismic resilience of concrete structures exposed to corrosion*, PhD Thesis, Supervisor: Prof. F. Biondini, Politecnico di Milano, Milan, Italy.
- CAPOZUCCA, R. (1995), «Damage to reinforced concrete due to reinforcement corrosion», *Construction and Building Materials*, vol. 9 (5), p. 295–303.
- CAPSONI, A. and CORRADI, L. (1997), «A finite element formulation of the rigid-plastic limit analysis problem», *International Journal for Numerical Methods in Engineering*, vol. 40 (11), p. 2063–2086.
- CASTELLANI, A. and CORONELLI, D. (1999), «Beams with corroded reinforcement: Evaluation of the effects of cross-section losses and bond deterioration by finite element analysis», *Studi e ricerche-Politecnico di Milano. Scuola di specializzazione in costruzioni in cemento armato.*, vol. 20, p. 53–69.

- CEA (2000), «CASTEM 2000, Guide d'Utilisation», *CEA, Saclay, France*.
- C.E.B. (1978), «Manual of Buckling and Instability», *C.E.B.*, vol. 123.
- C.E.B. (1985), «Cracking and deformations», *Ecole Polytechnique Federale, Lausanne*.
- C.E.B. (1992), *Durable Concrete Structures: Design Guide*, 183, Comité Euro-International du Béton, Thomas Telford.
- C.E.B. (1996), «Reinforced concrete elements under cyclic loading state-of-the-art report», *C.E.B.*, vol. 230.
- CERADINI, G. and GAVARINI, C. (1965), «Calcolo a rottura e programmazione lineare», *Giornale del Genio Civile*, vol. 103 (1-2), p. 48–64.
- CERESA, P., PETRINI, L. and PINHO, R. (2007), «Flexure-shear fiber beam-column elements for modeling frame structures under seismic loading - state of the art», *Journal of Earthquake Engineering*, vol. 11 (S1), p. 46–88.
- CERESA, P., PETRINI, L., PINHO, R. and SOUSA, R. (2009), «A fibre flexure-shear model for seismic analysis of RC-framed structures», *Earthquake Engineering & Structural Dynamics*, vol. 38 (5), p. 565–586.
- CERVENKA, V. (1970), *Inelastic finite element analysis of reinforced concrete panels under in-plane loads*, PhD Thesis, University of Colorado.
- CIAMPI, A. and DI CARLO, A. (1977), «Sulla pressoflessione dei cosiddetti solidi non reagenti a trazione», *Università degli Studi de L'Aquila, Facoltà di Ingegneria, Istituto di Scienza delle Costruzioni*, vol. 25 (1), p. 1–18.
- COCCHETTI, G. and MAIER, G. (2003), «Elastic-plastic and limit-state analyses of frames with softening plastic-hinge models by mathematical programming», *International Journal of Solids and Structures*, vol. 40 (25), p. 7219–7244.
- COLLINS, M. P. (1978), «Towards a rational theory for RC members in shear», *Journal of the Structural Division*, vol. 104 (4), p. 649–666.
- COLLINS, M. P. and LAMPERT, P. (1973), «Redistribution of Moments at Cracking-The Key to Simpler Torsion Design?», *ACI Special Publication*, vol. 35.
- COLUSSI, M. (2013), *Modified Compression Field & Disturbed Stress Field Theories: Applicabilità, Confronti, Contributi*, Master Thesis, Supervisors: Prof. P.G. Malerba and Eng. M. Quagliaroli, Politecnico di Milano, Milan, Italy.
- CONTI, E. (2013), *Analisi Limite e Non Lineare di Ponti in Calcestruzzo Armato*, Master Thesis, Supervisors: Prof. P.G. Malerba and Eng. M. Quagliaroli, Politecnico di Milano, Milan, Italy.
- CORIGLIANO, A. and TALIERCIO, A. (2005), *Meccanica Computazionale. Soluzione del problema elastico lineare*, Progetto Leonardo Bologna, Società Editrice Euscalapio.

- CORONELLI, D. and GAMBAROVA, P. (2004), «Structural assessment of corroded reinforced concrete beams: Modeling guidelines», *Journal of Structural Engineering*, vol. 130 (8), p. 1214–1224.
- DE DONATO, O. and MAIER, G. (1972), «Mathematical programming methods for the inelastic analysis of reinforced concrete frames allowing for limited rotation capacity», *International Journal for Numerical Methods in Engineering*, vol. 4 (3), p. 307–329.
- DELL'ACQUA, L. C. (1994), *Meccanica delle strutture*, McGraw-Hill.
- DM (2008), *Nuove norme tecniche per le costruzioni*, Ministero delle Infrastrutture, Ministero dell'Interno, Dipartimento della Protezione Civile, pubblicato su S.O. n.30 alla G.U. 4 febbraio 2008, n.29.
- DRUCKER, D. C., GREENBERG, H. J. and PRAGER, W. (1952), «Extended limit design theorems for continuous media», *Q. Appl. Math.*, vol. 9, p. 381–389.
- DRUCKER, D. C. and LI, M. (1992), «Non-associated plastic deformation and genuine instability», in «Advances in Dynamic Systems and Stability», p. 161–171, Springer.
- EN-206-1 (2001), «Concrete - Part 1. Specification, Performance, Production and Conformity», *European Committee for Standardization*.
- EXNER, H. (1979), «On the Effectiveness Factor in Plastic Analysis of Concrete», *Plasticity in Reinforced Concrete, IABSE Colloquium*, vol. 29, p. 35–42.
- FERREIRA, D. (2013), *A model for the nonlinear, time-dependent and strengthening analysis of shear critical frame concrete structures*, PhD Thesis, Supervisors: Prof. A.R. Marí, Prof. J.M. Bairán, Prof. R.M. Marques, Technical University of Catalonia, Barcelona, Spain.
- FERREIRA, D., BAIRÁN, J. and MARÍ, A. (2013a), «Numerical simulation of shear-strengthened RC beams», *Engineering Structures*, vol. 46, p. 359–374.
- FERREIRA, D., MARÍ, A. and BAIRÁN, J. (2013b), «Assessment of prestressed concrete bridge girders with low shear reinforcement by means of a non-linear filament frame model», *Structure and Infrastructure Engineering*, vol. ahead-of-print, p. 1–16.
- FERREIRA, D., OLLER, E., MARÍ, A. and BAIRÁN, J. (2013c), «Numerical Analysis of Shear Critical RC Beams Strengthened in Shear with FRP Sheets», *Journal of Composites for Construction*, vol. 17 (6).
- FRANCIOSI, V. (1959), *Scienza delle costruzioni*, Pellerano-Del Gaudio.
- FURLONG, R. W., HSU, C.-T. T. and MIRZA, S. A. (2004), «Analysis and design of concrete columns for biaxial bending-overview», *ACI Structural Journal*, vol. 101 (3).

- GALLI, A. and FRANCIOSI, V. (1955), «Il calcolo a rottura dei ponti a volta sottile ed impalcato irrigidente», *Giornale del Genio Civile*, vol. 11, p. 686–700.
- GARDNER, M. (1970), «Mathematical games: The fantastic combinations of John Conway's new solitaire game "life"», *Scientific American*, vol. 223 (4), p. 120–123.
- GJØRV, O. E. (2009), *Durability design of concrete structures in severe environments*, Taylor & Francis.
- GLICKSMAN, M. E. (2000), *Diffusion in solids: field theory, solid-state principles, and applications*, Wiley New York.
- GONZALEZ, J., ANDRADE, C., ALONSO, C. and FELIU, S. (1995), «Comparison of rates of general corrosion and maximum pitting penetration on concrete embedded steel reinforcement», *Cement and Concrete Research*, vol. 25 (2), p. 257–264.
- GUEDES, J., PEGON, P. and PINTO, A. (1994), «A fibre/Timoshenko beam element in CASTEM 2000», *special publication Nr. I*, vol. 94.
- GÜNER, S. (2008), *Performance assessment of shear-critical reinforced concrete plane frames*, PhD Thesis, Supervisor: Prof. F.J. Vecchio, University of Toronto, Canada.
- GÜNER, S. and VECCHIO, F. J. (2010), «Analysis of Shear-Critical Reinforced Concrete Plane Frame Elements under Cyclic Loading», *Journal of Structural Engineering*, vol. 137 (8), p. 834–843.
- GVOZDEV, A. (1938), «Opređenje veličiny razrushayushchei nagruzki dlya staticheski neopredelimykh sistem, preterpevayushchikh plasticheskie deformatsii», *Akademia Nauk SSSR, Moscow/Leningrad*, p. 19–38.
- HERNÁNDEZ-DÍAZ, A. and GIL-MARTÍN, L. (2012), «Analysis of the equal principal angles assumption in the shear design of reinforced concrete members», *Engineering Structures*, vol. 42, p. 95–105.
- HSU, T. T. (1998), «Stresses and crack angles in concrete membrane elements», *Journal of Structural Engineering*, vol. 124 (12), p. 1476–1484.
- JIRÁSEK, M. and BAZANT, Z. P. (2002), *Inelastic analysis of structures*, Wiley.com.
- KENT, D. C. and PARK, R. (1971), «Flexural members with confined concrete», *Journal of the Structural Division*, vol. 97 (7), p. 1969–1990.
- KOBAYASHI, K. (2006), «The seismic behavior of RC member suffering from chloride-induced corrosion», in «Proceedings of the second fib Congress», p. 19–3.
- KOSTIC, S. M. and FILIPPOU, F. C. (2011), «Section discretization of fiber beam-column elements for cyclic inelastic response», *Journal of Structural Engineering*, vol. 138 (5), p. 592–601.

- KUPFER, H. (1964), «Expansion of Mörsch's truss analogy by application of the principle of minimum strain energy», *CEB bulletin*, vol. 40.
- LE CORVEC, V. (2012), *Nonlinear 3d frame element with multi-axial coupling under consideration of local effects*, PhD Thesis, Supervisors: Prof. Filip C. Filippou, University of California, Berkeley.
- LEE, C. and FILIPPOU, F. (2009), «Frame elements with mixed formulation for singular section response», *International Journal for Numerical Methods in Engineering*, vol. 78, p. 1320–1344.
- LEONDARDT, F. (1965), «Reducing the shear reinforcement in reinforced concrete beams and slabs», *Magazine of Concrete Research*, vol. 17 (53), p. 187–198.
- LEONHARDT, F. and WALTHER, R. (1962), «Schubversuche an einfeldrigen Stahlbetonbalken mit und ohne Schubbewehrung», *Deutscher Ausschuss für Stahlbeton*, vol. 151.
- LIU, T. and WEYERS, R. (1998), «Modeling the dynamic corrosion process in chloride contaminated concrete structures», *Cement and Concrete Research*, vol. 28 (3), p. 365–379.
- MAIER, G. (1973), «A shakedown matrix theory allowing for workhardening and second-order geometric effects», in «International Symposium on Foundations of Plasticity, Warsaw, Poland», p. 417–433.
- MALERBA, P. (1984), «Aspetti numerici dell'analisi di sezioni in C.A. soggette a sforzo normale», *Atti del IV Congresso C.T.E. (Collegio dei Tecnici dell'Industrializzazione Edilizia) Firenze*, p. 165–171.
- MALERBA, P. (1998), *Analisi limite e non lineare di strutture in calcestruzzo armato*, International centre for mechanical sciences CISM, Collana di Ingegneria strutturale - no.10.
- MALERBA, P. (2005), «I ponti strallati. Il contributo di Francesco Martinez Y Cabrera», *Politecnico di Milano, P.za L. da Vinci, Milano, Italy*.
- MALERBA, P. and BONTEMPI, F. (1989), «Analisi di telai in c.a. in presenza di non linearità meccaniche e geometriche.», *Studi e ricerche - Politecnico di Milano. Scuola di specializzazione in costruzioni in cemento armato.*, vol. 11 (1), p. 209–224.
- MALERBA, P., BONTEMPI, F. and BARBERA, E. (1996), «Una formulazione del metodo delle strisce finite per l'analisi di elementi in cemento armato. Parte I: Impostazione», *Studi e ricerche - Politecnico di Milano. Scuola di specializzazione in costruzioni in cemento armato*, vol. 17, p. 189–222.
- MANDER, J. B., PRIESTLEY, M. J. and PARK, R. (1988), «Theoretical stress-strain model for confined concrete», *Journal of structural engineering*, vol. 114 (8), p. 1804–1826.

- MARÍ, A. R. (1984), «Nonlinear geometric, material and time dependent analysis of three dimensional reinforced and prestressed concrete frames», *Division of Structural Engineering and Structural Mechanics, Department of Civil Engineering, University of California, Berkeley*.
- MARÍ, A. R. (2000), «Numerical simulation of the segmental construction of three dimensional concrete frames», *Engineering Structures*, vol. 22, p. 585–596.
- MARTI, P. (1985), «Basic tools of reinforced concrete beam design», *ACI Journal Proceedings*, vol. 82 (1).
- MARTINELLI, L. (2008), «Modeling Shear-Flexure Interaction in Reinforced Concrete Elements Subjected to Cyclic Lateral Loading», *ACI Structural Journal*, vol. 105 (6).
- MEEK, J. L. (1991), *Computer methods in structural analysis*, Taylor & Francis.
- MOHR, S. (2011), *Nonlinear static and dynamic model for the analysis of reinforced concrete frames under high shear forces*, PhD Thesis, Supervisors: Prof. A.R. Marí, Prof. J.M. Bairán, Technical University of Catalonia, Barcelona, Spain.
- MOHR, S., BAIRÁN, J. M. and MARÍ, A. R. (2010), «A frame element model for the analysis of reinforced concrete structures under shear and bending», *Engineering Structures*, vol. 32 (12), p. 3936–3954.
- MOHR, S., BAIRÁN, J. M. and MARÍ, A. R. (2012), «Seismic response of reinforced concrete frames considering the influence of high shear stresses by means of a new numerical model», *15 WCEE, Lisboa*.
- MONTI, G. and SPACONE, E. (2000), «Reinforced concrete fiber beam element with bond-slip», *Journal of Structural Engineering*, vol. 126 (6), p. 654–661.
- MÖRSCH, E. (1902), «Le béton armé, étude théorique et pratique (Der Eisenbetonbau: Seine Theorie Und Anwendung)», *Paris, Liège: C. Béranger*, vol. 1.
- NEUENHOFER, A. and FILIPPOU, F. C. (1997), «Evaluation of nonlinear frame finite-element models», *Journal of Structural Engineering*, vol. 123 (7), p. 958–966.
- NIELSEN, M. P. and HOANG, L. C. (2011), *Limit analysis and concrete plasticity*, Taylor & Francis US.
- NUKALA, P. and WHITE, D. (2004), «Variationally consistent state determination algorithms for nonlinear mixed beam finite elements», *Computer Methods in Applied Mechanics and Engineering*, vol. 193, p. 3647–3666.
- OLSEN, P. C. (1998), «The influence of the linearisation of the yield surface on the load-bearing capacity of reinforced concrete slabs», *Computer Methods in Applied Mechanics and Engineering*, vol. 162 (1), p. 351–358.
- PANG, X.-B. D. and HSU, T. T. (1996), «Fixed angle softened truss model for reinforced concrete», *ACI Structural Journal*, vol. 93 (2).

- PASTORE, T. and PEDEFERRI, P. (1994), «La corrosione e la protezione delle opere metalliche esposte all'atmosfera», *Edilizia*, p. 75–92.
- PETRANGELI, M. (1999), «Fiber element for cyclic bending and shear of RC structures. II: Verification», *Journal of engineering mechanics*, vol. 125 (9), p. 1002–1009.
- PETRANGELI, M. and CIAMPI, V. (1997), «Equilibrium based iterative solutions for the non-linear beam problem», *International Journal for Numerical Methods in Engineering*, vol. 40, p. 423–437.
- PETRANGELI, M., PINTO, P. E. and CIAMPI, V. (1999), «Fiber element for cyclic bending and shear of RC structures. I: Theory», *Journal of Engineering Mechanics*, vol. 125 (9), p. 994–1001.
- PRAGER, W. (1952), «The general theory of limit design», in «Proceedings of the 8th International Congress on theoretical and Applied Mechanics, Istanbul», vol. 19, p. 65–72.
- RANZO, G. and PETRANGELI, M. (1998), «A fibre finite beam element with section shear modelling for seismic analysis of RC structures», *Journal of earthquake engineering*, vol. 2 (03), p. 443–473.
- RITTER, W. (1899), «Die Bauweise Hennebique», *Schweizerische Bauzeitung*, vol. 33/34.
- ROBINSON, J. and DEMORIEUX, J. (1968), «Essais de traction, compression sur modèles d'âme de poutre en béton armé», *Institute de Recherches appliquees du Beton (IRABA)*, vol. 1.
- ROGOWSKY, D. and MACGREGOR, J. (1986), «Design of reinforced concrete deep beams», *Concrete International*, vol. 8 (8), p. 49–58.
- RONCA, P. and COHN, M. (1979a), «Limit analysis of reinforced concrete arch bridges», *Journal of the Structural Division*, vol. 105 (2), p. 313–326.
- RONCA, P. and COHN, M. (1979b), «Matrix-MP method for the analysis of inelastic arch structures», *International Journal for Numerical Methods in Engineering*, vol. 14 (5), p. 703–725.
- SAETTA, A., SCOTTA, R. and VITALIANI, R. (1999), «Coupled environmental-mechanical damage model of RC structures», *Journal of engineering mechanics*, vol. 125 (8), p. 930–940.
- SCAPERROTTA, D. (2013), *Ponti in C.A. soggetti a Fenomeni Corrosivi*, Master Thesis, Supervisors: Prof. P.G. Malerba and Eng. M. Quagliaroli, Politecnico di Milano, Milan, Italy.
- SEIF, S. and DILGER, H. (1990), «Nonlinear Analysis and Collapse Load of P/C Cable-Stayed Bridges», *Journal of Structural Engineering*, vol. 116 (3), p. 829–849.

- SGAMBI, L., MALERBA, P. G., GOTTI, G. and IELMINI, D. (2012), «The influence of degradation phenomena on collapse modes in prestressed concrete beams», *International Journal of Lifecycle Performance Engineering*, vol. 1 (1), p. 41–63.
- SPACONE, E., CIAMPI, V. and FILIPPOU, F. (1996), «Mixed formulation of non-linear beam finite element», *Computers & Structures*, vol. 58 (1), p. 71–83.
- SPACONE, E., CIAMPI, V. and FILIPPOU, F. C. (1995), *A beam element for seismic damage analysis*, Earthquake Engineering Research Center, University of California.
- STEWART, M. G. (2009), «Mechanical behaviour of pitting corrosion of flexural and shear reinforcement and its effect on structural reliability of corroding RC beams», *Structural safety*, vol. 31 (1), p. 19–30.
- TAUCER, F., SPACONE, E. and FILIPPOU, F. (1991), *A fiber beam-column element for seismic response analysis of reinforced concrete structures*, Report No. UCB/EERC-91/17, University of California, Berkeley, National Science Foundation.
- TAYLOR, R., FILIPPOU, F., SARITAS, A. and AURICCHIO, F. (2003), «A mixed finite element method for beam and frame problems», *Computational Mechanics*, vol. 31 (1-2), p. 192–203.
- TITI, A. (2012), *Lifetime Probabilistic Seismic Assessment of Multistory Precast Buildings*, PhD Thesis, Supervisor: Prof. F. Biondini, Politecnico di Milano, Milan, Italy.
- TOFFOLI, T. and MARGOLUS, N. (1987), *Cellular Automata Machines: A new environment for modelling*, MIT press.
- VECCHIO, F. J. (2000a), «Analysis of shear-critical reinforced concrete beams», *ACI Structural Journal*, vol. 97 (1), p. 102–110.
- VECCHIO, F. J. (2000b), «Disturbed stress field model for reinforced concrete: Formulation», *Journal of Structural Engineering*, vol. 126 (9), p. 1070–1077.
- VECCHIO, F. J. (2001), «Disturbed stress field model for reinforced concrete: implementation», *Journal of Structural Engineering*, vol. 127 (1), p. 12–20.
- VECCHIO, F. J. and COLLINS, M. P. (1986), «The modified compression-field theory for reinforced concrete elements subjected to shear.», *ACI J.*, vol. 83 (2), p. 219–231.
- VECCHIO, F. J. and COLLINS, M. P. (1988), «Predicting the response of reinforced concrete beams subjected to shear using modified compression field theory», *ACI Structural Journal*, vol. 85 (3), p. 258–268.
- VECCHIO, F. J. and COLLINS, M. P. (1993), «Compression response of cracked reinforced concrete», *Journal of Structural Engineering*, vol. 119 (12), p. 3590–3610.



- VERGANI, M. (2010), *Modellazione del degrado di strutture in calcestruzzo armato soggette a corrosione*, Master Thesis, Supervisor: Prof. F. Biondini, Politecnico di Milano, Milan, Italy.
- VIDAL, T., CASTEL, A. and FRANCOIS, R. (2004), «Analyzing crack width to predict corrosion in reinforced concrete», *Cement and Concrete Research*, vol. 34 (1), p. 165–174.
- VINCIPROVA, F. and OLIVETO, G. (2013), «Ultimate Strength Domain of Reinforced Concrete Sections under Biaxial Bending and Axial Load», *ACI Structural Journal*, vol. 110 (1).
- VON NEUMANN, J., BURKS, A. W. *et al.* (1966), «Theory of self-reproducing automata», *University of Illinois press Urbana*.
- WAGNER, H. (1929), «Ebene blechwandträger mit sehr dünnem stegblech», *Z. Flugtechn. Motorluftschiffahrt*, vol. 65 (73).
- WALRAVEN, J. C. (1981), «Fundamental analysis of aggregate interlock», *Journal of the Structural Division*, vol. 107 (11), p. 2245–2270.
- WEAVER, W., JOHNSTON, P. R. and DOUGLAS, A. (1984), «Finite elements for structural analysis», *Journal of Applied Mechanics*, vol. 51, p. 705.
- WHITNEY, C. A. (1990), *Random processes in physical systems: an introduction to probability-based computer simulations*, John Wiley & Sons, Inc.
- WOLFRAM, S. (2002), *A new kind of science*, vol. 5, Wolfram media Champaign.
- XI, Y. and BAZANT, Z. P. (1999), «Modeling chloride penetration in saturated concrete», *Journal of Materials in Civil Engineering*, vol. 11 (1), p. 58–65.
- XI, Y., WILLAM, K. and FRANGOPOL, D. M. (2000), «Multiscale modeling of interactive diffusion processes in concrete», *Journal of engineering mechanics*, vol. 126 (3), p. 258–265.



# Index

- aggregate interlock, 54, 60, 61
- basic forces, 18
- bisection method, 167
- cable stayed bridge, 120
- carbonated concrete, 109
- cellular automata, 105
- chlorides, 5, 104, 114
- collapse mechanism, 185
- compatibility matrix, 181
- compression field, 53
- compression softening, 54, 58, 64
- computer code, 67, 185
- corrosion, 5, 104
- crack
  - check control, 60
  - models, 55, 62
  - slip, 66
  - width limit, 61
- cracking initiation, 111
- damage indexes, 107
- delamination, 111
- diffusion processes, 106
- distributed loads, 26, 179
- Disturbed Stress Field Model, 55, 62, 69
- effectiveness factor, 125, 130
- element
  - displacement-based, 16, 26
  - force-based, 17, 27, 180
  - state determination, 15, 17, 23, 35
- equilibrium matrix, 180
- evolutionary rule, 105
- fiber approach, 36
- finite difference, 44
- Fixed-Angle Softened Truss Model, 55
- flow chart, 73, 89
- flow rule, 183
- game of life, 105
- Generalized Beam Theory, 38
- geometric non linearities, 28
- geometric stiffness matrix, 29
- influence line, 137
- integration rule
  - Gauss-Legendre, 157
  - Gauss-Lobatto, 157, 169, 173–175
  - midpoint integration, 157
  - Newton-Cotes, 157
- interaction domain, 125, 130, 162, 166, 173–175, 178
- kinematic undetermined structure, 182
- lifetime, 101
- lower bound theorem, 184
- material degradation laws, 107
- Modified Compression Field Theory, 54, 55
- moment-curvature diagrams, 162
- Navier-Bernoulli Beam Theory, 38
- neutral axis, 169, 170
- Newton-Raphson, 21, 165
- numerical integration, 155
- optimization problem, 185
- pitting corrosion, 110
- plastic hinge, 24, 178
- prestressing forces, 122

- principle
  - of Virtual Displacements, 14, 48, 84, 163
  - of Virtual Forces, 15, 20, 181
  - of Virtual Work, 14, 19
- residual tension, 61
- Rotating-Angle Softened Truss Model, 55
- secant approach, 72
- secant formulation, 67
- section state determination, 87
- shear collapse, 79
- shear locking, 33
- simplex method, 185
- smearred approaches, 53
- spalling, 107, 110
- statically determined structure, 181
- statically undetermined structure, 182
- strut & tie, 41
- tension stiffening, 58
- Timoshenko Beam Theory, 38
- triangular element, 67
- truss analogy, 41
- truss model, 53
- upper bound theorem, 185
- warping, 47
- yield condition, 182





---

M. QUAGLIAROLI

*From Bidimensional towards Monodimensional Modeling  
of Sound and Damaged Reinforced Concrete Structures*

© March 2014

[manuel.quagliaroli@polimi.it](mailto:manuel.quagliaroli@polimi.it)

Department of Civil & Environmental Engineering  
Politecnico di Milano  
Piazza Leonardo da Vinci 32  
20133, Milan, Italy

---